

with or without elevations in bilirubin. Cholestasis can present as an acute or chronic condition and is thought to affect up to 20% of the population.⁷³ The impairment of flow leads to an increase in the concentration of bile salts in the serum and hepatocytes. As the bile salts accumulate in the liver, they dissolve hepatocyte cell membranes, leading to the release of AP and GGT, resulting in an increase in the serum concentrations of these enzymes.⁷⁴ Serum concentrations of AST and ALT, which are found in the cytoplasm of hepatocytes, are not increased to as great an extent. As the disease progresses, the serum concentration of conjugated bilirubin increases, giving rise to jaundice.³¹ The majority of cases of cholestasis are benign; however, severe and prolonged cholestasis can lead to cirrhosis.

Signs and symptoms of cholestasis include fatigue, pruritus, dark urine, and pale stools. An elevation of AP on screening laboratory studies may be the first indication in asymptomatic patients. The evaluation consists of a history and physical exam followed by abdominal ultrasonography. Abdominal ultrasonography is used to distinguish between extrahepatic and intrahepatic cholestasis. Extrahepatic cholestasis results from mechanical obstruction of the extrahepatic bile ducts, typically by stones, strictures, or masses leading to ductal dilation. Definitive diagnosis and treatment is by endoscopic retrograde pancreatography (ERCP). If the etiology is unclear, further imaging can be conducted using endoscopic ultrasound or magnetic resonance cholangiopancreatography to identify the biliary lesion leading to obstruction.⁷⁵ Normal imaging results indicate intrahepatic cholestasis. Intrahepatic cholestasis can have several etiologies including immune-mediated, infectious, drug-induced, paraneoplastic, and ischemic. The first step in the evaluation is the measurement of anti-mitochondrial antibody (AMA) titers to rule out primary biliary cholangitis (PBC). Further evaluation may require ERCP and liver biopsy.

PRIMARY BILIARY CHOLANGITIS

Formerly known as primary biliary cirrhosis, PBC is an autoimmune disease that is characterized by the destruction of intrahepatic cholangiocytes and the presence of AMAs. It is one of the most common cholestatic liver disorders.⁷⁶ Reported prevalence rates vary from 20 to 490 cases per million inhabitants with the highest rates reported in the United States.⁷⁷ Over 90% of patients are female and the average age at diagnosis is typically in the sixth decade. The diagnosis is made based on an elevation of AP over 1.5 times the upper limit of normal for a duration greater than 24 weeks along with the presence of an AMA titer greater than 1:40.⁷⁶ A liver biopsy in these patients will reveal interlobular bile duct lesions. Up to 60% of patients may be asymptomatic at diagnosis. If present, the most common symptoms at presentation are fatigue and pruritus. A large number of patients may present with other autoimmune disorders such as keratoconjunctivitis sicca and Raynaud phenomenon. PBC may be associated with osteopenia as well as hyperlipidemia.⁷⁶ The disease develops as a result of the loss of tolerance to mitochondrial antigens, leading to autoimmune-mediated destruction of biliary epithelial cells (cholangiocytes). PBC can lead to cirrhosis and liver failure, ultimately requiring transplantation.

Treatment consists of ursodeoxycholic acid (UDCA) administration. UDCA, a bile acid, is thought to act by modifying the bile acid pool and reducing inflammation. Approximately 60% to 70% of patients with PBC respond to UDCA with improvement in serum AP and bilirubin levels and a delay in the progression to cirrhosis and liver transplantation. Patients who have a suboptimal response to UDCA have an increased risk of developing complications and liver failure. In these patients, the administration of obeticholic acid, a farnesoid-X receptor agonist, has been shown to reduce the serum levels of AP. Fibrates and corticosteroids have also shown benefit when combined with UDCA in patients who are unresponsive to UDCA alone.⁷⁸⁻⁸³

PRIMARY SCLEROSING CHOLANGITIS

PSC is a rare cholestatic, immune-mediated disease that occurs most frequently in men aged 30 to 40 years old. It is characterized by inflammation and fibrosis of the bile ducts. The majority of patients with PSC have ulcerative colitis as well. Approximately half of the patients are asymptomatic at diagnosis. The most common presenting symptoms are fatigue and pruritus. Blood tests demonstrate a cholestatic pattern. Patients may also have hypergammaglobulinemia and elevations in serum autoantibodies. Diagnosis is made based on the presence of multifocal strictures and segmental biliary dilations on cholangiography, and the exclusion of a number of other possible etiologies including bacterial cholangitis, choledocholithiasis, and surgical biliary trauma.⁸⁴ Patients have an increased risk of developing hepatobiliary carcinoma. The disease is progressive, with biliary fibrosis leading to cirrhosis and ultimately end-stage liver disease (ESLD). Liver transplantation is the only effective therapy.

CIRRHOSIS

Cirrhosis is the common pathologic endpoint of a variety of mechanisms of hepatic injury. In the United States, it is the 14th most common cause of death and has a prevalence of 0.3%.⁸⁵ The most common causes of cirrhosis in western countries are alcoholic liver disease, hepatitis C, and nonalcoholic steatohepatitis. In the Asia-Pacific region the most common cause is hepatitis B.⁸⁶ The morbidity and mortality associated with cirrhosis result mainly from portal hypertension. Chronic liver disease promotes apoptosis and regeneration of hepatocytes. The resultant inflammation leads to parenchymal injury and fibrosis, causing distortion and obstruction of the hepatic vascular architecture. These structural changes increase hepatic resistance to portal blood flow (PBF) and give rise to portal hypertension. Hepatic vascular resistance is further increased due to hepatic endothelial dysfunction, which results in a reduction of vasodilator (primarily nitric oxide [NO]) production and an increase in vasoconstrictor (i.e., thromboxane) production.⁸⁷ Portal hypertension and the release of angiogenic factors lead to the development of gastroesophageal varices as well as portosystemic shunts. As portal hypertension worsens, the locally released NO and prostaglandins cause the splanchnic circulation to vasodilate. This further increases portal inflow and exacerbates portal hypertension. Splanchnic vasodilation also leads to systemic hypotension that, in turn, increases sympathetic tone, activates

the renin-angiotensin-aldosterone system, and increases antidiuretic hormone release, leading to the development of ascites and the hepatorenal syndrome (HRS). Other significant complications of cirrhosis and portal hypertension are spontaneous bacterial peritonitis, encephalopathy, HRS, portopulmonary hypertension (PoPH), cirrhotic cardiomyopathy, and HCC.⁸⁸

Laboratory abnormalities in cirrhotic patients include elevations in ALT, AST, AP, GGT, as well as serum bilirubin. Hypoalbuminemia and elevations in the PT are indications of hepatic synthetic dysfunction. Although liver biopsy is the gold standard for diagnosing cirrhosis, it is often not necessary in the presence of an appropriate patient history, and laboratory and radiologic data. In patients who are suspected of having cirrhosis, abdominal ultrasonography is used to aid in the diagnosis and evaluation for HCC and portal hypertension. Serologic studies and ultrasound-based techniques for evaluating hepatic fibrosis are also available.⁸⁹

The risk stratification of patients with cirrhosis is based on the presence and degree of portal hypertension, gastroesophageal varices, and synthetic dysfunction.⁹⁰ There are two stages of cirrhosis: compensated and decompensated. Decompensated cirrhosis is characterized by the presence of ascites, variceal hemorrhage, and/or hepatic encephalopathy (HE). Compensated cirrhosis is characterized by the absence of these clinical conditions. While the median survival in patients with compensated cirrhosis is greater than 12 years, in those with decompensated cirrhosis it is approximately 2 years.⁹¹ Patients with compensated cirrhosis can be further stratified based on their degree of portal hypertension. Portal hypertension is defined as a hepatic venous pressure gradient (HVPG) greater than 5 mm Hg. Patients with an HVPG greater than 10 mm Hg are deemed to have clinically significant portal hypertension. They are at increased risk of developing varices, overt hepatic decompensation, postsurgical decompensation, and HCC compared to those with mild portal hypertension (HVPG between 5 mm Hg and 10 mm Hg).⁹²⁻⁹⁴ Although HVPG is the gold standard for monitoring portal hypertension, its invasive nature precludes its routine use. A noninvasive measure of clinically significant portal hypertension is LS using transient elastography, an ultrasound-based approach. An LS value greater than 20 kPa has been shown to effectively discriminate mild from clinically significant portal hypertension.⁹⁵ Liver Doppler ultrasound may also aid in the diagnosis. The presence of portosystemic collaterals or reversal of portal venous flow on ultrasound imaging is also sufficient to diagnose clinically significant portal hypertension.⁹⁶ In patients with clinically significant portal hypertension, the presence of gastroesophageal varices portends a worse prognosis.⁹⁷

The management of patients with compensated cirrhosis who don't have gastroesophageal varices focuses on preventing the advancement of the disease by treating the underlying etiology.⁹⁰ Patients with varices are treated with nonspecific beta-blockers (i.e., propranolol, timolol), carvedilol or endoscopic variceal ligation to prevent variceal hemorrhage. Nonspecific beta-blocker therapy reduces HVPG.⁹⁸⁻¹⁰⁰

Acute variceal hemorrhage is a medical emergency. Management consists of airway protection, volume resuscitation, and endoscopy with variceal ligation. The concomitant

initiation of antibiotic prophylaxis (ceftriaxone 1 g/24 h) and vasopressor infusion (somatostatin, octreotide, or terlipressin) has been shown to improve outcome and is the standard of care. Once stabilized, preemptive TIPS may be performed in patients who are at high risk of rebleeding.⁹⁰

ASCITES

The presence of ascites is a marker of decompensated cirrhosis. The 1-year mortality rate of patients who develop ascites is 20%.¹⁰⁰ Patients who develop ascites are at increased risk of developing further complications including spontaneous bacterial peritonitis and acute kidney injury (AKI). Management consists of dietary sodium restriction, non-specific beta-blocker therapy to reduce portal pressure, and diuretic administration (spironolactone, furosemide). Midodrine can be added for refractory ascites. TIPS can improve transplant-free survival in certain patients with refractory ascites.⁸⁶

Renal Failure and Hepatorenal Syndrome

Up to 40% of patients admitted to the hospital with ESLD develop renal failure. Renal failure is a sign of advanced disease and has a poor prognosis in liver failure. Seventy to 80% of cases are precipitated by hypovolemia or bacterial infections. HRS is less common and associated with a worse prognosis.^{101,102} The diagnosis of HRS is one of exclusion. It is characterized by AKI in the absence of any apparent cause (shock, nephrotoxic drugs, obstruction, renal parenchymal disease) that is unresponsive to volume expansion and diuretic withdrawal. AKI is defined as a rise in creatinine greater than or equal to 0.3 mg/dL within 48 hours or a greater than 50% increase from baseline within 7 days.¹⁰³ HRS is subcategorized into Type 1 and Type 2 based on the rapidity of onset and degree of injury. Type 1 is rapidly progressive with a doubling of serum creatinine within 2 weeks. It is usually associated with a precipitating factor and has a worse prognosis. The treatment for HRS is aimed at increasing perfusion pressure to the kidneys. For critically ill patients, norepinephrine infusion with albumin boluses can be used. In more stable patients, terlipressin (if available) or midodrine with octreotide is administered along with albumin.¹⁰⁴ Dialysis may be used in the absence of response to medical therapy. Liver transplantation is the definitive treatment for HRS.¹⁰⁵

HEPATIC ENCEPHALOPATHY

HE is brain dysfunction secondary to hepatic insufficiency or portosystemic shunting. It is a sign of decompensated cirrhosis. It occurs in 30% to 40% of patients with cirrhosis and 50% of patients with portosystemic shunts.¹⁰⁶ The clinical presentation is variable and can range from mild changes in personality to disorientation, somnolence, and coma. Asterixis is usually present in the early to middle stages.¹⁰⁷ The severity of HE is typically graded from I to IV using the West Haven criteria with Grade I indicating mild symptoms and Grade IV, coma (Table 16.4).¹⁰⁸ Common precipitating factors of HE include infections, variceal hemorrhage, and diuretic overdose. Diagnosis is based on the exclusion of other causes of brain dysfunction and the application of clinical criteria. Treatment consists of amelioration of

TABLE 16.4 West Haven Criteria for Grading Hepatic Encephalopathy

Grade	Description
I	Trivial lack of awareness; shortened attention span; disordered sleep
II	Lethargy; behavioral change; asterixis
III	Somnolence; confusion; gross disorientation; bizarre behavior
IV	Coma

Modified from Table 2, Page 719 in: Vilstrup H, Amodio P, Bajaj J, et al. Hepatic encephalopathy in chronic liver disease: 2014 practice guideline by the American Association for the Study of Liver Diseases and the European Association for the Study of the Liver. *Hepatol*. 2014;60:715–735.

precipitating factors and the administration of lactulose, a nonabsorbable disaccharide. Rifaximin can be added on to prevent recurrence.¹⁰⁸

PULMONARY COMPLICATIONS

Hepatopulmonary syndrome (HPS), PoPH, and hepatic hydrothorax (HH) are pulmonary conditions that can develop in patients with cirrhosis and advanced liver disease. HPS has been reported in up to 30% of patients presenting for liver transplantation evaluation and is associated with increased mortality independent of the severity of liver disease.¹⁰⁹ It is defined as abnormal alveolar to arterial oxygen gradient (≥ 15 mm Hg) while breathing room air in sitting position. It is caused by intrapulmonary vascular dilation in the setting of cirrhosis. Its severity is determined by the PaO_2 : greater than 80 mm Hg is mild, 60 to 80 mm Hg is moderate, 50 to 60 mm Hg is severe, and less than 50 mm Hg is very severe.¹¹⁰ Patients may present with dyspnea at rest or on exertion. Approximately 25% of patients have platypnea (dyspnea when moving from supine to standing) or orthodeoxia (decrease in PaO_2 more than 5% or 4 mm Hg when moving from supine to standing). In advanced disease, patients may exhibit digital clubbing and cyanosis. Patients can be screened with pulse oximetry ($\text{SpO}_2 < 96\%$ on room air) and diagnosed based on PaO_2 values. Contrast-enhanced transthoracic echocardiography (TTE) may demonstrate intrapulmonary vascular dilation. No medical therapy has been shown to change outcome in patients with HPS. Supplemental oxygen is provided to maintain SpO_2 over 88%. Liver transplantation is the only effective treatment.¹¹¹ As such, MELD exception points are granted for patients with severe HPS (PaO_2 50–60 mm Hg). Patients with very severe HPS ($\text{PaO}_2 < 50$ mm Hg) have an increased risk for complications and mortality following liver transplantation although this risk may be lower in experienced centers.^{111,112}

PoPH is pulmonary arterial hypertension in the setting of portal hypertension.¹¹³ It is found in 5% of patients presenting for liver transplant evaluation and, in the absence of treatment, is associated with a 1-year survival of 46%.^{114,115} The diagnosis is made by right heart catheterization showing a mean pulmonary artery pressure (mPAP) greater than 25 mm Hg, pulmonary vascular resistance (PVR) greater than 240 dynes/s/cm⁵, and a pulmonary artery wedge pressure less than 15 mm Hg. PoPH is classified

as mild (mPAP: 25–35 mm Hg), moderate (mPAP: 35–45 mm Hg), and severe (mPAP more than 45 mm Hg).¹¹⁰ The pathophysiology of the disease remains to be elucidated. Patients are typically screened using TTE to measure right ventricular systolic pressure (RVSP). Those with RVSP greater than 50 mm Hg undergo right heart catheterization to confirm the diagnosis and determine the degree of PoPH. PoPH is treated with phosphodiesterase-5 inhibitors, prostacyclin analogs, and endothelin receptor antagonists to reduce PVR. mPAP greater than 45 mm Hg is an absolute contraindication to liver transplantation. MELD exception is considered for treatment-responsive PoPH.¹¹⁰

HH has a prevalence of 5% to 10% in cirrhotic patients.¹¹⁶ It develops due to the passage of ascitic fluid from the peritoneal cavity into the pleural space through defects in the diaphragm, most often on the right side. Patients may present with dyspnea, cough, chest discomfort, and hypoxia. Chest radiography and thoracentesis are used for diagnosis. Medical therapy consists of sodium restriction and diuretic administration. Refractory HH is treated with TIPS placement. For patients who have failed TIPS, VATS with pleurodesis is an option.¹¹⁷

HEPATOCELLULAR CARCINOMA

HCC is the most common primary liver malignancy and the third most common cause of cancer death globally. It occurs with greater frequency in men than women and with a higher incidence in Asia and Africa, although the incidence has been increasing in the United States.¹¹⁸ Chronic liver disease is the most important risk factor for the development of HCC. Hepatitis B, hepatitis C, hemochromatosis, alcohol use, nonalcoholic fatty liver disease, diabetes mellitus, and obesity all increase the risk of developing HCC.¹¹⁹ Screening is recommended for all patients with cirrhosis at 6-month intervals using ultrasound with or without serum AFP measurement. Masses over 1 cm should be imaged with dynamic MRI or four-phase multidetector CT to make the diagnosis noninvasively. A percutaneous biopsy is obtained for nodules that have nontypical appearance on imaging.¹²⁰ Staging is based on the size of the tumor, degree of extension into adjacent structures, presence of metastases, liver function, and the patient's physical status. There is no universally accepted system for staging. The tumor, node, metastasis and the Barcelona staging system (BCLC) are two of the more commonly used systems.¹²⁰

Surgical resection of HCC is the definitive treatment for the disease. However, the diagnosis of HCC is typically made late in the course of the disease. In patients with preserved liver function and a solitary tumor confined to the liver, treatment with surgical resection carries a 5-year survival rate from 40% to 75%.¹²¹ Transplantation may be an option for patients with hepatic dysfunction and tumors confined to the liver that meet certain size criteria.¹²² Non-surgical options for patients who are ineligible for resection or transplantation include radiofrequency ablation, transarterial chemoembolization, and systemic therapy.¹²⁰

HEPATIC EFFECTS OF ANESTHETIC AGENTS

Inhalational Anesthetics

(See also chapter on pharmacokinetics/dynamics of volatile anesthetics.)

The hepatic effects of volatile anesthetics result primarily from alterations in liver perfusion. Total hepatic blood flow (THBF) is the sum of PBF and hepatic arterial blood flow (HABF). Reductions in PBF are matched by increases in HABF to maintain THBF through the hepatic arterial buffer response (HABR).¹²³ Volatile anesthetics reduce mean arterial pressure (MAP) and CO, leading to a reduction in PBF in a dose-dependent manner. The HABR is preserved with isoflurane, sevoflurane, and desflurane leading to preservation of THBF, but not with halothane.¹²⁴⁻¹²⁶

Xenon is an inert gas that can be used as an anesthetic.¹²⁷ It has favorable anesthetic properties including a low blood-gas partition coefficient (0.115) and a stable hemodynamic profile.^{128,129} Hepatic perfusion during xenon anesthesia has been studied in pigs. In one study using radiolabeled microspheres, there was no difference in hepatic perfusion in pigs anesthetized with xenon when compared to propofol.¹³⁰ However, a second study using ICG reported a 17% reduction in portal venous blood flow in pigs anesthetized with a ketamine infusion that received a xenon anesthetic compared to controls. They reported no significant difference in hepatic arterial perfusion or hepatic function.¹³¹ In a porcine model, the use of xenon anesthesia was associated with significantly higher hepatic venous oxygen content when compared with propofol.¹³² It is not clear that there are relevant clinical consequences to these findings. The successful use of xenon anesthesia for the conduct of liver transplantation has been reported in a series of four cases.¹³³

In general, intravenous anesthetics such as propofol, thiopental, etomidate, and methohexitol do not adversely affect the liver. Furthermore, the pharmacokinetic properties of these agents are unchanged in patients with cirrhosis.¹³⁴⁻¹³⁷ Cirrhotic patients may be more sensitive to their central nervous system depressant effects. Propofol has been found to increase hepatic blood flow and oxygen consumption in both animal and human studies that have measured flow using radiolabeled microspheres, Doppler, and electromagnetic flow meters.¹³⁸⁻¹⁴¹ Studies using ICG clearance to measure hepatic flow, however, have reported that propofol reduced hepatic flow.^{142,143} These findings were confounded by the fact that propofol itself interferes with ICG clearance.^{141,144} Clinically, propofol has no adverse effect on hepatic function. Midazolam elimination is impaired in liver dysfunction leading to prolongation of sedative effects.¹⁴⁵ Dexmedetomidine elimination is reduced in patients with hepatic impairment, necessitating dose reduction.¹⁴⁶

In patients with significant cirrhosis, the metabolism of morphine, meperidine, and alfentanil is reduced and their durations of action are prolonged.¹⁴⁷⁻¹⁴⁹ In patients with mild hepatic insufficiency, the pharmacokinetics of fentanyl, sufentanil, and remifentanil are unchanged when compared to normal controls.¹⁵⁰⁻¹⁵²

Reduced levels of pseudocholinesterase in patients with hepatic dysfunction may prolong the effects of succinylcholine and mivacurium.^{153,154} The time to recovery from cisatracurium is unchanged as it is subject to Hoffman degradation.¹⁵⁵

Aminosteroid neuromuscular blocking agents (vecuronium, rocuronium, pancuronium) have a larger volume of distribution in cirrhotic patients. They have a slower

rate of onset and a longer duration of action, necessitating judicious dosing and close train-of-four monitoring.¹⁵⁶⁻¹⁵⁸ Sugammadex has been shown to be effective for reversing rocuronium in patients with hepatic dysfunction.¹⁵⁹ The use of neostigmine for reversal is likewise unaffected by the presence of hepatic dysfunction.

Five studies have examined the effect of epidural anesthesia on hepatic blood flow. Four have shown a reduction in hepatic blood flow in response to lumbar or thoracic epidural anesthesia when measured using the PDR of ICG and transgastric hepatic vein Doppler. In one study, blood flow was restored with the infusion of colloid and dopamine.¹⁶⁰⁻¹⁶² Maintenance of MAP with ephedrine or norepinephrine further reduced hepatic blood flow. Unlike these studies, a study by Kortgen et al. found that thoracic epidural anesthesia increased hepatic blood flow when measured by PDR-ICG, whereas lumbar epidural anesthesia resulted in an overall reduction.¹⁶³ The clinical significance of these findings is uncertain.

Nonhepatic Surgery in Patients With Liver Disease

The preoperative evaluation of patients with liver disease should determine the severity of the disease and the presence of comorbid conditions associated with hepatic dysfunction. Given the mortality risk, elective surgery is contraindicated in patients with acute hepatitis or acute liver failure.¹⁶⁴ In the absence of cirrhosis and significant hepatic dysfunction, patients with chronic liver disease generally have no increased risk for undergoing elective surgery. Patients with cirrhosis who undergo nonhepatic surgery have a higher incidence of postoperative morbidity and mortality when compared to patients without cirrhosis.¹⁶⁵ A wide range of mortality rates has been reported in the literature (1%-50%), mostly in small, uncontrolled, institutional studies spanning 30 years. Mortality in these patients is a function of the severity of liver disease, its attendant comorbidities, and the type of surgical procedure.¹⁶⁵ The largest study of in-hospital mortality in patients with cirrhosis used data from the Nationwide Inpatient Sample. The outcomes of 22,569 cirrhotic patients undergoing one of four index operations (cholecystectomy, colectomy, coronary artery bypass grafting [CABG], and abdominal aortic aneurysm repair) from 1998 to 2005 were compared to those of 2.8 million control patients. It was found that 4214 of the cirrhotic patients had portal hypertension. Patients with cirrhosis had a three- to eight-fold increase in the risk of in-hospital mortality, depending on the operation, compared to control patients. Mortality risk worsened in those with more severe liver disease, ranging from 12- to 23-fold, depending on the specific operation. The greatest risk was seen in patients undergoing CABG.¹⁶⁶ A Taiwanese study comparing 24,282 cirrhotic patients undergoing major nonhepatic surgery with 97,128 matched control patients found an over two-fold increased risk of 30-day mortality in patients with cirrhosis (1.2% vs. 0.7%). Mortality was further increased in those cirrhotic patients with viral hepatitis, jaundice, ascites, gastrointestinal hemorrhage, and hepatic coma.¹⁶⁷

In cirrhotic patients undergoing nonhepatic surgery, the Child-Turcotte-Pugh (CTP) and MELD scores have been shown to identify those who are at higher risk of morbidity and mortality.¹⁶⁸⁻¹⁷² The CTP score is calculated based on

TABLE 16.5 Child-Turcotte-Pugh (CTP) Score

POINTS ASSIGNED			
	1	2	3
Ascites	Absent	Slight	Moderate
Bilirubin	<2 mg/dL	2-3 mg/dL	>3 mg/dL
Albumin	>3.5 g/dL	2.8-3.5 g/dL	<2.8 g/dL
PROTHROMBIN TIME			
Seconds over control	<4	4-6	>6
International normalized ratio	<1.7	1.7-2.3	>2.3
Encephalopathy	None	Grades 1-2	Grades 3-4
Point total	CTP class	Operative mortality	
5-6	A	2-10%	
7-9	B	12-31%	
10-15	C	12-82%	

The 30-day postoperative mortality predicted by the **Child-Turcotte-Pugh (CTP) score** is based on retrospective studies cited in text. Lower mortality rates have been reported in more recent studies.

From Pugh RN, Murray-Lyon IM, Dawson JL, et al. Transection of the oesophagus for bleeding oesophageal varices. *Br J Surg*. 1973;60(8):646-649. <https://doi.org/>.

the values of five variables: degree of HE, degree of ascites, INR, serum albumin, and total bilirubin (Table 16.5). The score is then used to classify the patient into one of three groups: Class A (score of 5-6), Class B (score of 7-9), and Class C (score > 10).¹⁷³ A higher CTP class is associated with a greater risk of mortality. The mortality risk associated with each CTP class has decreased in more recent studies. In early retrospective series of cirrhotic patients undergoing abdominal surgery, the mortality risks associated with CTP Class A, B, and C were 10%, 30%, and 73% to 82%, respectively.^{174,175} In a more recent series of 194 patients undergoing 212 general surgical procedures, 30-day mortality was reported to be 6%, 13%, and 53% for CTP Classes A, B, and C, respectively.¹⁶⁹ The risk has been found to be even lower in patients undergoing laparoscopic procedures (Class A: 2%; Class B: 12%; Class C: 12%), suggesting that improvements in perioperative care and surgical techniques have made surgery safer for patients with cirrhosis.¹⁷⁰ A disadvantage of the CTP score is that the grading of encephalopathy and ascites is subjective. Furthermore, the score doesn't take into account other predictors of operative risk such as the type of surgery or the etiology of the cirrhosis.¹⁷⁶

As described above, the MELD score, calculated using the patient's INR, serum creatinine, serum bilirubin, and etiology of liver disease (Fig. 16.5)¹⁷⁷ is a validated measure of mortality risk in patients with ESLD and is the basis of the liver allocation system for transplantation.¹⁷⁸ A number of studies have validated the MELD score as a predictor of risk in cirrhotic patients undergoing abdominal, orthopedic, and cardiac surgery.^{168,179-181} In a large, retrospective study of cirrhotic patients undergoing major abdominal, orthopedic, or cardiac surgery, MELD score was a predictor for mortality at 30 days, 90 days, 1 year, and 5 years. The 30-day mortality ranged from 5.8% in patients with a

MELD under 8 to over 50% in patients with a MELD score greater than 20.¹⁸² The incorporation of serum sodium into the MELD score (MELD-Na) as well as a combination of serum sodium and patient age (integrated MELD or iMELD) have been shown to improve the accuracy of predictions of survival over MELD.^{183,184} The use of MELD-Na and iMELD may allow more accurate prediction of mortality following nonhepatic surgery; however more studies are needed.^{169,185,186}

Studies comparing the predictive power of CTP to MELD have yielded conflicting results likely due to small sample sizes and differences in primary outcome measures and surgical procedures. Small studies in cardiac and general surgical patients have found the abilities of CTP and MELD to predict postoperative mortality to be comparable.^{168,179} A study in cirrhotic patients undergoing extrahepatic abdominal surgery found MELD to be a better predictor than CTP for mortality or hepatic decompensation within 90 days of surgery.¹⁸⁰ A more recent study found neither to be a good predictor for death and hepatic decompensation in cirrhotic patients undergoing elective surgery requiring general anesthesia.¹⁷¹ It has been suggested that both scores should be used in conjunction with other available patient data when attempting to risk-stratify cirrhotic patients for nonhepatic surgery.¹⁸⁷

Apart from the severity of cirrhosis and the specific surgical procedure, risk factors associated with increased postoperative morbidity and mortality in cirrhotic patients include emergency surgery, American Society of Anesthesiologists (ASA) physical status classification, the presence of renal insufficiency, male gender, and advanced age.^{168,170,188}

In addition to determining the severity of cirrhosis, the preoperative evaluation should determine the presence and severity of comorbidities associated with cirrhosis, including HE, pulmonary disease, cardiac disease, and renal dysfunction (see previous discussion). Preoperative laboratory evaluation should include a complete blood count to evaluate for anemia, thrombocytopenia, and leukocytosis. Additionally, INR, fibrinogen, serum electrolytes, creatinine, glucose, transaminases, bilirubin, and albumin should be measured.

Anesthetic Considerations for Procedures Involving the Liver

Transjugular Intrahepatic Portosystemic Shunt. TIPS placement is a catheter-based, endovascular procedure during which a shunt is created between the portal and hepatic venous systems through the parenchyma of the liver (Fig. 16.6). The goal of the procedure is to reduce portal hypertension.¹⁸⁹ The main indications for TIPS are the secondary prevention of variceal hemorrhage and the management of refractory ascites.¹⁹⁰ During acute variceal hemorrhage in high-risk patients (HVPG > 20), TIPS placement following endoscopic intervention has been shown to reduce rebleeding.¹⁹¹ Contraindications to the procedure include congestive heart failure, tricuspid regurgitation, and moderate to severe pulmonary hypertension. During the procedure, a catheter is typically inserted through the right internal jugular vein into a hepatic venous branch. A needle is then passed through the hepatic vein into the portal vein. The tract is dilated and a stent is placed across it. HVPG should be

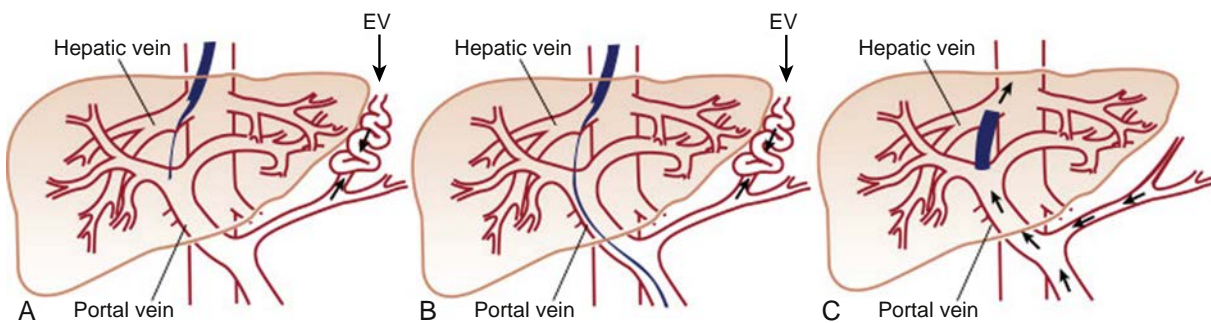


Fig. 16.6 Transjugular intrahepatic portosystemic shunt procedure. A stent (or stents) is passed through the internal jugular vein over a wire into the hepatic vein (A); dilated esophageal varices (EV) are apparent. The wire and stent or stents are then advanced into the portal vein (B), after which blood can pass through the portal vein into the hepatic vein and bypass and decompress dilated esophageal veins (C). (Reproduced with permission from University of Michigan Health System: www.med.umich.edu/1ibr/topics/liver09.htm/ (not able to access/TG 9-21-18)

less than 12 mm Hg following the procedure. The incidence of major complications such as intra abdominal hemorrhage is on the order of 1% to 2%.¹⁹²

TIPS may be carried out electively or emergently. The preoperative assessment should determine the extent of liver dysfunction and associated morbidity. Patients with advanced liver disease may be in a hyperdynamic state. They may have significant ascites with reductions in FRC as well as HH or HPS. Pulmonary function may be further compromised when the patient is in a supine position for the procedure. Patients may also have renal dysfunction, anemia, coagulopathy, and thrombocytopenia. Laboratory studies should screen for anemia, thrombocytopenia, and coagulopathy, as well as hyponatremia and elevations of creatinine and potassium. Patients should be transfused for a hemoglobin concentration less than 7 to 9 mg/dL, INR greater than 2, and a platelet count less than 50,000/ μ L.¹⁹³ The procedure can be conducted under local anesthesia, sedation, or general anesthesia. Consideration should be given to the acuity of the patient, their ability to tolerate supine positioning, and the anticipated length of the case. In patients with significant ascites or recent variceal hemorrhage, general anesthesia with rapid sequence induction for airway protection is preferred. Intraoperative pain may be experienced during the establishment of the intrahepatic shunt and the dilation of the stent. In a series of 150 patients undergoing TIPS with general anesthesia using TIVA, the authors reported a postoperative ICU admission rate of 6.6% primarily for intraoperative hemodynamic instability. They advocated for the use of general anesthesia for all TIPS procedures, given the concerns for airway protection, ability to maintain supine position, and pain associated with the procedure.¹⁹⁴ Postprocedure complications include heart failure due to increased venous return, HE, contrast-induced nephropathy, hemolytic anemia, and sepsis.^{195,196}

Hepatic Resection. The most common indications for hepatic resection are for the treatment of secondary metastases (i.e., metastatic colon cancer), primary hepatic malignancies, biliary tract malignancies, and benign hepatic masses.¹⁹⁷ Hepatic resection is carried out along the functional segments of the liver. The liver is divided into eight functional segments based on the distribution of blood supply and biliary drainage. The left liver is comprised of segments II, III, and IV, while the right liver is comprised of

segments V, VI, VII, and VIII. Segment I is the caudate lobe (see Fig. 16.1). Right hepatectomy involves resection of segments V–VIII. Left hepatectomy involves resection of segments II–IV. Right lobectomy, also described as an extended right hepatectomy or right trisegmentectomy, involves resection of segments IV–VIII with or without segment I. An extended left hepatectomy (left trisegmentectomy) is the resection of segments II–V and VIII.¹⁹⁸ Mortality and morbidity rates are impacted by the extent of the resection. A review of the 4881 hepatic resections over a 5-year period in the American College of Surgeons – National Surgical Quality Improvement Program database reported 30-day mortality and morbidity rates of 1.9% and 13.1%, respectively, for patients undergoing partial hepatectomy. Those mortality and morbidity rates increased significantly for patients undergoing extended hepatectomies (lobectomies or trisegmentectomies) to 5.8% and 22.5%, respectively.^{199,200} Other factors which have been shown to impact outcomes are the case volume of the performing center, patient age, history of cardiac, pulmonary or renal disease, blood loss, the presence of ascites, and reduced hepatic function.^{199,200}

Laparoscopic hepatic resection is considered most appropriate for small (<5 cm), solitary lesions located in peripheral segments (II–VI), when performed in experienced institutions.^{201,202} More extensive resections have been reported in experienced centers. A metaanalysis of 83 comparative case series (2900 patients) found a significantly lower rate of complications, transfusions, blood loss, and hospital stay in case-matched cohort of patients undergoing laparoscopic liver resection compared to open liver resection.²⁰³ To date, the only randomized, controlled trial comparing laparoscopic to open liver resection found a significant reduction in postoperative complications in patients undergoing laparoscopic hepatic resection (19% vs. 31%; 95% confidence interval [CI], 1.67–21.8; $P = .021$) for colorectal cancer liver metastases requiring resection of fewer than three consecutive segments. Although the hospital length of stay was significantly shorter, there were no differences in blood loss or mortality.²⁰⁴ Conversion from a laparoscopic to an open procedure is usually due to intraoperative hemorrhage and is reported to occur in 6% to 14% of cases. Risk factors for conversion include elevated BMI, increased age, diabetes mellitus, hypertension, and large tumor size.^{205,206} A number of recent observational, retrospective studies have described the performance of robot-assisted hepatectomy for both minor and major resections.²⁰⁷ A metaanalysis of

seven studies published between 2010 and 2014, comparing laparoscopic to robotic hepatectomy, found that the laparoscopic approach is associated with significant reductions in blood loss and operative time without any difference in the conversion rate, postoperative morbidity, and the hospital length of stay.²⁰⁸

The preoperative evaluation of the patient should focus on determining the severity of liver disease and the presence of other comorbidities. Both cirrhosis and steatosis have been associated with increased mortality in patients undergoing liver resection. The decision to proceed is made based on the anticipated future liver remnant (FLR) that will remain following resection.^{209,210} In patients with an anticipated FLR size that is considered unsafe, selective portal vein embolization (PVE) may be conducted in the weeks prior to the hepatic resection. Disruption of portal flow to the diseased portion of the liver leads to atrophy of the portion to be resected and hypertrophy of the FLR, allowing the patient to have adequate liver mass following resection. PVE is typically indicated for patients with an anticipated FLR less than 20% in the absence of cirrhosis, and less than 40% in the presence of cirrhosis.^{120,211} Further preoperative evaluation and risk assessment should take place as outlined above. Laboratory investigations prior to hepatic resection should include a complete blood count, serum electrolytes, liver chemistries, albumin, coagulation studies, and a type and screen.

Strategies for Minimizing Blood Loss

Intraoperative blood loss during liver resection is associated with an increased risk of morbidity and mortality.²¹²⁻²¹⁴ Several preoperative factors have been associated with an increased risk of transfusion. These include preoperative anemia, the need for an extrahepatic procedure, the need for caval exposure, major hepatectomy (>3 segments), tumor size, thrombocytopenia, cirrhosis, and a repeat operation.²¹⁵⁻²¹⁷ For patients at increased risk of significant intraoperative hemorrhage, the use of techniques such as acute normovolemic hemodilution and intraoperative cell salvage have been shown to reduce the transfusion of allogeneic units.²¹⁸⁻²²¹

A number of strategies have been adopted to reduce blood loss in open hepatic resection and case series from high-volume centers routinely report losses less than 500 mL.^{213,222,223} Such strategies include the use of temporary hepatic vascular occlusion and the intraoperative maintenance of low central venous pressure (CVP).^{224,225}

Hepatic vascular occlusion techniques may be used by surgeons to limit blood loss by limiting blood flow to the liver. Although not routinely used in simple resections, familiarity with these techniques is important as they may be employed in more complex resections. The most commonly used vascular occlusion technique is occlusion of the hepatic artery and portal vein by clamping the hepatoduodenal ligament. Otherwise known as the Pringle maneuver, total hepatic inflow occlusion was first described in 1908 as a means of controlling hemorrhage in hepatic trauma (Fig. 16.7A).²²⁶ The drawback of this maneuver is the potential for hepatic ischemia and reperfusion injury.²²⁷ To

mitigate this effect, surgeons typically make use of intermittent clamping with 15- to 20-minute intervals of clamping interspersed with 5- to 10-minute intervals of unclamping for a total ischemic time of less than 120 minutes.²²⁸ Tolerance of longer cumulative ischemic times has been reported.²²⁹ The application of sevoflurane for 30 minutes of preconditioning prior to the Pringle maneuver has been shown in one single-center randomized, controlled trial to significantly reduce postoperative transaminitis and complications in cases with greater than 30 minutes of continuous inflow occlusion.²³⁰ In a subsequent three-armed randomized controlled trial, the same group reported reductions in postoperative transaminitis and complications when sevoflurane was administered after the Pringle maneuver ("post-conditioning") or with the use of intermittent clamping.²³¹

The utility of the Pringle maneuver for reducing blood loss in modern hepatic resection has been called into question. While two early randomized, controlled trials showed a significant reduction in blood loss with intermittent Pringle maneuver compared to no inflow occlusion, three, more recent, randomized controlled trials have reported no benefit.²³²⁻²³⁶ The median blood loss values reported in these three more recent trials were much lower than those reported in the initial two studies. This finding suggests that in the context of current intraoperative approaches to hepatic resection, the routine use of the Pringle maneuver may not be necessary.^{236,237}

An alternative technique that may be utilized is hemi-hepatic inflow occlusion. This maneuver involves exclusively clamping the branches of the portal vein and hepatic artery which supply the hemi-liver which is being resected in order to reduce ischemic injury to the remnant liver (see Fig. 16.7B and C).²³⁸ Hemi-hepatic inflow occlusion hasn't been shown to reduce blood loss when compared to Pringle maneuver.²³⁹⁻²⁴² Total hepatic vascular exclusion (THVE) involves occlusion of the suprahepatic and infrahepatic IVC in addition to the portal vein and hepatic artery (see Fig. 16.7D).²⁴³ THVE can result in significant hypotension due to the reduction in venous return as well as increased morbidity. It has not been shown to offer any benefit compared to the Pringle maneuver and its use is typically reserved for patients with tumor extension into the IVC. In such complex resections, it has been combined with hypothermic portal perfusion and venovenous bypass to mitigate the risks of hypotension and hepatic ischemia; however the reported mortality is high.^{244,245} To avoid the hemodynamic effects of THVE, selective hepatic vascular exclusion (SHVE), which involves clamping the hepatic veins instead of the IVC, may be employed by the surgeon.²⁴⁶ Some studies have shown that SHVE results in fewer complications than THVE; however it is technically demanding and has a limited role in uncomplicated hepatic resections.^{247,248}

LOW CENTRAL VENOUS PRESSURE

While the Pringle maneuver occludes inflow to the liver, retrograde flow through the hepatic veins can still lead to substantial venous hemorrhage. The pressure in the hepatic veins is directly related to vena caval pressure, hence the strategy of maintaining a low CVP (<5 mm Hg) to minimize intraoperative blood loss.²⁴⁹ Retrospective

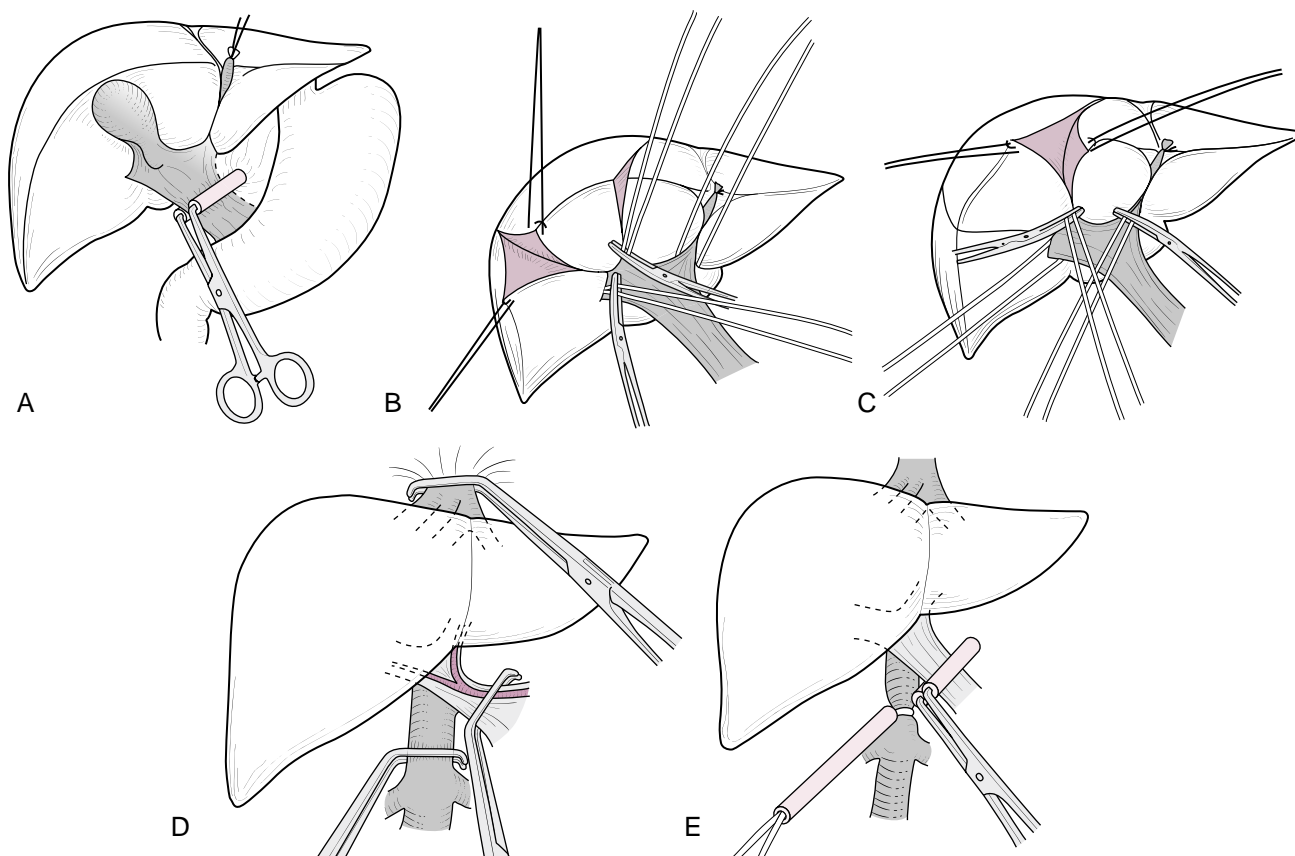


Fig. 16.7 (A–E) Vascular occlusion techniques in hepatic surgery. Surgical vascular occlusive techniques to reduce hemorrhage during hepatic resection include the Pringle maneuver (7A) during which a clamp is placed across the hepatoduodenal ligament to occlude hepatic arterial and portal venous inflow to the liver. Selective hepatic vascular exclusion (7B and C) involves clamping of the vessels perfusing the hemi-liver which is being resected. Total hepatic vascular exclusion (7D) is achieved by clamping the inferior vena cava above and below the liver along with the hepatoduodenal ligament. Another technique combines the application of a clamp across the infrahepatic IVC clamp with one across the hepatoduodenal ligament (7E). IVC, Inferior vena cava. (From Otsubo T. Control of the inflow and outflow system during liver resection. *J Hepatobiliary Pancreat Sci*. 2012;19:15–18.)

observational studies have reported reduced blood loss in patients managed with CVP less than 5 mm Hg without any significant adverse events.^{250–253} Two randomized controlled trials comparing patients with CVP under 5 mm Hg with liberal volume administration have shown reductions in both intraoperative blood loss and the need for transfusion.^{254,255} These studies have all been at risk for significant bias. Furthermore, in some of the trials the difference in estimated blood loss, though statistically significant, was clinically inconsequential.²⁵⁶ Although standard practice in hepatic resections is to maintain low CVP, some studies have found no association between CVP and intraoperative blood loss. In retrospective studies of patients undergoing donor hepatectomies, no correlation was found between the CVP and intraoperative blood loss. This finding may be due to the fact that living liver donors are healthy patients with normal livers.^{257,258} The largest of these studies consisted of over 900 patients. Although it found no correlation between CVP and estimated blood loss, nearly all of the patients were managed with CVPs less than 10 mm Hg, and the majority had CVPs in the 4 to 6 mm Hg range.²⁵⁸

A number of techniques have been described for reducing CVP during hepatic resection. The most commonly reported approach is the use of intraoperative fluid restriction with rates of 1 mL/kg/h. Vasopressors are used as needed to maintain SBP over 90 mm Hg and urine output

more than 25 mL/h. Though seldom required, vasodilation using nitroglycerin or morphine, or forced diuresis with furosemide, can be instituted if fluid restriction is insufficient.^{250,251,254,255,259} The use of milrinone, reverse Trendelenburg position, and epidural anesthesia have also been described, though there is insufficient data to recommend one particular approach.^{256,260–262}

Clamping of the infrahepatic IVC (IIVC) has been described as a means of minimizing hemorrhage in the setting of an elevated CVP despite the interventions described earlier (see Fig. 16.7E).²⁶³ A number of randomized controlled trials have demonstrated a significant reduction in blood loss and transfusion with the use of IIVC clamping in patients who tolerate the clamp or have a CVP greater than 5 mm Hg.^{262,264–268} A metaanalysis of these trials, comprising of 714 patients, showed a significant reduction in intraoperative blood loss (mean difference –353 mL) with no difference in the rates of postoperative complications. Of note, in pooled analysis, there was no significant difference in reported CVP values between the two groups.²⁶⁹

OTHER APPROACHES TO REDUCE BLOOD LOSS

Two multicenter, randomized, placebo-controlled trials have examined the efficacy of prophylactic recombinant Factor VIIa (rFVIIa) administration to reduce transfusion

patients undergoing hepatic resection. The studies found no benefit of prophylactic rFVIIa with respect to mortality, red blood cell transfusions, or adverse events.^{270,271} A single randomized, controlled trial in 214 patients undergoing primarily minor hepatic resections (82% of cases) found that the administration of tranexamic acid (TXA) resulted in fewer transfusions and less blood loss compared to placebo. In the study group, 500 mg of TXA was administered intravenously prior to incision followed by 250 mg every 6 hours for 3 days.²⁷²

A recent Cochrane database analysis of 67 randomized clinical trials of methods to decrease blood loss during liver resection found a high risk of bias in all trials. Based on the outcomes that were available in more than one trial, there is low-quality evidence that the “clamp and crush” parenchymal resection technique may be associated with fewer adverse events than radiofrequency resection techniques. They reported very low quality evidence that blood loss, operating time, and total hospital stay were reduced with intraoperative low CVP management.²⁷³

ANESTHETIC MANAGEMENT

The anesthetic management of these cases should be tailored to the comorbidities of the patients, the surgical approach (open, laparoscopic), the anticipated extent of resection, and the need for vascular occlusive maneuvers. Adequate venous access should be obtained for the anticipated degree of hemorrhage. In cases where significant blood loss is anticipated, red blood cell salvage can be used and consideration should be given to the use of acute normovolemic hemodilution. In addition to standard ASA monitors, intra-arterial blood pressure monitoring should be used in cases during which significant hemorrhage or the need for vascular occlusion maneuvers is anticipated. Central venous catheters may be inserted for both vascular access and CVP monitoring, although some high-volume centers forgo the routine use of CVP monitoring.^{274,275} Peripheral venous pressure monitoring may be considered as an alternative. Values are obtained through transduction of an antecubital vein and have been shown to correlate with the CVP in patients undergoing hepatic resection.^{276,277} Stroke volume variation (SVV) has been investigated as an alternative to CVP for volume management in patients undergoing liver resection. A study of patients undergoing donor hepatectomy showed an SVV value $\leq 6\%$ to be predictive of blood loss over 700 mL.²⁷⁸ In two studies, targeting SVV values greater than 12% to 15% in patients undergoing open or laparoscopic hepatic resection yielded blood loss comparable to, or better than, maintaining low CVP.^{279,280} In a study using milrinone to reduce CVP, SVV of 9% yielded a favorable surgical field. No correlation with CVP was noted in this study, possibly due to the lusitropic effects of milrinone.²⁸¹ The use of transesophageal echocardiography may be considered in patients with cardiac risk factors, although care must be taken in the presence of significant esophageal varices.

Hepatic resection may be associated with hemorrhage and, in extensive cases, the development of coagulopathy. There is insufficient data to recommend the routine use of viscoelastic hemostatic assays (rotational thromboelastography (TEG) or rotational thromboelastometry).

A single randomized, controlled trial of TEG-guided transfusion in cirrhotic patients with coagulopathy (INR > 1.8 and/or platelet count $< 50 \times 10^9/\text{L}$) undergoing invasive procedures found a significant reduction in blood product administration with TEG compared to the standard lab value-based group. However, only half of the patients enrolled in the trial were undergoing procedures associated with greater than 3% risk of hemorrhage.²⁸²

With respect to pain management, thoracic epidural analgesia is a highly effective means of pain control for hepatic resection.^{283,284} Although its use for this purpose has been described in a number of case series, it remains controversial due to the development of postoperative coagulopathy and thrombocytopenia following hepatic resection and the associated risk of epidural hematoma.^{276,285-288} Postoperative coagulopathy and thrombocytopenia occur in 21% to 100% of patients undergoing liver resection, depending on the volume of tissue resected. The INR peaks around postoperative day (POD) one or two while the platelet count is lowest on POD three or four. The values typically return to baseline by POD four or five; however in some patients they may remain elevated for up to a week, leading to delays in epidural catheter removal or the decision to transfuse FFP to facilitate catheter removal.^{276,285-289} An additional concern is the accidental dislodgment of the epidural catheter while the patient is coagulopathic which has been reported to occur in up to 7% of patients.^{276,286} The degree of coagulopathy is influenced by the extent of the resection. In a review of 759 patients undergoing hepatic resection, the incidence of coagulopathy was 39.1% in patients who had undergone major hepatectomies (> 2 segments) versus 21.3% in patients who had undergone minor hepatectomies (≤ 2 segments).²⁸⁹ Other factors that are independently associated with postoperative coagulopathy included preexisting cirrhosis, preoperative INR ≥ 1.3 , preoperative platelet count $< 150,000/\mu\text{L}$, estimated blood loss $\geq 1000 \text{ mL}$, and the duration of surgery.^{285,287,289} Although no case series has reported the complication of an epidural hematoma, epidural hematoma is quite rare and the numbers of published cases may have been inadequate to detect its occurrence.^{290,291}

Rapid sequence induction should be considered in patients with significant ascites. Maintenance of general anesthesia has been described with both volatile anesthetics and intravenous anesthetics. There is no compelling clinical evidence for the benefit of one specific agent over another.²⁹²⁻²⁹⁴ Regardless of the approach, anesthetic dosing should be titrated to the patient's requirements, taking into account the pharmacokinetics and pharmacodynamics of common anesthetic agents in patients with liver disease. The anesthesiologist should understand the vascular occlusion strategies that may be employed during the operation along with their hemodynamic effects. The Pringle maneuver, both during open and laparoscopic hepatic resections, leads to an increase in MAP and systemic vascular resistance and a decrease in CO.^{295,296} During open hepatic resection, portal triad clamping leads to a decrease in left ventricular (LV) end-diastolic area (i.e., LV preload). During laparoscopic hepatic resection, in the presence of pneumoperitoneum, PTC also increases LV end-systolic wall stress (i.e., LV afterload).²⁹⁷

ENHANCED RECOVERY AFTER SURGERY AND LIVER RESECTION

A number of randomized controlled trials have been conducted comparing the use of enhanced recovery after surgery (ERAS) protocols with traditional management in patients undergoing both open and laparoscopic liver resections.^{250,298-301} Although ERAS Society consensus guidelines exist, these trials differed with respect to the number and nature of ERAS elements.³⁰² Most incorporated preoperative education, early enteral nutrition, and early mobilization. The implementation of an ERAS protocol for liver resection surgery has been shown to reduce minor adverse events, hospital length of stay, hospital cost, and to improve patient quality of life. A metaanalysis published by the Cochrane group found that the use of ERAS protocols resulted in a reduction in mild adverse events, hospital length of stay, and cost. However, all studies were at high risk of bias and the quality of available evidence was determined to be low.³⁰³

Acknowledgment

The editors and publisher would like to thank Drs. Phillip S. Mushlin and Simon Gelman for contributing a chapter on this topic in the prior edition of this work. It has served as the foundation for the current chapter.

 Complete references available online at expertconsult.com.

References

1. Molina DK, et al. *Am J Forensic Med Pathol*. 2015;36(3):182.
2. Molina DK, DiMaio VJM. *Am J Forensic Med Pathol*. 2012;33(4):368.
3. Pryce JW, et al. *BMC Clin Pathol*. 2014;14(18).
4. Abdel-Misih SRZ, Bloomston M. *Surg Clin North Am*. 2010;90(4):643.
5. van Gulik TM, van den Esschert JW. *HPB (Oxford)*. England; 2010;12:81.
6. Juza RM, Pauli EM. *Clin Anat*. 2014;27(5):764.
7. Strasberg SM. *J Hepatobiliary Pancreat*. 2005;12(5):351.
8. Strasberg SM, Phillips C. *Ann Surg*. 2013;257(3):377.
9. Bismuth H. Revisiting liver anatomy and terminology of hepatectomies. *Ann Surg*. 2013;257(3):383.
10. Poisson J, et al. *J Hepatol*. 2017;66(1):212.
11. Blouin A, et al. *J Cell Biol*. 1977;72(2):441.
12. Treyer A, Müsch A. *Physiol*. 2013;3(1):243.
13. T K. Metabolic Zonation of the Liver: The Oxygen Gradient Revisited; 2018. PubMed - NCBI. <https://phstwlp2.partners.org:2052/pu/bmed/28126520>.
14. Geerts A. *Semin Liver Dis*. 2001;21(3):311.
15. Tsuchida SL, Friedman T. Mechanisms of Hepatic Stellate Cell Activation; 2018. PubMed - NCBI. <https://phstwlp2.partners.org:2052/pu/bmed/28487545>.
16. Li P, et al. *Mol Immunol*. 2017;85:222.
17. Robinson MW, et al. *Cell Mol Immunol*. 2016;13(3):267.
18. Lau AH, Thomson AW. *Gut*. 2003;52(2):307.
19. Njoku DB. *Int J Mol Sci*. 2014;15(4):6990.
20. Almazroo OA, et al. *Clin Liver Dis*. 2017;21(1):1.
21. Trefts E, et al. *Curr Biol*. 2017;27(21):r1151.
22. Adeva-Andany MM, et al. *Biosci Rep*. 2016;36(6).
23. Nguyen P, et al. *J Anim Physiol Anim Nutr (Berl)*. 2008;92(3):272.
24. Boyer JL. *Compr Physiol*. 2013;3(3):1035.
25. Roberts MS, et al. *Clin Pharmacokinet*. 2002;41(10):751.
26. Malik MY, et al. *Drug Metab Rev*. 2016;48(2):281.
27. Borowski M, et al. *J Biol Chem*. 1986;261(4):1624.
28. Dimova EY, Kietzmann T. *Thromb Haemost*. 2008;100(6):992.
29. Ceserman-Maus G, Hajjar KA. *Br J Haematol*. 2005;129(3):307.
30. Stein PE, et al. Update Review of the Acute Porphyrias; 2018. PubMed - NCBI. <https://phstwlp2.partners.org:2052/pubmed/?term=27982422>.
31. Sticova E, Jirska M. *World J Gastroenterol*. 2013;19(38):6398-6407.
32. Ganz T, Nemeth E. *Biochim Biophys Acta*. 2012;1823(9):1434.
33. Yakar S, et al. *J Clin Invest*. 2002;110(6):771.
34. Lu H, et al. *Hypertens Res*. 2016;39(7):492.
35. Jelkmann W. *Eur J Gastroenterol Hepatol*. 2001;13(7):791.
36. Habib S, et al. Approach to jaundice and abnormal liver function test results. In: Sanyal AJ, et al., ed. *Zakim and Boyer's Hepatol: A Textbook of Liver Disease*. 7th ed. Philadelphia, PA: Elsevier; 2018:99-116.
37. Pratt DS. Liver chemistry and function tests. In: Feldman M, et al. ed. *Sleisenger and Fordtran's Gastrointestinal and Liver Disease: Pathophysiology, Diagnosis, Management*. 10th ed. Philadelphia: Saunders; 2016:1243-1253.
38. Kwo PY, et al. *Am J Gastroenterol*. 2017;112(1):18.
39. Eminler AT, Ayyildiz T, Irak K, et al. AST/ALT ratio is not useful in predicting the degree of fibrosis in chronic viral hepatitis patients. *Eur J Gastroenterol Hepatol*. 2015;27(12):1361.
40. Maina I, et al. *Jrnl App Lab Med*. 2016;1(2):119.
41. Redick JA, et al. *J Biol Chem*. 1982;257(24):15200.
42. Siddique A, Kowdley KV. *Clin Liver Dis*. 2012;16(2):199.
43. Fargo MV, et al. *Am Fam Physician*. 2017;95(3):164.
44. Liang TJ. Hepatitis B. The virus and disease. *Hepatology*. 2009; 49(suppl 5):13.
45. AASLD/IDSA HCV Guidance Panel. *Hepatology*. 2015;62(3):932.
46. Fourati S, et al. *J Int AIDS Soc*. 2018;21(suppl 2):e25058.
47. Freiman JM, et al. *Ann Intern Med*. 2016;165(5):345.
48. Ajisaka H, et al. *J Surg Oncol*. 2003;84(2):89.
49. Fujioka M, et al. *Hepatology*. 2001;34(6):1128.
50. Sugimoto H, et al. *Liver Int*. 2003;23(1):38.
51. Wong RJ, et al. *Clin Liver Dis*. 2015;19(2):309.
52. Song P, et al. *World J Gastroenterol*. 2016;22(1):262.
53. Yuen M, Lai C. Best Pract Res Clin Gastroenterol. 2005;19(1):91.
54. Tapper EB, Lok AS. *N Engl J Med*. 2017;377(23):2296.
55. Bolondi G, et al. *World J Gastroenterol*. 2016;22(26):5936.
56. Guerrini GP, et al. *Prog Transplant*. 2018;28(1):63.
57. Lin C, et al. *Intern Med*. 2008;47(7):569.
58. Younossi ZM, et al. *Hepatology*. 2018;68(1):349.
59. Sakka SG. *Curr Opin Crit Care*. 2007;13(2):207.
60. Denaro CP, et al. *Ther Drug Monit*. 1998;20(1):78.
61. Jover R, et al. *Am J Gastroenterol*. 1997;92(10):1905.
62. Wahlländer A, et al. *J Hepatol*. 1990;10(2):129.
63. Everson GT, et al. *Hepatology*. 2012;55(4):1019.
64. Chow PKH, et al. *J Surg Res*. 2003;112(1):1.
65. Helmke S, et al. *Curr Opin Gastroenterol*. 2015;31(3):199.
66. Kang HK, et al. *Radiographics*. 2002;22(5):1053.
67. Sharma S, et al. *World J Gastroenterol*. 2014;20(45).
68. Iranpour P, et al. *Ultrasound*. 2016;35(1):3.
69. Barr RG, et al. *Radiology*. 2015;276(3):845.
70. Younossi ZM, et al. *Hepatology*. 2018;68(1):349.
71. Tang A, et al. *Radiology*. 2018;286(1):29.
72. Bialecki ES, Di Bisceglie AM. *HPB (Oxford)*. 2005;7(1):26.
73. Pollock G, Minuk GY. *J Gastroenterol Hepatol*. 2017;32(7):1303.
74. Popper H, Schaffner F. Pathophysiology of cholestasis. *Hum Pathol*. 1970;1(1):1.
75. EASL. *J Hepatol*. 2009;51(2):237.
76. Lleo A, et al. *Hepatol Int*. 2017;11(6):485.
77. Boonstra K, et al. *J Hepatol*. 2012;56(5):1181.
78. Trivedi HD, et al. *Frontline Gastroenterol*. 2017;8(1):29.
79. Poupon RE, et al. *N Engl J Med*. 1991;324(22):1548.
80. Corpechot C, et al. *Hepatology*. 2008;48(3):871.
81. Hirschfield GM, et al. *Gastroenterol*. 2015;148(4):61.e8.
82. Lens S, et al. *Liver Int*. 2014;34(2):197.
83. Rautiainen H, et al. *Hepatology*. 2005;41(4):747.
84. Karlsen TH, et al. *J Hepatol*. 2017;67(6):1298.
85. Scaglione S, et al. *J Clin Gastroenterol*. 2015;49(8):690.
86. Tsouchatzis EA, et al. *Lancet*. 2014;383(9930):1749.
87. Garcia-Pagan JC, et al. *J Hepatol*. 2012;57(2):458.
88. Runyon BA. *Hepatology*. 2013;57(4):1651.
89. De Robertis R, et al. *World J Gastroenterol*. 2014;20(23):7231.
90. Garcia-Tsao G, et al. *Hepatology*. 2017;65(1):310.
91. D'Amico G, et al. *J Hepatol*. 2018;68(3):563.
92. Ripoll C, et al. *Gastroenterology*. 2007;133(2):481.
93. Ripoll C, et al. *J Hepatology*. 2009;50(5):923.
94. Abraldes JG, et al. *Clin Liver Dis*. 2014;18(4):779.

95. Shi KQ, et al. *Liver Int*. 2013;33(1):62.
96. Vilgrain V, et al. *Gastrointest Radiol*. 1990;15(3):218.
97. Zipprich A, et al. *Liver Int*. 2012;32(9):1407.
98. Gluud LL, Krag A, et al. *Cochrane Database Syst Rev*. 2012;8:CD004544.
99. Shah HA, et al. *J Hepatol*. 2014;60(4):757.
100. D'Amico G, et al. *Gastroenterology*. 2006;131(5):1611.
101. Carvalho GC, et al. *Ann Hepatol*. 2012;11(1):90.
102. Martin-Llahi M, et al. *Gastroenterology*. 2011;140(2):496.e4.
103. Angeli P, et al. *J Hepatol*. 2015;62(4):968.
104. de Mattos AZ, et al. *Ann Hepatol*. 2016;15(4):474.
105. Boyer TD, et al. *Liver Transpl*. 2011;17(11):1328.
106. Nolte W, et al. *Hepatology*. 1998;28(5):1215.
107. Montagnese S, et al. *Metab Brain Dis*. 2004;19(3–4):281.
108. Vilstrup H, et al. *Hepatology*. 2014;60(2):715.
109. Swanson KL, et al. *Hepatology*. 2005;41(5):1122.
110. Krowka MJ, et al. *Transplantation*. 2016;100(7):1440.
111. Iyer VN, et al. *Hepatology*. 2013;57(6):2427.
112. Schiffer E, et al. *Am J Transplant*. 2006;6(6):1430.
113. Simonneau G, et al. *J Am Coll Cardiol*. 2013;62(suppl 25):34.
114. Krowka MJ, et al. Portopulmonary hypertension: Results from a 10-year screening algorithm. *Hepatology*. 2006;44(6):1502.
115. Swanson KL, et al. *Am J Transplant*. 2008;8(11):2445.
116. Malagari K, et al. *Hepatogastroenterology*. 2005;52(62):558.
117. Machicao VI, et al. *Hepatology*. 2014;59(4):1627.
118. GBD 2016 Risk Factors Collaborators. *Lancet*. 2017;390(10100):1151.
119. Forner A, et al. *Lancet*. 2018;391(10127):1301.
120. Heimbach JK, et al. *Hepatology*. 2018;67(1):358.
121. Poon RT, et al. *Ann Surg*. 2002;235(3):373.
122. Mazzaferro V, et al. *N Engl J Med*. 1996;334(11):693.
123. Lautt WW. *Am J Physiol*. 1985;249(5 Pt 1):549.
124. Gelman S, et al. *Anesthesiology*. 1984;61(6):726.
125. Frink EJ Jr, et al. *Anesthesiology*. 1992;76(1):85.
126. Hartman JC, et al. *Can J Anaesth*. 1992;39(8):877.
127. Cullen SC, Gross EG. *Science*. 1951;113(2942):580.
128. Goto T, et al. *Br J Anaesth*. 1998;80(2):255.
129. Wappler F, et al. *Anesthesiology*. 2007;106(3):463.
130. Schmidt M, et al. *Anaesthesia*. 2001;56(12):1154.
131. Iber T, et al. *Minerva Anestesiol*. 2008;74(10):511.
132. Reinelt H, et al. *Acta Anaesthesiol Scand*. 2002;46(6):713.
133. Wilke HJ, et al. *Transplant Proc*. 2011;43(7):2683.
134. Servin F, et al. *Br J Anaesth*. 1990;65(2):177.
135. Pandele G, et al. *Anesthesiology*. 1983;59(2):123.
136. van Beem H, et al. *Anaesthesia*. 1983;38(Suppl):61.
137. Duvaldestin P, et al. *Acta Anaesthesiol Scand*. 1991;35(2):159.
138. Carmichael FJ, et al. *Anesthesiology*. 1993;79(5):1051.
139. Wouters PF, et al. *Anesth Analg*. 1995;81(1):125.
140. Zhu T, et al. *Can J Anaesth*. 2008;55(6):364.
141. Meierhenrich R, et al. *Anaesthesia*. 2010;65(11):1085.
142. Leslie K, et al. *Anesth Analg*. 1995;80(5):1007.
143. Runciman WB, et al. *Br J Anaesth*. 1990;65(3):353.
144. Sear JW, et al. *Br J Anaesth*. 1994;72(4):451.
145. MacGilchrist AJ, et al. *Gut*. 1986;27(2):190.
146. Weerink MAS, et al. *Clin Pharmacokinet*. 2017;56(8):893.
147. Mazoit JX, et al. *Anesth Analg*. 1987;66(4):293.
148. Klotz U, et al. *Clin Pharmacol Ther*. 1974;16(4):667.
149. Ferrier C, et al. *Anesthesiology*. 1985;62(4):480.
150. Haberer JP, et al. *Br J Anaesth*. 1982;54(12):1267.
151. Chauvin M, et al. *Anesth Analg*. 1989;68(1):1.
152. Dershawitz M, et al. *Anesthesiology*. 1996;84(4):812.
153. Devlin JC, et al. *Br J Anaesth*. 1993;71(2):227.
154. Viby-Mogensen J, Hanel HK. *Acta Anaesthesiol Scand*. 1978;22(4):371.
155. De Wolf AM, et al. *Br J Anaesth*. 1996;76(5):624.
156. Lebrault C, et al. *Anesthesiology*. 1985;62(5):601.
157. Khalil M, et al. *Anesthesiology*. 1994;80(6):1241.
158. Duvaldestin P, et al. *Br J Anaesth*. 1978;50(11):1131.
159. Fujita A, et al. *Acta Anaesthesiol Taiwan*. 2014;52(2):54.
160. Tanaka N, et al. *Anesth Analg*. 1997;85(2):286.
161. Meierhenrich R, et al. *Anesth Analg*. 2009;108(4):1331.
162. Trepennaitis D, et al. *Medicina (Kaunas)*. 2010;46(7):465.
163. Kortgen, et al. *Eur J Anaesthesiol*. 2009;26(2):111.
164. Friedman LS. *Trans Am Clin Climatol Assoc*. 2010;121:204. discussion 205.
165. de Goede B, et al. *Best Pract Res Clin Gastroenterol*. 2012;26(1):47.
166. Csikesz NG, et al. *J Am Coll Surg*. 2009;208(1):96.
167. Lin CS, et al. *Br J Surg*. 2013;100(13):1784.
168. Farnsworth N, et al. *Am J Surg*. 2004;188(5):580.
169. Neff HP, et al. *Surgery*. 2014;155(4):623.
170. Telem DA, et al. *Clin Gastroenterol Hepatol*. 2010;8(5):7. quz e58.
171. Hoteit MA, et al. *World J Gastroenterol*. 2008;14(11):1774.
172. Pantel HJ, et al. *J Gastrointest Surg*. 2016;20(8):1511.
173. Pugh RN, et al. *Br J Surg*. 1973;60(8):646.
174. Garrison RN, et al. *Ann Surg*. 1984;199(6):648.
175. Mansouri A, et al. *Surgery*. 1997;122(4):6.
176. Kiamanesh D, et al. *Br J Anaesth*. 2013;111(suppl 1):50.
177. Malinchoc M, et al. *Hepatology*. 2000;31(4):864.
178. Kamath PS, et al. *Hepatology*. 2001;33(2):464.
179. Suman A, et al. *Clin Gastroenterol Hepatol*. 2004;2(8):719.
180. Befeler AS, et al. *Arch Surg*. 2005;140(7):4. discussion 655.
181. Northup PG, et al. *Ann Surg*. 2005;242(2):244.
182. Teh SH, et al. *Gastroenterol*. 2007;132(4):1261.
183. Biggins SW, et al. *Gastroenterology*. 2006;130(6):1652.
184. Luca A, et al. *Liver Transpl*. 2007;13(8):1174.
185. Cho HC, et al. *Eur J Gastroenterol Hepatol*. 2011;23(1):51.
186. Kim DH, et al. *ANZ J Surg*. 2014;84(11):832.
187. Bhangui P, et al. *J Hepatol*. 2012;57(4):874.
188. Kim TH, et al. *Liver Int*. 2015;35(3):713.
189. Boyer TD, Haskal ZJ. *Hepatology*. 2010;51(1):306.
190. Parker R. *Clin Liver Dis*. 2014;18(2):319.
191. Monescillo A, et al. *Hepatology*. 2004;40(4):793.
192. Suhocki PV, et al. *Semin Intervent Radiol*. 2015;32(2):123.
193. Chana A, et al. *BJA Education*. 2016;16(12):405.
194. DeGasperi A, et al. *J Clin Monit Comput*. 2009;23(6):341.
195. Modha K, et al. *Cardiovasc Intervent Radiol*. 2018;41(4):564.
196. Suhocki PV, et al. *Semin Intervent Radiol*. 2015;32(2):123.
197. Dimick JB, et al. *Arch Surg*. 2003;138(2):185.
198. Aragon RJ, Solomon NL. *J Gastrointest Oncol*. 2012;3(1):28.
199. Kneuerz PJ, et al. *J Gastrointest Surg*. 2012;16(9):1727.
200. Chang CM, et al. *Medicine (Baltimore)*. 2014;93(12):e59.
201. Wakabayashi G, et al. *Ann Surg*. 2015;261(4):619.
202. Abu Hilal M, et al. *Ann Surg*. 2018;268(1):11.
203. Ciria R, et al. *Ann Surg*. 2016;263(4):761.
204. Fretland AA, et al. *Ann Surg*. 2018;267(2):199.
205. Cauchy F, et al. *Br J Surg*. 2015;102(7):785.
206. Goh BK, et al. *Surg Endosc*. 2015;29(9):2636.
207. Nota CL, et al. *HPB (Oxford)*. 2016;18(2):113.
208. Montalti R, et al. *World J Gastroenterol*. 2015;21(27):8441.
209. Capussotti L, et al. *Eur J Surg Oncol*. 2005;31(9):986.
210. Reddy SK, et al. *Hepatology*. 2012;56(6):2221.
211. van Lienden KP, et al. *Cardiovasc Intervent Radiology*. 2013;36(1):25.
212. Kamiyama T, et al. *J Am Coll Surg*. 2010;211(4):443.
213. Aramaki O, et al. *J Hepatobiliary Pancreat Sci*. 2014;21(8):585.
214. Katz SC, et al. *Am Surg*. 2009;249(4):617.
215. McNally SJ, et al. *HPB (Oxford)*. 2012;14(4):236.
216. Nanashima A, et al. *Surg Today*. 2013;43(5):485.
217. Janny S, et al. *HPB (Oxford)*. 2015;17(4):357.
218. Fujimoto J, et al. *Arch Surg*. 1993;128(9):1065.
219. Matot I, et al. *Anesth Analg*. 2002;97(4):794.
220. Jarnagin WR, et al. *Ann Surg*. 2008;248(3):360.
221. Frankel TL, et al. *J Am Coll Surg*. 2013;217(2):210–220.
222. Imamura H, et al. *Arch Surg*. 2003;138(11):1206. discussion 1206.
223. Grazi GL, et al. *Ann Surg*. 2001;234(1):71.
224. Huntington JT, et al. *J Surg Oncol*. 2014;109(2):81.
225. Jiang B, et al. *Hepatol Res*. 2018;48(8):635.
226. Pringle JHV. *Ann Surg*. 1908;48(4):541.
227. Kim YI. *J Hepatobiliary Pancreat*. 2003;10(3):195.
228. Hoekstra LT, et al. *Dig Surg*. 2012;29(1):35.
229. Torzilli G, et al. *Ann Surg*. 2012;255(2):270.
230. Beck-Schimmer B, et al. *Ann Surg*. 2008;248(6):909.
231. Beck-Schimmer B, Breitenstein S, Bonvini JM, et al. *Ann Surg*. 2012;256(5):5.
232. Man K, et al. *Ann Surg*. 1997;226(6):3.
233. Man K, et al. *Br J Surg*. 2003;90(2):183.
234. Capussotti L, et al. *Br J Surg*. 2006;93(6):685.
235. Lee KF, et al. *Br J Surg*. 2012;99(9):1203.
236. Lee KF, et al. *World J Surg*. 2018.
237. Hanyong S, et al. *Eur J Surg Oncol*. 2015;41(2):243.
238. Makuuchi M, et al. *Surg Gynecol Obstet*. 1987;164(2):155.
239. Figueiras J, et al. *Ann Surg*. 2005;241(4):582.

240. Liang G, et al. *HepatoGastroenterology*. 2009;56(91–92):745.
241. Fu SY, et al. *Am J Surg*. 2011;201(1):62.
242. Ni JS, et al. *J Gastrointest Surg*. 2013;17(8):1414.
243. Huguet C, et al. *Surg Gynecol Obstet*. 1978;147(5):689.
244. Belghiti J, et al. *Ann Surg*. 1995;224(2):155.
245. Azoulay D, et al. *Ann Surg*. 2015;262(1):93.
246. Elias D, et al. *Br J Surg*. 1995;82(11):1535.
247. Smyrniotis VE, et al. *Am J Surg*. 2002;183(2):173.
248. Smyrniotis VE, et al. *World J Surg*. 2003;27(7):765.
249. Melendez JA, et al. *J Am Coll Surg*. 1998;187(6):620.
250. Jones RM, et al. *Br J Surg*. 1998;85(8):1058.
251. Smyrniotis V, et al. *Am J Surg*. 2004;187(3):398.
252. Bui LL, et al. *HPB (Oxford)*. 2002;4(1):5.
253. Chen H, et al. *J Gastrointest Surg*. 2000;4(2):162.
254. Wang WD, et al. *World J Gastroenterol*. 2006;12(6):935.
255. Liu Y, et al. *Chin–Germ J Clin Oncol*. 2008;7:7.
256. Hughes MJ, et al. *HPB (Oxford)*. 2015;17(10):863.
257. Chhibber A, et al. *Liver Transpl*. 2007;13(4):537.
258. Kim YK, et al. *Acta Anaesthesiol Scand*. 2009;53(5):601.
259. Melendez JA, et al. *J Am Coll Surg*. 1998;187(6):620.
260. Ryu HG, et al. *Am J Transplant*. 2010;10(4):877.
261. Sand L, et al. *Acta Anaesthesiol Scand*. 2011;55(9):1106.
262. Rahbari NN, et al. *Ann Surg*. 2011;253(6):1102.
263. Otsubo T, et al. *Surgery*. 2004;135(1):67.
264. Chen XP, et al. *Langenbecks Arch Surg*. 2006;391(3):209.
265. Kato M, et al. *World J Surg*. 2008;32(6):1082.
266. Zhu P, et al. *Br J Surg*. 2012;99(6):781.
267. Zhou YM, et al. *Medicine (Baltimore)*. 2016;95(27):e4159.
268. Ueno M, et al. *Surgery*. 2017;161(6):1502.
269. Fancellu A, et al. *J Gastrointest Surg*. 2018;22(5):941.
270. Lodge JP, Jonas S, Oussoultzoglou E, et al. *Anesthesiology*. 2005;102(2):269.
271. Shao YF, et al. *Am J Surg*. 2006;191(2):245.
272. Wu CC, et al. *Ann Surg*. 2006;243(2):173.
273. Moggia E, et al. *Cochrane Database Syst Rev*. 2016;10:CD010683.
274. Wax DB, et al. *Eur J Surg Oncol*. 2016;42(10):1608.
275. Niemann CU, et al. *Liver Transpl*. 2007;13(2):266.
276. Choi SJ, et al. *Liver Transpl*. 2007;13(10):1414.
277. Stephan F, et al. *Acta Anaesthesiol Scand*. 2008;52(3):388.
278. Kim YK, et al. *Transplant Proc*. 2011;43(5):1407.
279. Ratti F, et al. *HPB (Oxford)*. 2016;18(2):136.
280. Dunki-Jacobs EM, et al. *Ann Surg Oncol*. 2014;21(2):473.
281. Lee J, et al. *Anesth Analg*. 2017;125(2):423.
282. De Pietri L, et al. *Hepatol*. 2016;63(2):566.
283. Schreiber KL, et al. *Reg Anesth Pain Med*. 2016;41(4):460.
284. Ali M, et al. *Br J Anaesth*. 2010;104(3):292.
285. Matot I, et al. *Anesth Analg*. 2002;95(5):81.
286. Tsui SL, et al. *Anaesth Intensive Care*. 2004;32(5):630.
287. Yuan FS, et al. *J Clin Anesth*. 2012;24(5):398.
288. Elterman KG, Xiong Z. *J Anesth*. 2015;29(3):367.
289. Jacquenod P, et al. *Anesth Analg*. 2018;126(4):1142.
290. Christie IW, McCabe S. *Anesthesia*. 2007;62(4):335.
291. Cook TM, et al. *Br J Anaesth*. 2009;102(2):179.
292. Ko JS, et al. *Transpl Int*. 2010;23(7):736.
293. Toprak HI, et al. *Transplant Proc*. 2012;44(6):1635.
294. Ko JS, et al. *Liver Transpl*. 2008;14(8):1150.
295. Decailliot F, et al. *Br J Anaesth*. 2001;87(3):493.
296. Delva E, et al. *Anesth Analg*. 1987;66(9):864.
297. Decailliot F, et al. *Anesth Analg*. 2005;100(3):864.
298. Ni CY, et al. *Eur J Surg Oncol*. 2013;39(6):542.
299. Qi S, et al. *J Clin Lab Anal*. 2018;e22434.
300. He F, et al. *Clin Transl Oncol*. 2015;17(9):694.
301. Liang X, et al. *Surg Endosc*. 2018;32(6):2746.
302. Melloul E, et al. *World J Surg*. 2016;40(10):2425.
303. Bond-Smith G, et al. *Cochrane Database Syst Rev*. 2016;2:CD011382.

References

1. Molina DK, DiMaio VJM. Normal organ weights in women: part II—the brain, lungs, liver, spleen, and kidneys. *Am J Forensic Med Pathol*. 2015;36(3):182–187.
2. Molina DK, DiMaio VJM. Normal organ weights in men: Part II—the brain, lungs, liver, spleen, and kidneys. *Am J Forensic Med Pathol*. 2012;33(4):368–372.
3. Pryce JW, Bamber AR, Ashworth MT, Kiho L, Malone M, Sebire NJ. Reference ranges for organ weights of infants at autopsy: results of >1,000 consecutive cases from a single centre. *BMC Clin Pathol*. 2014;14:18.
4. Abdel-Misih SRZ, Bloomston M. Liver anatomy. *Surg Clin North Am*. 2010;90(4):643–653.
5. van Gulik TM, van den Esschert JW. James Cantlie's Early Messages for Hepatic Surgeons: How the Concept of Pre-Operative Portal Vein Occlusion was Defined. *HPB (Oxford)*. 12(2):81–83. 2010. <https://doi.org/10.1111/j.1477-2574.2009.00124.x>.
6. Juza RM, Pauli EM. Clinical and surgical anatomy of the liver: a review for clinicians. *Clin Anat*. 2014;27(5):764–769. <https://doi.org/10.1002/ca.22350>.
7. Strasberg SM. Nomenclature of hepatic anatomy and resections: a review of the brisbane 2000 system. *J Hepatobiliary Pancreat*. 2005;12(5):351–355. <https://doi.org/10.1007/s00534-005-0999-7>.
8. Strasberg SM, Phillips C. Use and dissemination of the brisbane 2000 nomenclature of liver anatomy and resections. *Ann Surg*. 2013;257(3):377–382. <https://doi.org/10.1097/SLA.0b013e31825a01f6>.
9. Bismuth H. Revisiting liver anatomy and terminology of hepatectomies. *Ann Surg*. 2013;257(3):383–386. <https://doi.org/10.1097/SLA.0b013e31827f17f1>.
10. Poisson J, Lemoine S, Boulanger C, et al. Liver sinusoidal endothelial cells: physiology and role in liver diseases. *J Hepatol*. 2017;66(1):212–227.
11. Blouin A, Bolender RP, Weibel ER. Distribution of organelles and membranes between hepatocytes and nonhepatocytes in the rat liver parenchyma. A stereological study. *J Cell Biol*. 1977;72(2):441–455.
12. Treyer A, Müsch A. Hepatocyte polarity. *Compr Physiol*. 2013;3(1):243–287.
13. T K. Metabolic zonation of the liver: the oxygen gradient revisited – PubMed – NCBI; 2018. <https://phstwlp2.partners.org:2052/pubmed/28126520>.
14. Geerts A. History, heterogeneity, developmental biology, and functions of quiescent hepatic stellate cells. *Semin Liver Dis*. 2001;21(3):311–335.
15. Tsuchida T, Friedman SL. Mechanisms of hepatic stellate cell activation – PubMed – NCBI; 2018. <https://phstwlp2.partners.org:2052/pubmed/28487545>.
16. Li P, He K, Li J, Liu Z, Gong J. The role of kupffer cells in hepatic diseases. *Mol Immunol*. 2017;85:222–229.
17. Robinson MW, Harmon C, O'Farrelly C. Liver immunology and its role in inflammation and homeostasis. *Cell Mol Immunol*. 2016;13(3):267–276.
18. Lau AH, Thomson AW. Dendritic cells and immune regulation in the liver. *Gut*. 2003;52(2):307–314.
19. Njoku DB. Drug-induced hepatotoxicity: metabolic, genetic and immunological basis. *Int J Mol Sci*. 2014;15(4):6990–7003.
20. Almazroo OA, Miah MK, Venkataraman R. Drug metabolism in the liver. *Clin Liver Dis*. 2017;21(1):1–20.
21. Trefts E, Gannon M, Wasserman DH. The liver. *Curr Biol*. 2017;27(21):r1151. <https://doi.org/10.1016/j.cub.2017.09.019>.
22. Adeva-Andany MM, Perez-Felipe N, Fernandez-Fernandez C, Donapetry-Garcia C, Pazos-Garcia C. Liver glucose metabolism in humans. *Biosci Rep*. 2016;36(6). <https://doi.org/10.1042/bsr20160385>.
23. Nguyen P, Leray V, Diez M, et al. Liver lipid metabolism. *J Anim Physiol Anim Nutr (Berl)*. 2008;92(3):272–283.
24. Boyer JL. Bile formation and secretion. *Compr Physiol*. 2013;3(3):1035–1078. <https://doi.org/10.1002/cphy.c120027>.
25. Roberts MS, Magnusson BM, Burczynski FJ, Weiss M. Enterohepatic circulation: physiological, pharmacokinetic and clinical implications. *Clin Pharmacokinet*. 2002;41(10):751–790.
26. Malik MY, Jaiswal S, Sharma A, Shukla M, Lal J. Role of enterohepatic recirculation in drug disposition: cooperation and complications. *Drug Metab Rev*. 2016;48(2):281–327. <https://doi.org/10.3109/03602532.2016.1157600>.
27. Borowski M, Furie BC, Furie B. Distribution of gamma-carboxyglutamic acid residues in partially carboxylated human prothrombins. *J Biol Chem*. 1986;261(4):1624–1628.
28. Dimova EY, Kietzmann T. Metabolic, hormonal and environmental regulation of plasminogen activator inhibitor-1 (PAI-1) expression: lessons from the liver. *Thromb Haemost*. 2008;100(6):992–1006.
29. Ceserman-Maus G, Hajjar KA. Molecular mechanisms of fibrinolysis. *Br J Haematol*. 2005;129(3):307–321.
30. Stein PE ea. Update review of the acute porphyrias – PubMed – NCBI; 2018. <https://phstwlp2.partners.org:2052/pubmed/?term=27982422>.
31. Sticova E, Jirska M. New insights in bilirubin metabolism and their clinical implications. *World J Gastroenterol*. 2013;19(38):6398–6407. <https://doi.org/10.3748/wjg.v19.i38.6398>.
32. Ganz T, Nemeth E. Hepcidin and iron homeostasis. *Biochim Biophys Acta*. 2012;1823(9):1434–1443.
33. Yakar S, Rosen CJ, Beamer WG, et al. Circulating levels of IGF-1 directly regulate bone growth and density. *J Clin Invest*. 2002;110(6):771–781.
34. Lu H, Cassis LA, Kooi CWV, Daugherty A. Structure and functions of angiotensinogen. *Hypertens Res*. 2016;39(7):492–500.
35. Jelkmann W. The role of the liver in the production of thrombopoietin compared with erythropoietin. *Eur J Gastroenterol Hepatol*. 2001;13(7):791–801.
36. Habib S, Shaikh OS. Approach to jaundice and abnormal liver function test results. In: Sanyal AJ, Boyer TD, Lindor KD, Terrault NH, eds. *Zakim and Boyer's Hepatology: A Textbook of Liver Disease*. 7th ed. Philadelphia, PA: Elsevier; 2018:99–116.
37. Pratt DS. Liver chemistry and function tests. In: Feldman M, Friedman LS, Brandt LJ, eds. *Sleisenger and Fordtran's Gastrointestinal and Liver Disease: Pathophysiology, Diagnosis, Management*. 10th ed. Philadelphia: Saunders; 2016:1243–1253.
38. Kwo PY, Cohen SM, Lim JK. ACG clinical guideline: evaluation of abnormal liver chemistries. *Am J Gastroenterol*. 2017;112(1):18–35.
39. Eminler AT, Ayyildiz T, Irak K, et al. AST/ALT ratio is not useful in predicting the degree of fibrosis in chronic viral hepatitis patients. *Eur J Gastroenterol Hepatol*. 2015;27(12):1361–1366. <https://doi.org/10.1097/MEG.0000000000000468>.
40. Maina I, Rule JA, Wians FH, Poirier M, Grant L, Lee WM. A-glutathione S-transferase: a new biomarker for liver injury? *Jml App Lab Med*. 2016;1(2):119. <http://jalm.aaccjnl.org/content/1/2/119.abstract>.
41. Redick JA, Jakoby WB, Baron J. Immunohistochemical localization of glutathione S-transferases in livers of untreated rats. *J Biol Chem*. 1982;257(24):15200–15203.
42. Siddique A, Kowdley KV. Approach to a patient with elevated serum alkaline phosphatase. *Clin Liver Dis*. 2012;16(2):199–229. <https://doi.org/10.1016/j.cld.2012.03.012>.
43. Fargo MV, Grogan SP, Saguil A. Evaluation of jaundice in adults. *Am Fam Physician*. 2017;95(3):164–168.
44. Liang TJ. Hepatitis B: the virus and disease. *Hepatology*. 2009;49(5 Suppl):13. <https://doi.org/10.1002/hep.22881>.
45. Hepatitis C guidance: AASLD–IDSA recommendations for testing, managing, and treating adults infected with hepatitis C virus. *Hepatology*. 2015;62(3):932–954. <https://doi.org/10.1002/hep.27950>.
46. Fourati S, Feld JJ, Chevaliez S, Luhmann N. Approaches for simplified HCV diagnostic algorithms. *J Int AIDS Soc*. 2018;21(suppl 2):e25058. <https://doi.org/10.1002/jia2.25058>.
47. Freiman JM, Tran TM, Schumacher SG, et al. Hepatitis C core antigen testing for diagnosis of hepatitis C virus infection: a systematic review and meta-analysis. *Ann Intern Med*. 2016;165(5):345–355. <https://doi.org/10.7326/M16-0065>.
48. Ajisaka H, Shimizu K, Miwa K. Immunohistochemical study of protein induced by vitamin K absence or antagonist II in hepatocellular carcinoma. *J Surg Oncol*. 2003;84(2):89–93. <https://doi.org/10.1002/jso.10298>.
49. Fujioka M, Nakashima Y, Nakashima O, Kojiro M. Immunohistologic study on the expressions of alpha-fetoprotein and protein induced by vitamin K absence or antagonist II in surgically resected small hepatocellular carcinoma. *Hepatology*. 2001;34(6):1128–1134. <https://doi.org/10.1053/jhep.2001.29202>.
50. Sugimoto H, Takeda S, Inoue S, Kaneko T, Watanabe K, Nakao A. Des-gamma-carboxy prothrombin (DCP) ratio, a novel parameter measured by monoclonal antibodies MU-3 and 19B7, as a new prognostic indicator for hepatocellular carcinoma. *Liver Int*. 2003;23(1):38–44.

51. Wong RJ, Ahmed A, Gish RG. Elevated alpha-fetoprotein: differential diagnosis—hepatocellular carcinoma and other disorders. *Clin Liver Dis.* 2015;19(2):309–323. <https://doi.org/10.1016/j.cld.2015.01.005>.
52. Song P, Xia J, Inagaki Y, et al. Controversies regarding and perspectives on clinical utility of biomarkers in hepatocellular carcinoma. *World J Gastroenterol.* 2016;22(1):262–274. <https://doi.org/10.3748/wjg.v22.i1.262>.
53. Yuen M, Lai C. Serological markers of liver cancer. *Best Pract Res Clin Gastroenterol.* 2005;19(1):91–99. <https://doi.org/10.1016/j.bpg.2004.10.003>.
54. Tapper EB, Lok AS. Use of liver imaging and biopsy in clinical practice. *N Engl J Med.* 2017;377(23):2296–2297. <https://doi.org/10.1056/NEJMcl1712445>.
55. Bolondi G, Mocchegiani F, Montalti R, Nicolini D, Vivarelli M, De Petti L. Predictive factors of short term outcome after liver transplantation: a review. *World J Gastroenterol.* 2016;22(26):5936–5949. <https://doi.org/10.3748/wjg.v22.i26.5936>.
56. Guerrini GP, Pinelli D, Marini E, et al. Value of HCC-MELD score in patients with hepatocellular carcinoma undergoing liver transplantation. *Prog Transplant.* 2018;28(1):63–69. <https://doi.org/10.1177/1526924817746686>.
57. Lin C, Chang C, Yang S, Yeh H, Lin C. Retrospective evaluation of serum markers APRI and AST/ALT for assessing liver fibrosis and cirrhosis in chronic hepatitis B and C patients with hepatocellular carcinoma. *Intern Med.* 2008;47(7):569–575.
58. Younossi ZM, Loomba R, Anstee QM, et al. Diagnostic modalities for nonalcoholic fatty liver disease, nonalcoholic steatohepatitis, and associated fibrosis. *Hepatology.* 2018;68(1):349–360. <https://doi.org/10.1002/hep.29721>.
59. Sakka SG. Assessing liver function. *Curr Opin Crit Care.* 2007;13(2):207–214. <https://doi.org/10.1097/MCC.0b013e328012b268>.
60. Denaro CP, Jacob P, Benowitz NL. Evaluation of pharmacokinetic methods used to estimate caffeine clearance and comparison with a bayesian forecasting method. *Ther Drug Monit.* 1998;20(1):78–87.
61. Jover R, Carnicer F, Sánchez-Payá J, Climent E, Sirvent M, Marco JL. Salivary caffeine clearance predicts survival in patients with liver cirrhosis. *Am J Gastroenterol.* 1997;92(10):1905–1908.
62. Wahlländer A, Mohr S, Paumgartner G. Assessment of hepatic function. Comparison of caffeine clearance in serum and saliva during the day and at night. *J Hepatol.* 1990;10(2):129–137.
63. Everson GT, Shiffman ML, Hoefs JC, et al. Quantitative liver function tests improve the prediction of clinical outcomes in chronic hepatitis C: results from the hepatitis C antiviral long-term treatment against cirrhosis trial. *Hepatology.* 2012;55(4):1019–1029.
64. Chow PKH, Yu W, Soo K, Chan STF. The measurement of liver blood flow: a review of experimental and clinical methods. *J Surg Res.* 2003;112(1):1–11.
65. Helmke S, Colmenero J, Everson GT. Noninvasive assessment of liver function. *Curr Opin Gastroenterol.* 2015;31(3):199–208.
66. Kang HK, Jeong YY, Choi JH, et al. Three-dimensional multi-detector row CT portal venography in the evaluation of portosystemic collateral vessels in liver cirrhosis. *Radiographics.* 2002;22(5):1053–1061.
67. Sharma S, Khalili K, Nguyen GC. Non-invasive diagnosis of advanced fibrosis and cirrhosis. *World J Gastroenterol.* 2014;20(45):16820–16830.
68. Iranpour P, Lall C, Houshyar R, et al. Altered Doppler flow patterns in cirrhosis patients: an overview. *Ultrasonography.* 2016;35(1):3–12.
69. Barr RG, Ferraioli G, Palmeri ML, et al. Elastography assessment of liver fibrosis: society of radiologists in ultrasound consensus conference statement. *Radiology.* 2015;276(3):845–861.
70. Younossi ZM, Loomba R, Anstee QM, et al. Diagnostic modalities for nonalcoholic fatty liver disease, nonalcoholic steatohepatitis, and associated fibrosis. *Hepatology.* 2018;68(1):349–360. <https://doi.org/10.1002/hep.29721>.
71. Tang A, Bashir MR, Corwin MT, et al. Evidence supporting LI-RADS major features for CT- and MR imaging-based diagnosis of hepatocellular carcinoma: a systematic review. *Radiology.* 2018;286(1):29–48.
72. Bialecki ES, Di Bisceglie AM. Diagnosis of hepatocellular carcinoma. *HPB (Oxford).* 2005;7(1):26–34.
73. Pollock G, Minuk GY. Diagnostic considerations for cholestatic liver disease. *J Gastroenterol Hepatol.* 2017;32(7):1303–1309. <https://doi.org/10.1111/jgh.13738>. <https://www.ncbi.nlm.nih.gov/pubmed/28106928>.
74. Popper H, Schaffner F. Pathophysiology of cholestasis. *Hum Pathol.* 1970;1(1):1–24. <https://doi.org/>.
75. EASL clinical practice guidelines: management of cholestatic liver diseases. *J Hepatol.* 2009;51(2):237–267. <https://doi.org/10.1016/j.jhep.2009.04.009>.
76. Lleo A, Marzorati S, Anaya JM, Gershwin ME. Primary biliary cholangitis: a comprehensive overview. *Hepatol Int.* 2017;11(6):485–499. <https://doi.org/10.1007/s12072-017-9830-1>.
77. Boonstra K, Beuers U, Ponsioen CY. Epidemiology of primary sclerosing cholangitis and primary biliary cirrhosis: a systematic review. *J Hepatol.* 2012;56(5):1181–1188. <https://doi.org/10.1016/j.jhep.2011.10.025>.
78. Trivedi HD, Lizaola B, Tapper EB, Bonder A. Primary biliary cholangitis: new treatments for an old disease. *Frontline Gastroenterol.* 2017;8(1):29–36. <https://doi.org/10.1136/flgastro-2016-100741>.
79. Poupon RE, Balkau B, Eschwege E, Poupon R. A multicenter, controlled trial of ursodiol for the treatment of primary biliary cirrhosis. UDCA–PBC study group. *N Engl J Med.* 1991;324(22):1548–1554. <https://doi.org/10.1056/nejm199105303242204>.
80. Corpechot C, Abenavoli L, Rabahi N, et al. Biochemical response to ursodeoxycholic acid and long-term prognosis in primary biliary cirrhosis. *Hepatology.* 2008;48(3):871–877. <https://doi.org/10.1002/hep.22428>.
81. Hirschfield GM, Mason A, Luketic V, et al. Efficacy of obeticholic acid in patients with primary biliary cirrhosis and inadequate response to ursodeoxycholic acid. *Gastroenterology.* 2015;148(4):61.e8. <https://doi.org/10.1053/j.gastro.2014.12.005>.
82. Lens S, Leoz M, Nazal L, Bruguera M, Pares A. Bezafibrate normalizes alkaline phosphatase in primary biliary cirrhosis patients with incomplete response to ursodeoxycholic acid. *Liver Int.* 2014;34(2):197–203. <https://doi.org/10.1111/liv.12290>.
83. Rautiainen H, Karkkainen P, Karvonen AL, et al. Budesonide combined with UDCA to improve liver histology in primary biliary cirrhosis: a three-year randomized trial. *Hepatology.* 2005;41(4):747–752. <https://doi.org/10.1002/hep.20646>.
84. Karlsson TH, Folseraas T, Thorburn D, Vesterhus M. Primary sclerosing cholangitis – a comprehensive review. *J Hepatol.* 2017;67(6):1298–1323. <https://doi.org/10.1016/j.jhep.2017.07.022>.
85. Scaglione S, Kliethermes S, Cao G, et al. The epidemiology of cirrhosis in the United States: a population-based study. *J Clin Gastroenterol.* 2015;49(8):690–696. <https://doi.org/10.1097/mcg.0000000000000208>.
86. Tschoatzis EA, Bosch J, Burroughs AK. Liver cirrhosis. *Lancet.* 2014;383(9930):1749–1761. [https://doi.org/10.1016/s0140-6736\(14\)60121-5](https://doi.org/10.1016/s0140-6736(14)60121-5).
87. Garcia-Pagan JC, Gracia-Sancho J, Bosch J. Functional aspects on the pathophysiology of portal hypertension in cirrhosis. *J Hepatol.* 2012;57(2):458–461. <https://doi.org/10.1016/j.jhep.2012.03.007>.
88. Runyon BA. Introduction to the revised American Association for the Study of Liver Diseases practice guideline management of adult patients with ascites due to cirrhosis 2012. *Hepatology.* 2013;57(4):1651–1653. <https://doi.org/10.1002/hep.26359>.
89. De Robertis R, D'Onofrio M, Demozzi E, Crosara S, Canestrini S, Pozzi Mucelli R. Noninvasive diagnosis of cirrhosis: a review of different imaging modalities. *World J Gastroenterol.* 2014;20(23):7231–7241. <https://doi.org/10.3748/wjg.v20.i23.7231>.
90. Garcia-Tsao G, Abraldes JG, Berzigotti A, Bosch J. Portal hypertensive bleeding in cirrhosis: risk stratification, diagnosis, and management: 2016 practice guidance by the American Association for the Study of Liver Diseases. *Hepatology.* 2017;65(1):310–335. <https://doi.org/10.1002/hep.28906>.
91. D'Amico G, Morabito A, D'Amico M, et al. Clinical states of cirrhosis and competing risks. *J Hepatol.* 2018;68(3):563–576. <https://doi.org/10.1016/j.jhep.2017.10.020>.
92. Ripoll C, Groszmann RJ, Garcia-Tsao G, et al. Hepatic venous pressure gradient predicts clinical decompensation in patients with compensated cirrhosis. *Gastroenterology.* 2007;133(2):481–488. <https://doi.org/10.1053/j.gastro.2007.05.024>.
93. Ripoll C, Groszmann RJ, Garcia-Tsao G, et al. Hepatic venous pressure gradient predicts development of hepatocellular carcinoma

- independently of severity of cirrhosis. *J Hepatol.* 2009;50(5):923–928. <https://doi.org/10.1016/j.jhep.2009.01.014>.
94. Abraldes JG, Sarlieve P, Tandon P. Measurement of portal pressure. *Clin Liver Dis.* 2014;18(4):779–792. <https://doi.org/10.1016/j.cld.2014.07.002>.
95. Shi KQ, Fan YC, Pan ZZ, et al. Transient elastography: a meta-analysis of diagnostic accuracy in evaluation of portal hypertension in chronic liver disease. *Liver Int.* 2013;33(1):62–71. <https://doi.org/10.1111/liv.12003>.
96. Vilgrain V, Lebrec D, Menu Y, Scherrer A, Nahum H. Comparison between ultrasonographic signs and the degree of portal hypertension in patients with cirrhosis. *Gastrointest Radiol.* 1990;15(3):218–222. <https://doi.org/>.
97. Zipprich A, Garcia-Tsao G, Rogowski S, Fleig WE, Seufferlein T, Dollinger MM. Prognostic indicators of survival in patients with compensated and decompensated cirrhosis. *Liver Int.* 2012;32(9):1407–1414. <https://doi.org/10.1111/j.1478-3231.2012.02830.x>.
98. Gluud LL, Krag A. Banding ligation versus beta-blockers for primary prevention in oesophageal varices in adults. *Cochrane Database Syst Rev.* 2012;8:CD004544. <https://doi.org/10.1002/14651858.CD004544.pub2>.
99. Shah HA, Azam Z, Rauf J, et al. Carvedilol vs. esophageal variceal band ligation in the primary prophylaxis of variceal hemorrhage: a multicentre randomized controlled trial. *J Hepatol.* 2014;60(4):757–764. <https://doi.org/10.1016/j.jhep.2013.11.019>.
100. D'Amico G, Garcia-Pagan JC, Luca A, Bosch J. Hepatic vein pressure gradient reduction and prevention of variceal bleeding in cirrhosis: a systematic review. *Gastroenterology.* 2006;131(5):1611–1624. <https://doi.org/10.1053/j.gastro.2006.09.013>.
101. Carvalho GC, Regis Cde A, Kalil JR, et al. Causes of renal failure in patients with decompensated cirrhosis and its impact in hospital mortality. *Ann Hepatol.* 2012;11(1):90–95. <https://doi.org/>.
102. Martin-Llahi M, Guevara M, Torre A, et al. Prognostic importance of the cause of renal failure in patients with cirrhosis. *Gastroenterology.* 2011;140(2):496.e4. <https://doi.org/10.1053/j.gastro.2010.07.043>.
103. Angeli P, Gines P, Wong F, et al. Diagnosis and management of acute kidney injury in patients with cirrhosis: revised consensus recommendations of the International Club of Ascites. *J Hepatol.* 2015;62(4):968–974. <https://doi.org/10.1016/j.jhep.2014.12.029>.
104. de Mattos AZ, de Mattos AA, Mendez-Sanchez N. Hepatorenal syndrome: current concepts related to diagnosis and management. *Ann Hepatol.* 2016;15(4):474–481. <https://doi.org/>.
105. Boyer TD, Sanyal AJ, Garcia-Tsao G, et al. Impact of liver transplantation on the survival of patients treated for hepatorenal syndrome type 1. *Liver Transpl.* 2011;17(11):1328–1332. <https://doi.org/10.1002/lt.22395>.
106. Nolte W, Wiltfang J, Schindler C, et al. Portosystemic hepatic encephalopathy after transjugular intrahepatic portosystemic shunt in patients with cirrhosis: clinical, laboratory, psychometric, and electroencephalographic investigations. *Hepatology.* 1998;28(5):1215–1225. <https://doi.org/10.1002/hep.510280508>.
107. Montagnese S, Amodio P, Morgan MY. Methods for diagnosing hepatic encephalopathy in patients with cirrhosis: a multidimensional approach. *Metab Brain Dis.* 2004;19(3–4):281–312. <https://doi.org/>.
108. Vilstrup H, Amodio P, Bajaj J, et al. Hepatic encephalopathy in chronic liver disease: 2014 practice guideline by the American Association for the Study of Liver Diseases and the European Association for the Study of the Liver. *Hepatology.* 2014;60(2):715–735. <https://doi.org/10.1002/hep.27210>.
109. Swanson KL, Wiesner RH, Krowka MJ. Natural history of hepatopulmonary syndrome: impact of liver transplantation. *Hepatology.* 2005;41(5):1122–1129. <https://doi.org/10.1002/hep.20658>.
110. Krowka MJ, Fallon MB, Kawut SM, et al. International Liver Transplant Society practice guidelines: diagnosis and management of hepatopulmonary syndrome and portopulmonary hypertension. *Transplantation.* 2016;100(7):1440–1452. <https://doi.org/10.1097/tp.0000000000001229>.
111. Iyer VN, Swanson KL, Cartin-Ceba R, et al. Hepatopulmonary syndrome: favorable outcomes in the MELD exception era. *Hepatology.* 2013;57(6):2427–2435. <https://doi.org/10.1002/hep.26070>.
112. Schiffer E, Majno P, Mentha G, et al. Hepatopulmonary syndrome increases the postoperative mortality rate following liver transplantation: a prospective study in 90 patients. *Am J Transplant.* 2006;6(6):1430–1437. <https://doi.org/10.1111/j.1600-6143.2006.01334.x>.
113. Simonneau G, Gatzoulis MA, Adatia I, et al. Updated clinical classification of pulmonary hypertension. *J Am Coll Cardiol.* 2013;62(suppl 25):34. <https://doi.org/10.1016/j.jacc.2013.10.029>.
114. Krowka MJ, Swanson KL, Frantz RP, McGoon MD, Wiesner RH. Portopulmonary hypertension: results from a 10-year screening algorithm. *Hepatology.* 2006;44(6):1502–1510. <https://doi.org/10.1002/hep.21431>.
115. Swanson KL, Wiesner RH, Nyberg SL, Rosen CB, Krowka MJ. Survival in portopulmonary hypertension: Mayo Clinic experience categorized by treatment subgroups. *Am J Transplant.* 2008;8(11):2445–2453. <https://doi.org/10.1111/j.1600-6143.2008.02384.x>.
116. Malagari K, Nikita A, Alexopoulou E, et al. Cirrhosis-related intra-thoracic disease. imaging features in 1038 patients. *HepatoGastroenterology.* 2005;52(62):558–562. <https://doi.org/>.
117. Machicao VI, Balakrishnan M, Fallon MB. Pulmonary complications in chronic liver disease. *Hepatology.* 2014;59(4):1627–1637. <https://doi.org/10.1002/hep.26745>.
118. Global, regional, and national age–sex specific mortality for 264 causes of death, 1980–2016: a systematic analysis for the global burden of disease study 2016. *Lancet.* 2017;390(10100):1151–1210. [https://doi.org/10.1016/s0140-6736\(17\)32152-9](https://doi.org/10.1016/s0140-6736(17)32152-9).
119. Forner A, Reig M, Bruix J. Hepatocellular carcinoma. *Lancet.* 2018;391(10127):1301–1314. [https://doi.org/10.1016/s0140-6736\(18\)30010-2](https://doi.org/10.1016/s0140-6736(18)30010-2).
120. Heimbach JK, Kulik LM, Finn RS, et al. AASLD guidelines for the treatment of hepatocellular carcinoma. *Hepatology.* 2018;67(1):358–380. <https://doi.org/10.1002/hep.29086>.
121. Poon RT, Fan ST, Lo CM, Liu CL, Wong J. Long-term survival and pattern of recurrence after resection of small hepatocellular carcinoma in patients with preserved liver function: implications for a strategy of salvage transplantation. *Ann Surg.* 2002;235(3):373–382. <https://doi.org/>.
122. Mazzaferro V, Regalia E, Doci R, et al. Liver transplantation for the treatment of small hepatocellular carcinomas in patients with cirrhosis. *N Engl J Med.* 1996;334(11):693–699. <https://doi.org/10.1056/nejm199603143341104>.
123. Lautt WW. Mechanism and role of intrinsic regulation of hepatic arterial blood flow: hepatic arterial buffer response. *Am J Physiol.* 1985;249(5 Pt 1):549. <https://doi.org/10.1152/ajphl.1985.249.5.G549>.
124. Gelman S, Fowler KC, Smith LR. Liver circulation and function during isoflurane and halothane anesthesia. *Anesthesiology.* 1984;61(6):726–730. <https://doi.org/>.
125. Frink EJ Jr, Morgan SE, Coetzee A, Conzen PF, Brown BR Jr. The effects of sevoflurane, halothane, enflurane, and isoflurane on hepatic blood flow and oxygenation in chronically instrumented greyhound dogs. *Anesthesiology.* 1992;76(1):85–90. <https://doi.org/>.
126. Hartman JC, Pagel PS, Proctor LT, Kampine JP, Schmeling WT, Warltier DC. Influence of desflurane, isoflurane and halothane on regional tissue perfusion in dogs. *Can J Anaesth.* 1992;39(8):877–887. <https://doi.org/10.1007/bf03008300>.
127. Cullen SC, Gross EG. The anesthetic properties of xenon in animals and human beings, with additional observations on krypton. *Science.* 1951;113(2942):580–582. <https://doi.org/>.
128. Goto T, Suwa K, Uezono S, Ichinose F, Uchiyama M, Morita S. The blood–gas partition coefficient of xenon may be lower than generally accepted. *Br J Anaesth.* 1998;80(2):255–256. <https://doi.org/>.
129. Wappler F, Rossaint R, Baumert J, et al. Multicenter randomized comparison of xenon and isoflurane on left ventricular function in patients undergoing elective surgery. *Anesthesiology.* 2007;106(3):463–471. <https://doi.org/>.
130. Schmidt M, Marx T, Kotzerke J, et al. Cerebral and regional organ perfusion in pigs during xenon anaesthesia. *Anaesthesia.* 2001;56(12):1154–1159. <https://doi.org/>.
131. Iber T, Hecker K, Vagts DA, et al. Xenon anesthesia impairs hepatic oxygenation and perfusion in healthy pigs. *Minerva Anestesiol.* 2008;74(10):511–519. <https://doi.org/>.
132. Reinelt H, Marx T, Kotzerke J, et al. Hepatic function during xenon anesthesia in pigs. *Acta Anaesthesiol Scand.* 2002;46(6):713–716. <https://doi.org/>.
133. Wilke HJ, Moench C, Lotz G, Bechstein W, Zacharowski K. Xenon anesthesia for liver transplant surgery: a report of four cases. *Transplant Proc.* 2011;43(7):2683–2686. <https://doi.org/10.1016/j.transproceed.2011.06.029>.

134. Servin F, Cockshott ID, Farinotti R, Haberer JP, Winckler C, Desmonts JM. Pharmacokinetics of propofol infusions in patients with cirrhosis. *Br J Anaesth.* 1990;65(2):177–183. <https://doi.org/>.
135. Pandele G, Chaux F, Salvadori C, Farinotti M, Duvaldestin P. Thiopental pharmacokinetics in patients with cirrhosis. *Anesthesiology.* 1983;59(2):123–126. <https://doi.org/>.
136. van Beem H, Manger FW, van Boxtel C, van Bentem N. Etomidate anaesthesia in patients with cirrhosis of the liver: pharmacokinetic data. *Anaesthesia.* 1983;38(suppl):61–62. <https://doi.org/>.
137. Duvaldestin P, Chauvin M, Lebrault C, Bertrand F, Karolak FT, Farinotti R. Effect of upper abdominal surgery and cirrhosis upon the pharmacokinetics of methohexitol. *Acta Anaesthesiol Scand.* 1991;35(2):159–163. <https://doi.org/>.
138. Carmichael FJ, Crawford MW, Khayyam N, Saldivia V. Effect of propofol infusion on splanchnic hemodynamics and liver oxygen consumption in the rat. A dose–response study. *Anesthesiology.* 1993;79(5):1051–1060. <https://doi.org/>.
139. Wouters PF, Van de Velde MA, Marcus MA, Deruyter HA, Van Aken H. Hemodynamic changes during induction of anaesthesia with etlananolone and propofol in dogs. *Anesth Analg.* 1995;81(1):125–131. <https://doi.org/>.
140. Zhu T, Pang Q, McCluskey SA, Luo C. Effect of propofol on hepatic blood flow and oxygen balance in rabbits. *Can J Anaesth.* 2008;55(6):364–370. <https://doi.org/10.1007/bf03021492>.
141. Meierhenrich R, Gauss A, Muhling B, et al. The effect of propofol and desflurane anaesthesia on human hepatic blood flow: a pilot study. *Anaesthesia.* 2010;65(11):1085–1093. <https://doi.org/10.1111/j.1365-2044.2010.06504.x>.
142. Leslie K, Sessler DI, Bjorksten AR, Moayeri A. Mild hypothermia alters propofol pharmacokinetics and increases the duration of action of atracurium. *Anesth Analg.* 1995;80(5):1007–1014. <https://doi.org/>.
143. Runciman WB, Mather LE, Selby DG. Cardiovascular effects of propofol and of thiopentone anaesthesia in the sheep. *Br J Anaesth.* 1990;65(3):353–359. <https://doi.org/>.
144. Sear JW, Diedericks J, Foex P. Continuous infusions of propofol administered to dogs: effects on ICG and propofol disposition. *Br J Anaesth.* 1994;72(4):451–455. <https://doi.org/>.
145. MacGilchrist AJ, Birnie GG, Cook A, et al. Pharmacokinetics and pharmacodynamics of intravenous midazolam in patients with severe alcoholic cirrhosis. *Gut.* 1986;27(2):190–195. <https://doi.org/>.
146. Weerink MAS, Struys M, Hannivoort LN, Barends CRM, Absalom AR, Colin P. Clinical pharmacokinetics and pharmacodynamics of dexmedetomidine. *Clin Pharmacokinet.* 2017;56(8):893–913. <https://doi.org/10.1007/s40262-017-0507-7>.
147. Mazoit JX, Sandouk P, Zetlaoui P, Scherrmann JM. Pharmacokinetics of unchanged morphine in normal and cirrhotic subjects. *Anesth Analg.* 1987;66(4):293–298. <https://doi.org/>.
148. Klotz U, McHorse TS, Wilkinson GR, Schenker S. The effect of cirrhosis on the disposition and elimination of meperidine in man. *Clin Pharmacol Ther.* 1974;16(4):667–675. <https://doi.org/>.
149. Ferrier C, Marty J, Bouffard Y, Haberer JP, Levron JC, Duvaldestin P. Alfentanil pharmacokinetics in patients with cirrhosis. *Anesthesiology.* 1985;62(4):480–484. <https://doi.org/>.
150. Haberer JP, Schoeffler P, Couderc E, Duvaldestin P. Fentanyl pharmacokinetics in anaesthetized patients with cirrhosis. *Br J Anaesth.* 1982;54(12):1267–1270. <https://doi.org/>.
151. Chauvin M, Ferrier C, Haberer JP, et al. Sufentanil pharmacokinetics in patients with cirrhosis. *Anesth Analg.* 1989;68(1):1–4. <https://doi.org/>.
152. Dershawitz M, Hoke JF, Rosow CE, et al. Pharmacokinetics and pharmacodynamics of remifentanil in volunteer subjects with severe liver disease. *Anesthesiology.* 1996;84(4):812–820. <https://doi.org/>.
153. Devlin JC, Head-Rapson AG, Parker CJ, Hunter JM. Pharmacodynamics of mivacurium chloride in patients with hepatic cirrhosis. *Br J Anaesth.* 1993;71(2):227–231. <https://doi.org/>.
154. Viby-Mogensen J, Hanel HK. Prolonged apnoea after suxamethonium: an analysis of the first 225 cases reported to the danish cholinesterase research unit. *Acta Anaesthesiol Scand.* 1978;22(4):371–380. <https://doi.org/>.
155. De Wolf AM, Freeman JA, Scott VL, et al. Pharmacokinetics and pharmacodynamics of cisatracurium in patients with end–stage liver disease undergoing liver transplantation. *Br J Anaesth.* 1996;76(5):624–628. <https://doi.org/>.
156. Lebrault C, Berger JL, D'Hollander AA, Gomeni R, Henzel D, Duvaldestin P. Pharmacokinetics and pharmacodynamics of vecuronium (ORG NC 45) in patients with cirrhosis. *Anesthesiology.* 1985;62(5):601–605. <https://doi.org/>.
157. Khalil M, D'Honneur G, Duvaldestin P, Slavov V, De Hys C, Gomeni R. Pharmacokinetics and pharmacodynamics of rocuronium in patients with cirrhosis. *Anesthesiology.* 1994;80(6):1241–1247. <https://doi.org/>.
158. Duvaldestin P, Agoston S, Henzel D, Kersten UW, Desmonts JM. Pancuronium pharmacokinetics in patients with liver cirrhosis. *Br J Anaesth.* 1978;50(11):1131–1136. <https://doi.org/>.
159. Fujita A, Ishibe N, Yoshihara T, et al. Rapid reversal of neuromuscular blockade by sugammadex after continuous infusion of rocuronium in patients with liver dysfunction undergoing hepatic surgery. *Acta Anaesthesiol Taiwan.* 2014;52(2):54–58. <https://doi.org/10.1016/j.jaat.2014.04.007>.
160. Tanaka N, Nagata N, Hamakawa T, Takasaki M. The effect of dopamine on hepatic blood flow in patients undergoing epidural anaesthesia. *Anesth Analg.* 1997;85(2):286–290. <https://doi.org/>.
161. Meierhenrich R, Wagner F, Schutz W, et al. The effects of thoracic epidural anaesthesia on hepatic blood flow in patients under general anaesthesia. *Anesth Analg.* 2009;108(4):1331–1337. <https://doi.org/10.1213/ane.0b013e3181966e6f>.
162. Trepenaitis D, Pundzius J, Macas A. The influence of thoracic epidural anaesthesia on liver hemodynamics in patients under general anaesthesia. *Medicina (Kaunas).* 2010;46(7):465–471. <https://doi.org/>.
163. Kortgen A, Silomon M, Pape-Becker C, Buchinger H, Grundmann U, Bauer M. Thoracic but not lumbar epidural anaesthesia increases liver blood flow after major abdominal surgery. *Eur J Anaesthesiol.* 2009;26(2):111–116. <https://doi.org/10.1097/EJA.0b013e32831c8939>.
164. Friedman LS. Surgery in the patient with liver disease. *Trans Am Clin Climatol Assoc.* 2010;121:204; discussion 205 <https://doi.org/>.
165. de Goede B, Klitsie PJ, Lange JF, Metselaar HJ, Kazemier G. Morbidity and mortality related to non-hepatic surgery in patients with liver cirrhosis: a systematic review. *Best Pract Res Clin Gastroenterol.* 2012;26(1):47–59. <https://doi.org/10.1016/j.bpr.2012.01.010>.
166. Csiksz NG, Nguyen LN, Tseng JF, Shah SA. Nationwide volume and mortality after elective surgery in cirrhotic patients. *J Am Coll Surg.* 2009;208(1):96–103. <https://doi.org/10.1016/j.jamcollsurg.2008.09.006>.
167. Lin CS, Lin SY, Chang CC, Wang HH, Liao CC, Chen TL. Postoperative adverse outcomes after non-hepatic surgery in patients with liver cirrhosis. *Br J Surg.* 2013;100(13):1784–1790. <https://doi.org/10.1002/bjs.9312>.
168. Farnsworth N, Fagan SP, Berger DH, Awad SS. Child–Turcotte–Pugh versus MELD score as a predictor of outcome after elective and emergent surgery in cirrhotic patients. *Am J Surg.* 2004;188(5):580–583. <https://doi.org/10.1016/j.amjsurg.2004.07.034>.
169. Neff HP, Streule GC, Drogatz O, et al. Early mortality and long-term survival after abdominal surgery in patients with liver cirrhosis. *Surgery.* 2014;155(4):623–632. <https://doi.org/10.1016/j.surg.2013.11.009>.
170. Telem DA, Schiano T, Goldstone R, et al. Factors that predict outcome of abdominal operations in patients with advanced cirrhosis. *Clin Gastroenterol Hepatol.* 2010;8(5):7. <https://doi.org/10.1016/j.cgh.2009.12.015>, quiz e58.
171. Hoteit MA, Ghazale AH, Bain AJ, et al. Model for end–stage liver disease score versus Child score in predicting the outcome of surgical procedures in patients with cirrhosis. *World J Gastroenterol.* 2008;14(11):1774–1780. <https://doi.org/>.
172. Pantel HJ, Stensland KD, Nelson J, et al. Should we use the model for end–stage liver disease (MELD) to predict mortality after colorectal surgery? *J Gastrointest Surg.* 2016;20(8):1511–1516. <https://doi.org/10.1007/s11605-016-3167-2>.
173. Pugh RN, Murray–Lyon IM, Dawson JL, Pietroni MC, Williams R. Transection of the oesophagus for bleeding oesophageal varices. *Br J Surg.* 1973;60(8):646–649. <https://doi.org/>.
174. Garrison RN, Cryer HM, Howard DA, Polk HC Jr. Clarification of risk factors for abdominal operations in patients with hepatic cirrhosis. *Ann Surg.* 1984;199(6):648–655. <https://doi.org/>.
175. Mansour A, Watson W, Shayani V, Pickleman J. Abdominal operations in patients with cirrhosis: still a major surgical challenge. *Surgery.* 1997;122(4):6. <https://doi.org/>.

176. Kiamanesh D, Rumley J, Moitra VK. Monitoring and managing hepatic disease in anaesthesia. *Br J Anaesth.* 2013;111(suppl 1):50–61. <https://doi.org/10.1093/bja/aet378>.
177. Malinchoc M, Kamath PS, Gordon FD, Peine CJ, Rank J, ter Borg PC. A model to predict poor survival in patients undergoing transjugular intrahepatic portosystemic shunts. *Hepatology.* 2000;31(4):864–871. <https://doi.org/10.1053/he.2000.5852>.
178. Kamath PS, Wiesner RH, Malinchoc M, et al. A model to predict survival in patients with end-stage liver disease. *Hepatology.* 2001;33(2):464–470. <https://doi.org/10.1053/jhep.2001.22172>.
179. Suman A, Barnes DS, Zein NN, Levinthal GN, Connor JT, Carey WD. Predicting outcome after cardiac surgery in patients with cirrhosis: a comparison of Child–Pugh and MELD scores. *Clin Gastroenterol Hepatol.* 2004;2(8):719–723. <https://doi.org/>.
180. Befeler AS, Palmer DE, Hoffman M, Longo W, Solomon H, Di Bisceglie AM. The safety of intra-abdominal surgery in patients with cirrhosis: Model for End-Stage Liver Disease score is superior to Child–Turcotte–Pugh classification in predicting outcome. *Arch Surg.* 2005;140(7):4. <https://doi.org/10.1001/archsurg.140.7.650>. dsusson 655.
181. Northup PG, Wanamaker RC, Lee VD, Adams RB, Berg CL. Model for end-stage liver disease (MELD) predicts nontransplant surgical mortality in patients with cirrhosis. *Ann Surg.* 2005;242(2):244–251. <https://doi.org/>.
182. Teh SH, Nagorney DM, Stevens SR, et al. Risk factors for mortality after surgery in patients with cirrhosis. *Gastroenterology.* 2007;132(4):1261–1269. <https://doi.org/10.1053/j.gastro.2007.01.040>.
183. Biggins SW, Kim WR, Terrault NA, et al. Evidence-based incorporation of serum sodium concentration into MELD. *Gastroenterology.* 2006;130(6):1652–1660. <https://doi.org/10.1053/j.gastro.2006.02.010>.
184. Luca A, Angermayr B, Bertolini G, et al. An integrated MELD model including serum sodium and age improves the prediction of early mortality in patients with cirrhosis. *Liver Transpl.* 2007;13(8):1174–1180. <https://doi.org/10.1002/lt.21197>.
185. Cho HC, Jung HY, Sinn DH, et al. Mortality after surgery in patients with liver cirrhosis: comparison of Child–Turcotte–Pugh, MELD and MELDNa score. *Eur J Gastroenterol Hepatol.* 2011;23(1):51–59. <https://doi.org/10.1097/MEG.0b013e3283407158>.
186. Kim DH, Kim SH, Kim KS, et al. Predictors of mortality in cirrhotic patients undergoing extrahepatic surgery: comparison of Child–Turcotte–Pugh and Model for End-Stage Liver Disease-based indices. *ANZ J Surg.* 2014;84(11):832–836. <https://doi.org/10.1111/ans.12198>.
187. Bangui P, Laurent A, Amathieu R, Azoulay D. Assessment of risk for non-hepatic surgery in cirrhotic patients. *J Hepatol.* 2012;57(4):874–884. <https://doi.org/10.1016/j.jhep.2012.03.037>.
188. Kim TH, Um SH, Yim SY, et al. The risk of perioperative adverse events in patients with chronic liver disease. *Liver Int.* 2015;35(3):713–723. <https://doi.org/10.1111/liv.12529>.
189. Boyer TD, Haskal ZJ. The role of transjugular intrahepatic portosystemic shunt (TIPS) in the management of portal hypertension: update 2009. *Hepatology.* 2010;51(1):306. <https://doi.org/10.1002/hep.23383>.
190. Parker R. Role of transjugular intrahepatic portosystemic shunt in the management of portal hypertension. *Clin Liver Dis.* 2014;18(2):319–334. <https://doi.org/10.1016/j.cld.2013.12.004>.
191. Monescillo A, Martinez-Lagares F, Ruiz-del-Arbol L, et al. Influence of portal hypertension and its early decompression by TIPS placement on the outcome of variceal bleeding. *Hepatology.* 2004;40(4):793–801. <https://doi.org/10.1002/hep.20386>.
192. Suhocki PV, Lungren MP, Kapoor B, Kim CY. Transjugular intrahepatic portosystemic shunt complications: prevention and management. *Semin Intervent Radiol.* 2015;32(2):123–132. <https://doi.org/10.1055/s-0035-1549376>.
193. Chana A, James M, Veale P. Anaesthesia for transjugular intrahepatic portosystemic shunt insertion. *BJA Education.* 2016;16(12):405–409. <https://doi.org/10.1093/bjaed/mkw022>.
194. DeGasperi A, Corti A, Corso R, et al. Transjugular intrahepatic portosystemic shunt (TIPS): the anesthesiological point of view after 150 procedures managed under total intravenous anesthesia. *J Clin Monit Comput.* 2009;23(6):341–346. <https://doi.org/10.1007/s10877-009-9167-y>.
195. Modha K, Kapoor B, Lopez R, Sands MJ, Carey W. Symptomatic heart failure after transjugular intrahepatic portosystemic shunt placement: incidence, outcomes, and predictors. *Cardiovasc Interv Radiol.* 2018;41(4):564–571. <https://doi.org/10.1007/s00270-017-1848-1>.
196. Suhocki PV, Lungren MP, Kapoor B, Kim CY. Transjugular intrahepatic portosystemic shunt complications: prevention and management. *Semin Intervent Radiol.* 2015;32(2):123–132. <https://doi.org/10.1055/s-0035-1549376>.
197. Dimick JB, Cowan JA Jr, Knol JA, Upchurch GR Jr. Hepatic resection in the United States: indications, outcomes, and hospital procedural volumes from a nationally representative database. *Arch Surg.* 2003;138(2):185–191. <https://doi.org/>.
198. Aragon RJ, Solomon NL. Techniques of hepatic resection. *J Gastrointest Oncol.* 2012;3(1):28–40. <https://doi.org/10.3978/j.issn.2078-6891.2012.006>.
199. Kneuertz PJ, Pitt HA, Bilimoria KY, et al. Risk of morbidity and mortality following hepato-pancreato-biliary surgery. *J Gastrointest Surg.* 2012;16(9):1727–1735. <https://doi.org/10.1007/s11605-012-1938-y>.
200. Chang CM, Yin WY, Su YC, et al. Preoperative risk score predicting 90-day mortality after liver resection in a population-based study. *Medicine (Baltimore).* 2014;93(12):e59. <https://doi.org/10.1097/md.0000000000000059>.
201. Wakabayashi G, Cherqui D, Geller DA, et al. Recommendations for laparoscopic liver resection: a report from the Second International Consensus Conference held in Morioka. *Ann Surg.* 2015;261(4):619–629. <https://doi.org/10.1097/sla.0000000000001184>.
202. Abu Hilal M, Aldrighetti L, Dagher I, et al. The Southampton consensus guidelines for laparoscopic liver surgery: from indication to implementation. *Ann Surg.* 2018;268(1):11–18. <https://doi.org/10.1097/sla.0000000000002524>.
203. Ciria R, Cherqui D, Geller DA, Briceno J, Wakabayashi G. Comparative short-term benefits of laparoscopic liver resection: 9000 cases and climbing. *Ann Surg.* 2016;263(4):761–777. <https://doi.org/10.1097/sla.0000000000001413>.
204. Fretland AA, Dagenborg VJ, Bjornely GMW, et al. Laparoscopic versus open resection for colorectal liver metastases: the OSLO–COMET randomized controlled trial. *Ann Surg.* 2018;267(2):199–207. <https://doi.org/10.1097/sla.0000000000002353>.
205. Cauchy F, Fuks D, Nomi T, et al. Risk factors and consequences of conversion in laparoscopic major liver resection. *Br J Surg.* 2015;102(7):785–795. <https://doi.org/10.1002/bjs.9806>.
206. Goh BK, Chan CY, Wong JS, et al. Factors associated with and outcomes of open conversion after laparoscopic minor hepatectomy: initial experience at a single institution. *Surg Endosc.* 2015;29(9):2636–2642. <https://doi.org/10.1007/s00464-014-3981-0>.
207. Nota CL, Rinkes IHB, Molenaar IQ, van Santvoort HC, Fong Y, Hagendoorn J. Robot-assisted laparoscopic liver resection: a systematic review and pooled analysis of minor and major hepatectomies. *HPB (Oxford).* 2016;18(2):113–120. <https://doi.org/10.1016/j.hpb.2015.09.003>.
208. Montalenti R, Berardi G, Patriti A, Vivarelli M, Troisi RI. Outcomes of robotic vs laparoscopic hepatectomy: a systematic review and meta-analysis. *World J Gastroenterol.* 2015;21(27):8441–8451. <https://doi.org/10.3748/wjg.v21.i27.8441>.
209. Capussotti L, Muratore A, Amisano M, Polastri R, Bouzari H, Massucco P. Liver resection for hepatocellular carcinoma on cirrhosis: analysis of mortality, morbidity and survival—a European single center experience. *Eur J Surg Oncol.* 2005;31(9):986–993. <https://doi.org/10.1016/j.ejso.2005.04.002>.
210. Reddy SK, Marsh JW, Varley PR, et al. Underlying steatohepatitis, but not simple hepatic steatosis, increases morbidity after liver resection: a case-control study. *Hepatology.* 2012;56(6):2221–2230. <https://doi.org/10.1002/hep.25935>.
211. van Lienden KP, van den Esschert JW, de Graaf W, et al. Portal vein embolization before liver resection: a systematic review. *Cardiovasc Interv Radiol.* 2013;36(1):25–34. <https://doi.org/10.1007/s00270-012-0440-y>.
212. Kamiyama T, Nakanishi K, Yokoo H, et al. Perioperative management of hepatic resection toward zero mortality and morbidity: analysis of 793 consecutive cases in a single institution. *J Am Coll Surg.* 2010;211(4):443–449. <https://doi.org/10.1016/j.jamcoll-surg.2010.06.005>.

213. Aramaki O, Takayama T, Higaki T, et al. Decreased blood loss reduces postoperative complications in resection for hepatocellular carcinoma. *J Hepatobiliary Pancreat Sci.* 2014;21(8):585–591. <https://doi.org/10.1002/jhbp.101>.
214. Katz SC, Shia J, Liau KH, et al. Operative blood loss independently predicts recurrence and survival after resection of hepatocellular carcinoma. *Ann Surg.* 2009;249(4):617–623. <https://doi.org/10.1097/SLA.0b013e31819ed22f>.
215. McNally SJ, Revie EJ, Massie LJ, et al. Factors in perioperative care that determine blood loss in liver surgery. *HPB (Oxford).* 2012;14(4):236–241. <https://doi.org/10.1111/j.1477-2574.2011.00433.x>.
216. Nanashima A, Abo T, Hamasaki K, et al. Predictors of intraoperative blood loss in patients undergoing hepatectomy. *Surg Today.* 2013;43(5):485–493. <https://doi.org/10.1007/s00595-012-0374-7>.
217. Janny S, Eurin M, Dokmak S, Toussaint A, Farges O, Paugam-Burtz C. Assessment of the external validity of a predictive score for blood transfusion in liver surgery. *HPB (Oxford).* 2015;17(4):357–361. <https://doi.org/10.1111/hpb.12376>.
218. Fujimoto J, Okamoto E, Yamanaka N, et al. Efficacy of autotransfusion in hepatectomy for hepatocellular carcinoma. *Arch Surg.* 1993;128(9):1065–1069. <https://doi.org/>.
219. Matot I, Scheinin O, Jurim O, Eid A. Effectiveness of acute normovolemic hemodilution to minimize allogeneic blood transfusion in major liver resections. *Anesthesiology.* 2002;97(4):794–800. <https://doi.org/>.
220. Jarnagin WR, Gonen M, Maithel SK, et al. A prospective randomized trial of acute normovolemic hemodilution compared to standard intraoperative management in patients undergoing major hepatic resection. *Ann Surg.* 2008;248(3):360–369. <https://doi.org/10.1097/SLA.0b013e318184db08>.
221. Frankel TL, Fischer M, Grant F, et al. Selecting patients for acute normovolemic hemodilution during hepatic resection: a prospective randomized evaluation of nomogram-based allocation. *J Am Coll Surg.* 2013;217(2):210–220. <https://doi.org/10.1016/j.jamcoll-surg.2013.03.019>.
222. Imamura H, Seyama Y, Kokudo N, et al. One thousand fifty-six hepatectomies without mortality in 8 years. *Arch Surg.* 2003;138(11):1206; discussion 1206.
223. Grazi GL, Ercolani G, Pierangeli F, et al. Improved results of liver resection for hepatocellular carcinoma on cirrhosis give the procedure added value. *Ann Surg.* 2001;234(1):71–78. <https://doi.org/>.
224. Huntington JT, Royall NA, Schmidt CR. Minimizing blood loss during hepatectomy: a literature review. *J Surg Oncol.* 2014;109(2):81–88. <https://doi.org/10.1002/jso.23455>.
225. Jiang B, Yan X, Zhang J. Meta-analysis of laparoscopic versus open liver resection for hepatocellular carcinoma. *Hepatol Res.* 2018;48(8):635–663.
226. Pringle JHV. Notes on the arrest of hepatic hemorrhage due to trauma. *Ann Surg.* 1908;48(4):541–549. <https://doi.org/>.
227. Kim YI. Ischemia–reperfusion injury of the human liver during hepatic resection. *J Hepatobiliary Pancreat.* 2003;10(3):195–199. <https://doi.org/10.1007/s00534-002-0730-x>.
228. Hoekstra LT, van Trigt JD, Reiniers MJ, Busch OR, Gouma DJ, van Gulik TM. Vascular occlusion or not during liver resection: the continuing story. *Dig Surg.* 2012;29(1):35–42. <https://doi.org/10.1159/000335724>.
229. Torzilli G, Procopio F, Donadon M, Del Fabbro D, Cimino M, Montorsi M. Safety of intermittent Pringle maneuver cumulative time exceeding 120 minutes in liver resection: a further step in favor of the radical but conservative policy. *Ann Surg.* 2012;255(2):270–280. <https://doi.org/10.1097/SLA.0b013e318232b375>.
230. Beck-Schimmer B, Breitenstein S, Urech S, et al. A randomized controlled trial on pharmacological preconditioning in liver surgery using a volatile anesthetic. *Ann Surg.* 2008;248(6):909–918. <https://doi.org/10.1097/SLA.0b013e31818f3dda>.
231. Beck-Schimmer B, Breitenstein S, Bonvini JM, et al. Protection of pharmacological postconditioning in liver surgery: results of a prospective randomized controlled trial. *Ann Surg.* 2012;256(5):5. <https://doi.org/10.1097/SLA.0b013e318272df7c>.
232. Man K, Fan ST, Ng IO, Lo CM, Liu CL, Wong J. Prospective evaluation of Pringle maneuver in hepatectomy for liver tumors by a randomized study. *Ann Surg.* 1997;226(6):3. <https://doi.org/>.
233. Man K, Lo CM, Liu CL, et al. Effects of the intermittent Pringle manoeuvre on hepatic gene expression and ultrastructure in a randomized clinical study. *Br J Surg.* 2003;90(2):183–189. <https://doi.org/10.1002/bjs.4027>.
234. Capussotti L, Muratore A, Ferrero A, Massucco P, Ribero D, Polastri R. Randomized clinical trial of liver resection with and without hepatic pedicle clamping. *Br J Surg.* 2006;93(6):685–689. <https://doi.org/10.1002/bjs.5301>.
235. Lee KF, Cheung YS, Wong J, Chong CC, Wong JS, Lai PB. Randomized clinical trial of open hepatectomy with or without intermittent Pringle manoeuvre. *Br J Surg.* 2012;99(9):1203–1209. <https://doi.org/10.1002/bjs.8863>.
236. Lee KF, Wong J, Cheung SYS, et al. Does intermittent Pringle maneuver increase postoperative complications after hepatectomy for hepatocellular carcinoma? A randomized controlled trial. *World J Surg.* 2018. <https://doi.org/10.1007/s00268-018-4637-3>.
237. Hanyong S, Wankee L, Siyuan F, et al. A prospective randomized controlled trial: comparison of two different methods of hepatectomy. *Eur J Surg Oncol.* 2015;41(2):243–248. <https://doi.org/10.1016/j.ejso.2014.10.057>.
238. Makuuchi M, Mori T, Gunven P, Yamazaki S, Hasegawa H. Safety of hemihepatic vascular occlusion during resection of the liver. *Surg Gynecol Obstet.* 1987;164(2):155–158. <https://doi.org/>.
239. Figueiras J, Llado L, Ruiz D, et al. Complete versus selective portal triad clamping for minor liver resections: a prospective randomized trial. *Ann Surg.* 2005;241(4):582–590. <https://doi.org/>.
240. Liang G, Wen T, Yan L, et al. A prospective randomized comparison of continuous hemihepatic with intermittent total hepatic inflow occlusion in hepatectomy for liver tumors. *HepatoGastroenterology.* 2009;56(91–92):745–750. <https://doi.org/>.
241. Fu SY, Lau WY, Li GG, et al. A prospective randomized controlled trial to compare Pringle maneuver, hemihepatic vascular inflow occlusion, and main portal vein inflow occlusion in partial hepatectomy. *Am J Surg.* 2011;201(1):62–69. <https://doi.org/10.1016/j.amjsurg.2009.09.029>.
242. Ni JS, Lau WY, Yang Y, et al. A prospective randomized controlled trial to compare pringle manoeuvre with hemi-hepatic vascular inflow occlusion in liver resection for hepatocellular carcinoma with cirrhosis. *J Gastrointest Surg.* 2013;17(8):1414–1421. <https://doi.org/10.1007/s11605-013-2236-z>.
243. Huguet C, Nordlinger B, Galopin JJ, Bloch P, Gallot D. Normothermic hepatic vascular exclusion for extensive hepatectomy. *Surg Gynecol Obstet.* 1978;147(5):689–693. <https://doi.org/>.
244. Belghiti J, Noun R, Zante E, Ballet T, Sauvanet A. Portal triad clamping or hepatic vascular exclusion for major liver resection. A controlled study. *Ann Surg.* 1996;224(2):155–161. <https://doi.org/>.
245. Azoulay D, Lim C, Salloum C, et al. Complex liver resection using standard total vascular exclusion, venovenous bypass, and in situ hypothermic portal perfusion: an audit of 77 consecutive cases. *Ann Surg.* 2015;262(1):93–104. <https://doi.org/10.1097/SLA.0000000000000787>.
246. Elias D, Lasser P, Debaene B, et al. Intermittent vascular exclusion of the liver (without vena cava clamping) during major hepatectomy. *Br J Surg.* 1995;82(11):1535–1539. <https://doi.org/>.
247. Smyrniotis VE, Kostopanagiotou GG, Gamaletsos EL, et al. Total versus selective hepatic vascular exclusion in major liver resections. *Am J Surg.* 2002;183(2):173–178. <https://doi.org/>.
248. Smyrniotis VE, Kostopanagiotou GG, Contis JC, et al. Selective hepatic vascular exclusion versus Pringle maneuver in major liver resections: prospective study. *World J Surg.* 2003;27(7):765–769. <https://doi.org/>.
249. Melendez JA, Arslan V, Fischer ME, et al. Perioperative outcomes of major hepatic resections under low central venous pressure anesthesia: blood loss, blood transfusion, and the risk of postoperative renal dysfunction. *J Am Coll Surg.* 1998;187(6):620–625. <https://doi.org/>.
250. Jones RM, Moulton CE, Hardy KJ. Central venous pressure and its effect on blood loss during liver resection. *Br J Surg.* 1998;85(8):1058–1060. <https://doi.org/10.1046/j.1365-2168.1998.00795.x>.
251. Smyrniotis V, Kostopanagiotou G, Theodoraki K, Tsantoulas D, Contis JC. The role of central venous pressure and type of vascular control in blood loss during major liver resections. *Am J Surg.* 2004;187(3):398–402. <https://doi.org/10.1016/j.amjsurg.2003.12.001>.
252. Bui LL, Smith AJ, Bercovici M, Szalai JP, Hanna SS. Minimising blood loss and transfusion requirements in hepatic resection. *HPB (Oxford).* 2002;4(1):5–10. <https://doi.org/10.1080/136518202753598672>.
253. Chen H, Merchant NB, Didolkar MS. Hepatic resection using intermittent vascular inflow occlusion and low central venous pressure anesthesia improves morbidity and mortality. *J Gastrointest Surg.* 2000;4(2):162–167. <https://doi.org/>.

254. Wang WD, Liang LJ, Huang XQ, Yin XY. Low central venous pressure reduces blood loss in hepatectomy. *World J Gastroenterol*. 2006;12(6):935–939. <https://doi.org/>.
255. Liu Y, Duan S, Peng X, Lai Y, Li Y. Effect of controlled low central venous pressure on renal function in major liver resection. *Chin-Germ J Clin Oncol*. 2008;7:7–9.
256. Hughes MJ, Ventham NT, Harrison EM, Wigmore SJ. Central venous pressure and liver resection: a systematic review and meta-analysis. *HPB (Oxford)*. 2015;17(10):863–871. <https://doi.org/10.1111/hpb.12462>.
257. Chhibber A, Dzialk J, Kolano J, Norton JR, Lustik S. Anesthesia care for adult live donor hepatectomy: our experiences with 100 cases. *Liver Transpl*. 2007;13(4):537–542. <https://doi.org/10.1002/lt.21074>.
258. Kim YK, Chin JH, Kang SJ, et al. Association between central venous pressure and blood loss during hepatic resection in 984 living donors. *Acta Anaesthesiol Scand*. 2009;53(5):601–606. <https://doi.org/10.1111/j.1399-6576.2009.01920.x>.
259. Melendez JA, Arslan V, Fischer ME, et al. Perioperative outcomes of major hepatic resections under low central venous pressure anesthesia: blood loss, blood transfusion, and the risk of postoperative renal dysfunction. *J Am Coll Surg*. 1998;187(6):620–625. <https://doi.org/>.
260. Ryu HG, Nahm FS, Sohn HM, Jeong EJ, Jung CW. Low central venous pressure with milrinone during living donor hepatectomy. *Am J Transplant*. 2010;10(4):877–882. <https://doi.org/10.1111/j.1600-6143.2010.03051.x>.
261. Sand L, Rizell M, Houltz E, et al. Effect of patient position and PEEP on hepatic, portal and central venous pressures during liver resection. *Acta Anaesthesiol Scand*. 2011;55(9):1106–1112. <https://doi.org/10.1111/j.1399-6576.2011.02502.x>.
262. Rahbari NN, Koch M, Zimmermann JB, et al. Infrahepatic inferior vena cava clamping for reduction of central venous pressure and blood loss during hepatic resection: a randomized controlled trial. *Ann Surg*. 2011;253(6):1102–1110. <https://doi.org/10.1097/SLA.0b013e318214bee5>.
263. Otsubo T, Takasaki K, Yamamoto M, et al. Bleeding during hepatectomy can be reduced by clamping the inferior vena cava below the liver. *Surgery*. 2004;135(1):67–73. <https://doi.org/10.1016/s0039>.
264. Chen XP, Zhang ZW, Zhang BX, et al. Modified technique of hepatic vascular exclusion: effect on blood loss during complex mesohepatectomy in hepatocellular carcinoma patients with cirrhosis. *Langenbecks Arch Surg*. 2006;391(3):209–215. <https://doi.org/10.1007/s00423-006-0043-7>.
265. Kato M, Kubota K, Kita J, Shimoda M, Rokkaku K, Sawada T. Effect of infra-hepatic inferior vena cava clamping on bleeding during hepatic dissection: a prospective, randomized, controlled study. *World J Surg*. 2008;32(6):1082–1087. <https://doi.org/10.1007/s00268-007-9445-0>.
266. Zhu P, Lau WY, Chen YF, et al. Randomized clinical trial comparing infrahepatic inferior vena cava clamping with low central venous pressure in complex liver resections involving the Pringle manoeuvre. *Br J Surg*. 2012;99(6):781–788. <https://doi.org/10.1002/bjs.8714>.
267. Zhou YM, Sui CJ, Zhang XF, Li B, Yang JM. Anterior approach combined with infrahepatic inferior vena cava clamping right hepatic resection for large hepatocellular carcinoma: a prospective randomized controlled trial. *Medicine (Baltimore)*. 2016;95(27):e4159. <https://doi.org/10.1097/md.00000000000004159>.
268. Ueno M, Kawai M, Hayami S, et al. Partial clamping of the infrahepatic inferior vena cava for blood loss reduction during anatomic liver resection: a prospective, randomized, controlled trial. *Surgery*. 2017;161(6):1502–1513. <https://doi.org/10.1016/j.surg.2016.12.010>.
269. Fancellu A, Petrucciani N, Melis M, et al. Usefulness of infra-hepatic inferior vena cava clamping during liver resection: a meta-analysis of randomized controlled trials. *J Gastrointest Surg*. 2018;22(5):941–951. <https://doi.org/10.1007/s11605-018-3720-2>.
270. Lodge JP, Jonas S, Oussoultzoglou E, et al. Recombinant coagulation factor VIIa in major liver resection: a randomized, placebo-controlled, double-blind clinical trial. *Anesthesiology*. 2005;102(2):269–275. <https://doi.org/>.
271. Shao YF, Yang JM, Chau GY, et al. Safety and hemostatic effect of recombinant activated factor VII in cirrhotic patients undergoing partial hepatectomy: a multicenter, randomized, double-blind, placebo-controlled trial. *Am J Surg*. 2006;191(2):245–249. <https://doi.org/10.1016/j.amjsurg.2005.10.019>.
272. Wu CC, Ho WM, Cheng SB, et al. Perioperative parenteral tranexamic acid in liver tumor resection: a prospective randomized trial toward a blood transfusion-free hepatectomy. *Ann Surg*. 2006;243(2):173–180. <https://doi.org/10.1097/01.sla.0000197561.70972.73>.
273. Moggia E, Rouse B, Simillis C, et al. Methods to decrease blood loss during liver resection: a network meta-analysis. *Cochrane Database Syst Rev*. 2016;10:CD010683. <https://doi.org/10.1002/14651858.CD010683.pub3>.
274. Wax DB, Zerillo J, Tabrizian P, et al. A retrospective analysis of liver resection performed without central venous pressure monitoring. *Eur J Surg Oncol*. 2016;42(10):1608–1613. <https://doi.org/10.1016/j.ejso.2016.03.025>.
275. Niemann CU, Feiner J, Behrends M, Eilers H, Ascher NL, Roberts JP. Central venous pressure monitoring during living right donor hepatectomy. *Liver Transpl*. 2007;13(2):266–271. <https://doi.org/10.1002/lt.21051>.
276. Choi SJ, Gwak MS, Ko JS, et al. Can peripheral venous pressure be an alternative to central venous pressure during right hepatectomy in living donors? *Liver Transpl*. 2007;13(10):1414–1421. <https://doi.org/10.1002/lt.21255>.
277. Stephan F, Rezaioglu-Delclaux S. Usefulness of a central venous catheter during hepatic surgery. *Acta Anaesthesiol Scand*. 2008;52(3):388–396. <https://doi.org/10.1111/j.1399-6576.2007.01553.x>.
278. Kim YK, Shin WJ, Song JG, Jun IG, Hwang GS. Does stroke volume variation predict intraoperative blood loss in living right donor hepatectomy? *Transplant Proc*. 2011;43(5):1407–1411. <https://doi.org/10.1016/j.transproceed.2011.02.056>.
279. Ratti F, Cipriani F, Reineke R, et al. Intraoperative monitoring of stroke volume variation versus central venous pressure in laparoscopic liver surgery: a randomized prospective comparative trial. *HPB (Oxford)*. 2016;18(2):136–144. <https://doi.org/10.1016/j.hpb.2015.09.005>.
280. Dunki-Jacobs EM, Philips P, Scoggins CR, McMasters KM, Martin RC. Stroke volume variation in hepatic resection: a replacement for standard central venous pressure monitoring. *Ann Surg Oncol*. 2014;21(2):473–478. <https://doi.org/10.1245/s10434-013-3323-9>.
281. Lee J, Kim WH, Ryu HG, et al. Stroke volume variation–guided versus central venous pressure–guided low central venous pressure with milrinone during living donor hepatectomy: a randomized double-blinded clinical trial. *Anesth Analg*. 2017;125(2):423–430. <https://doi.org/10.1213/ane.0000000000002197>.
282. De Pietri L, Bianchini M, Montalti R, et al. Thrombelastography–guided blood product use before invasive procedures in cirrhosis with severe coagulopathy: a randomized, controlled trial. *Hepatology*. 2016;63(2):566–573. <https://doi.org/10.1002/hep.28148>.
283. Schreiber KL, Chelly JE, Lang RS, et al. Epidural versus paravertebral nerve block for postoperative analgesia in patients undergoing open liver resection: a randomized clinical trial. *Reg Anesth Pain Med*. 2016;41(4):460–468. <https://doi.org/10.1097/aap.0000000000000422>.
284. Ali M, Winter DC, Hanly AM, O'Hagan C, Keaveny J, Broe P. Prospective, randomized, controlled trial of thoracic epidural or patient–controlled opiate analgesia on perioperative quality of life. *Br J Anaesth*. 2010;104(3):292–297. <https://doi.org/10.1093/bja/aeq006>.
285. Matot I, Scheinin O, Eid A, Jurim O. Epidural anesthesia and analgesia in liver resection. *Anesth Analg*. 2002;95(5):81; table of contents <https://doi.org/>.
286. Tsui SL, Yong BH, Ng KF, Yuen TS, Li CC, Chui KY. Delayed epidural catheter removal: the impact of postoperative coagulopathy. *Anaesth Intensive Care*. 2004;32(5):630–636. <https://doi.org/>.
287. Yuan FS, Ng SY, Ho KY, Lee SY, Chung AY, Poopalalingam R. Abnormal coagulation profile after hepatic resection: the effect of chronic hepatic disease and implications for epidural analgesia. *J Clin Anesth*. 2012;24(5):398–403. <https://doi.org/10.1016/j.jclinane.2011.11.005>.
288. Elterman KG, Xiong Z. Coagulation profile changes and safety of epidural analgesia after hepatectomy: a retrospective study. *J Anesth*. 2015;29(3):367–372. <https://doi.org/10.1007/s00540-014-1933-4>.
289. Jacquinod P, Wallon G, Gazon M, et al. Incidence and risk factors of coagulation profile derangement after liver surgery: implications for the use of epidural analgesia—a retrospective cohort study. *Anesth Analg*. 2018;126(4):1142–1147. <https://doi.org/10.1213/ane.0000000000002457>.

290. Christie IW, McCabe S. Major complications of epidural analgesia after surgery: results of a six-year survey. *Anaesthesia*. 2007;62(4):335–341.
291. Cook TM, Counsell D, Wildsmith JA. Major complications of central neuraxial block: report on the third national audit project of the Royal College of Anaesthetists. *Br J Anaesth*. 2009;102(2):179–190. <https://doi.org/10.1093/bja/aen360>.
292. Ko JS, Gwak MS, Choi SJ, et al. The effects of desflurane and sevoflurane on hepatic and renal functions after right hepatectomy in living donors*. *Transpl Int*. 2010;23(7):736–744. <https://doi.org/10.1111/j.1432-2277.2009.01050.x>.
293. Toprak HI, Sahin T, Aslan S, Karahan K, Sanli M, Ersoy MO. Effects of desflurane and isoflurane on hepatic and renal functions and coagulation profile during donor hepatectomy. *Transplant Proc*. 2012;44(6):1635–1639. <https://doi.org/10.1016/j.transproceed.2012.05.047>.
294. Ko JS, Gwak MS, Choi SJ, et al. The effects of desflurane and propofol–remifentanil on postoperative hepatic and renal functions after right hepatectomy in liver donors. *Liver Transpl*. 2008;14(8):1150–1158. <https://doi.org/10.1002/lt.21490>.
295. Decailliot F, Cherqui D, Leroux B, et al. Effects of portal triad clamping on haemodynamic conditions during laparoscopic liver resection. *Br J Anaesth*. 2001;87(3):493–496. <https://doi.org/>.
296. Delva E, Camus Y, Paugam C, Parc R, Huguet C, Lienhart A. Hemodynamic effects of portal triad clamping in humans. *Anesth Analg*. 1987;66(9):864–868. <https://doi.org/>.
297. Decailliot F, Streich B, Heurtematte Y, Duvaldestin P, Cherqui D, Stephan F. Hemodynamic effects of portal triad clamping with and without pneumoperitoneum: an echocardiographic study. *Anesth Analg*. 2005;100(3):864–868; table of contents. <https://doi.org/10.1213/01.ane.0000144592.20499.12>.
298. Ni CY, Yang Y, Chang YQ, et al. Fast-track surgery improves post-operative recovery in patients undergoing partial hepatectomy for primary liver cancer: a prospective randomized controlled trial. *Eur J Surg Oncol*. 2013;39(6):542–547. <https://doi.org/10.1016/j.ejso.2013.03.013>.
299. Qi S, Chen G, Cao P, et al. Safety and efficacy of enhanced recovery after surgery (ERAS) programs in patients undergoing hepatectomy: a prospective randomized controlled trial. *J Clin Lab Anal*. 2018;e22434. <https://doi.org/10.1002/jcla.22434>.
300. He F, Lin X, Xie F, Huang Y, Yuan R. The effect of enhanced recovery program for patients undergoing partial laparoscopic hepatectomy of liver cancer. *Clin Transl Oncol*. 2015;17(9):694–701. <https://doi.org/10.1007/s12094-015-1296-9>.
301. Liang X, Ying H, Wang H, et al. Enhanced recovery care versus traditional care after laparoscopic liver resections: a randomized controlled trial. *Surg Endosc*. 2018;32(6):2746–2757. <https://doi.org/10.1007/s00464-017-5973-3>.
302. Melloul E, Hubner M, Scott M, et al. Guidelines for perioperative care for liver surgery: Enhanced Recovery after Surgery (ERAS) Society recommendations. *World J Surg*. 2016;40(10):2425–2440. <https://doi.org/10.1007/s00268-016-3700-1>.
303. Bond-Smith G, Belgaumkar AP, Davidson BR, Gurusamy KS. Enhanced recovery protocols for major upper gastrointestinal, liver and pancreatic surgery. *Cochrane Database Syst Rev*. 2016;2:CD011382. <https://doi.org/10.1002/14651858.CD011382.pub2>.

RICHARD M. PINO and ABRAHAM SONNY

KEY POINTS

- A molecule in the plasma must pass in succession through the endothelial fenestration, glomerular basement membrane (GBM), and epithelial slit diaphragm to cross the filtration barrier and enter the tubular fluid. The capillary endothelium restricts the passage of cells, while the GBM restricts albumin and larger molecules. The negatively charged glycoproteins of the GBM limit the passage of other negatively charged proteins. Thus, the filtration barrier is size selective and charge selective. The epithelial cells maintain the integrity of this capillary bed by producing several key signaling molecules and endocytosis of membrane receptors.
- A primary determinant of glomerular filtration rate (GFR) is glomerular filtration pressure, which depends on renal artery perfusion pressure and the balance between afferent and efferent arteriolar tone. With decreases in afferent arteriolar pressure or blood flow, mediators such as catecholamines, angiotensin II, and arginine vasopressin (AVP) constrict efferent arterioles to maintain glomerular filtration pressure. This is reflected by an increase in GFR.
- Tubuloglomerular feedback is a critical mechanism for renal autoregulation. When GFR is increased, distal tubular NaCl delivery is enhanced and the increase in chloride concentration is sensed by the macula densa to trigger the renin-angiotensin cascade. The result is afferent arteriolar vaso constriction as efferent arteriolar vasoconstriction increases GFR. Autoregulation enables the kidney to maintain solute and water regulation independently of wide fluctuations in arterial blood pressure. Tubular water reabsorption determines urinary flow rate and is closely related to the hydrostatic pressure in the peritubular capillaries. Hypotension of any cause results in decreased urinary flow rate that may be correctable only when arterial blood pressure is restored toward normal.
- The tubule has an enormous capacity for reabsorption of water and NaCl. Each day, 180 L of protein-free glomerular ultrafiltrate is formed, of which almost 99% of the water and 99% of the sodium is reabsorbed. The ability of the kidney to concentrate urine is dependent on the interaction of at least three processes: (1) generation of a hypertonic medullary interstitium by the countercurrent mechanism and urea recycling, (2) concentration and then dilution of tubular fluid in the loop of Henle, and (3) the action of AVP, also known as antidiuretic hormone, in increasing water permeability in the last part of the distal tubule and collecting ducts. The juxtaglomerular apparatus provides an important regulating system for arterial blood pressure, salt, and water homeostasis.
- The interactions of the sympathoadrenal axis, renin-angiotensin-aldosterone system, and AVP will respond to hypotension and hypovolemia by promoting vasoconstriction and the retention of salt and water. Prostaglandins and natriuretic peptides facilitate vasodilation and the excretion of salt and water excretion when there is hypertension and hypervolemia.
- Plasma osmolality is tightly controlled. The threshold for AVP secretion by the neurohypophysis between 280 and 290 mOsm/kg. Even mild dehydration results in rapid antidiuresis, and urine osmolality can increase from 300 to 1200 mOsm/kg. Decreases in intravascular volume stimulate AVP secretion.
- Serum creatinine reflects the balance between creatinine production from muscle and creatinine excretion by the kidney, which is dependent on GFR. Creatinine generation rate varies with muscle mass, physical activity, protein intake, and catabolism. However, when these processes are in equilibrium and renal function is stable, serum creatinine is a useful marker of GFR. The relationship between serum creatinine and GFR is inverse and exponential. A doubling of the serum creatinine implies a halving of GFR.

Introduction

The kidney exemplifies an exquisite structure-function relationship to regulate intravascular volume, osmolality, acid-base and electrolyte balance, and to excrete end products of metabolism and drugs. The kidney also produces hormones involved with fluid homeostasis (renin, prostaglandins, kinins), bone metabolism (1,25-dihydroxycholecalciferol) and hematopoiesis (erythropoietin).¹ In addition to these multiple roles in the healthy patient, almost every systemic disease will affect renal function. This chapter will describe the normal anatomy and physiology of the kidney and the basics for the clinical evaluation of renal function.

Organization of the Kidney

THE NEPHRON

The fundamental unit of the kidney is the nephron (Figs. 17.1 and 17.2). The nephron is composed of a vascular network close to a series of tubules with distinct physiologic functions that empty into collecting ducts to form urine. There are approximately 1 million nephrons in the normal kidney. The kidneys receive about 20% of the cardiac output and are responsible for 7% of total body oxygen consumption, although they account for only 0.5% of the total body weight.² Afferent arterioles from the renal arteries

branch extensively to supply the renal and peritubular capillaries. Kidney disease can result from perturbations of these vascular, glomerular, and tubular components (see Chapter 42). Knowledge of these factors is important to the anesthesiologist to limit decrements in renal function during the perioperative period.

The kidney is divided into an outer layer, the cortex, which receives 85% to 90% of the renal blood flow (RBF), and an inner medulla (see Fig. 17.1). In the cortex are glomeruli (see Figs. 17.2 and 17.3), tufts of capillaries originating from afferent arterioles. The glomerular capillary endothelial cells have fenestrations that are barriers to red blood cells but allow the transit of plasma proteins and smaller molecules (Fig. 17.4). Their glycocalyx is an anionic barrier that repels large macromolecules and albumin. Knowledge of this is through experimental studies and diseases where albuminuria is seen after alteration of anionic sites in the glomerular basement membrane (GBM).^{3,4} During development, these capillaries invaginate epithelial cells to form tufts of visceral epithelial cells with footlike morphologies called podocytes that are rich in actin cytoskeletons. These podocytes anchor to the GBM, closely interdigitate, and envelope the renal capillaries (Fig. 17.5). A thin membrane called the slit diaphragm has an ultrastructural zipper-like complex that spans the space between each of the foot processes of the podocytes.⁵ Additional epithelial cells and their extravascular matrix make up the parietal

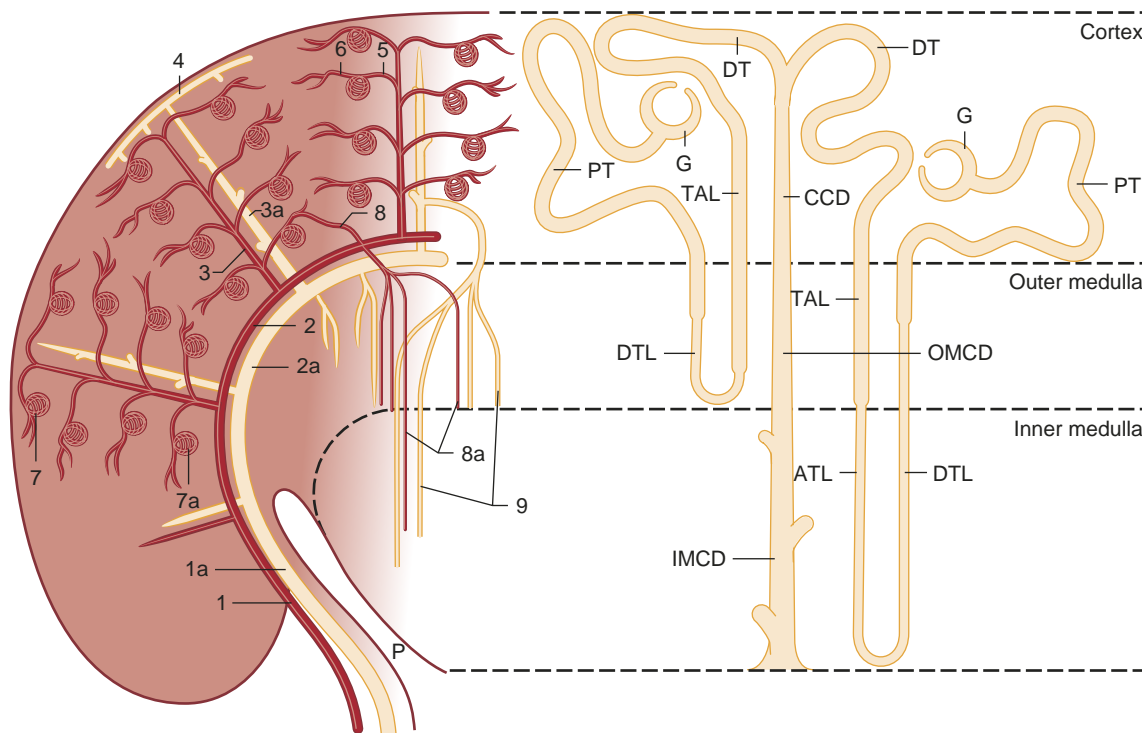


Fig. 17.1 Anatomic relationships of the nephron and the renal vasculature. The left side of the diagram represents the renal vasculature as distributed through the inner medulla, outer medulla, and cortex. Arteries are drawn as solid lines, veins as hollow tubes. The renal artery divides serially into interlobar arteries (1), arcuate arteries (2), and interlobular arteries (3). The afferent arterioles (5) branch off laterally and provide the capillary tufts of the renal glomeruli in the outer cortex (7a), whose efferent arterioles (6) supply the cortical capillary network (not shown). In the juxamedullary zone (7b), the efferent arterioles become the vasa recta, which are closely applied to the long loops of Henle (8, 8a, 9). The venous drainage consists of stellate veins (4), interlobular veins (3a), arcuate veins (2a), and interlobar veins (1a). (Modified from Kriz W, Bankir L. A standard nomenclature for structures of the kidney. The Renal Commission of the International Union of Physiological Sciences (IUPS). *Kidney Int*. 1988;33[1]:1-7.)

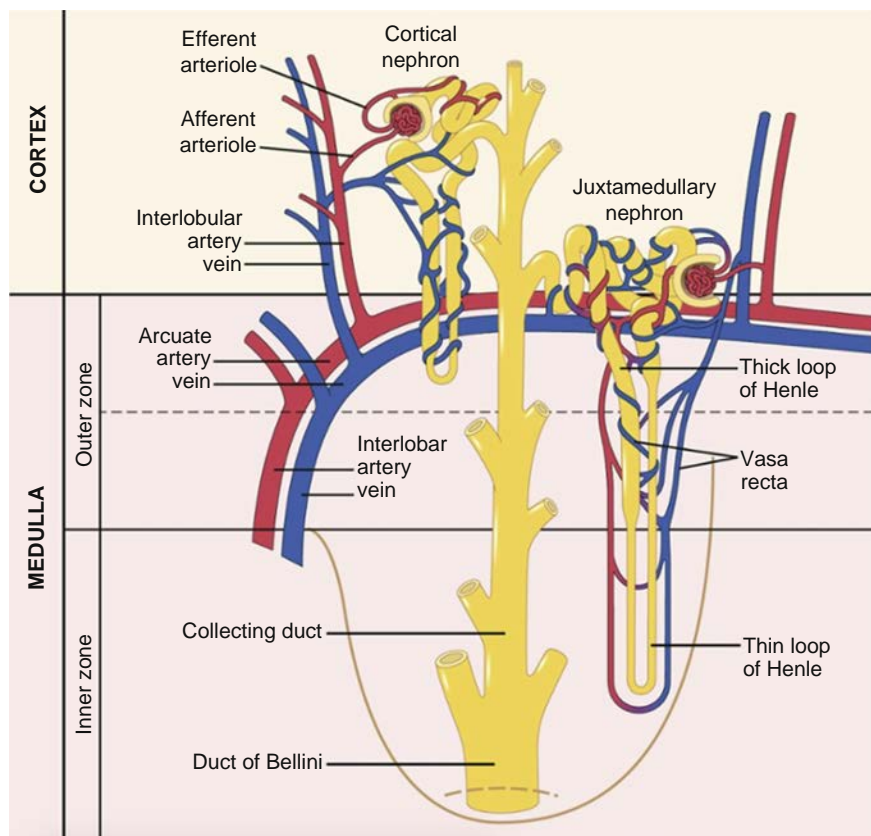


Fig. 17.2 Schematic of relations between blood vessels and tubular structures. (Redrawn from Hall JE. *Guyton and Hall Textbook of Medical Physiology*. 13th ed. Philadelphia: Elsevier; 2016.)

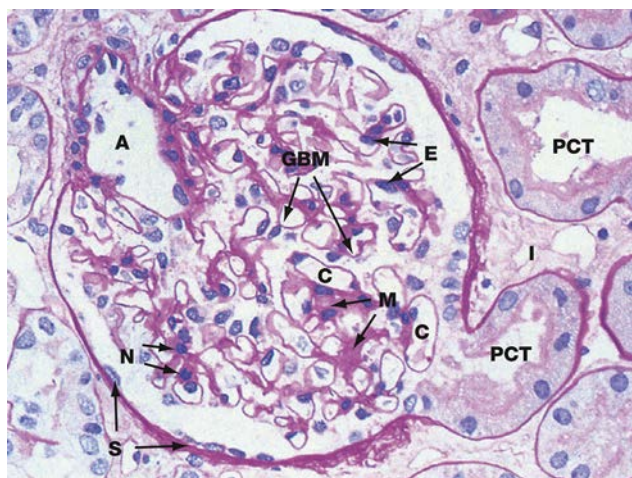


Fig. 17.3 Glomerulus. An afferent arteriole (A) enters the glomerulus and divides into numerous capillaries (C) adjacent to the glomerular basement membrane (GBM). The squamous epithelial cells (S) lining Bowman space lead to the cuboidal proximal convoluted tubules (PCT) with brush borders. E, Nuclei of endothelial cells; M, mesangium; N, nuclei of mesangial cells. (From Young B, Woodford P, O'Dowd G. *Urinary system*. In: *Wheaton's Functional Histology. A Text and Colour Atlas*. 6th ed. Philadelphia: Elsevier Churchill Livingstone; 2014.)

epithelium that lines a pouch-like cistern, called Bowman space, which is the beginning of the renal tubular system.

The vasculature of the kidney is unique in that it has two capillary beds. Upon leaving the glomerulus, the glomerular

capillary then forms the efferent artery that in turn leads to an anastomosing network of 10 to 25 long peritubular capillaries called vasa recta. The vasa recta are close around the ascending limb of the loop of Henle before anastomosis into veins that leave the kidney (see Fig. 17.2).

The endothelial and epithelial cells synthesize proteins that are essential components of the filtration barrier of the kidney, the GBM (see Fig. 17.5).⁶ The GBM is rich in the anionic glycosaminoglycan heparin sulfate, Type IV collagen, and laminin.^{6,7} The epithelial cells maintain the integrity of this capillary bed by producing several key molecules including vascular endothelial growth factor⁸ and families of signaling proteins and receptors. The transmembrane protein nephrin supports the integrity of the slit pore diaphragms and its maintenance is dependent on the endocytosis of slit diaphragm proteins and plasma membrane components.^{7,9,10} The interplay between the foot processes of the podocytes, slit diaphragms, and organization of the actin intracellular scaffolds is centered on nephrin and related proteins.¹¹ The functions of these numerous factors are often elucidated in experimental studies when found as etiologies of renal disease.^{7,11}

THE RENAL TUBULES

The kidneys receive 20% of the total cardiac output but extract relatively little oxygen. The renal arteriovenous oxygen difference is only 1.5 mL/dL. However, there is marked dissimilarity between the renal cortex and medulla with regard to blood flow, oxygen delivery, and oxygen consumption (Table 17.1). The medulla receives only 6% of the

RBF and has an average oxygen tension (PO_2) of 8 mm Hg. Thus, severe hypoxia could develop in the medulla despite a relatively adequate total RBF; the metabolically active medullary thick ascending loop of Henle (mTAL) is particularly vulnerable.¹²

The terminology of the renal tubular system is based on morphology as seen with light microscopy. The system begins with the proximal convoluted tubule (PCT) that starts as a continuation of the parietal epithelium of the nephron (see Fig. 17.3). A high density of mitochondria and the extensive surface area of the apical (referred as the

brush border) and basilar cell membranes mark the renal tubules and indicate high-energy requirements. In normal kidneys, 80% of the energy is required for Na^+/K^+ -ATPase that maintains the osmotic gradient needed for the resorption of filtered molecules (Fig. 17.6).² In spite of this high-energy demand, the tubular system is supplied by only 10% to 15% of the RBF and is a key etiology for acute tubular necrosis after hypotension (see Chapter 42).

A distal short straight length of the proximal tubule leads to the thinner epithelium of the descending thin limb of the loop of Henle. This makes a hairpin 180-degree turn to ascend toward the cortex and eventually becomes the medullary thick ascending limb of the loop of Henle (mTAL) and distal convoluted tube (see Fig. 17.2). Seventy to 80% of nephrons begin in the cortex and have short loops of Henle that enter only the outer margin of the medulla. The remaining juxamedullary nephrons start at the corticomedullary junction and have elongated loops of Henle that descend into the most distal extent of the medulla. At the end of the distal tubule is the juxtaglomerular apparatus that is comprised of specialized epithelial cells, called the macula densa (by virtue of light microscopic image), cells of the afferent glomerular arteriole, and mesangial cells (Fig. 17.7). The juxtaglomerular apparatus is essential for the maintenance of blood pressure, as described later. The most distal end of the nephron is the collecting duct that empties the ultrafiltrate into the renal pelvis and then the ureters.



Fig. 17.4 Electron micrograph of glomerulus. The several glomerular capillaries (C) are lined by fenestrated endothelial cells. The podocytes (P) give rise to foot processes (P_1, P_2) that rest on the glomerular basement membrane (BM). Mesangial cells (M) support the capillary loops. Bowman space (BS) is delineated by the podocyte bodies on one side and the parietal epithelial cells on the other. E, Nucleus of capillary; IPS, interpodocyte space; MM, mesangial matrix; SPS, subpodocyte space. (From Young B, Woodford P, O'Dowd G. Urinary system. In: *Wheaton's Functional Histology. A Text and Colour Atlas*. 6th ed. Philadelphia: Elsevier Churchill Livingstone; 2014.)

FORMATION OF URINE

Urine is formed by the interaction of three processes: glomerular filtration, tubular reabsorption, and tubular secretion.

Glomerular Filtration

The formation of the glomerular filtrate is dependent on the balance of Starling forces regulating fluid flux across the filtration barrier.¹³ Central to this process is the pressure difference between the afferent and efferent arteries (Fig. 17.8). The hydrostatic pressure in the glomerular

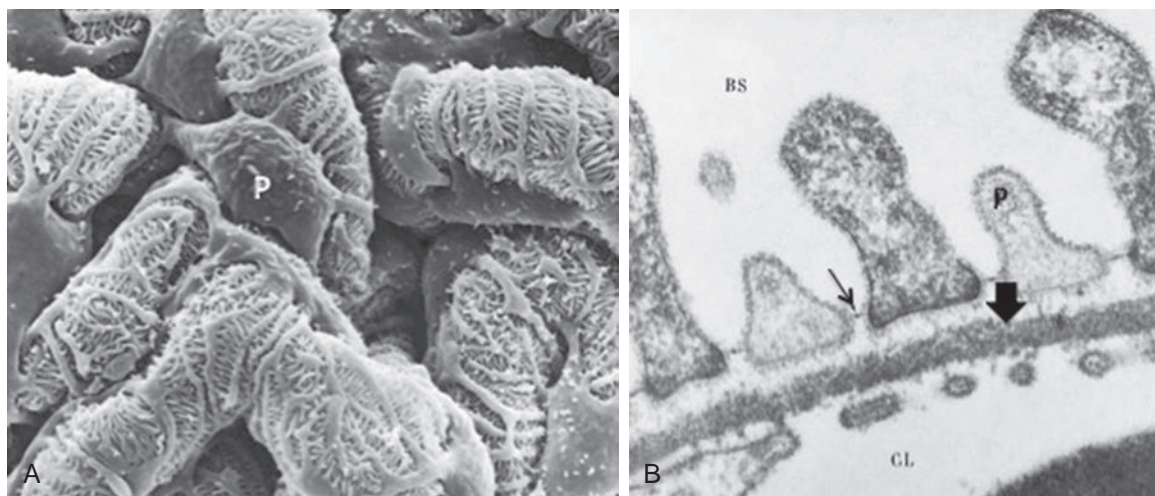


Fig. 17.5 (A) Scanning electron micrograph of podocytes (P) and their processes. (B) Electron micrograph of podocyte processes (P), the glomerular basement membrane, and glomerular capillaries. Slit diaphragms (arrow) span the podocyte processes. Large arrow points to the lamina densa of the glomerular basement membrane. BS, Bowman space; CL, glomerular capillary lumen. (Modified from Gartner LP. Urinary system. In: *Textbook of Histology*. 4th ed. Philadelphia: Elsevier; 2017.)

capillaries is 60 mm Hg, which is three times higher than in most capillary beds. This pressure difference drives plasma across the endothelial and epithelial filtration barriers (Table 17.2). A delicate balance in pressure maintenance is necessary because reduced pressures will decrease filtration, as increased pressures may cause renal damage. The glomerular filtration rate (GFR) depends upon the glomerular capillary pressure that is opposed by the hydrostatic pressure in Bowman space and the colloid osmotic pressure within the glomerular capillaries (Figs. 17.8 and 17.9). In healthy patients, the colloid osmotic pressure in Bowman

TABLE 17.1 Distribution of Renal Blood Flow Between Cortex and Medulla

	Cortex	Medulla*
Percentage of renal blood flow	94	6
Blood flow (mL/min/g)	5.0	0.03
PO ₂ (mm Hg)	50	8
O ₂ extraction ratio (VO ₂ /DO ₂)	0.18	0.79

*The renal medulla receives only a small fraction of the total renal blood flow, and flow rates are extremely slow. As a result, the tissue oxygen tension is extremely low, and the medulla extracts almost 80% of the oxygen delivered to it. A very mild reduction in total and cortical renal blood flow may therefore induce ischemia and hypoxia in the renal medulla. DO₂, Oxygen delivery; O₂, oxygen; PO₂, oxygen tension; VO₂, oxygen consumption.

Data from Brezis M, Rosen S, Epstein F. The pathophysiological implications of medullary hypoxia. *Am J Kidney Dis*. 1989;13:253–258.

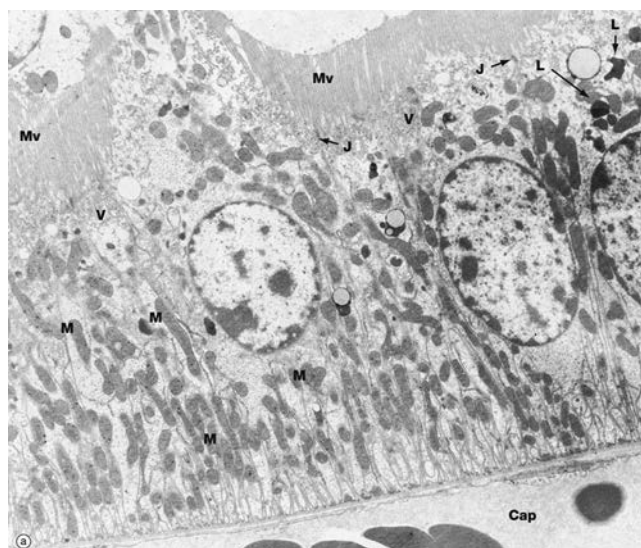


Fig. 17.6 Proximal convoluted tubule. The apical surface of the proximal convoluted tubule epithelium is marked by tall microvilli (Mv) that are seen as the brush border in light micrographs. The cytoplasm at the basal surface is filled with mitochondria (M) that are reflective of the high oxygen requirement needed for the maintenance of the basal lateral Na⁺/K⁺ ATPase. Cap, tubular capillary; J, tight intercellular junction; L, lysosome; V, vesicle. (From Young B, Woodford P, O'Dowd G. Urinary system. In: *Wheaton's Functional Histology. A Text and Colour Atlas*. 6th ed. Philadelphia: Elsevier Churchill Livingstone; 2014.)

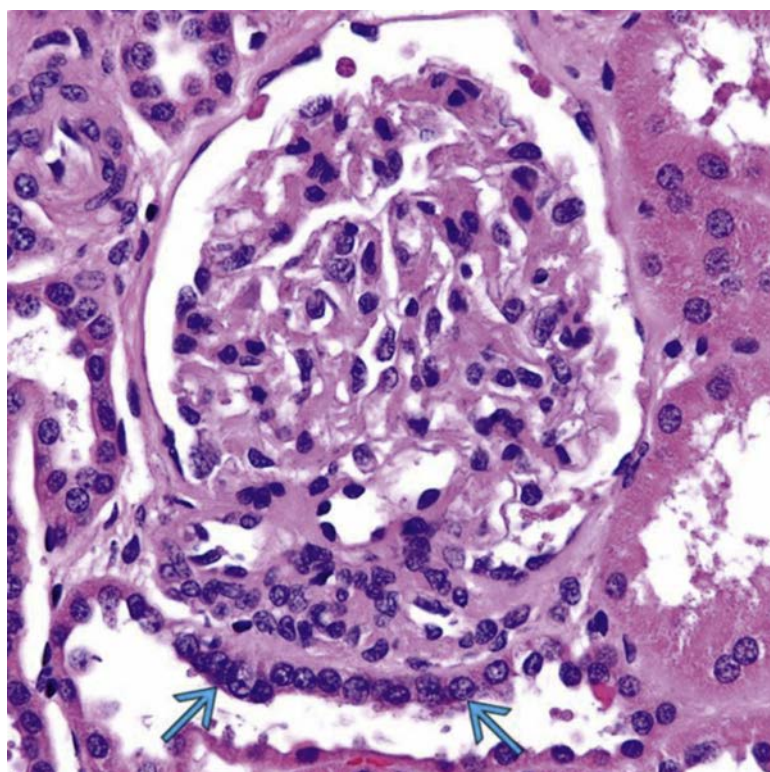
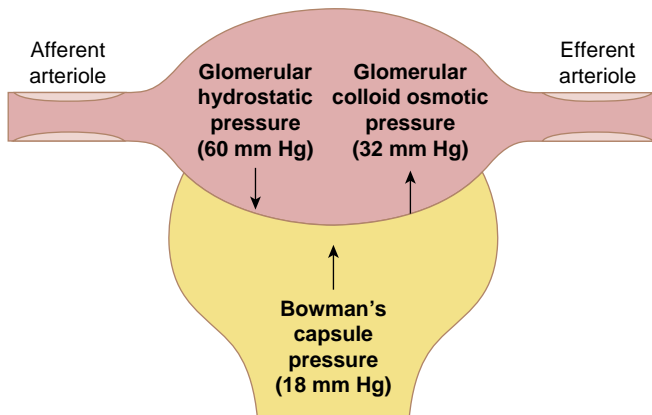


Fig. 17.7 The macula densa (arrows). The cells of the macula densa represent a special portion of the distal tubule that is adjacent to the juxtaglomerular apparatus. (From Genitourinary and male genital tract. In: Lindberg MR, Lamps LW, eds. *Diagnostic Pathology: Normal Histology*. 2nd ed. Philadelphia: Elsevier; 2018.)



$$\text{Net filtration pressure (10 mm Hg)} = \text{Glomerular hydrostatic pressure (60 mm Hg)} - (\text{Glomerular colloid osmotic pressure (32 mm Hg)} + \text{Bowman's capsule pressure (18 mm Hg)})$$

Fig. 17.8 Summary of forces causing filtration by the glomerular capillaries. (Redrawn from Hall JE. Guyton and Hall Textbook of Medical Physiology. 13th ed. Philadelphia: Elsevier; 2016.)

TABLE 17.2 Approximate Pressures and Vascular Resistances in the Circulation of a Normal Kidney

Vessel	PRESSURE IN VESSEL (MM HG)		Percent of Total Renal Vascular Resistance
	Beginning	End	
Renal artery	100	100	≈0
Interlobar, arcuate, and interlobular arteries	≈100	85	≈16
Afferent arteriole	85	60	≈26
Glomerular capillaries	60	59	≈1
Efferent arteriole	59	18	≈43
Peritubular capillaries	18	8	≈10
Interlobar, arcuate, and interlobular veins	8	4	≈4
Renal vein	4	≈4	≈0

From Hall JE. Guyton and Hall Textbook of Medical Physiology. 13th ed. Philadelphia: Elsevier; 2016.

space is negligible, since the GBM restricts the passage of proteins. The normal GFR is about 180 L/day.

Mediator Control of the Glomerular Filtration Rate

Control of this glomerular capillary pressure is exquisite. Hormones, peptides, and autacoids interact with receptors in the kidney to assure maintenance of RBF and GFR (Fig. 17.10).

α-Adrenergic Effect. The vascular myocytes of afferent and efferent arterioles have the pressure-dependent ability to contract or relax. This prevents increased diuresis, appropriately called pressure diuresis, when the blood pressure is elevated. Mild α-adrenergic stimulation

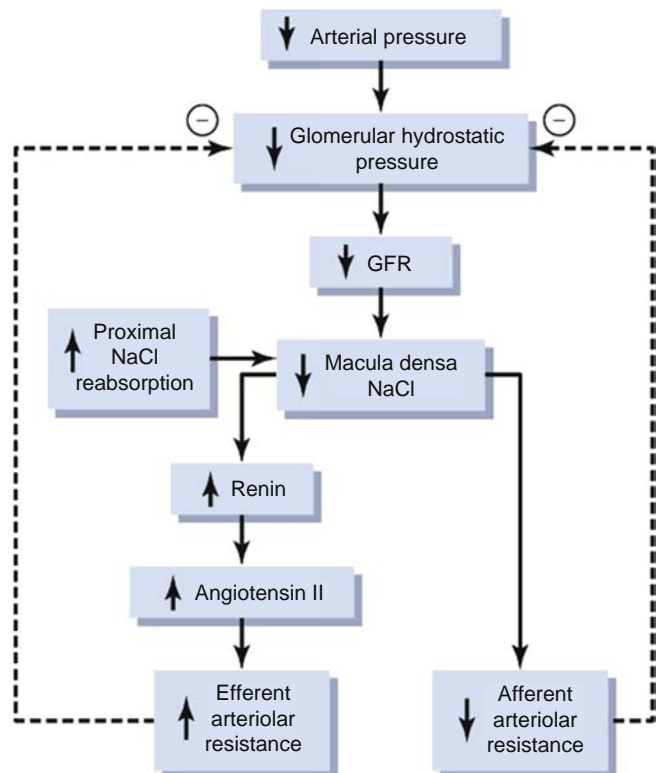


Fig. 17.9 Macula densa feedback mechanism for autoregulation of glomerular hydrostatic pressure and glomerular filtration rate (GFR) during decreased renal artery pressure. (Redrawn from Hall JE. Guyton and Hall Textbook of Medical Physiology. 13th ed. Philadelphia: Elsevier; 2016.)

Vasoconstrictor Systems	Vasodilator Systems
Sympathoadrenal system Renin-angiotensin system Aldosterone Antidiuretic hormone (ADH)	Prostaglandins Kinins Atrial natriuretic peptide (ANP)
↓ RBF ↓ GFR ↓ Urine flow ↓ Na excretion	↑ RBF ↑ GFR ↑ Urine flow ↑ Na excretion

Fig. 17.10 Neurohormonal renal regulatory systems. GFR, Glomerular filtration rate; Na, sodium; RBF, renal blood flow; ↓, decreased; ↑, increased. Modified from Sladen RN. Effect of anesthesia and surgery on renal function. *Crit Care Clin*. 1987;3(2):380–393.

constricts the efferent arteriole that preserves GFR (Fig. 17.11). Severe α-adrenergic activity decreases the filtration fraction by constricting the afferent and efferent arterioles to prevent a flow-induced decrease in GFR. This is the reason norepinephrine administration during sepsis may preserve diuresis. This is important to understand during shock, when the endogenous adrenergic response or the use of α agonists may worsen renal hypoperfusion and decrease the GFR. The kidney is relatively devoid of β₂ receptors, so epinephrine release induces predominant vasoconstriction through α receptor or angiotensin activation.

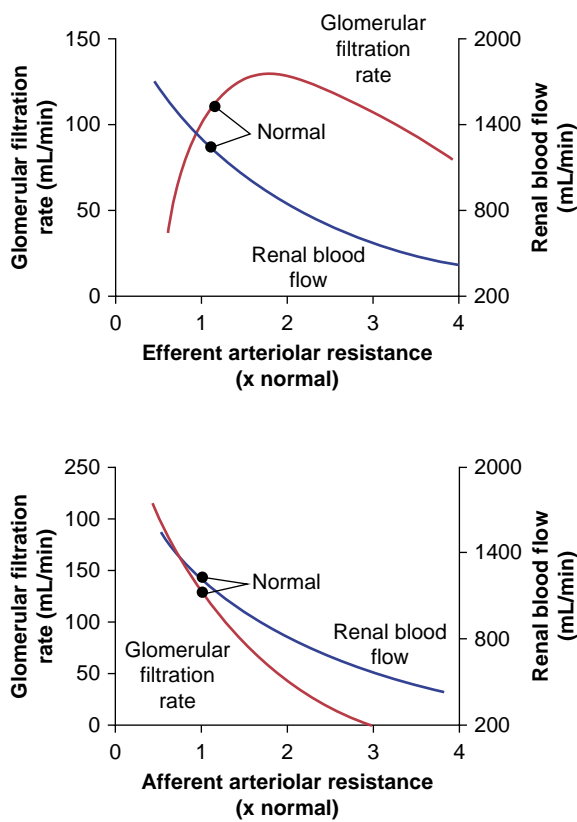


Fig. 17.11 Effect of change in afferent arteriolar resistance or efferent arteriolar resistance on glomerular filtration rate and renal blood flow. (Redrawn from Hall JE. *Guyton and Hall Textbook of Medical Physiology*. 13th ed. Philadelphia: Elsevier; 2016.)

Renin-Angiotensin. Adrenergic stimulation of the juxtaglomerular apparatus releases the enzyme renin from the cells of the macula densa and principal cells of the collecting ducts.¹⁴ Renin, more appropriately called angiotensinogenase, converts the hepatic synthesized glycoprotein angiotensinogen to angiotensin I. Angiotensin-converting enzymes (ACEs) are present in diverse cell types,¹² including leukocytes and smooth muscle. The vascular endothelial cells of the kidney and lung are the major source of ACE that converts angiotensin I to angiotensin II.^{12,15-17}

Angiotensin II stimulates two pathways that have opposing effects (Fig. 17.12). The principal receptor is AT₁ that is found on the luminal epithelial surface of the proximal tubular cell (PTC), mTAL, macula densa, distal tubules, and collecting ducts.^{14,18} The angiotensin II-AT₁ interaction serves to maintain systemic blood pressure through vasoconstriction, and enhancement of tubular transport mechanisms to reabsorb sodium and water.^{14,15,19} The binding of angiotensin II to “non-classical” receptors such as AT₇ opposes these actions and causes vasodilatation through nitric oxide (NO) and prostaglandin-mediated natriuresis, diuresis, and reduced oxidative stress.¹⁹

Angiotensin II is a potent vasoconstrictor of efferent arterioles, which increases the pressure difference and enhances filtration.¹⁸ This maintains the glomerular filtration fraction in the face of mild to moderate decreases in RBF or perfusion pressure that may result from hypovolemia or systemic hypotension. Angiotensin II promotes systemic vasoconstriction at about one tenth of its renal effect. Renin

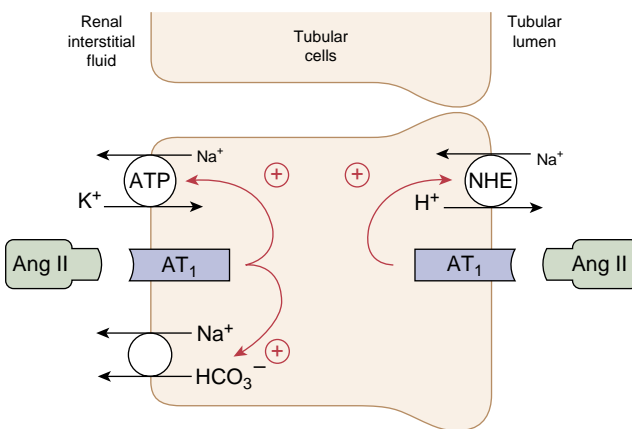


Fig. 17.12 Direct effects of angiotensin II (Ang II) to increase proximal tubular sodium reabsorption. Ang II stimulates sodium-hydrogen exchange (NHE) on the luminal membrane and the sodium-potassium ATPase transporter and sodium-bicarbonate co-transport on the basolateral membrane. ATP, Adenosine triphosphate. (Redrawn from Hall JE. *Guyton and Hall Textbook of Medical Physiology*. 13th ed. Philadelphia: Elsevier; 2016.)

secretion is stimulated by hypovolemia from hemorrhage, diuresis, or sodium loss/restriction and by reductions in perfusion as seen with positive pressure ventilation, congestive heart failure, sepsis, or cirrhosis with ascites. Angiotensin II feeds back to the juxtaglomerular apparatus to inhibit renin secretion. It also stimulates phospholipase A₂ to trigger the synthesis of vasodilatory prostaglandins.

Prostaglandins and Kinins. Intrarenal prostaglandins play an important role in endogenous renal protection by vasodilating juxtaglomerular blood vessels and maintaining inner cortical blood flow.²⁰ Prostaglandins are called autacoids because, unlike true hormones, they are produced in minute amounts and have a local, evanescent action. Because their structure is based on a 20-carbon fatty acid, they are also referred to as eicosanoids, after *eicosa*, the Greek word for the number 20.

Phospholipase A₂ resides in the inner lipid layer of the cell membrane and controls prostaglandin production through its formation of the prime precursor, arachidonic acid. It is stimulated by ischemia, hypotension, norepinephrine, angiotensin II, and arginine vasopressin (AVP). Thus, the factors that induce and mediate the stress response simultaneously activate prostaglandins, which defend the kidney against their actions. Cyclooxygenase-1 acts on arachidonic acid to form the vasodilator prostaglandins that include PGD₂, PGE₂, and PGI₂ (prostacyclin).²¹ Vasodilation is through activation of cyclic adenosine monophosphate (cAMP) to oppose the action of catecholamines, angiotensin II, and AVP. Prostaglandins may be particularly important in decreasing the vasoconstrictor activity of angiotensin II on the afferent arteriole and mesangial cells. Drugs that inhibit prostaglandin synthesis, such as nonsteroidal anti-inflammatory agents, can upset this compensatory mechanism and result in medullary ischemia.

Kinins act directly as vasodilators, as well as stimulate phospholipase A₂, prostacyclin production, and endothelial cell NO formation.²² Kinins are produced by cleavage of kininogen by the serine protease kallikrein. Over 90% of renal kallikrein is produced by the distal convoluted tubules

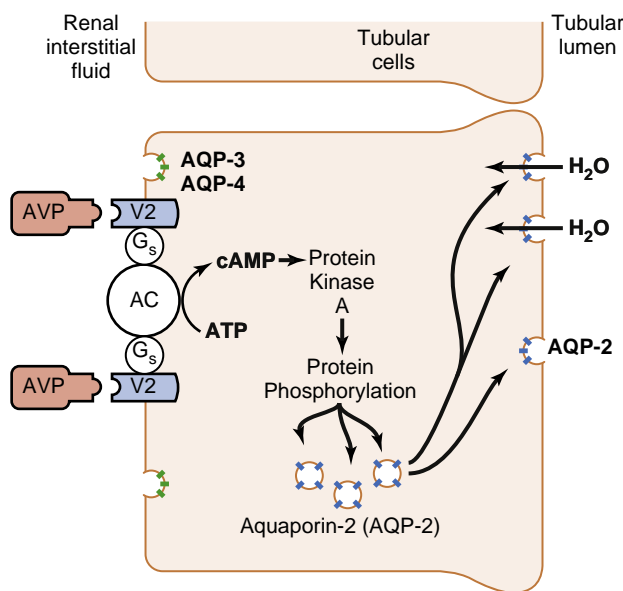


Fig. 17.13 Mechanism of action of arginine vasopressin. Arginine vasopressin (AVP) binds to receptors (V_2) that are coupled to G proteins (G_s) to activate adenylate cyclase (AC) and stimulate the formation of cyclic adenosine monophosphate (cAMP). This will then activate protein kinase A to phosphorylate intracellular proteins and allow aquaporin-2 (AQP-2) to form water channels at the luminal side of the membrane. Other aquaporins (AQP-3, AQP-4) that are not controlled by AVP allow water to exit the cell at the basolateral cell membrane. ATP, Adenosine triphosphate. (Redrawn from Hall JE. *Guyton and Hall Textbook of Medical Physiology*. 13th ed. Philadelphia: Elsevier; 2016.)

in the cortex with decreased concentrations from outer to inner zones.²² Renal kininase, which controls the level of bradykinin, is inhibited by ACE inhibitors and is the reason for angioedema.²³

Arginine Vasopressin. AVP, also known as antidiuretic hormone (ADH), is produced by the posterior pituitary, and its release is stimulated by hyperosmolality or hypovolemia.²⁴ By far the most potent trigger for AVP release is systemic arterial hypotension, mediated by aortic and carotid baroreceptors. It overrides all other triggers, and plasma AVP may reach levels 10- to 1000-fold greater than normal. At these concentrations, AVP acts as a vasoconstrictor, especially in the outer renal cortex. It does so by stimulating the V_{1A} receptor that exists on vascular smooth muscle, glomerular mesangial cells, and the vasa recta and promotes vasoconstriction through the phosphatidylinositol pathway.²⁵ AVP maintains effective glomerular filtration pressure because it is an extremely potent constrictor of the efferent arteriole, and unlike catecholamines and angiotensin, it has little effect on the afferent arteriole, even at high plasma levels.²⁶ The binding to V_2 receptors on the medullary collecting ducts stimulates adenylate cyclase to form cAMP that enhances aquaporin-2 channels of the principal cells to increase water reabsorption (Fig. 17.13).^{24,27} Anesthetics have little direct effect on AVP secretion, except via the changes that they induce in arterial blood pressure, venous volume, and serum osmolality. Surgical stimulation is a major stimulus to AVP secretion. This stress response, whether mediated by pain or by intravascular volume changes, is profound and lasts at least 2 to 3 days after the surgical procedure.

Natriuretic Peptides. Natriuretic peptides dilate vascular smooth muscle through activation of cyclic guanosine monophosphate by blocking the phospholipase C-linked receptors to the actions of norepinephrine and angiotensin II. Atrial natriuretic peptide (ANP)²⁸ is released from atrial myocytes in response to atrial wall stretch and increased atrial volume, brain (B-type) natriuretic peptide is released in response to cerebral ventricle stretch, and C-type is released from the endothelium of major blood vessels. Urodilatin is secreted by the epithelium of the distal tubules and collecting ducts in response to increases in mean arterial pressure and blood volume.

The natriuretic peptides cause prompt, sustained increases in GFR and glomerular filtration fractions even when RBF is not increased or when arterial pressure is decreased. They promote afferent arteriolar dilatation with or without efferent arteriolar constriction, antagonize endothelin (the endogenous vasoconstrictor peptide produced by vascular endothelial cells), inhibit renin secretion, and decrease angiotensin-stimulated aldosterone. These peptides also inhibit the release of aldosterone in the adrenal cortex and block its actions at the distal tubules and collecting ducts. Moreover, they inhibit the secretion of AVP through their effects on the brain and pituitary, which can lead to an enhanced diuresis. NaCl is resorbed, and diuresis is promoted.²⁹ These actions are important in oliguric patients (such as those with acute renal failure and chronic renal failure) to increase urine output.

Aldosterone. Aldosterone is a steroid hormone secreted by the zona glomerulosa of the adrenal cortex in response to hyperkalemia or hyponatremia.³⁰ Angiotensin II and adrenocorticotropic hormone also trigger its release. It acts at the thick ascending limb of the loop of Henle, the principal cells of the distal tubule, and the collecting duct to increase active absorption of sodium and passive absorption of water, culminating in an expanded blood volume. Sodium retention in vessel walls appears to enhance their response to vasoconstrictor agents. In contrast to the immediate sympathetic angiotensin II response to hypovolemia, there is a delay of about 1 to 2 hours from the secretion of aldosterone to its action on sodium reabsorption.

Aldosterone forms a complex with a receptor at the cell membrane in the principal cells of the distal tubule (Fig. 17.14). The aldosterone-receptor complex travels to the cell nucleus, where it induces cytoplasmic transcription of messenger ribonucleic acid. This fosters synthesis of proteins that form sodium channels in the apical cell membrane and enhance the Na^+/K^+ /ATPase pump in the basolateral cell membrane.³¹ Sodium is transported from the tubular fluid into the peritubular capillary in exchange for potassium. Long-standing stimulation of aldosterone secretion, characteristically induced by the intravascular volume depletion of chronic ascites, culminates in potassium depletion and hypokalemic alkalosis.

The Dopaminergic System

There are at least two subtypes of dopaminergic (DA) receptors.³² DA1 receptors are present on the renal and splanchnic vasculature and also on the proximal tubule. Stimulation of the DA1 receptor activates cAMP and induces renal vasodilation, increased RBF and GFR, natriuresis, and diuresis. Dopamine inhibits the sodium-hydrogen antiporter system

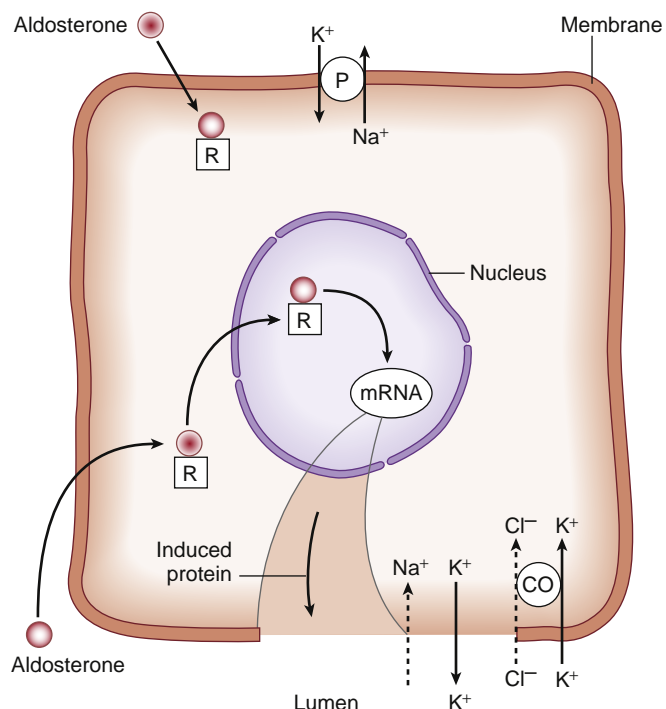


Fig. 17.14 Action of aldosterone. Aldosterone enters the distal tubular cytoplasm and attaches to a receptor, then migrates to the nucleus, where it induces the formation of messenger ribonucleic acid (mRNA). The mRNA in turn induces the synthesis of a protein that enhances the permeability of the apical (luminal) membrane to sodium and potassium. The reabsorption of sodium stimulates the basolateral membrane Na-K-ATPase pump, the intracellular concentration of potassium rises, and it follows its concentration gradient out into the lumen. The net effect of aldosterone's action is sodium reabsorption and potassium loss. Cl^- , Chloride; CO , cotransporter (= symporter); K^+ , potassium; Na^+ , sodium; P , sodium-potassium ATPase pump; R , receptor. (From Wingard LB, Brody TM, Larner J, et al. Diuretics: drugs that increase excretion of water and electrolytes. In: Wingard LB, Brody TM, Larner J, et al., eds. *Human Pharmacology: Molecular-To-Clinical*. London: Wolfe Publishing Ltd; 1991:249, Fig. 19.4.)

at the brush-border membrane of the proximal tubule and the Na^+/K^+ /ATPase pump at the basolateral membrane of the thick ascending limb of the loop of Henle to enhance NaCl reabsorption.

Stimulation of D2 receptors on the presynaptic terminal of postganglionic sympathetic nerves inhibits the release of norepinephrine from presynaptic vesicles to facilitate vasodilation. The DA system plays an integral role in the endogenous vasodilator-natriuresis system and the maintenance of normal blood pressure. Endogenous dopamine constitutively activates the DA2 receptor, which synergistically enhances the activation of the DA1 receptor and inhibits tubular Na^+/K^+ -ATPase activity, especially when sodium intake is increased. It also opposes the anti-natriuretic effects of norepinephrine, angiotensin II, and aldosterone. Endogenous ANP acts via the renal dopamine system by recruiting "silent" DA1 receptors from the interior of the cell toward the plasma membrane and also enhances dopamine accumulation.^{32,33}

Urinary dopamine excretion is increased with salt loading; decreased DA activity may contribute to the pathogenesis of idiopathic edema, which manifests as retention of salt and water in the upright position. There is evidence that the endogenous dopamine system is activated in compensated cirrhosis and helps to maintain renal sodium excretion.^{32,33}

Adenosine

Adenosine is present in all tissues and in the extracellular space as a signaling molecule. It plays a role during conditions of cellular distress such as hypoxia, inflammation, and acute cellular injury.³⁴ Extracellular adenosine mainly exerts its biologic actions through activation of four adenosine receptors that lead to the attenuation or activation of intracellular cAMP levels through modulation of adenylate cyclase activity. This modulation of cAMP affects the production of nucleotides adenosine monophosphate, adenosine diphosphate (ADP), and adenosine triphosphate (ATP) that have essential roles in most cellular functions.³⁴ Adenosine is implicated in the regulation of RBF by tubuloglomerular feedback and protects the kidney from ischemia.³⁵ During periods of ischemia, there is a fivefold increase in extracellular adenosine. In animal models, receptors for adenosine have been effective in preventing or treating acute kidney injury (AKI) from ischemia.³⁵

Nitric Oxide

Endogenous NO is a potent vasodilator of vascular smooth muscle. It is produced in many nephron segments including the cortical and medullary thick ascending limb of the loop of Henle (mTAL).³⁶ During oxidative stress, reactive oxygen species (ROS), including superoxide (O_2^-), hydrogen peroxide (H_2O_2), and the hydroxyl radical (OH), are produced. Under normal conditions, NO minimizes the influence of these ROS. NO acts at multiple points in the citric acid cycle and increases the efficiency of oxygen utilization within the kidney.³⁶ NO inhibits apical Na^+/H^+ cotransport and basolateral Na^+/K^+ -ATPase activity in the proximal tubule, inhibits sodium reabsorption in the mTAL by blocking the $\text{Na}^+/\text{K}^+/2\text{Cl}^-$ cotransporter, and has a direct effect on apical sodium channels of the cortical collecting ducts to inhibit sodium transport.^{36,37} NO produced in the epithelial cells of mTAL buffers the vasoconstriction in the medullary circulation in response to sympathetic stimulation and angiotensin II.³⁸ As for antagonism of O_2^- tubular activity, endogenous NO counteracts the vasoconstrictor effects of O_2^- .

Renal Tubular System Physiology

The renal tubular system compensates for the large glomerular filtration by resorption so that only 1.5 L/day of fluid is excreted as urine. The tubules also conserve and regulate molecules within appropriate physiologic ranges that are freely filtered such as ions, glucose, and amino acids (Table 17.3). Under most conditions, the kidneys excrete more than 95% of the ingested Na^+ at rates that match dietary Na^+ intake.³⁹ Approximately 65% of filtered sodium, chloride, and water is reabsorbed by the PCTs (Fig. 17.15). In the first segment of the PCT, sodium moves across the apical lumen by cotransport with amino acids, bicarbonate, and glucose and counter-transport mechanisms (Fig. 17.16). This reabsorption increases the concentration of chloride ions to 140 mEq/L from the initial filtrate concentration of 105 mEq/L and favors its diffusion through the intercellular junctions into the interstitial space. Organic acids and bases including waste products of metabolism, such as bile salts and urea, and multiple exogenous molecules are cleared by the PCT. This clearance has additional clinical importance since doses of drugs that are removed by the kidney, such as β -lactam antibiotics, will require dose

TABLE 17.3 Filtration, Reabsorption, and Excretion Rates of Different Substances by the Kidneys

	Amount Filtered	Amount Reabsorbed	Amount Excreted	Percent of Filtered Load Reabsorbed
Glucose (g/day)	180	180	0	100
Bicarbonate (mEq/day)	4,320	4,318	2	>99.9
Sodium (mEq/day)	25,560	25,410	150	99.4
Chloride (mEq/day)	19,440	19,260	180	99.1
Potassium (mEq/day)	756	664	92	87.8
Urea (g/day)	46.8	23.4	23.4	50
Creatinine (g/day)	1.8	0	1.8	0

From Hall JE. *Guyton and Hall Textbook of Medical Physiology*. 13th ed. Philadelphia: Elsevier; 2016.

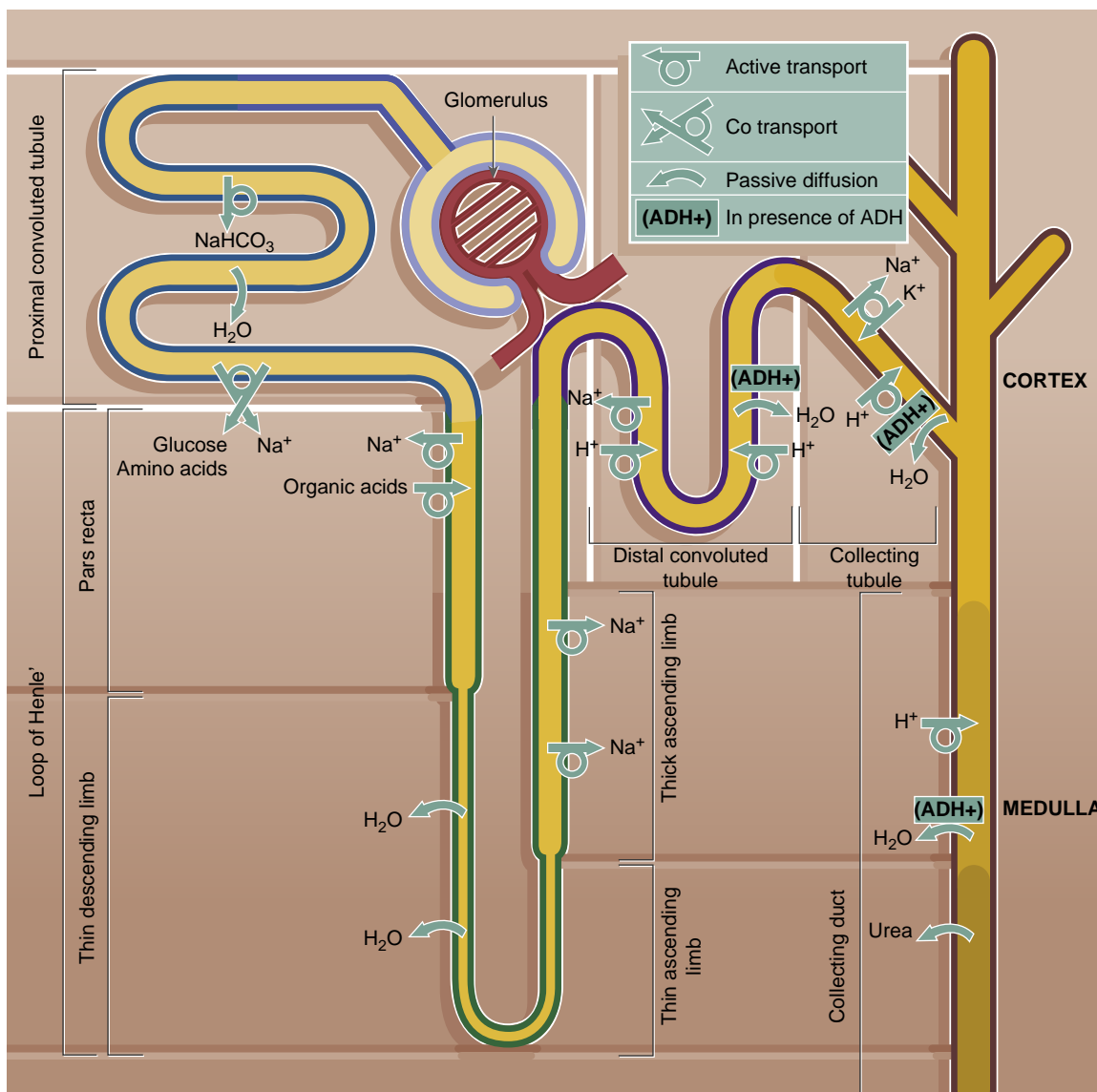


Fig. 17.15 Summary of major activities of different parts of the renal tubule. The ability of the tubule to produce concentrated urine is dependent on the high osmolality of the renal medulla created by the counter-current multiplier mechanism. This is dependent upon the active transport of NaCl in the water-impermeable thick ascending limb of the loop of Henle NaCl , the action of arginine vasopressin (antidiuretic hormone, ADH) on the collecting tubule and duct, the high concentration of urea created by passive diffusion, and the reabsorption of water reabsorbed into the hyperosmolar medulla by the vasa recta. (Redrawn from Young B, Woodford P, O'Dowd G. Urinary system. *Wheaton's Functional Histology. A Text and Colour Atlas*. 6th ed. Philadelphia: Elsevier Churchill Livingstone; 2014.)

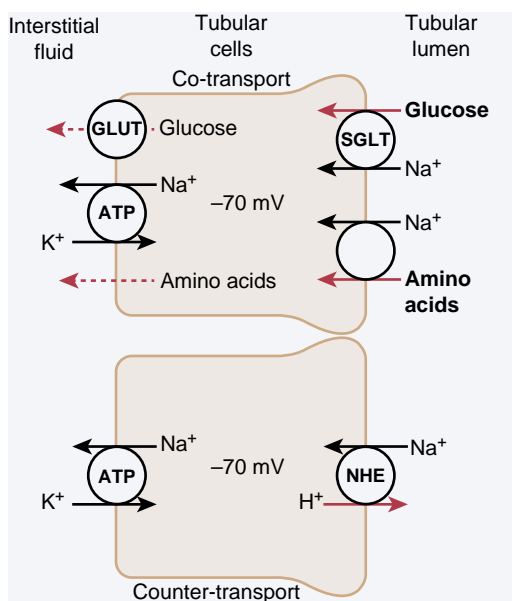


Fig. 17.16 Mechanism of secondary active transport. The upper cell shows the cotransport of glucose and amino acids along with Na^+ through the apical side of the tubular epithelial cells followed by facilitated diffusion through the basolateral membranes. The lower cell shows the counter-transport of hydrogen ions from the interior of the cell across the apical membrane and into the tubular lumen. The movement of sodium ions into the cell is down an electrochemical gradient established by the sodium-potassium pump at the basolateral membrane and provides the energy for transport of the hydrogen ions from the inside of the cell into the tubular lumen. ATP, Adenosine triphosphate; GLUT, glucose transporter; NHE, sodium hydrogen exchanger; SGLT, sodium-glucose co-transporter. (Redrawn from Hall JE. *Guyton and Hall Textbook of Medical Physiology*. 13th ed. Philadelphia: Elsevier; 2016.)

adjustments to achieve therapeutic levels or to prevent toxicity in other organs. **Fig. 17.17** outlines changes in the concentrations of different substances in the tubular system relative to the concentration in plasma and the glomerular filtrate.

The Loop of Henle

The loop of Henle is comprised of a thin descending limb, thin ascending limb, a medullary thick ascending limb (mTAL) as well as a cortical portion that leads to the distal convoluted tubule. The macula densa (see **Fig. 17.1**) is an area of closely packed cells lining the wall of the distal tubule at the point where it meets the thick ascending limb. The major function of the loop of Henle is the maintenance of an osmotic gradient in the interstitium by a countercurrent system to allow the resorption of 40% of the filtered sodium and 25% of filtered water (see later).³⁹ Differential permeability to water, transport of ions, and urea carriers provide the interstitial environment to concentrate urine (see **Fig. 17.15**). The tubules of the descending loop of Henle are freely permeable to water and allow for the reabsorption of about 20% of the filtered water. Both the medullary and cortical thick limbs are impermeable to water and function to concentrate urine. Urea, which comprises 90% of waste nitrogen, is passively absorbed in the tubules by osmosis and is facilitated by specific transporters. An increased concentration of urea in the tubular lumen favors its movement into the interstitium to create an extremely high interstitial osmolality at the tip that approaches 1200 mOsm/kg. Since the tubules are less permeable to urea than water, most of the urea is excreted into the urine.

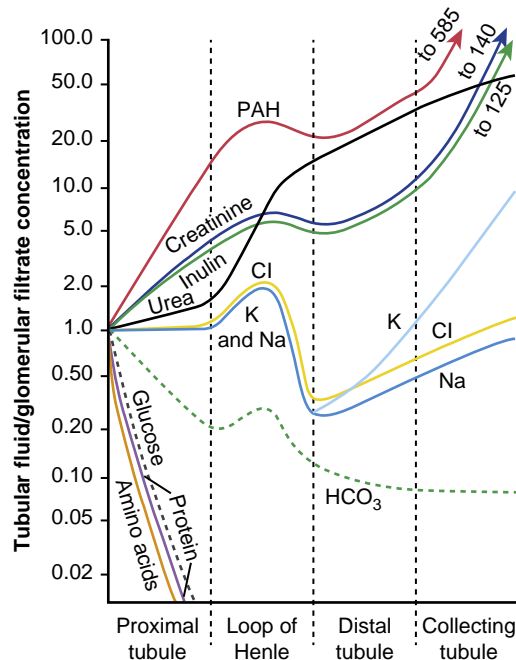


Fig. 17.17 Changes in the average concentrations of different substances at different points in the tubular system relative to the concentration of that substance in the plasma and in the glomerular filtrate. A value of 1.0 indicates that the concentration in the tubular fluid is the same as in the plasma, values below 1.0 indicate that the substance is reabsorbed more avidly than water, while values greater than 1.0 indicate that the substance is reabsorbed to a lesser extent than water or is secreted into the tubules. (Redrawn from Hall JE. *Guyton and Hall Textbook of Medical Physiology*. 13th ed. Philadelphia: Elsevier; 2016.)

As with the cells of the PCT, the mTAL cells have high metabolic activity. A $\text{Na}^+/\text{K}^+/2\text{Cl}^-$ cotransporter in this segment absorbs Na^+ , Cl^- , and K^+ from the tubular lumen. Inhibition of this cotransporter is the mechanism of cationic (positively charged) loop diuretics such as furosemide. The positive charge of the tubular lumen compared to the interstitium allows the paracellular reabsorption of magnesium and calcium in addition to sodium and potassium. ATPase-dependent Na^+/K^+ pumps in the basilar membrane will reabsorb 25% of the filtered sodium and potassium.

DISTAL TUBULES AND MACULA DENSA

The first part of the distal tubule forms the macula densa of the juxtaglomerular apparatus. Approximately 5% of sodium is reabsorbed in the first part of the distal tubule by a sodium chloride cotransporter that moves ions from the tubular lumen into the cell and a Na^+/K^+ ATPase that moves Na^+ out of the cell.^{39,40} Thiazide diuretics inhibit this cotransporter (see **Fig. 17.16**). The movement of chloride is passive. The permeability to water of the distal tubules, as well as the collecting tubules described later, is regulated by AVP (Fig. 17.18). With increased AVP, the tubules become more permeable and water is absorbed.

COLLECTING TUBULES

The collecting tubules are extensions of the distal tubules and have the same function of Na^+ resorption. The two cell types lining the collecting tubules are the principal

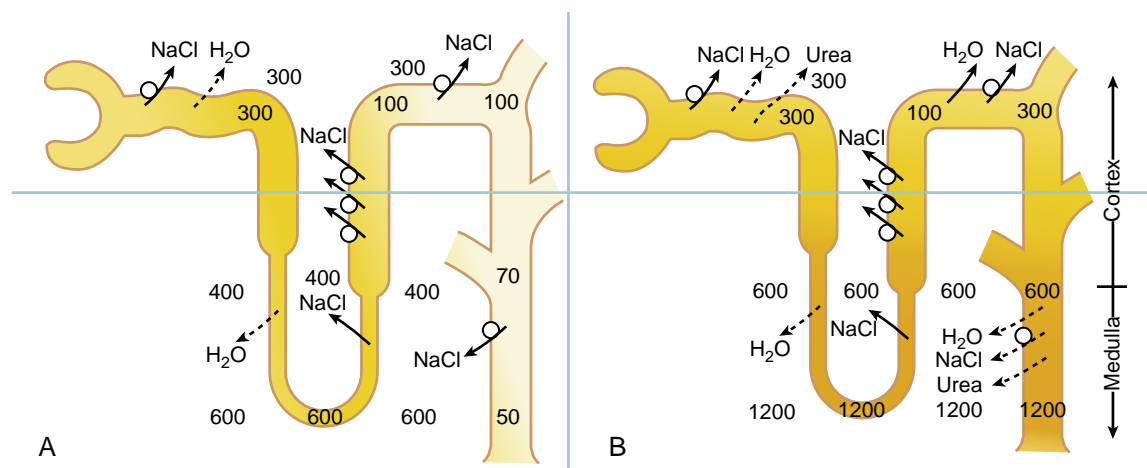


Fig. 17.18 Effect of arginine vasopressin on the formation of urine. (A) With low levels of arginine vasopressin (AVP), fluid in the ascending limb of the loop of Henle is dilute and becomes further diluted in the distal and collecting tubules by continued reabsorption of solutes (indicated as millimoles per liter) while water is not resorbed. (B) Urine is concentrated when AVP is high. Fluid leaving the loop of Henle becomes more concentrated as water is absorbed from the distal and collecting tubules. With high AVP levels, the osmolality of the urine (indicated as milliosmoles) is the same as in the renal medullary interstitial fluid. (Modified from Hall JE. *Guyton and Hall Textbook of Medical Physiology*. 13th ed. Philadelphia: Elsevier; 2016.)

cells and two types of intercalated cells. Principal cells use Na^+/K^+ ATPase to resorb Na^+ and K^+ . These cells are the sites of action for the potassium-sparing diuretics such as spironolactone, a competitor of aldosterone. An additional mechanism is Na^+ channel blockade by diuretics such as amiloride.

Type A intercalated cells use H^+/ATPase and H^+/K^+ ATPase transporters to secrete hydrogen ions formed by carbonic anhydrase against a large concentration gradient. Bicarbonate ions are absorbed from the basolateral membrane. In contrast, the Type B intercalated cells transport hydrogen out of the cell on the basolateral side while bicarbonate is excreted into the tubular lumen. These cells are critical to the maintenance of acid-base balance, sodium reabsorption, and intravascular volume.⁴¹

COLLECTING DUCTS

The collecting ducts form as distal anastomoses of collecting tubules in the medulla and determine the final composition of urine. The principal cell of the collecting duct is a highly regulated epithelial cell. AVP controls water resorption. Urea is reabsorbed via transporters into the medullary interstitium, thereby raising the osmolality to assist in the concentration of urine. Hydrogen can also be secreted against a high concentration gradient to regulate acidosis.

RENAL AUTOREGULATION

The formation of urine is tightly controlled by complex autoregulation that maintains consistency of the RBF, GFR, and the resorption rate in tubules when there are changes in tubular flow. This autoregulation protects the kidney from injury secondary to elevated blood pressure by two mechanisms: autoregulation of RBF and tubuloglomerular feedback.⁴²

Autoregulation of Renal Blood Flow

The smooth muscles of the afferent arterioles, as in other vascular beds, have the intrinsic ability to contract, called a myogenic response, to increases in blood pressure. The

response can compensate for changes in pressure within 3 to 10 seconds over a mean arterial blood pressure range of 70 to 130 mm Hg.⁴³

The Myogenic Mechanism of the Renal Blood Flow Autoregulation

Glomerulotubular balance compensates for increased GFR when blood pressure is elevated by preventing fluid loss through an augmented rate of tubular absorption in the PTC and loop of Henle. This process is more adaptable to slow changes in arterial pressure (>20 seconds) and more critical in maintaining GFR and RBF during sustained reductions in blood pressure (Fig. 17.19).⁴³ An increase in GFR provides enhanced NaCl delivery to the distal tubules. The increased chloride concentration is sensed by the macula densa and triggers the renin-angiotensin cascade to decrease the GFR through angiotensin II constriction of the afferent arteriole. This trigger is sent by the macula densa through the complex of mesangial cells to the smooth muscle of the vasculature by paracrine signaling. There are no intercellular connections between the macula densa, other components of the juxtaglomerular apparatus, and the blood vessels.⁴⁴ The increases in resorption proportionate to the GFR prevent distention of the distal tubular segments.

TUBULOGLOMERULAR FEEDBACK

The dynamic range of tubuloglomerular feedback is a NaCl concentration between 15 and 60 mmol/L with maximal responses at greater than 60 mmol/L.⁴⁴ In the tubules, more than 99% of water and most of the solutes are absorbed, pass through the interstitium, and enter the capillaries at a rate of 124 mL/min. As demonstrable for most capillary beds, the transit of fluids is dependent upon balance of hydrostatic and colloid forces (see Fig. 17.8). Intravascular pressure (13 mm Hg) and colloid osmotic pressure of the interstitium (15 mm Hg) oppose resorption, whereas the hydrostatic pressure in the interstitium (6 mm Hg), intravascular colloid osmotic pressure (32 mm Hg), and large surface area of the capillaries favor resorption.

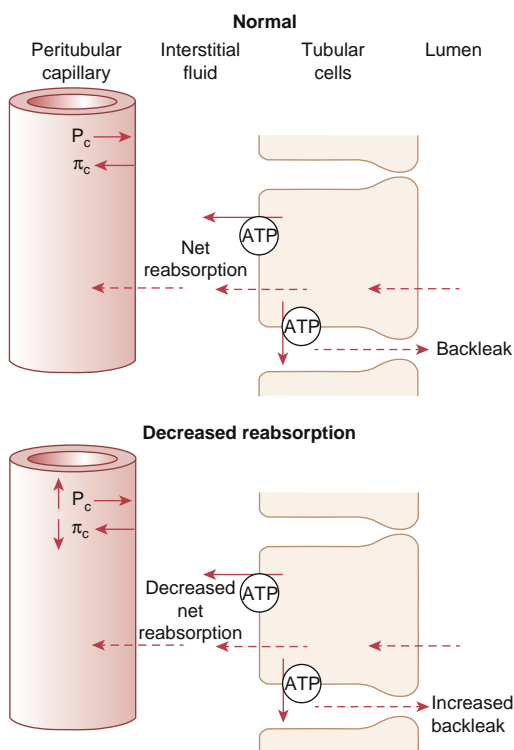


Fig. 17.19 Proximal and peritubular capillary reabsorption under normal conditions (top) and during decreased peritubular capillary reabsorption caused by increased hydrostatic pressure (P_c) or decreased colloid osmotic pressure (π_c). As peritubular capillary reabsorption decreases, the net reabsorption of solutes and water is lowered by the increase in solutes and water that leak back into the tubular lumen through the tight junctions of the tubular epithelial cells. ATP, Adenosine triphosphate. (Redrawn from Hall JE. *Guyton and Hall Textbook of Medical Physiology*. 13th ed. Philadelphia: Elsevier; 2016.)

MAINTENANCE OF PLASMA OSMOLALITY

Definition

Prior to any description of this process, the definitions of osmolarity and osmolality should be reviewed. Osmolality is a measure of the osmoles (Osm) of solute per kilogram of solvent (Osm/kg) while osmolarity is defined as the number of osmoles of solute per liter of solution (Osm/L). Osmolarity is affected by changes in water content, temperature, and pressure. Osmolarity is slightly less than osmolality because the total solvent weight excludes any solutes. Clinically, the values for osmolarity and osmolality are very similar, and the terms are usually used interchangeably. The bedside calculation from laboratory data ($2[\text{Na}^+ \text{ mmol/L}] + 2[\text{K}^+ \text{ mmol/L}] + \text{BUN mg/dL}/2.8 + \text{glucose mg/dL}/18$) is in units of osmolarity. The clinical laboratory measurements determined with osmometers are reported as osmolality.

Regulation of Osmolality

Plasma osmolality is closely regulated between 275 and 300 mOsm/L. Acute alterations in osmolality, either hypoosmolality or hyperosmolality, can result in serious neurologic symptoms and death as the result of water movement in the brain. Normal patients can dilute and concentrate urine within the range of 40 to 1400 mOsm/L.⁴⁵ Maintenance of plasma osmolality is linked to the regulation of sodium

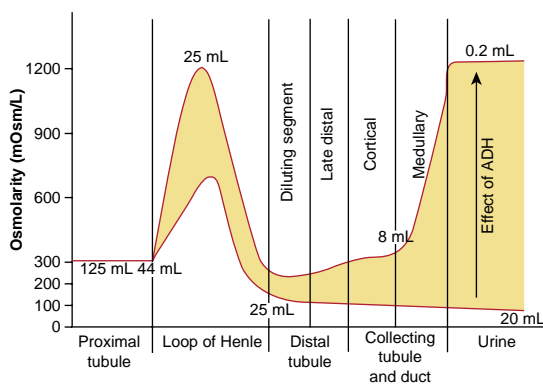


Fig. 17.20 Changes in osmolality of the tubular fluid as it passes through the different tubular segments (milliliters per minute) in the presence of high and low levels of arginine vasopressin (indicated here as the alternative term antidiuretic hormone [ADH]). (Redrawn from Hall JE. *Guyton and Hall Textbook of Medical Physiology*. 13th ed. Philadelphia: Elsevier; 2016.)

concentration and water balance by the tubular system and the collecting ducts in concert with the vasa recta blood supply of the tubules through differences in tubular permeability to water and the control of sodium transport (Fig. 17.20). It is dependent on the interaction of at least three processes: the generation of a hypertonic medullary interstitium by the countercurrent mechanism and urea recycling, the concentration and then dilution of tubular fluid in the loop of Henle, and the action of AVP to increase water permeability in the last part of the distal tubule and collecting ducts.

ROLE OF PROXIMAL TUBULES AND LOOP OF HENLE

Osmosis, the spontaneous net movement of solvent molecules through a selectively permeable membrane into a region of higher solute concentration to equalize the solute concentrations on the two sides, takes place in the proximal tubule. Proximal tubule solutes and water are equally reabsorbed so that the fluid in the tubules is isosmotic with plasma. In contrast, the organization of the loop of Henle is designed to maintain hyperosmolality of the medullary interstitium that can approach 1200 mOsm/L. The major process for this is the active transport of Na^+ and co-transport of K^+ and Cl^- from the lumen of the thick limb of the loop of Henle that is impermeable to water to the interstitium. This allows for a concentration gradient of 200 mOsm/L.

Medullary Interstitium

The medullary interstitium becomes hypertonic by the countercurrent multiplier effect of the loop of Henle that is best understood diagrammatically (Fig. 17.21). The primary mechanism is by the combination of NaCl reabsorption and water impermeability in the ascending limb. The descending limb is freely permeable to water, which diffuses into the interstitium along the osmotic gradient, and the tubular fluid becomes progressively hyperosmotic at the bend of the loop.

Water entering the distal convoluted tubule after leaving the loop of Henle is dilute (about 100 mOsm/L).

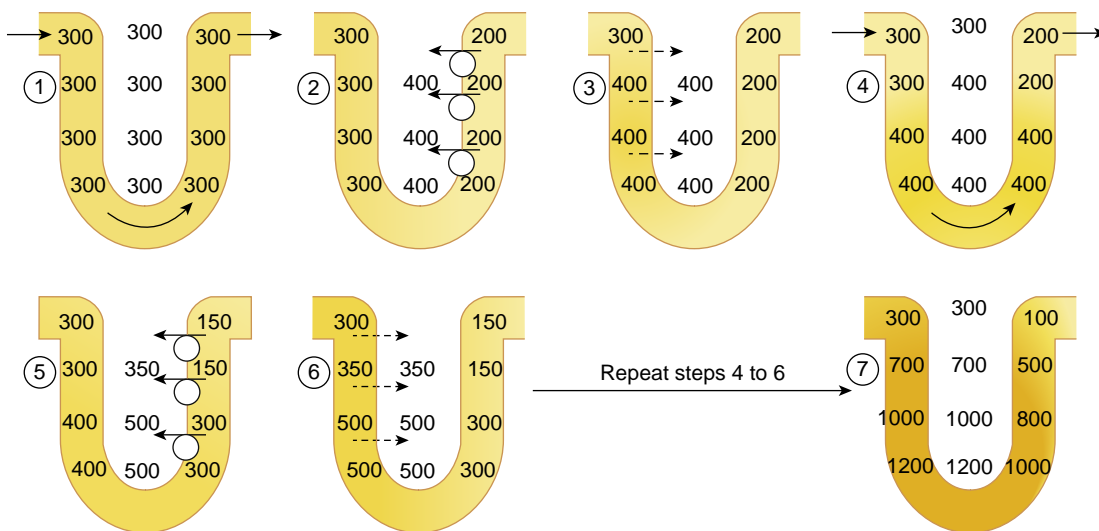


Fig. 17.21 Countercurrent multiplier system in the loop of Henle for producing a hyperosmotic (millimoles per liter) renal medulla. (Redrawn from Hall JE. *Guyton and Hall Textbook of Medical Physiology*. 13th ed. Philadelphia: Elsevier; 2016.)

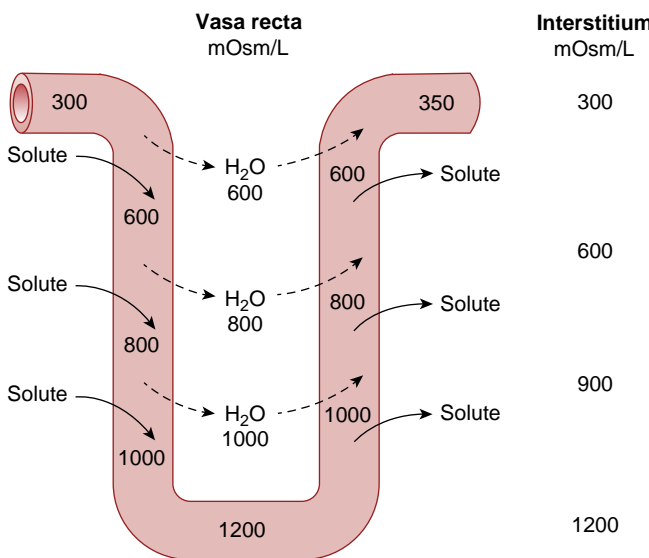


Fig. 17.22 Countercurrent exchange in the vasa recta. Plasma flowing down the descending limb of the loop of the vasa recta becomes more hyperosmotic (in millimoles per liter) as water diffuses out of the blood while solutes from the interstitial fluid flow into the blood. In the ascending limb, solutes diffuse back to the interstitial fluid and water diffuses back into the vasa recta. (Redrawn from Hall JE. *Guyton and Hall Textbook of Medical Physiology*. 13th ed. Philadelphia: Elsevier; 2016.)

This dilution is increased because of the active transport of NaCl and the impermeability of the epithelium. In the collecting tubule, resorption of water is dependent upon the action of AVP (ADH), since the epithelium is normally impermeable to water. With the action of AVP, large amounts of water are reabsorbed into the interstitium of the cortex and removed by the peritubular capillaries (see Fig. 17.18).

Vasa Recta

The vasa recta or straight arterioles of kidney are a series of straight capillaries that lie parallel to the loops of Henle of the juxamedullary nephrons (Fig. 17.22). Only 5% of the RBF is through the vasa recta, creating a sluggish flow. As the capillaries descend into the medulla, the blood becomes

more concentrated by solute entry from the interstitium. This high concentration in the ascending vasa recta in turn facilitates the entry of water from the ascending tubules. The combined interactions of tubular permeability and the vasa recta create the standing osmotic gradients in the cortex (300 mOsm/L), juxamedullary zone (600 mOsm/L), and deep medulla (1200 mOsm/L).

The Role of Urea

A healthy person excretes 20% to 50% of the filtered load of urea. The concentration of urea entering the tubular system is related to the prerenal plasma concentration and the GFR. Urea contributes 40% to 50% of the osmolality of the medullary interstitium. The PCT are freely permeable whereas the loop of Henle, distal tubules, and the collecting ducts have little permeability to urea (Fig. 17.23). As water absorption increases with AVP action, the concentration of urea in the tubules progressively increases. With this high concentration, urea diffuses into the interstitial fluid facilitated by specific urea transporters that are activated by AVP. The simultaneous movement of urea and water out of the inner medullary collecting ducts maintains a high concentration of urea in the tubular fluid. As the concentration of urea increases in the medullary interstitium, it diffuses through the thin limb of the loop of Henle and transits through the ascending system again before it is excreted. This recirculation enhances the increased osmotic pressure in the medulla.

RENAL CONTROL OF INTRAVASCULAR VOLUME

Hypovolemia

Patients with hypovolemia, for example, from hemorrhage, gastrointestinal loss, or preoperative fasting, are commonly encountered in the perioperative period. Contraction of the extracellular volume by hypovolemia increases sympathetic outflow, activates the renin-angiotensin-aldosterone response, and releases AVP. Initially, the GFR and filtered load of sodium decrease. Sodium reabsorption in the proximal tubule is increased from about 66% to 80%

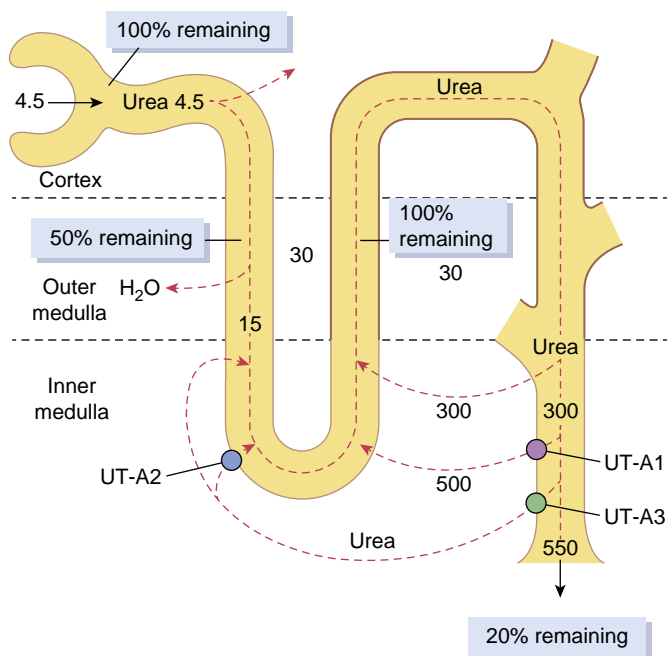


Fig. 17.23 Recirculation of urea absorbed from the medullary collecting duct into the interstitial fluid. Urea diffuses into the thin loop of Henle assisted by urea transporter UT-A2 through to the distal tubules and finally passes back to the collecting duct aided by urea transporters (UT-A1 and UT-A3). This recirculation helps to trap urea in the renal medulla contributing to its hyperosmolality (millimoles per liter). Heavy lines indicate segments that are not very permeable to urea. (Redrawn from Hall JE. Guyton and Hall Textbook of Medical Physiology. 13th ed. Philadelphia: Elsevier; 2016.)

by sympathetic activity and angiotensin II, as well as by the decline in peritubular capillary pressure induced by renal vasoconstriction. Sodium delivery to the thick ascending loop of Henle, distal tubule, and collecting duct is decreased, but aldosterone promotes reabsorption of sodium at these sites. Under the influence of AVP, water is also avidly reabsorbed in the collecting duct so that the urine becomes highly concentrated (osmolality 600 mOsm/kg) but with virtually no sodium (10 mEq/L).

Hypervolemia

Expansion of the extracellular volume by hypervolemia is countered by an increase in the GFR and filtered sodium load due to a combination of reflex decreases in sympathetic and angiotensin II activity and the release of ANP. Together with the increase in peritubular capillary hydrostatic pressure, these responses cause sodium reabsorption in the proximal tubule to decrease from 67% to 50%. The decline in plasma aldosterone decreases sodium absorption from the thick ascending loop of Henle to the collecting duct. The presence of ANP and absence of AVP impairs water absorption at the collecting duct so that a dilute urine (osmolality 300 mOsm/kg) with abundant sodium (80 mEq/L) is produced.

CLINICAL TESTS FOR RENAL FUNCTION^{46,47}

Urine Output

The measurement of urine output is simple and has been the traditional intraoperative and postoperative clinical evaluation of renal function in the absence of laboratory data. By

consensus, oliguria is defined as a urine flow rate less than 0.5 mL/kg/h; it is often interpreted as a sign of renal dysfunction⁴⁸ and was first described by Galen and Ephesus between 100 and 200 AD. Urine output was listed as one of the most widely used indicators for volume expansion with intravenous fluids by 77% to 83% of anesthesiologists surveyed and based on a survey of United States and European anesthesiologists.⁴⁹ However, studies have shown that low urine output was not necessarily associated with renal failure.⁵⁰ Reduced intraoperative urinary output (<1 mL/kg/h) for patients undergoing anesthesia for thoracic resections was not associated with postoperative renal dysfunction regardless of the amount of fluid administered.⁵¹ Although traditionally oliguria is taken as a sign of hypovolemia and subsequent reduction in kidney perfusion, perioperative oliguria is not always abnormal, especially when no other signs of hypoperfusion are present. Tolerance of modest oliguria is necessary when considering the relatively recent push for fluid limitations with enhanced recovery after surgery protocols.⁵² Targeting urine output does not affect 30-day mortality, and oliguria is not a modifiable risk factor for mortality.⁵³ Oliguria has been correlated with AKI and may be a better threshold for the guidance of fluid administration.⁵⁴

In the perioperative period, transient oliguria is almost inevitable, whether induced by hypotension, as an appropriate prerenal response to intravascular hypovolemia, or as a manifestation of the physiologic response to surgical stress.⁵⁵ It is a relative condition that depends on *expected* urine flow, and it may bear little, if any, relationship to GFR. When arterial blood pressure and intravascular volume are restored to normal levels, normal urinary flow should resume. Complete, often abrupt, cessation of urine flow (anuria) suggests postrenal obstruction. For patients with indwelling urinary catheters, obstruction of the catheter by malposition, blood, or kinking is the first diagnosis that must be ruled out and corrected immediately if confirmed. When the catheter is patent, obstruction from the surgical field must be considered dependent upon the procedure.

Creatinine

Creatine phosphate in muscle transfers high-energy phosphate to ADP, creating ATP necessary for contraction, and creatine. Creatinine results from the metabolism of creatine in the liver. Serum creatinine is a reasonable approximation of GFR since it is freely filtered by the glomerulus, is soluble, distributes through the total body water, and is not reabsorbed by the tubules. Creatinine varies with muscle mass, rate of catabolism, protein intake, and physical activity. Low GFR tends to overestimate renal function since little creatinine is secreted. The relationship between serum creatinine and GFR is inverse and exponential; that is, a doubling of serum creatinine implies a halving of GFR. The normal serum creatinine range is 0.5 to 1.2 mg/dL. Muscle mass must be taken into consideration since a normal creatinine in a malnourished, cachectic patient may reflect reduced GFR.

Blood Urea Nitrogen

Urea is formed in the liver by the deamination of amino acids and conversion to ammonia by the arginine cycle. It is not an indicator of GFR since it is rapidly reabsorbed by the

tubules. Absorption of blood from the gastrointestinal tract, steroids, and sepsis may increase the blood urea nitrogen (BUN), whereas malnutrition or liver disease might result in its decrease. The normal ratio of BUN to serum creatinine ratio is between 10 and 15 to 1. The BUN to creatinine ratio may be useful in the diagnosis of renal failure from prerenal causes versus acute tubular necrosis (see [Chapter 42](#)).

RENAL CLEARANCE TECHNIQUES

Clearance is the pharmacokinetic measurement of the volume of plasma that is removed of a specific substance over a period of time. Classic renal physiology experiments used the plant polysaccharide that is freely filtered by the glomerulus and not secreted or reabsorbed by the tubules. ^{131}I -iothalamate has the same renal properties as inulin and is used in radiographic studies to assess clearance.⁵⁶

In routine clinical practice, GFR [urine creatinine (mg/dL) \times volume of urine (mL)/plasma creatinine (mg/dL)] has been employed. The traditional collection period is 24 hours but since the collection of urine can sometimes be impractical, shorter intervals can be used for estimations. A volume of urine is carefully collected over a defined time period and the creatinine concentration is measured. A comparison is then made with a blood sample that is taken during the midpoint of urine flow to determine the creatinine. The GFR may decrease significantly before serum creatinine increases above normal and can be inaccurate due to its variable tubular secretion, extrarenal elimination, and variable rates of generation. For these reasons, estimated GFR (eGFR) that is based on age, sex, and race is often calculated using either the Modification of Diet in Renal Disease (MDRD) or the Chronic Kidney Disease Epidemiology Collaboration (CKD-EPI) equation.⁵⁷

Both methods normalize for sex, age, and race and are based on a stable steady-state production of creatinine and are not accurate with AKI when creatinine clearance is in flux. The MDRD formula is normalized to an average adult 1.73 m^2 body surface area. The CKD-EPI equation is more accurate for values less than $60\text{ mL/min}/1.73\text{ m}^2$. Clinical laboratories will state which method is used when eGFR is reported. Extremes of muscle mass, pregnancy, dietary intake, and comorbidities are factors that will lead to errors in eGFR. Creatinine clearance is more accurate when drugs are dosed based on renal function.⁵⁸

Measurement of Tubular Function

When oliguria is present, tests of renal tubular function may be useful to distinguish dehydration (prerenal azotemia) from acute tubular necrosis. In dehydration, the tubules function normally to retain Na^+ and water to maintain the blood volume. The osmolality of plasma is 280 to 300 mOs/kg but with dehydration, the urine osmolality can increase to greater than 450 mOs/kg. Acute tubular necrosis is a pathologic state (see [Chapter 42](#)) in which the concentrating ability of the tubules is defective. Sodium and water may be lost in the urine if nonoliguric.

The most common method of assessing for tubular concentration ability is the fractional excretion of sodium (FE_{Na}), which is a measure of sodium clearance as a percentage of

creatinine clearance. FE_{Na} is calculated by the following from simultaneous samples of blood and urine collection:

$$\text{FE}_{\text{Na}} = (\text{urine Na/plasma Na}) / (\text{urine creatinine/plasma creatinine}) \times 100$$

Effect of Anesthetics on Renal Function

All general anesthetics tend to decrease GFR and intraoperative urine flow as a consequence of decreased cardiac output and arterial blood pressure.⁵⁹ Some drugs also decrease RBF, but filtration fraction is usually increased, which implies that angiotensin-induced efferent arteriolar constriction limits the decrease in GFR that resolves after emergence from anesthesia. Any anesthetic technique that induces hypotension will result in decreased urine flow because of altered peritubular capillary hydrostatic gradients, even if renal autoregulation is preserved. Injury to kidneys seldom occurs unless there is preexisting kidney disease, nephrotoxic injury, hypovolemia, or a combination thereof, which will exacerbate renal dysfunction.⁶⁰ Volatile anesthetics induce mild to moderate reductions in RBF and GFR, primarily because of their myocardial depression and vasodilatory effects⁶¹ that can be attenuated by prior intravenous hydration. Opioid-based anesthetics are considerably more effective than volatile anesthetics in suppressing the release of catecholamines, angiotensin II, aldosterone, and AVP. Ketamine increases RBF but decreases urine flow rate, possibly through sympathetic activation; it preserves RBF during hemorrhagic hypovolemia.⁶²

The potential for AKI after the breakdown of volatile anesthetics to free fluoride ions causing tubular lesions is now of only historical interest.⁶³ The “older” volatile drug isoflurane produces minimal peak fluoride levels (<4 $\mu\text{M/L}$).⁶⁴ Initial studies of sevoflurane in rats reported nephrotoxicity through the formation of Compound A, a vinyl ether formed by degradation of sevoflurane at low flow through carbon dioxide absorbents.⁶⁵ Clinically significant renal injury has not been shown with desflurane, sevoflurane, or propofol in patients even with moderate preexisting renal dysfunction.⁶⁶

There is growing evidence to support anesthetics as agents that ameliorate ischemia-reperfusion injury in the kidney and other organs.⁶⁷ The volatile anesthetics desflurane, sevoflurane, isoflurane, and halothane attenuated the increase in serum creatinine compared with pentobarbital or ketamine in animal models.⁶⁸ The mechanism is related to an induction of cytoprotective factors and suppression of proinflammatory cytokine and chemokine activation in response to ischemia-reperfusion. There is experimental evidence that propofol can prevent renal ischemia-reperfusion injury through inhibition of oxidative stress pathways.⁶⁹

EFFECTS OF MECHANICAL VENTILATION ON RENAL FUNCTION

Mechanical ventilation and positive end-expiratory pressure (PEEP) may cause decreases in RBF, GFR, sodium excretion, and urine flow rate through changes in hemodynamics.⁷⁰ The increased airway and intrapleural pressures lead to decreased venous return, cardiac filling pressures, and cardiac output. Positive pressure ventilation increases

inferior vena caval pressure and through increased renal venous pressure, may increase peritubular capillary pressure to increase tubular sodium reabsorption. The decrease in cardiac output and systemic arterial pressure results in a carotid and aortic baroreceptor-mediated increase in sympathetic nerve tone to the kidney, with renal vasoconstriction, antidiuresis, and anti-natriuresis. Volume receptors in the atria respond to decreased filling by decreased ANP secretion, resulting in increased sympathetic tone, renin activation, and AVP activity.

The renin-angiotensin-aldosterone system undoubtedly augments the renal responses to positive pressure ventilation. An increase in PEEP can depress cardiac output, RBF, GFR, and urine volume, and increase renin and aldosterone. Although the extent of depression of renal function depends on the mean airway pressure, there is no difference in creatinine clearance and FE_{Na} between volume-controlled and pressure support ventilation.⁷¹ Permissive hypercapnia as employed during acute respiratory distress syndrome may promote renal vasoconstriction.⁷⁰

Induced Hypotension

During anesthesia with induced hypotension, substantial reduction of GFR and urine flow rate is common. Although earlier studies suggested that hypotensive anesthesia can be well tolerated without permanent impairment of renal function, a more recent retrospective analysis suggests that mean arterial pressures less than 60 mmHg for 11 to 20 min or less than 55 mmHg for more than 10 min are associated with acute kidney injury.⁷² Vasodilators used to induce hypotension differ in their effect on RBF. Administration of sodium nitroprusside decreases renal vascular resistance but tends to shunt blood flow away from the kidney. Moreover, its administration is associated with marked renin-angiotensin activation and catecholamine release, which results in rebound hypertension if the infusion is suddenly discontinued. Nitroglycerin decreases RBF less than sodium nitroprusside.⁷³ The selective DA1-dopaminergic agonist fenoldopam is capable of providing induced hypotension without any significant decrease in RBF.⁷⁴ Nicardipine increased creatinine clearance and attenuated the increase in FE_{Na} in patients undergoing spine surgery under deliberate hypotension⁷⁵ and improved renal function when given to patients with preexisting renal insufficiency who had robotic-assisted radical prostatectomy.⁷⁶

Acknowledgment

The editors and publisher would like to thank Drs. David McIlroy and Robert N. Sladen for contributing a chapter on this topic in the prior edition of this work. It has served as the foundation for the current chapter.

 Complete references available online at expertconsult.com.

References

1. Jelkmann W. *J Physiol*. 2011;589:1251–1258.
2. Hansell P, et al. *Clin Exp Pharmacol Physiol*. 2014;40:123–137.
3. Washizawa K, et al. *Pediatr Nephrol*. 1993;7:1–5.
4. Raats CJ, et al. *Kidney Int*. 2000;57:385–400.
5. Rodewald R, Karnovsky MJ. *J Cell Biol*. 1974;217:423–433.
6. Farquhar MG. *J Clin Invest*. 2006;116:2090–2093.
7. Neal CR. *Front Endocrinol*. 2015;6:9.
8. Schrijvers BF, et al. *Kidney Int*. 2004;65:2003–2017.
9. Inoue K, Ishibe S. *Am J Physiol Renal Physiol*. 2015;309:F398–F405.
10. Pulameni T, et al. *J Am Soc Nephrol*. 2002;13:1766–1772.
11. New LA, et al. *Curr Opin Nephrol Hypertens*. 2014;23:420–430.
12. Wu C-H, et al. *Arterioscler Thromb Vasc Biol*. 2018;38:e108–e116.
13. Koeppen BM, Stanton BA. Glomerular filtration and renal blood flow. In: Koeppen BM, Stanton BA, eds. *Renal Physiology*. 4th ed. Philadelphia: Mosby Elsevier; 2007:31.
14. Navar LG, et al. *Hypertension*. 2011;57:355–362.
15. Wilson BA, et al. *Am J Physiol Regul Integr Comp Physiol*. 2014;307:R487–R489.
16. Herichova I, Szantoova K. *Endocr Regul*. 2013;47:39–52.
17. Sparks MA, et al. *Compr Physiol*. 2014;4:1201–1228.
18. Li C, et al. *Am J Physiol Renal Physiol*. 2011;300:F1255–F1261.
19. Chappell MC. *Compr Physiol*. 2012;2:2733–2752.
20. Hao C-M, Breyer MD. *Am Rev Physiol*. 2008;70:357–377.
21. Kim G-H. *Electrolyte and Blood Pressure*. 2008;6:35–41.
22. Scicli AG, Carretero OA. *Kidney Int*. 1986;29:120–130.
23. Baram M, et al. *J Allergy Clin Immunol Pract*. 2013;1:442–445.
24. Kortenoeven ML, et al. *Am J Physiol Renal Physiol*. 2015;15:F280–299.
25. Bayless PH. Posterior pituitary function in health and disease. *Clin Endocrin Metabolism*. 1983;12:747–770.
26. Edwards RM, et al. *Am J Physiol*. 1989;256:F526–F534.
27. Olesen ET, Fenton RA. *Am J Physiol Renal Physiol*. 2017;312:F744–F747.
28. de Bold AJ. *Can J Physiol Pharmacol*. 2011;89:527–531.
29. Inoue T, et al. *Cardiovasc Res*. 2001;15:470–480.
30. Heras MM, et al. *J Diabetes Metab*. 2012;3:171.
31. Genuth SM. The adrenal glands. In: Berne RM, Levy EM, eds. *Physiology*. 4th ed. St Louis: Mosby; 1998:930–964.
32. Choi MR, et al. *Biomed Res Int*. 2014.
33. Sansoè G, et al. *Dig Dis Sci*. 2002;247:392–400.
34. Eltzschig HK. *Anesthesiology*. 2009;111:904–915.
35. Bauerle JD, et al. *J Am Soc Nephrol*. 2011;22:14–20.
36. Evans RG, Fitzgerald SM. *Curr Opin Nephrol Hypertens*. 2005;14:9–15.
37. Ortiz PA, Garvin JL. *Am J Physiol Renal Physiol*. 2002;282:F777–F784.
38. Cowley AW Jr, et al. *Am J Physiol Renal Physiol*. 2015;308:F179–F197.
39. Palmer LG, Schnermann J. *Clin J Am Soc Nephrol*. 2015;10:676–687.
40. McCormick JA, Ellison DH. *Compr Physiol*. 2015;5:45–98.
41. Roy A, et al. *Clin J Am Soc Nephrol*. 2015;10:305–324.
42. Carlström M, et al. *Physiol Rev*. 2015;95:405–511.
43. Burke M, et al. *Curr Vasc Pharmacol*. 2014;12:845–858.
44. Komlosi P, et al. *Acta Physiol Scand*. 2004;181:463–469.
45. Rose BD. Regulation of plasma osmolality. In: Rose BD, ed. *Clinical Physiology of Acid-Base and Electrolyte Disorders*. 4th ed. New York, NY: McGraw-Hill; 1994:261–273.
46. Winter WE. *The Kidney*. In: Laposata's *Laboratory Medicine Diagnosis of Disease in Clinical Laboratory*. 2nd ed. New York, NY: McGraw Hill; 2014:385–396.
47. Prowle JR, Forni LG. Functional biomarkers. In: Ronco C, Bellomo R, Kellum JA, Ricci Z, eds. *Critical Care Nephrology*. 3rd ed. Philadelphia: Elsevier, Inc; 2019:141–145.
48. Kunst G, Ostermann M. *Brit J Anaesth*. 2017;119:1075–1077.
49. Cannesson M, et al. *Critical Care*. 2011;15:R197.
50. Khetpal S, et al. *Anesthesiology*. 2007;107:892–902.
51. Matot I, et al. *J Thorac Cardiovasc Surg*. 2013;146:461–466.
52. Makaryus R, et al. *Brit J Anaesth*. 2018;120:376–383.
53. van der Zee EN, et al. *BMC Anesthesiol*. 2017;17:22.
54. Matot I, et al. *Arch Surg*. 2012;147:228–234.
55. Sladen RN. *Anesthesiol Clin North America*. 2000;18:739–752. viii.
56. Seegmiller JC, et al. *Adv Chronic Kidney Dis*. 2018;25:84–92.
57. <http://www.niddk.nih.gov/health-information/communication-programs/nkdep/laboratory-evaluation/glomerular-filtration-rate/estimating>.
58. Hermans ED, et al. *Pharmacotherapy*. 2009;29:649–655.
59. Priano LL. Effects of anesthetic agents on renal function. In: Barash PG, ed. *Refresher Courses in Anesthesiology*. Philadelphia: Lippincott; 1985:143–156.
60. Fukazawa K, Lee T. *J Am Soc Nephrol*. 2014;25:884–892.

61. Gelman S, et al. *Anesth Analg*. 1984;63:557–565.
62. Priano LL. *Anesth Analg*. 1982;61:853–862.
63. Mazze RI, et al. *Anesthesiology*. 1971;35:247.
64. Mazze RI, et al. *Anesthesiology*. 1974;40:536–542.
65. Higuchi H, et al. *Anesth Analg*. 2000;91:434–439.
66. Ebert TJ, Arain SR. *Anesthesiology*. 2000;93:1401–1406.
67. Motayagheni N, et al. *Am J Nephrol*. 2017;46:380–389.
68. Lee HT, et al. *Anesthesiology*. 2004;101:1313–1324.
69. Li Y, et al. *Cell Physiol Biochem*. 2015;37:14–26.
70. Kuiper JW, et al. *Crit Care Med*. 2005;33:1408–1415.
71. Botha J, et al. *Crit Care Resusc*. 2005;7:303–309.
72. Thompson GE, et al. *Anesthesiology*. 1978;48:91–96.
73. Colley PS, Silverjan M. *Anesth Analg*. 1984;63:503–510.
74. Aronson S, et al. *J Cardiothorac Vasc Anesth*. 1991;5:29–32.
75. Park C, et al. *Clin Spine Surg*. 2017;30:E954–E958.
76. Huh H, et al. *J Int Med Res*. 2014;42:427–435.

References

- Jelkmann W. Regulation of erythropoietin production. *J Physiol*. 2011;589:1251–1258.
- Hansell P, Welch WJ, Blantz RC, Fredrik Palm. Determinants of kidney oxygen consumption and their relationship to tissue oxygen tension in diabetes and hypertension. *Clin Exp Pharmacol Physiol*. 2014;40:123–137.
- Washizawa K, Kasai S, Mori T, Komiyama A, Shigematsu H. Ultrastructural alteration of glomerular anionic sites in nephrotic patients. *Pediatr Nephrol*. 1993;7:1–5.
- Raats CJ, Van Den Born J, Berden JH. Glomerular heparan sulfate alterations: mechanisms and relevance for proteinuria. *Kidney Int*. 2000;57:385–400.
- Rodewald R, Karnovsky MJ. Porous substructure of the glomerular slit diaphragm in the rat and mouse. *J Cell Biol*. 1974;217:423–433.
- Farquhar MG. The glomerular basement membrane: not gone, just forgotten. *J Clin Invest*. 2006;116:2090–2093.
- Neal CR. Podocytes...what's under yours? (Podocytes and foot processes and how they change in nephropathy). *Front Endocrinol*. 2015;6:6–9.
- Schrijvers BF, Flyvbjerg A, De Vries AS. The role of vascular endothelial growth factor (VEGF) in renal pathophysiology. *Kidney Int*. 2004;65:2003–2017.
- Inoue K, Ishibe S. Podocyte endocytosis in the regulation of the glomerular filtration barrier. *Am J Physiol Renal Physiol*. 2015;309:F398–F405.
- Pulamneni T, Lehtonen S, Ora A, et al. Interaction of endogenous nephrine and CD2-associated protein in mouse epithelia M-1 cell line. *J Am Soc Nephrol*. 2002;13:1766–1772.
- New LA, Martin CE, Jones N. Advances in slit diaphragm signaling. *Curr Opin Nephrol Hypertens*. 2014;23:420–430.
- Wu C-H, Mohammadmoradi S, Chen JZ, Sawada H, Daugherty A, Lu HS. Renin-angiotensin system and cardiovascular functions. *Arterioscler Thromb Vasc Biol*. 2018;38:e108–e116.
- Koeppen BM, Stanton BA. Glomerular filtration and renal blood flow. In: Koeppen BM, Stanton BA, eds. *Renal Physiology*. 4th ed. Philadelphia: Mosby Elsevier; 2007:31.
- Navar LG, Kobori H, Prieto MC, Gonzalez-Villalobos RA. Intratubular renin-angiotensin system in hypertension. *Hypertension*. 2011;57:355–362.
- Wilson BA, Marshall AC, Alzayadneh EM, Chappell MC. The ins and outs of angiotensin processing within the kidney. *Am J Physiol Regul Integr Comp Physiol*. 2014;307:R487–R489.
- Herichova I, Szantoova K. Renin-angiotensin system: upgrade of recent knowledge and perspectives. *Endocr Regul*. 2013;47:39–52.
- Sparks MA, Crowley SD, Gurley SB, Mirotsou M, Coffman TM. Classical renin-angiotensin system in kidney physiology. *Compr Physiol*. 2014;4:1201–1228.
- Li C, Wang W, Rivard CJ, Lanaska MA, Summer S, Schrier RW. Molecular mechanisms of angiotensin II stimulation on aquaporin-2 expression and trafficking. *Am J Physiol Renal Physiol*. 2011;300:F1255–F1261.
- Chappell MC. Nonclassical renin-angiotensin system and renal function. *Compr Physiol*. 2012;2:2733–2752.
- Hao C-M, Breyer MD. The physiologic regulation of prostaglandins in the kidney. *Ann Rev Physiol*. 2008;70:357–377.
- Kim G-H. Renal effects of prostaglandins and cyclooxygenase-2 inhibitors. *Electrolyte and Blood Pressure*. 2008;6:35–41.
- Scicli AG, Carretero OA. Renal kallikrein-kinin system. *Kidney Int*. 1986;29:120–130.
- Baram M, Kommuri A, Sellers SA, Cohn JR. ACE inhibitor-induced angioedema. *J Allergy Clin Immunol Pract*. 2013;1:442–445.
- Kortenoeven ML, Petersen NB, Rosenbaek LL, Fenton RA. Vasopressin regulation of sodium transport in the distal nephron and collecting duct. *Am J Physiol Renal Physiol*. 2015;15:F280–299.
- Bayless PH. Posterior pituitary function in health and disease. *Clin Endocrin Metabolism*. 1983;12:747–770.
- Edwards RM, Rizna W, Kinter LB. Renal microvascular effects of vasopressin and vasopressin antagonist. *Am J Physiol*. 1989;256:F526–F534.
- Olesen ET, Fenton RA. Aquaporin-2 membrane targeting: still a conundrum. *Am J Physiol Renal Physiol*. 2017;312:F744–F747.
- de Bold AJ. Thirty years of research on atrial natriuretic factor: historical background and emerging concepts. *Can J Physiol Pharmacol*. 2011;89:527–531.
- Inoue T, Nonoguchi H, Tomita K. Physiological effects of vasopressin and atrial natriuretic peptide in the collecting duct. *Cardiovasc Res*. 2001;15:470–480.
- Heras MM, del Castillo Rodrígues N, Navarro JF. The renin-angiotensin-aldosterone system in renal and cardiovascular disease and the effects of its pharmacological blockade. *J Diabetes Metab*. 2012;3:171. <https://doi.org/10.4172/2155-6156.1000171>.
- Genuth SM. The adrenal glands. In: Berne RM, Levy EM, eds. *Physiology*. 4th ed. St Louis: Mosby; 1998:930–964.
- Choi MR, Mikusic NLR, Kouyoumdzian NM, Kravetz MC, Fernández BE. Atrial natriuretic peptide and renal dopaminergic system: a positive friendly relationship? *Biomed Res Int*. 2014. <https://doi.org/10.1155/2014/710781>.
- Sansoè G, Ferrari A, Baraldi E, et al. Dopaminergic control of renal tubular function in patients with compensated cirrhosis. *Dig Dis Sci*. 2002;247:392–400.
- Eltzschig HK. Adenosine: an old drug newly discovered. *Anesthesiology*. 2009;111:904–915.
- Bauerle JD, Grenz A, Kim J-H, Lee HT, Eltzschig HK. Adenosine generation and signaling during acute kidney injury. *J Am Soc Nephrol*. 2011;22:14–20.
- Evans RG, Fitzgerald SM. Nitric oxide and superoxide in the renal medulla: a delicate balancing act. *Curr Opin Nephrol Hypertens*. 2005;14:9–15.
- Ortiz PA, Garvin JL. Role of nitric oxide in the regulation of nephron transport. *Am J Physiol Renal Physiol*. 2002;282:F777–F784.
- Cowley AW Jr, Abe M, Mori T, Connor PM, Ohsaki Y, Zheleznova NN. Reactive oxygen species as important determinants of medullary flow, sodium excretion, and hypertension. *Am J Physiol Renal Physiol*. 2015;308:F179–F197.
- Palmer LG, Schnermann J. Integrated control of Na transport along the nephron. *Clin J Am Soc Nephrol*. 2015;10:676–687.
- McCormick JA, Ellison DH. Distal convoluted tubule. *Compr Physiol*. 2015;5:45–98.
- Roy A, Al-bataineh MM, Pastor-soler NM. Collecting duct intercalated cell function and regulation. *Clin J Am Soc Nephrol*. 2015;10:305–324.
- Carlström M, Wilcox CS, Arendshorst WJ. Renal autoregulation in health and disease. *Physiol Rev*. 2015;95:405–511.
- Burke M, Pabbidi MR, Farley J, Roman RJ. Molecular mechanisms of renal blood flow autoregulation. *Curr Vasc Pharmacol*. 2014;12:845–858.
- Komlosi P, Fintha A, Bell PD. Current mechanisms of macula densa signalling. *Acta Physiol Scand*. 2004;181:463–469.
- Rose BD. Regulation of plasma osmolality. In: Rose BD, ed. *Clinical Physiology of Acid-Base and Electrolyte Disorders*. 4th ed. New York, NY: McGraw-Hill; 1994:261–273.
- Winter WE. The Kidney. In: *Lapostata's Laboratory Medicine Diagnosis of Disease in Clinical Laboratory*. 2nd ed. New York, NY: McGraw Hill; 2014:385–396.
- Prowle JR, Forni LG. Functional biomarkers. In: Ronco C, Bellomo R, Kellum JA, Ricci Z, eds. *Critical Care Nephrology*. 3rd ed. Philadelphia: Elsevier, Inc; 2019:141–145.
- Kunst G, Ostermann M. Intraoperative permissive oliguria – how much is too much? *Brit J Anaesth*. 2017;119:1075–1077.
- Cannesson M, Pestel G, Ricks C, Hoeft A, Perel A. Hemodynamic monitoring and management in patients undergoing high risk surgery: a survey among North American and European anesthesiologists. *Critical Care*. 2011;15:R197.
- Kheterpal S, Tremper KK, Englesbe MJ, et al. Predictors of postoperative acute renal failure after noncardiac surgery in patients with previously normal renal function. *Anesthesiology*. 2007;107:892–902.
- Matot I, Dery E, Bulgov Y, Cohen B, Paz J, Nesher N. Fluid management during video-assisted thoracoscopic surgery for lung resection: a randomized, controlled trial of effects on urinary output and postoperative renal function. *J Thorac Cardiovasc Surg*. 2013;146:461–466.
- Makaryus R, Miller TE, Gan TJ. Current concepts of fluid management in enhanced recovery pathways. *Brit J Anaesth*. 2018;120:376–383.
- van der Zee EN, Egal M, Gommers D, Groeneveld AB. Targeting urine output and 30-day mortality in goal-directed therapy: a systematic review with meta-analysis and meta-regression. *BMC Anesthesiol*. 2017;17:22. <https://doi.org/10.1186/s12871-017-0316-4>.
- Matot I, Paskaleva R, Eid L, et al. Effect of the volume of fluids administered on intraoperative oliguria in laparoscopic bariatric surgery: a randomized controlled trial. *Arch Surg*. 2012;147:228–234.

55. Sladen RN. Oliguria in the ICU. Systematic approach to diagnosis and treatment. *Anesthesiol Clin North America*. 2000;18:739–752, viii.
56. Seegmiller JC, Eckfeldt JH, Lieske JC. Challenges in measuring glomerular filtration rate: a clinical laboratory perspective. *Adv Chronic Kidney Dis*. 2018;25:84–92.
57. <http://www.niddk.nih.gov/health-information/communication-programs/nkdep/laboratory-evaluation/glomerular-filtration-rate/estimating>.
58. Hermans ED, Maiefski M, Florescu MC, Qiu F, Rupp ME. Comparison of the modification of diet in renal disease and Cockcroft-Gault equations for dosing antimicrobials. *Pharmacotherapy*. 2009;29:649–655.
59. Priano LL. Effects of anesthetic agents on renal function. In: Barash PG, ed. *Refresher Courses in Anesthesiology*. Philadelphia: Lippincott; 1985:143–156.
60. Fukazawa K, Lee T. Volatile anesthetics and AKI: risks, mechanisms, and a potential therapeutic window. *J Am Soc Nephrol*. 2014;25:884–892.
61. Gelman S, Gowler KC, Smith LR. Regional blood flow during isoflurane and halothane anesthesia. *Anesth Analg*. 1984;63:557–565.
62. Priano LL. Alteration of renal hemodynamics by thiopental, diazepam and ketamine in conscious dogs. *Anesth Analg*. 1982;61:853–862.
63. Mazze RI, Trudell JR, Cousins MJ. Methoxyflurane metabolism and renal dysfunction: clinical correlation in man. *Anesthesiology*. 1971;35:247.
64. Mazze RI, Cousins MJ, Barr GA. Renal effects and metabolism of isoflurane in man. *Anesthesiology*. 1974;40:536–542.
65. Higuchi H, Adachi Y, Arimura S, Kanno M, Satoh T. Compound A concentrations during low-flow sevoflurane anesthesia correlate directly with the concentration of monovalent bases in carbon dioxide absorbents. *Anesth Analg*. 2000;91:434–439.
66. Ebert TJ, Arain SR. Renal responses to low-flow desflurane, sevoflurane, and propofol in patients. *Anesthesiology*. 2000;93:1401–1406.
67. Motayagheni N, Phan S, Eshraghi C, Nozari A, Atala A. A review of anesthetic effects on renal function: potential organ protection. *Am J Nephrol*. 2017;46:380–389.
68. Lee HT, Ota-Setlik A, Fu Y. Differential protective effects of volatile anesthetics against renal ischemia-reperfusion injury in vivo. *Anesthesiology*. 2004;101:1313–1324.
69. Li Y, Zhong D, Lei L, Jia Y, Zhou H, Yang B. Propofol prevents renal ischemia-reperfusion injury via inhibiting the oxidative stress pathways. *Cell Physiol Biochem*. 2015;37:14–26.
70. Kuiper JW, Groeneveld AB, Slutsky AS, Plotz FB. Mechanical ventilation and acute renal failure. *Crit Care Med*. 2005;33:1408–1415.
71. Botha J, Mudholkar P, Le Blanc V. The effect of changing from pressure support ventilation to volume control ventilation on renal function. *Crit Care Resusc*. 2005;7:303–309.
72. Thompson GE, Miller RD, Stevens WC, et al. Hypotensive anesthesia for total hip arthroplasty: a study of blood loss and organ function, brain, heart, liver and kidneys. *Anesthesiology*. 1978;48:91–96.
73. Colley PS, Silvarjan M. Regional blood flow in dogs during halothane anesthesia and controlled hypotension produced by nitroprusside or nitroglycerin. *Anesth Analg*. 1984;63:503–510.
74. Aronson S, Goldberg LI, Glock D, et al. Effects of fenoldopam on renal blood flow and systemic hemodynamics during isoflurane anesthesia. *J Cardiothorac Vasc Anesth*. 1991;5:29–32.
75. Park C, Kim JY, Kim C, Chang CH. Nicardipine effects on renal function during spine surgery. *Clin Spine Surg*. 2017;30:E954–E958.
76. Huh H, Kim NY, Park SJ, Cho JE. Effect of nicardipine on renal function following robot-assisted laparoscopic radical prostatectomy in patients with pre-existing renal insufficiency. *J Int Med Res*. 2014;42:427–435.

TAE KYUN KIM, SHINJU OBARA, and KEN B. JOHNSON

KEY POINTS

- Pharmacokinetics describes the relationship between drug dose and drug concentration in plasma or at the site of drug effect over time. For anesthetic drugs, the processes of distribution and elimination (metabolism and excretion) govern this relationship.
- The time course of intravenously administered drugs is a function of distribution volume and clearance. Estimates of distribution volumes and clearances, pharmacokinetic parameters, are derived from mathematical formulas fit to measured blood or plasma concentrations over time following a known drug dose.
- Front-end kinetics refer to alterations in cardiac output that substantially influence the pharmacokinetic behavior of anesthetic drugs in terms of onset and duration of effect. Context-sensitive decrement time, which is defined as the time required to reach a certain plasma concentration after a termination of long infusion, characterizes the back-end kinetics.
- Hysteresis refers to the time delay between changes in plasma concentration and drug effect. Hysteresis accounts for the time required for drug to diffuse from the plasma to the site of action plus the time required, once drug is at the site of action, to elicit a drug effect.
- Pharmacodynamics describes what the drug does to the body. In particular, pharmacodynamics describes the relationship between drug concentration and pharmacologic effect.
- The effect-site concentration describes a mathematically derived virtual location where an anesthetic drug exerts its effect. This approach cannot describe a mechanism of drug action (e.g., drug-receptor interaction).
- A single anesthetic drug has multiple effects (i.e., analgesia, ventilatory depression, loss of response to laryngoscopy, and changes in the electroencephalogram) that typically occur at various effect-site concentrations.
- The concentration range where changes in drug effect occur is known as the dynamic range. Concentrations outside the dynamic range do not yield much change in drug effect. Levels below the dynamic range are ineffective and those above the dynamic range do not provide additional effect.
- Anesthesia is the practice of applied drug interactions. Anesthetics rarely consist of one drug, but rather a combination of drugs to achieve desired levels of hypnosis, analgesia, and muscle relaxation. Hypnotics, analgesics, and muscle relaxants all interact with one another such that rarely does one drug, when administered in the presence of other drugs, behave as if it were administered alone.
- Pharmacokinetic and pharmacodynamic principles characterize the magnitude and time course of drug effect, but because of complex mathematics, they have limited clinical utility. Advances in computer simulation have brought this capability to the point of real-time patient care in the form of drug displays.
- Special populations: many aspects of a patient's demographics and medical history are considered in finding the *correct dose*. Some of these include age; body habitus; gender; chronic exposure to opioids, benzodiazepines, or alcohol; presence of heart, lung, kidney, or liver disease; and the extent of blood loss or dehydration.
- Some patient characteristics (e.g., obesity and age) influence anesthetic drug behavior, while other patient characteristics (chronic opioid use, hepatic and renal failure) remain poorly described.

Introduction

The basic principles of pharmacology are fundamental to an anesthesia provider's knowledge base. The aim of this chapter is to provide an overview of key principles in clinical pharmacology used to describe anesthetic drug behavior.

This chapter is divided into three major sections: pharmacokinetic principles, pharmacodynamic principles, and the importance of patient characteristics. Pharmacokinetics is the relationship between drug administration and drug concentration at the site of action. Core concepts include volumes of distribution, drug clearance, and transfer of

drugs between plasma and tissues. The section on pharmacokinetics introduces both the physiologic processes that determine pharmacokinetics and the mathematical models used to relate dose to concentration.

Pharmacodynamics is the relationship between drug concentration and pharmacologic effect. An anesthetic rarely consists of only one drug. In fact, most anesthetics are a combination of several drugs with specific goals in analgesia, sedation, and muscle relaxation. This section reviews common pharmacodynamic interactions and how they influence anesthetic effect.

The last section briefly addresses patient demographics and how they influence anesthetic behavior. When formulating an anesthetic, the following factors need to be considered in determining the correct dose: age; body habitus; gender; chronic exposure to opioids, benzodiazepines, or alcohol; presence of heart, lung, kidney, or liver disease; and the extent of blood loss or dehydration. This section focuses on body habitus and age, both known to influence the pharmacology of many anesthetic drugs and both of which serve as excellent examples of altered pharmacokinetics and pharmacodynamics.

FUNDAMENTAL PHARMACOKINETIC CONCEPTS

Pharmacokinetics describes the relationship between drug dose and drug concentration in plasma or at the site of drug effect over time. The processes of absorption, distribution, and elimination (metabolism and excretion) govern this relationship. Absorption is not relevant to intravenously administered drugs but is relevant to all other routes of drug delivery. The time course of intravenously administered drugs is a function of distribution volume and clearance. Estimates of distribution volumes and clearances are described by pharmacokinetic parameters. Pharmacokinetic parameters are derived from mathematical formulas fit to measured blood or plasma concentrations over time following a known amount of drug dose.

Volume of Distribution

An over-simplified model of drug distribution throughout plasma and tissues is the dilution of a drug dose into a tank of water. The volume of distribution (V_d) is the apparent size of the tank in which a known amount of drug distributes to produce a measured drug concentration once the drug has had enough time to thoroughly mix within the tank (Fig. 18.1). If an injected drug disperses and distributes instantaneously throughout the tank without any drug degradation, the distribution volume is estimated using the simple relationship between dose (e.g., mg) and measured concentration (e.g., mg/L) as presented in Eq. (18.1).

$$\text{Volume of distribution} = \frac{\text{Amount of dose}}{\text{Concentration}} \quad (18.1)$$

With an estimate of tank volume, drug concentration after any bolus dose can be calculated. Human bodies are not like water tanks. As soon as a drug is injected, it begins to be cleared from the body. To account for this in the schematic presented in Fig. 18.1, a faucet is added to the tank to mimic drug elimination from the body (Fig. 18.2). Considering the elimination of drug from the tank and the changes

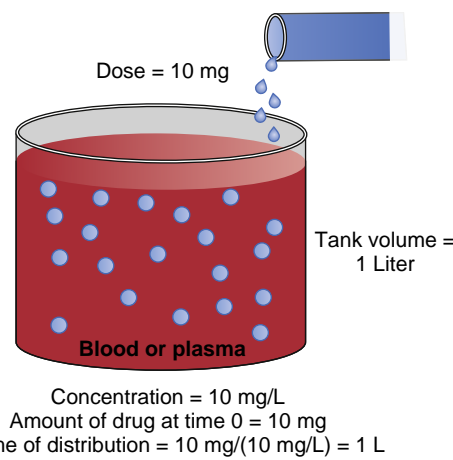


Fig. 18.1 Schematic of a single-tank model of distribution volume. The group of blue drops emerging from the pipe at the top right represent a bolus dose that, when administered to the tank of water, evenly distributes within the tank.

in concentration, the definition of distribution volume in Eq. (18.1) should be refined with the amount of drug and the concentration at a given time t .

$$V_d = \frac{\text{Amount} (t)}{\text{Concentration} (t)} \quad (18.2)$$

If drug elimination occurs as a first-order process (i.e., elimination is proportional to the concentration at that time), in a tank model, the volume of distribution calculated by Eq. (18.2) will be constant (Fig. 18.3; see also Fig. 18.2). When a drug is administered intravenously, some drug stays in the vascular volume, but most of the drug distributes to peripheral tissues. This distribution is often represented as additional tanks (peripheral distribution volumes) connected to a central tank (blood or plasma volume). Peripheral distribution volumes increase the total volume of distribution (Fig. 18.4). For the calculation of distribution volumes, peripheral tissue concentrations are difficult to measure whereas plasma concentrations are easily measured.

The schematic in Fig. 18.4 presents two tanks that represent plasma and peripheral tissue volumes. The peripheral tank represents the drug volume of distribution in peripheral tissues. There may be more than one peripheral tank (volume) to best describe the entire drug disposition in the body. The size of the peripheral volumes represents a drug's solubility in tissue relative to blood or plasma. The more soluble a drug is in peripheral tissue relative to blood or plasma, the larger the peripheral volumes of distribution.

An important point illustrated in Fig. 18.4 is that drug not only distributes to the peripheral tank and thus increases the volume of distribution, but it also binds to tissue in that tank. This process further lowers the measurable concentration in the central tank. Thus, the total volume of distribution may even be larger than the two tanks added together. In fact, some anesthetics have huge distribution volumes (e.g., fentanyl has an apparent distribution volume of 4 L/kg) that are substantially larger than an individual's vascular volume (0.07 L/kg) or extracellular volume (0.2 L/kg).

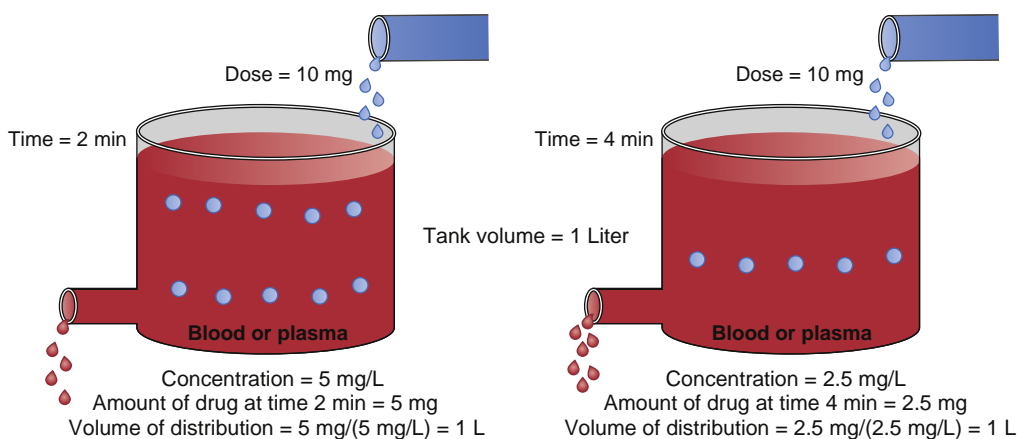


Fig. 18.2 Schematic of a single-tank model of elimination as a first-order process (eliminated at a rate of 50% to the amount of drug present at every two minutes). At 2 minutes (left panel) and 4 minutes (right panel) following a 10-mg drug bolus, tank concentrations are decreasing from 5 to 2.5 mg/mL. Accounting for elimination, estimates of the distribution volume at each time point are both 1 L.

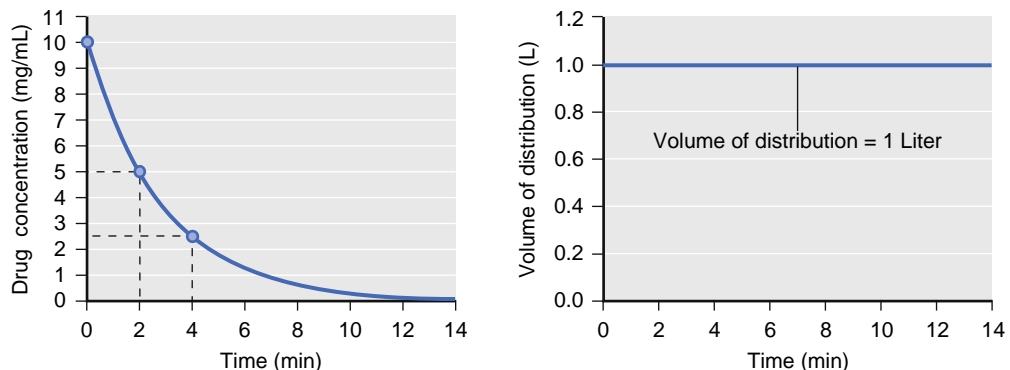


Fig. 18.3 Simulation of concentration (left panel) and distribution volume (right panel) changes over time following a bolus dose for a single-tank (one-compartment) model. The distribution volume remains constant throughout.

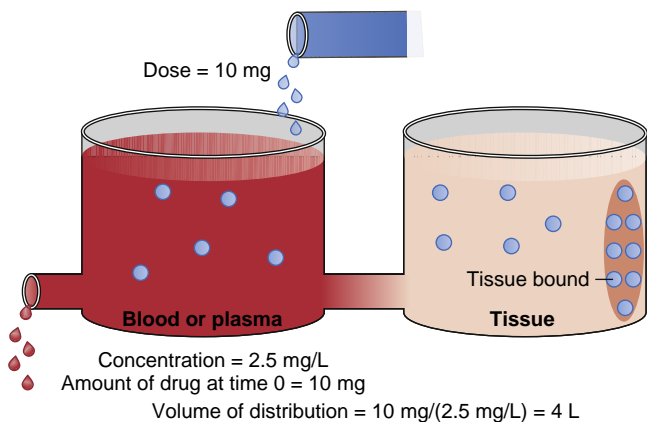


Fig. 18.4 Schematic of a two-tank model. The total volume of distribution consists of the sum of the two tanks. The brown ellipse in the peripheral volume represents tissue that binds up drugs. The measured concentration in the blood or plasma is 2.5 mg/mL just after a bolus dose of 10 mg. Using Fig. 18.1, this leads to a distribution volume of 4 L.

With additional distribution volumes, the overall volume of distribution can change over time and is a function of how drug is administered as well (e.g., as a bolus or a continuous infusion). For example, consider simulations of concentrations and distribution volumes over time following a bolus dose or a continuous infusion of an intravenous anesthetic

as presented in Fig. 18.5. For a bolus dose, assume that the volume of distribution is 1 L at time = 0 and that it then increases to 14 L as the plasma concentration falls over the next 10 minutes. The increase of the distribution volume is due to the distribution of drug to peripheral tissue and a decrease in the plasma concentration. For a constant infusion, assume the volume of distribution is again 1 L at time = 0 and that it then increases to 5 L as the plasma concentrations also increase to a steady-state concentration over the next several hours. This is known as the steady-state volume of distribution. It is estimated as the sum of the central and peripheral apparent distribution volumes.

Clearance

Clearance describes the rate of drug removal from the plasma/blood. Two processes contribute to drug clearance: systemic (removal from the tank) and intercompartmental (between tanks) clearance (Fig. 18.6). Systemic clearance permanently removes drug from the body, either by eliminating the parent molecule or by transforming it into metabolites. Intercompartmental clearance moves drug between plasma and peripheral tissue tanks. By way of clarification, in this chapter, the words compartment and tank are interchangeable.

Clearance is defined in units of flow, that is, the volume completely cleared of drug per unit of time (e.g., L/min).

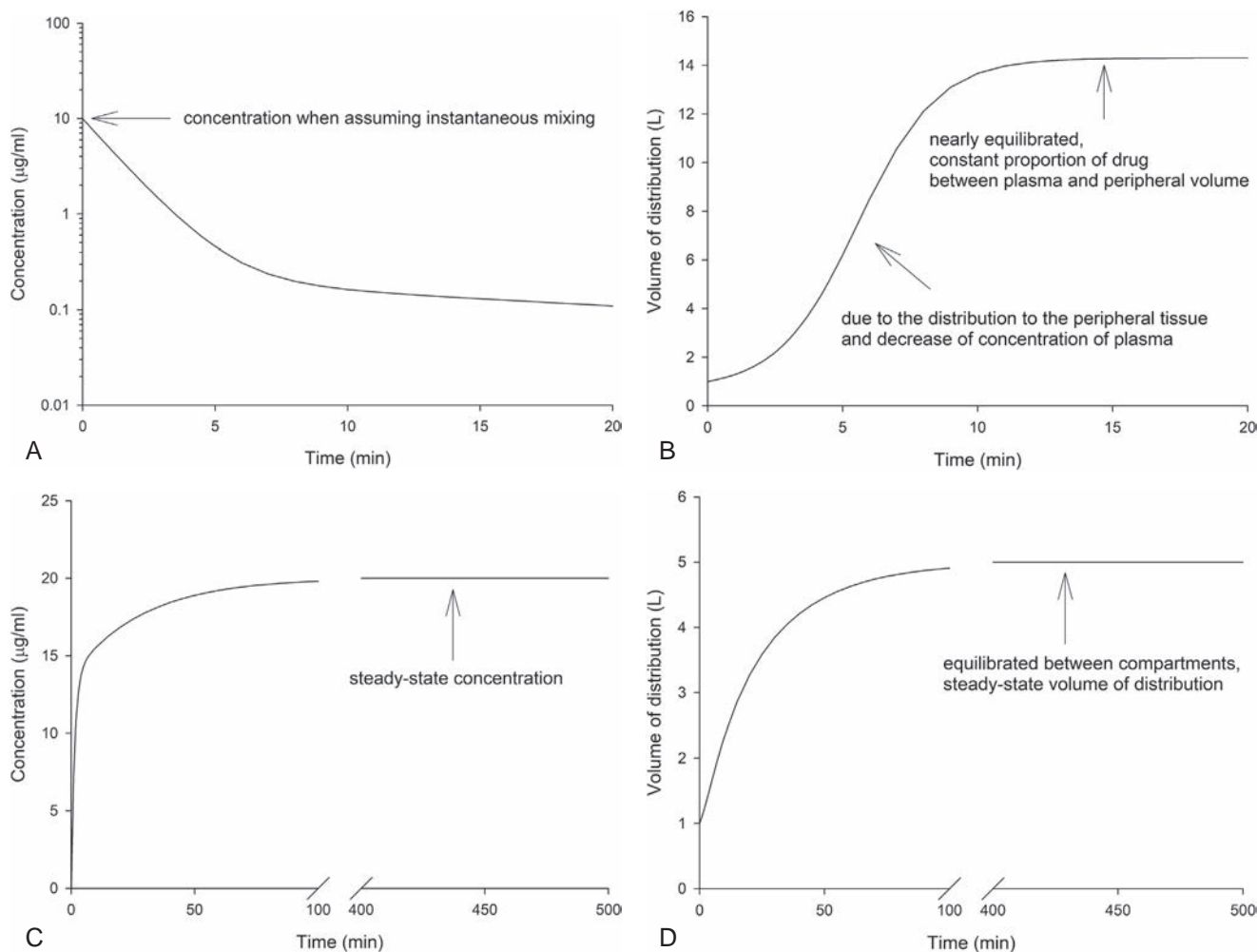


Fig. 18.5 Simulation of concentration and apparent distribution volume changes over time following a bolus dose for a two-tank (two-compartment) model. Panels A and C present drug concentrations over time. Panels B and D present the apparent distribution volume over time.

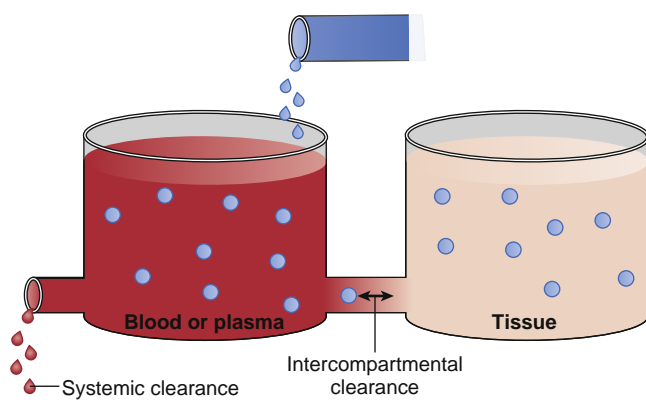


Fig. 18.6 Schematic of a two-tank model illustrating two sources of drug removal from the central tank (blood or plasma): systemic and intercompartmental clearance.

Clearance is not to be confused with elimination rate (e.g., mg/min). The elimination rate is not an accurate method of describing the mass of drug removed over time. For example, assuming a first-order process, when plasma concentrations are high, the rate of drug elimination is high. When low, the rate is also low. Clearance is a better descriptor as it is independent of drug concentration.

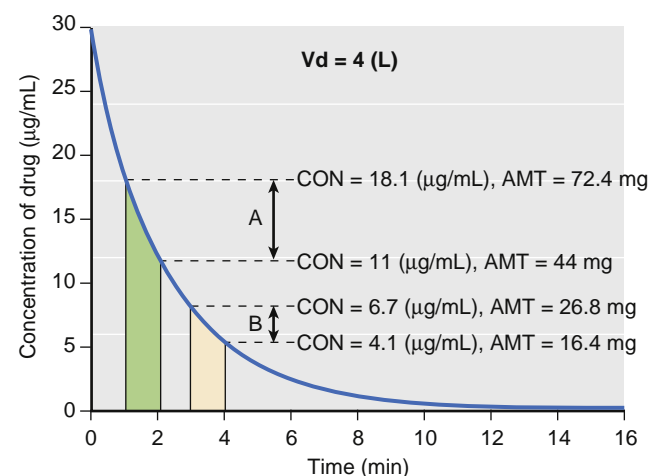


Fig. 18.7 Simulation of drug concentration changes when a drug is administered to a single-tank model with first-order elimination (see **Fig. 18.2**). The concentration changes for two time windows are labeled with dashed lines from 1 to 2 minutes (time window A) and from 3 to 4 minutes (time window B), respectively. The concentrations (CON) at the beginning and end of each time window are used to calculate the amount (AMT) of drug that is eliminated (see text). V_d , Volume of distribution.

To illustrate this point, consider the simulation presented in Fig. 18.7. In this simulation, the total amount of drug at each time can be calculated from the known volume of distribution and measured concentration. The concentration change in time window A is larger than in time window B even though they are both 1 minute in duration. The elimination rates are 28.4 and 10.4 mg/min for time windows A and B, respectively. They are different, and neither can be used as a parameter to represent a measure of drug removal from the body. Because of this limitation with elimination rate, clearance was developed to provide a single number to describe the decay in drug concentration presented in Fig. 18.7.

For discussion purposes, assume that concentration is the power necessary to push drug out of the water tank. The higher the concentration, the larger the amount of drug eliminated. To standardize the elimination rate, the eliminated amount of drug is scaled to concentration. For example, when the elimination rate in time window A (28.4 mg/min) is scaled to the concentration at the middle of the time window (14.2 μ g/mL), the clearance is 2 L/min. When the elimination rate in time window B (10.4 mg/min) is scaled to the concentration at the middle of the time window (5.2 μ g/mL), the clearance is again 2 L/min. If the time interval is narrowed so that the time window approaches zero, the definition of clearance becomes:

$$\text{Clearance} = \frac{\frac{dA(t)}{dt}}{C(t)} \quad (18.3)$$

where $dA(t)/dt$ is the rate of drug elimination at given time t , and $C(t)$ is the corresponding concentration at that time. Rearranging Eq. (18.3) and integrating both numerator and denominator, the following relationship holds:

$$\text{Clearance} = \frac{\int_0^\infty dA(t)}{\int_0^\infty C(t) dt} \quad (18.4)$$

because the term $\int_0^\infty dA(t)$ is equal to the total amount of drug eliminated and $\int_0^\infty C(t) dt$ is the area under curve (AUC) in concentration versus time plot, then the following equation can be derived:

$$\text{Clearance} = \frac{\text{Dose}}{\text{AUC}} \quad (18.5)$$

With long infusions, drug concentrations reach a steady-state condition where the rate of drug elimination $\left(\frac{dA(t)}{dt}\right)$ is in equilibrium with the rate of drug administration (infusion rate). Clearance in a steady-state condition can be obtained using Eq. (18.3) as follows:

$$\text{Clearance} = \frac{\text{Infusion rate}}{\text{Css}} \quad (18.6)$$

where Css is the plasma concentration at steady state.

To illustrate the relationship between clearance and volume of distribution, consider the following simulation using a generic drug dosed in milligrams into a single compartment (tank) representing the distribution volume that has a clearance of 1 L/min. Assume that when drug is administered, the tank is well stirred and has instantaneous mixing throughout the entire volume. Assume the distribution volume is 4 L, the total dose of drug is 64 mg, and that drug elimination is proportional to the amount of drug present inside the tank at any given time. This rate of drug elimination is known as first-order elimination kinetics. When the drug is injected into the 4 L distribution volume, the drug will instantly evenly distribute throughout

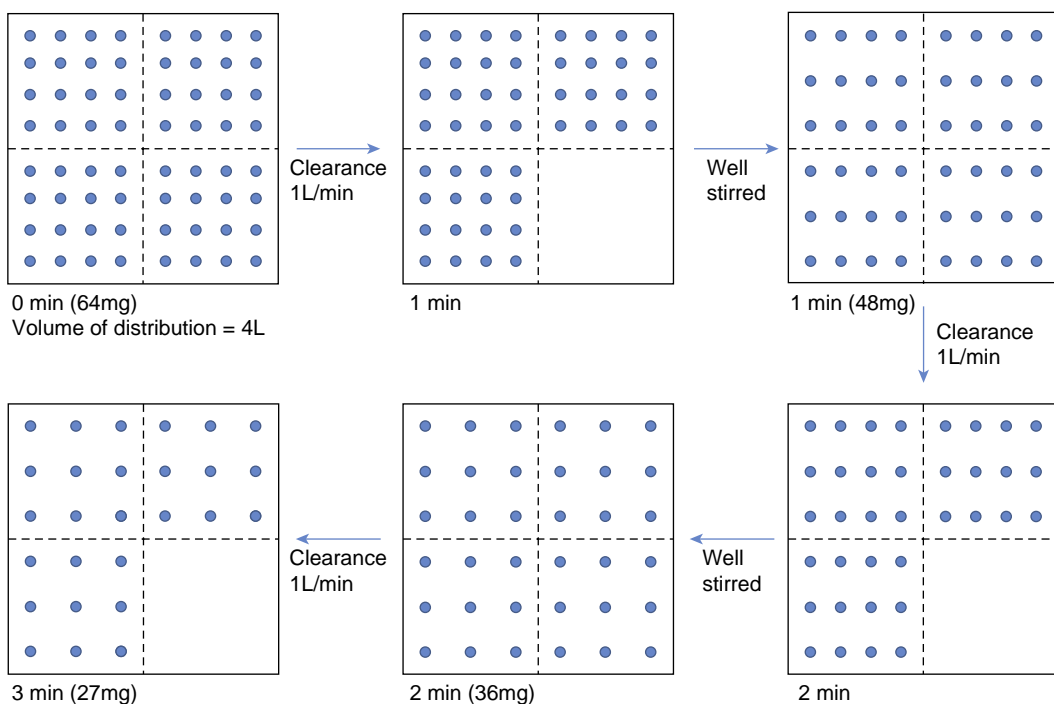


Fig. 18.8 Schematic representation of relationship among clearance, volume of distribution, and elimination rate constant. A generic drug dose of 64 mg is administered into a single compartment volume of 4 L that has a clearance of 1 L/min. Drug elimination is proportional to the amount of drug present inside the compartment at any given time, otherwise known as first-order elimination kinetics. At 1-minute intervals, one of the 4 L is cleared along with all drug contained in that liter. The drug amount decreases by 16, 12, and 9 mg at 1, 2, and 3 minutes.

the compartment (Fig. 18.8). With a clearance of 1 L/min, the amount of drug distributed to one fourth of compartment volume (1 L) will be cleared every minute. In the first minute, 16 mg drug is cleared. The remaining 48 mg will be redistributed evenly throughout the compartment. For the next minute, one fourth of the compartment volume (1 L) is again cleared. In the second minute, 12 mg of drug is cleared. This process repeats every minute. When assuming instantaneously mixing, the ratio of the amount of drug removed within the cleared portion of the distribution volume to the amount of drug within the total distribution volume will remain the same as illustrated in Eq. (18.7).

$$\frac{16\text{mg}}{64\text{mg}} = \frac{12\text{mg}}{48\text{mg}} = \frac{9\text{mg}}{36\text{mg}} = \frac{\text{cleared volume}}{\text{volume of distribution}} \quad (18.7)$$

This ratio, known as the elimination rate constant (k), is described in Eq. (18.8).

$$\frac{\text{CL}}{\text{Vd}} = k \text{ or } \text{CL} = \text{Vd} \times k \quad (18.8)$$

Where CL is clearance with units of volume/time (L/min), Vd is the compartment distribution volume with units of liters (L), and k is the first-order elimination rate constant with units of inverse time (min^{-1}).

Physiologic Model for Clearance

Drug extraction by metabolic organs is illustrated in Fig. 18.9. This model contains a metabolic organ system responsible for drug elimination. According to mass balance, the rate at which drug flows *out* of metabolic organs is the rate at which drug flows *into* them minus the metabolic rate. The elimination rate (dA/dt) can be expressed as $Q(C_{\text{in}} - C_{\text{out}})$. Rearranging $C(t)$ in Eq. (18.3) with C_{in} , clearance can be expressed as

$$\text{Clearance} = \frac{Q(C_{\text{in}} - C_{\text{out}})}{C_{\text{in}}} \quad (18.9)$$

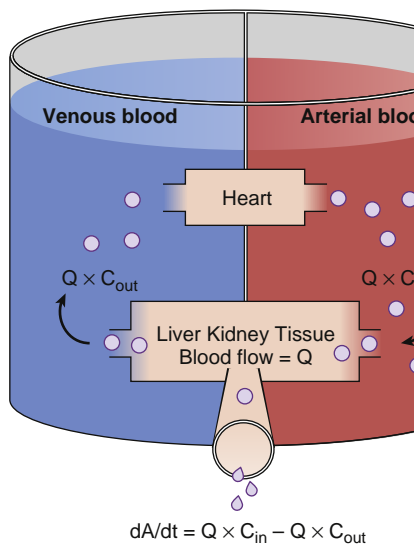


Fig. 18.9 Schematic of drug extraction. Q indicates blood flow. C_{in} and C_{out} indicate drug concentrations presented to and leaving metabolic organs. A indicates the amount of drug, and dA/dt is the drug elimination rate.

where Q is the blood flow to metabolic organs, C_{in} is the concentration of drug delivered to metabolic organs, and C_{out} is the concentration of drug leaving metabolic organs.

The fraction of inflowing drug extracted by the organ is $\frac{C_{\text{in}} - C_{\text{out}}}{C_{\text{in}}}$. This is called the extraction ratio (ER). Clearance

can be estimated as organ blood flow multiplied by the ER. Eq. (18.9) can be simplified to

$$\begin{aligned} \text{Clearance} &= \frac{Q(C_{\text{in}} - C_{\text{out}})}{C_{\text{in}}} \\ &= Q \times \frac{C_{\text{in}} - C_{\text{out}}}{C_{\text{in}}} = Q \times \text{ER} \quad (18.10) \end{aligned}$$

The total clearance is the sum of each clearance by metabolic organs such as the liver, kidney, and other tissues.

Hepatic clearance has been well characterized. For example, the relationship among clearance, liver blood flow, and the ER is presented in Fig. 18.10.¹ For drugs with an ER of nearly 1 (e.g., propofol), a change in liver blood flow produces a nearly proportional change in clearance. For drugs with a low ER (e.g., alfentanil), clearance is nearly independent of the rate of liver blood flow. If nearly 100% of the drug is extracted by the liver, this implies that the liver has a very large metabolic capacity for the drug. In this case, the rate-limiting step in metabolism is the flow of drug to the liver, and such drugs are said to be “flow limited.” As a consequence, any reduction in liver blood flow due to circulatory effects of anesthetic agents or changes in circulatory volumes in cases of perioperative bleeding or other situations of excessive fluid loss can be expected to reduce liver-dependent drug clearance. However, moderate changes in hepatic metabolic function per se will have little

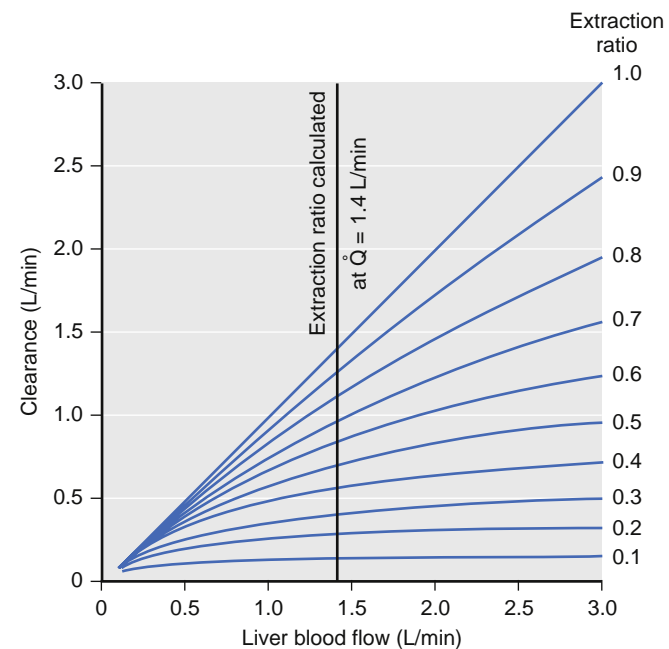


Fig. 18.10 Relationship among liver blood flow (Q), clearance, and extraction ratio. For drugs with a high extraction ratio, clearance is nearly identical to liver blood flow. For drugs with a low extraction ratio, changes in liver blood flow have almost no effect on clearance. (From Wilkinson GR, Shand DG. Commentary: a physiological approach to hepatic drug clearance. *Clin Pharmacol Ther*. 1975;18:377–390.)

impact on clearance because hepatic metabolic capacity is overwhelmingly in excess of demand.

For many drugs (e.g., alfentanil), the ER is considerably less than 1. For these drugs, clearance is limited by the capacity of the liver to take up and metabolize drug. These drugs are said to be “capacity limited.” Clearance will change in response to any change in the capacity of the liver to metabolize such drugs, as might be caused by liver disease or enzymatic induction. However, changes in liver blood flow caused by the anesthetic regimen or other changes in splanchnic circulation usually have little influence on clearance because the liver handles only a fraction of the drug that it sees.

Although most anesthetic drugs are cleared by hepatic metabolism, remifentanil, succinylcholine, and esmolol are cleared in the plasma and tissues by ester hydrolysis, and pancuronium is cleared via the kidney. The relationship between metabolism and clearance is complex.

Hepatic Biotransformation

Most anesthetic drugs are cleared by hepatic biotransformation. The synthetic pathways for biotransformation are covered in detail in many biochemistry texts. Briefly, the liver metabolizes drugs through oxidation, reduction, hydrolysis, or conjugation. Oxidation and reduction occur in the cytochrome P450 system. These enzymes can be induced by exposure to certain drugs (e.g., the herbal remedy St. John’s wort) and increase the liver’s intrinsic metabolic capacity. Other drugs or hepatic disease can inhibit these enzymes (e.g., selected calcium channel blockers and selected antibiotics). Routes of oxidative metabolism include hydroxylation, dealkylation, deamination, desulfuration, epoxidation, and dehalogenation. Conjugation and hydrolysis often occur outside the P450 system, although glucuronidation involves the P450 system as well. The effect of conjugation is to transform hydrophobic molecules into water-soluble molecules through the addition of polar groups and thus render the metabolites easier to excrete via the kidneys. The metabolites generated by the liver are generally inactive, although some drugs (e.g., morphine, midazolam) have metabolites that are as potent as the parent drug. Genetic polymorphism can occur in all of these pathways, and this accounts for part of the variability in clearance in the population.

Pharmacokinetic Models

To create a framework from which to compare drugs and describe drug behavior, pharmacologists developed pharmacokinetic models to characterize drug concentrations as a function of time. These models provide estimates of drug concentrations over time in response to dosing regimens (e.g., bolus vs. infusion). Several types of pharmacokinetic models have been developed. Examples include complex physiologic models and the more common compartmental models.

Physiologic Models

Physiologic models are based on organ and tissue physiologic and anatomic data. Drug concentrations into and out of an organ, organ blood flow, and organ drug distribution

volume are required. Capturing these metrics from all organs is nearly impossible in humans and very challenging in animal models. If obtained, this data is used to estimate volumes and clearances for each organ in the body. Individual organ models are assembled into a whole organism physiological model.² Once assembled, the combined models are complex and mathematically cumbersome. They may not offer a better prediction of plasma drug concentrations over time than simple compartmental models. If the intent of the model is to explore the ability of possible dosing regimens to achieve therapeutic plasma drug concentrations, compartmental models are usually adequate.

Compartmental Models

Compartmental models are built on the same basic concepts as physiologic models, but with significant simplifications. Compartment pharmacokinetic models are strictly empirical. They are based on fitting equations to measured plasma concentrations following a known dose. Kinetic models are transformed into models that characterize changes over time in terms of volumes and clearances. Part of the continuing popularity of pharmacokinetic models is that they can be transformed from an unintuitive exponential form to a more intuitive compartmental form as shown in Fig. 18.11.

Compartment models used to describe anesthetic drugs typically consist of one, two, or three compartments corresponding to the number of exponents in an equation needed to best fit the plasma versus concentration data (see Fig. 18.11). Exponents are difficult to work with and have little clinical meaning. Thus, they are converted into fictitious volumes and clearances. For example, in a three-compartment model, there is a central compartment and two peripheral compartments. The sum of the all volumes is the volume of distribution at steady state. Drug clearance

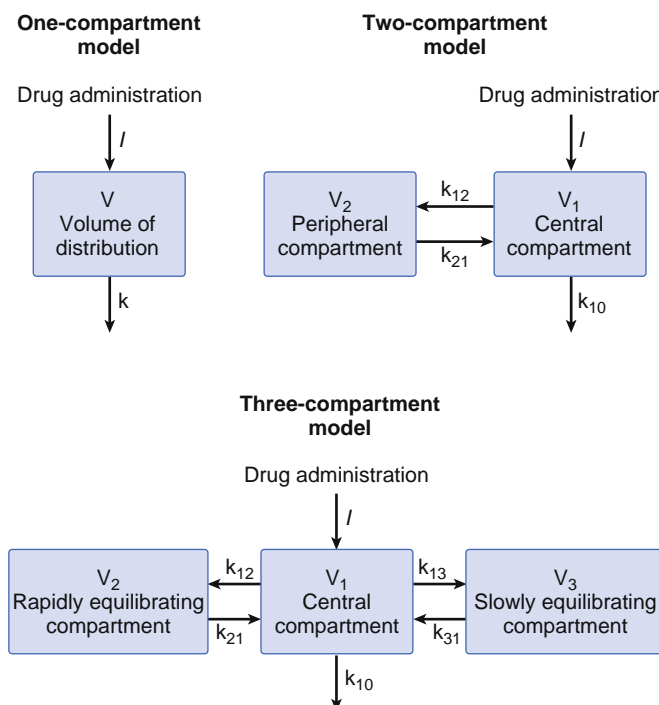


Fig. 18.11 One-, two-, and three-compartment mammillary models.

from the central compartment to the outside is the central clearance. Central clearance accounts for both metabolism and excretion. Clearances between the central and peripheral compartments is the “intercompartmental” clearance. Micro rate constants, expressed as k_{ij} , define the rate of drug transfer from compartment i to compartment j . For example, k_{10} is the micro rate constant describing drug transfer from central compartment to the outside. The intercompartmental micro rate constants (k_{12} , k_{21} , etc.) describe movement of drug between the central and peripheral compartments. Each peripheral compartment has at least two micro rate constants, one for drug entry and one for drug exit. The micro rate constants for the two- and three-compartment models are presented in Fig. 18.11.

Zero Versus First-Order Kinetics

Drug elimination can have one of two profiles, zero- and first-order kinetics. With zero-order kinetics, drug is eliminated at a constant rate. With first-order kinetics, drug is eliminated at a rate proportional to the amount of drug present at that time. These rates are expressed using the following equations.

$$\frac{dA(t)}{dt} = -k_0 \text{ for zero order kinetics} \quad (18.11)$$

$$\frac{dA(t)}{dt} = -k_1 E(t) \text{ for first - order kinetics} \quad (18.12)$$

where $A(t)$ is the amount of drug at time t , $dA(t)$ is the change in drug amount at time t . $-k_0$ is the zero-order elimination rate constant. Its units are mass/time (e.g., mg/min). $-k_1$ is the first-order elimination rate constant. Its units are the reciprocal time 1/time, (e.g., min⁻¹). Most anesthetic drugs have first-order kinetics. When the processes responsible for metabolism are saturated, the kinetics could change from first to zero order.

ONE-COMPARTMENT MODEL

For a one-compartment model with first-order kinetic elimination, the amount of drug at a given time t is described by Eq. (18.13).

$$A(t) = A_0 e^{-kt} \quad (18.13)$$

where A_0 is the initial drug amount (i.e., the initial dose), k is the first-order kinetic elimination rate constant. Note that k must be greater than 0. With this equation, there is an exponential decrease in drug amount.

The distribution volume (V_d) is a function of drug concentration and the total amount of drug in the compartment. Dividing Eq. (18.13) on both sides by V_d yields the following equation:

$$\frac{A(t)}{V_d} = \frac{A_0}{V_d} e^{-kt} \quad (18.14)$$

Drug concentration can be derived from this relationship with Eq. (18.15):

$$C(t) = C_0 \times e^{-kt} \quad (18.15)$$

where $C(t)$ is the concentration at time t , C_0 is the initial concentration at time 0.

Taking the natural logarithm on both sides, the following expression is obtained:

$$\log C(t) = \log C_0 - kt \quad (18.16)$$

A plot of this equation shows a straight line with slope of $-k$ and intercept of $\log C_0$. To yield the time required for the concentration to decrease by half, replacing $\log C(t)$ in Eq. (18.16) to $\log C_0/2$ and rearranging gives:

$$\log \frac{C_0}{2} = \log C_0 - kt \quad (18.17)$$

Solving this equation gives

$$t_{1/2} = \frac{0.693}{k} \quad (18.18)$$

where $t_{1/2}$ is the elimination half-life.

Multicompartment Models

Plasma concentrations over time after an intravenous bolus resemble the curve in Fig. 18.12. This curve has the characteristics common to most drugs when given by intravenous bolus. First, the concentrations continuously decrease over time. Second, the rate of decline is initially steep but continuously becomes less steep, until we get to a portion that is “log-linear.” For many drugs, three distinct phases can be distinguished, as illustrated in Fig. 18.12. A “rapid-distribution” phase (blue line) begins immediately after bolus injection. Very rapid movement of the drug from plasma to the rapidly equilibrating tissues characterizes this phase. Frequently there is a second “slow-distribution” phase (red line), which is characterized by movement of drug into more slowly equilibrating tissues and return of drug to plasma from the most rapidly equilibrating tissues. The terminal phase (green line) is a straight line when plotted on a semi-logarithmic graph. The terminal phase is often called the “elimination phase” because the primary mechanism for decreasing drug concentration during the terminal phase is elimination of drug from the body. The distinguishing

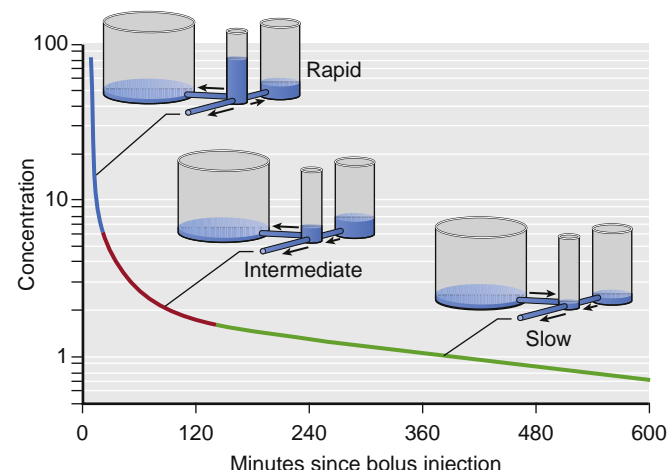


Fig. 18.12 Hydraulic model of fentanyl pharmacokinetics. Drug is administered into the central tank, from which it can distribute into two peripheral tanks, or it may be eliminated. The volume of the tanks is proportional to the volumes of distribution. The cross-sectional area of the pipes is proportional to clearance. (From Youngs EJ, Shafer SL. Basic pharmacokinetic and pharmacodynamic principles. In: White PF, ed. *Textbook of Intravenous Anesthesia*. Baltimore: Williams & Wilkins; 1997.)

characteristic of the terminal elimination phase is that the plasma concentration is lower than tissue concentrations and the relative proportion of drug in plasma and peripheral volumes of distribution remains constant. During this terminal phase, drug returns from the rapid- and slow-distribution volumes to plasma and is permanently removed from plasma by metabolism or excretion.

The presence of three distinct phases after bolus injection is a defining characteristic of a three-compartment model.³ A useful metaphor in describing the features of this model is hydraulics. This model has three tanks corresponding (from left to right) to the slowly equilibrating peripheral compartment, the central compartment (the plasma, into which drug is injected), and the rapidly equilibrating peripheral compartment. The horizontal pipes represent intercompartmental clearance or (for the pipe draining onto the page) metabolic clearance. The volumes of each tank correspond to the volumes of each compartment. The cross-sectional areas of the pipes correlate with fentanyl systemic and intercompartmental clearance. The height of water in each tank corresponds to drug concentration.

By using this hydraulic model, we can follow the processes that decrease drug concentration over time after bolus injection. Initially, drug flows from the central compartment to both peripheral compartments via intercompartmental clearance and completely out of the model via metabolic clearance. Because there are three places for drug to go, the concentration in the central compartment decreases very rapidly. At the transition between the blue line and the red line, a change occurs in the role of the most rapidly equilibrating compartment. At this transition, the concentration in the central compartment falls below the concentration in the rapidly equilibrating compartment, and the direction of flow between them is reversed. After this transition (red line), drug in plasma has only two places to go: into the slowly equilibrating compartment or out the drain pipe. These processes are partly offset by the return of drug to plasma from the rapidly equilibrating compartment. The net effect is that once the rapidly equilibrating compartment has come to equilibration, the concentration in the central compartment falls far more slowly than before.

Once the concentration in the central compartment falls below both the rapidly and slowly equilibrating compartments (green line), the only method of decreasing the plasma concentration is metabolic clearance, the drainpipe. Return of drug from both peripheral compartments to the central compartment greatly slows the rate of decrease in plasma drug concentration.

Curves that continuously decrease over time, with a continuously increasing slope (i.e., curves that look like Fig. 18.12), can be described by a sum of negative exponentials. In pharmacokinetics, one way of denoting this sum of exponentials is to say that the plasma concentration over time is

$$C(t) = Ae^{-\alpha t} + Be^{-\beta t} + Ce^{-\gamma t} \quad (18.19)$$

where t is the time since the bolus, $C(t)$ is the drug concentration after a bolus dose, and A , α , B , β , C , and γ are parameters of a pharmacokinetic model. A , B , and C are called coefficients, whereas α , β , and γ are called exponents. After a bolus injection, all six of the parameters in Eq. (18.19) will be greater than 0.

Special significance is often ascribed to the smallest exponent. This exponent determines the slope of the final log-linear portion of the curve. When the medical literature refers to the half-life of a drug, unless otherwise stated, the half-life will be the terminal half-life. Some literature occasionally refers to the half-life of the initial distribution phase as distribution half-life. The terminal half-life sets an upper limit on the time required for the concentrations to decrease by 50% after drug administration. Usually, the time needed for a 50% decrease will be much faster than that upper limit.

Special Interests in Anesthetic Pharmacokinetics

Front-End Kinetics

Front-end kinetics refers to the description of intravenous drug behavior immediately following administration. How a drug rapidly moves from the blood into peripheral tissues directly influences the peak plasma drug concentration. The amount of drug that moves to the peripheral tissue commonly surpasses the amount that is eliminated during the first few minutes after drug administration. As an example, consider a simulation of a propofol bolus that plots the accumulation of propofol in peripheral tissues and the amount eliminated over time (Fig. 18.13). During the first 4 minutes, the amount distributed to the peripheral tissue is larger than the amount eliminated out of the body. After 4 minutes, the amounts reverse.

With compartmental models, an important assumption is that an intravenous bolus instantly mixes in the central volume, with the peak concentration occurring at the moment of injection without elimination or distribution to peripheral tissues. For simulation purposes, the initial concentration and volume of distribution at time = 0 are extrapolated as if the circulation had been infinitely fast. This, of course, is not real. If drug is injected into an arm

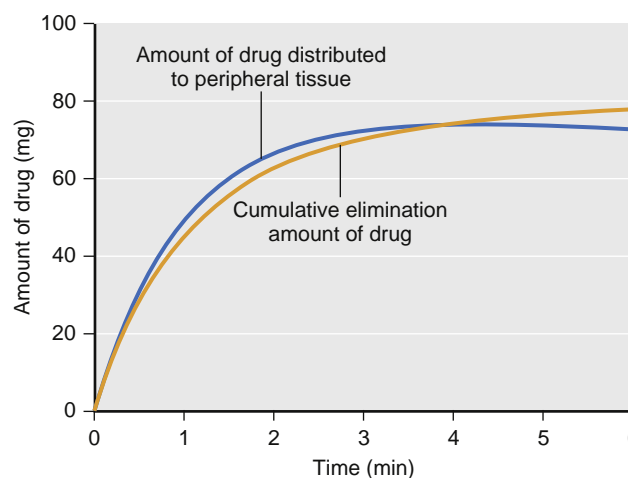


Fig.18.13 Simulation of propofol accumulation in the peripheral tissues (blue line) and the cumulative amount of propofol eliminated (gold line) following a 2-mg/kg propofol bolus to a 77-kg (170-lb), 53-year-old male who is 177 cm (5 ft 10 inch) tall, using published pharmacokinetic model parameters.³² Drug indicates propofol.

vein and the initial concentration is measured in a radial artery, drug appears in the arterial circulation 30 to 40 seconds after injection. The delay likely represents the time required for drug to pass through the venous volume of the upper part of the arm, heart, great vessels, and peripheral arterial circulation. More sophisticated models (e.g., a recirculatory model)⁴ account for this delay and are useful when characterizing the behavior of a drug immediately following bolus administration such as with induction agents where the speed of onset and duration of action are of interest (Fig. 18.14).

Back-End Kinetics

Using estimates of distribution volume and clearance, back-end kinetics is a useful tool that describes the behavior of intravenous agents when administered as continuous infusions. Back-end kinetics provides descriptors of how plasma drug concentrations decrease once a continuous infusion is terminated. An example is decrement time, which predicts the time required to reach a certain plasma concentration once an infusion is terminated. Decrement times are a function of infusion duration. Consider the example of decrement times for a set of continuous target- controlled infusions (TCIs; Fig. 18.15). In this simulation, TCI of propofol is set to maintain a concentration of 4 $\mu\text{g}/\text{mL}$ for 30, 60, and 120 minutes. Once the infusion is stopped, the time to reach 0.5 $\mu\text{g}/\text{mL}$ is estimated. As illustrated, the longer the infusion, the longer the time required to reach 0.5 $\mu\text{g}/\text{mL}$. This example demonstrates how drugs accumulate in peripheral tissues with prolonged infusions. This accumulation prolongs the decrement time.

Another use of decrement times is as a tool to compare drugs within a drug class (e.g., opioids). As a comparator, plots of decrement times are presented as a function of infusion duration. When used this way, decrement times are determined as the time required to reach a target percentage of the concentration just before the termination of a continuous infusion. Examples of 50% and 80% decrement times for selected opioids and sedatives are presented in Fig. 18.16. Of note, for shorter infusions, the decrement times are similar for both classes of anesthetic drugs. Once infusion duration exceeds 2 hours, the decrement times vary substantially. A popular decrement time is the 50% decrement time, also known as the context-sensitive half-time.⁵ The term “context-sensitive” refers to infusion duration and the term “half-time” refers to the 50% decrement time.

Hysteresis

Hysteresis refers to the time delay between changes in plasma concentration and drug effect. Hysteresis accounts for the time required for drug to diffuse from the plasma to the site of action plus the time required, once drug is at the site of action, to elicit a drug effect. A simulation of various propofol bolus doses and their predicted effect on bispectral index are presented in Fig. 18.17. Of note, the time to peak effect for each dose is identical (approximately 1.5 minutes following the peak plasma concentration). The difference between each dose is the magnitude and duration of effect. A key principle here is that when drug concentrations are in flux (e.g., during induction and emergence), changes in drug effect will lag behind changes in plasma drug concentration. This lag between the plasma concentration and

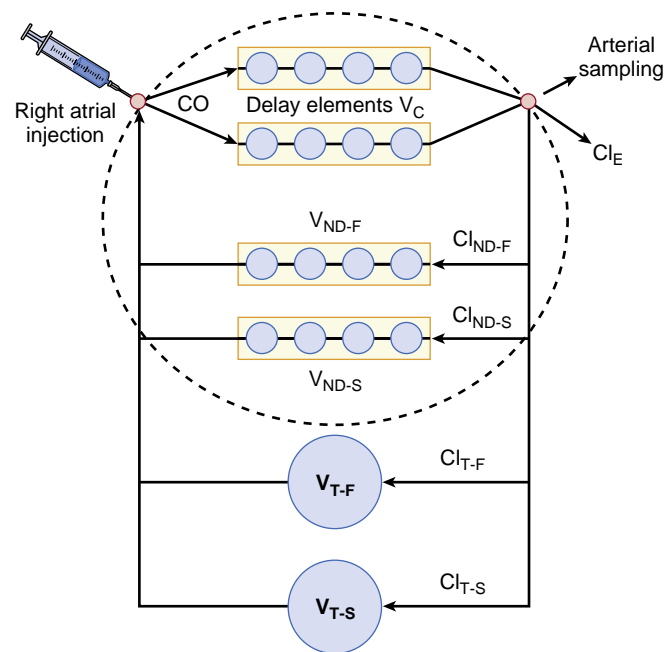


Fig. 18.14 A recirculatory model accounting for cardiac output (CO), transit delays, pulmonary uptake (delay elements V_C and V), and nondistributive mixing pathways (V_{ND} and Cl_{ND}). All the components within the dashed circle are required to accurately model the central volume of distribution. In most situations, this complexity is not required, and the simpler approach of assuming instantaneous mixing within the central volume is an adequate approximation. Cl_{ND-F} , Fast nondistributive clearance; Cl_{ND-S} , slow nondistributive clearance; Cl_{T-F} , fast tissue clearance; Cl_{T-S} , slow tissue clearance; V_{ND-F} , fast nondistributive volume; V_{ND-S} , slow nondistributive volume; V_{T-F} , fast tissue volume; V_{T-S} , slow tissue volume. (From Krejcie TC, Avram MJ, Gentry WB. A recirculatory model of the pulmonary uptake and pharmacokinetics of lidocaine based on analysis or arterial and mixed venous data from dogs. *J Pharmacokinet Biopharm*. 1997;25:169–190.)

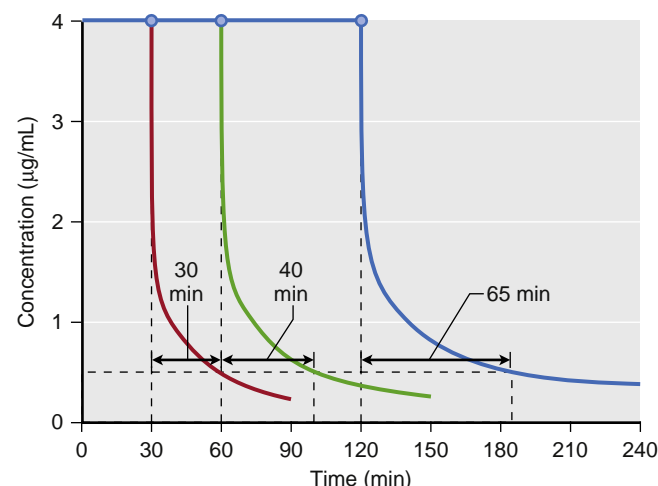


Fig. 18.15 Simulation of decrement times for a target-controlled infusion set to maintain a target propofol concentration of 4 $\mu\text{g}/\text{mL}$ for 30, 60, and 120 minutes. Once terminated, the time required to reach 0.5 $\mu\text{g}/\text{mL}$ was 30, 40, and 65 minutes for each infusion, respectively. Simulations of the decrement times used a published pharmacokinetic model. (From Schnider TW, Minto CF, Gambus PL, et al. The influence of method of administration and covariates on the pharmacokinetics of propofol in adult volunteers. *Anesthesiology*. 1998;88(5):1170–1182.)

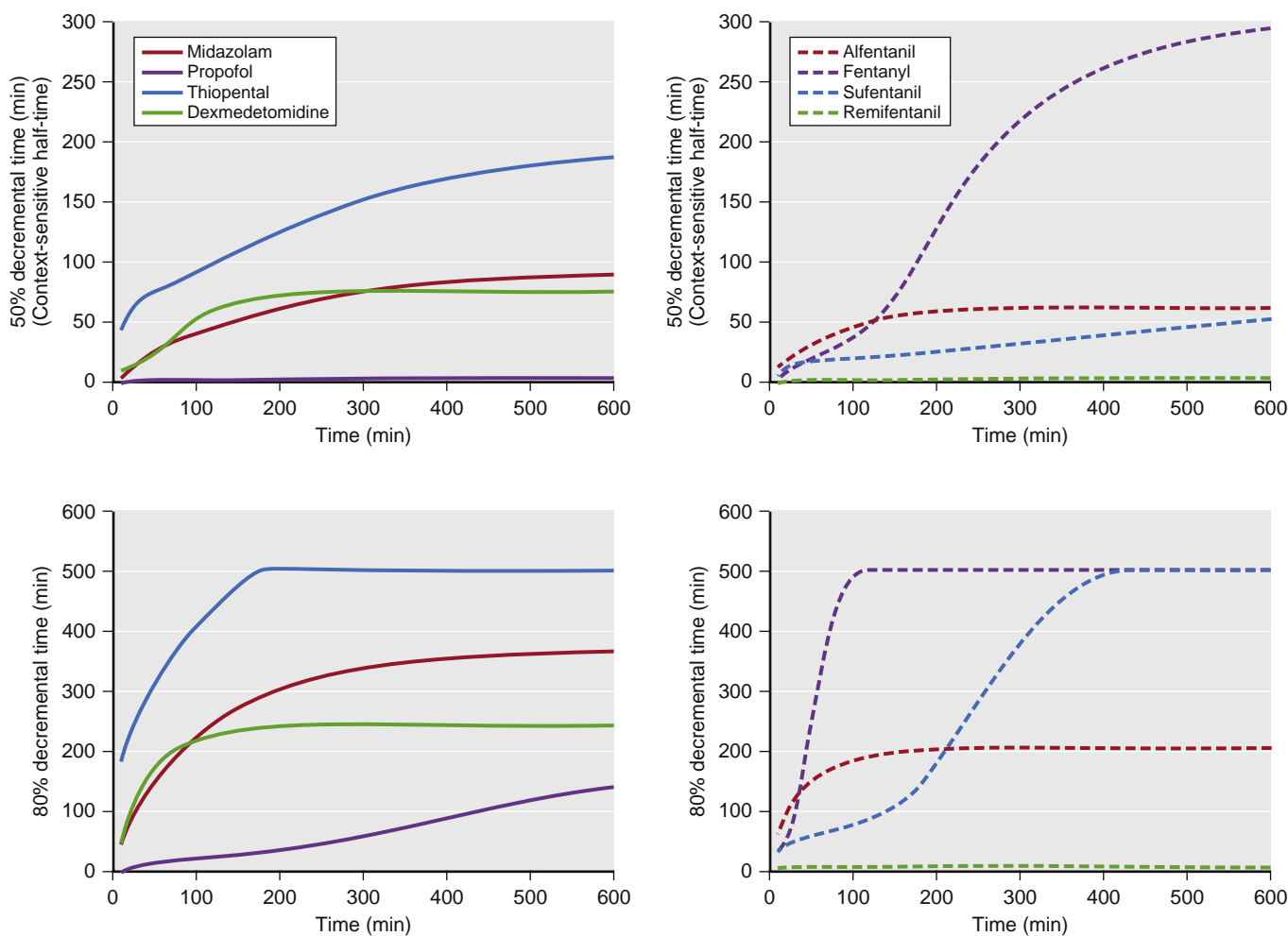


Fig. 18.16 Fifty percent and 80% decrement times for selected sedatives (left side) and opioids (right side). The vertical axes refer to the time required to reach the desired decrement time. The horizontal axes refer to infusion duration. Simulations of the decrement times used published pharmacokinetic models for each sedative and analgesic. (Data from references 5, 43, 57, and 68-70.)

effect usually results in the phenomenon called hysteresis in which two different plasma concentrations correspond to one drug effect or one plasma concentration corresponds to two drug effects. Fig. 18.17 shows that different concentrations, C and c , correspond to the same bispectral index scale (BIS). To collapse the hysteresis between plasma concentration and effect and to match one plasma concentration to one drug effect, this lag is often modeled with an effect-site compartment added to the central compartment. Kinetic micro rate constants used to describe biophase include k_{1e} and k_{e0} . The k_{1e} describes drug movement from the central compartment to the effect site, and k_{e0} describe the elimination of drug from the effect-site compartment. There are two important assumptions with the effect-site compartment: (1) the amount of drug that moves from the central compartment to the effect-site compartment is negligible and vice versa, and (2) there is no “volume” estimate to the effect-site compartment.

Typically, the relationship between plasma and the site of drug effect is modeled with an “effect-site” compartment model, as shown in Fig. 18.18. The site of drug effect is connected to plasma by a first-order process. The equation that relates effect-site concentration to plasma concentration is

$$\frac{dCe}{dt} = k_{e0} \times (Cp - Ce) \quad (18.20)$$

where Ce is the effect-site concentration, Cp is the plasma drug concentration, and k_{e0} is the rate constant for elimination of drug. The constant k_{e0} describes the rate of rise and offset of drug effect (Fig. 18.19).

In summary, although of interest to many clinicians, the conventional pharmacokinetic term *half-life* has limited meaning to anesthetic practice since the clinical behavior of drugs used in anesthesia is not well described by half-life. Instead, the pharmacokinetic principles discussed in this section (such as volume of distribution, clearance, elimination, front-end kinetics, back-end kinetics, context-sensitive half-time, and biophase) describe how drugs used in anesthesia will behave.

Pharmacodynamic Principles

Simply stated, pharmacokinetics describes what the body does to the drug, whereas pharmacodynamics describes what the drug does to the body. In particular, pharmacodynamics describes the relationship between drug concentration and pharmacologic effect.

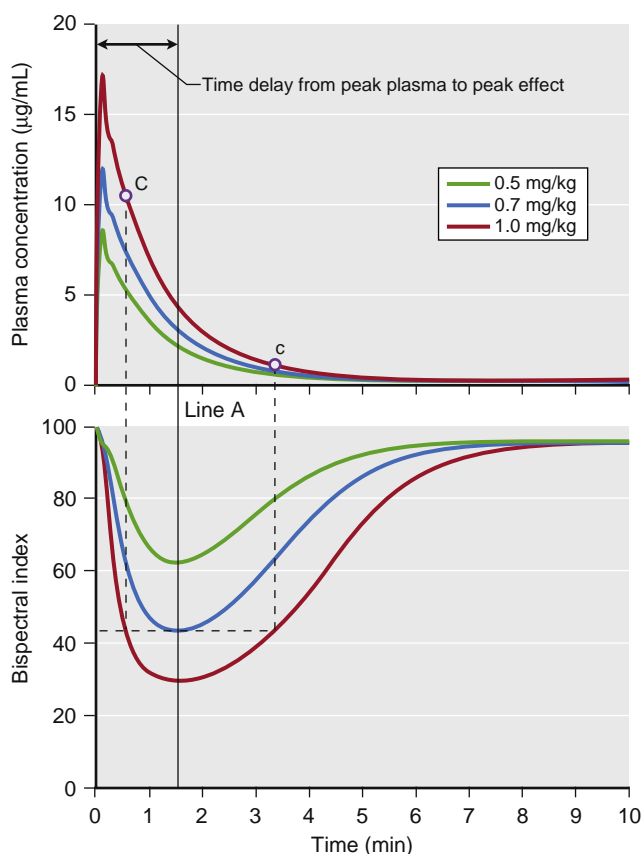


Fig. 18.17 Illustration of hysteresis. The top plot presents a simulation of three propofol doses and the resultant plasma concentrations. The bottom plot presents a simulation of the predicted effect on the bispectral index scale (BIS). These simulations assume linear kinetics: regardless of the dose, effects peak at the same time (*line A*) as do the plasma concentration. The time to peak effect is 1.5 minutes. Even the plasma concentrations of point C and c are different; the BIS of those two points are same. It shows the hysteresis between plasma concentration and BIS. Simulations used published pharmacokinetic and pharmacodynamic models. (Data from references 32 and 57.)

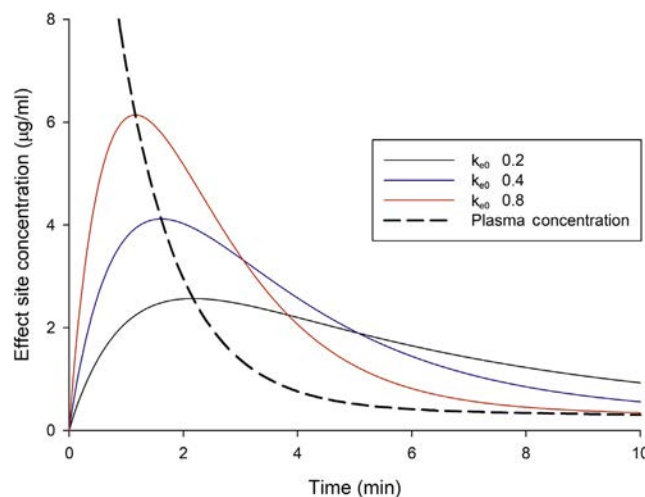


Fig. 18.19 Effect of the k_{e0} changes. As the k_{e0} decreases, the time to peak effect is prolonged. (Data from references 32, 57, 67.)

simultaneously. For example, consider the measured plasma concentrations of a drug following a bolus dose and the associated changes in the spectral edge from one individual presented in Fig. 18.20. Spectral edge is an easily captured metric used to quantify the electroencephalogram (EEG). Shortly after the plasma concentration peaks, the spectral edge starts to drop, reaches a nadir, and then returns to baseline as the plasma concentrations drop to near 0.

Combining data from several individuals and plotting the measured concentrations versus the observed effect (modified to be a percentage of the maximal effect across all individuals), the data create a hysteresis loop (Fig. 18.21). The ascending portion of the loop represents rising drug concentrations (see arrow). While rising, the increase in drug effect lags behind the increase in drug concentration. For the descending loop, the decrease in drug effect lags behind the decrease in drug concentration.

To create a pharmacodynamic model, the hysteresis loop is collapsed using modeling techniques that account for the lag time between plasma concentrations and the observed effect. These modeling techniques provide an estimate of the lag time, known as the $t_{1/2}k_{e0}$, and an estimate of the effect-site concentration (C_e) associated with a 50% probability of drug effect (C_{50}). Most concentration effect relationships in anesthesia are described with a sigmoid curve. The standard equation for this relationship is the “Hill Equation,” also known as the “sigmoid E_{max} relationship” (Eq. 18.21),

$$\text{Effect} = E_0 + (E_{max} - E_0) * \left(\frac{C^g}{C_{50}^g + C^g} \right) \quad (18.21)$$

where E_0 is the baseline effect, E_{max} is the maximal effect, C is the drug concentration, and γ (gamma) represents the slope of the concentration-effect relationship. Gamma (γ) is also known as the “Hill coefficient.” For values of $\gamma < 1$, the curve is hyperbolic; for values of $\gamma > 1$, the curve is sigmoid. Fig. 18.22 presents an example of this relationship: a fentanyl effect-site concentration-effect curve for analgesia. This example illustrates how C_{50} and γ characterize the concentration-effect relationship.

Potency and Efficacy

Two important concepts are relevant to this relationship: potency and efficacy. Potency describes the amount of drug

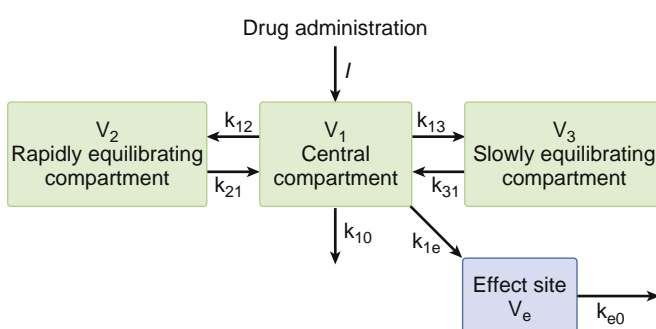


Fig. 18.18 A three-compartment model with an added effect site to account for the delay in equilibration between the rise and fall in arterial drug concentrations and the onset and offset of drug effect. The effect site is assumed to have a negligible volume.

Models used to describe the concentration-effect relationships are created in much the same way as pharmacokinetic models; they are based on observations and used to create a mathematical model. To create a pharmacodynamic model, plasma drug levels and a selected drug effect are measured

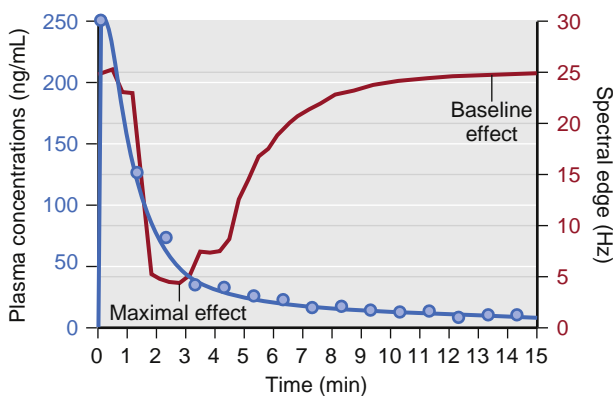


Fig. 18.20 Schematic representation of drug plasma concentrations (blue circles) following a bolus and the associated changes in the electroencephalogram's spectral edge (red line) measured in one individual. Note that changes in spectral edge lag behind changes in plasma concentrations.

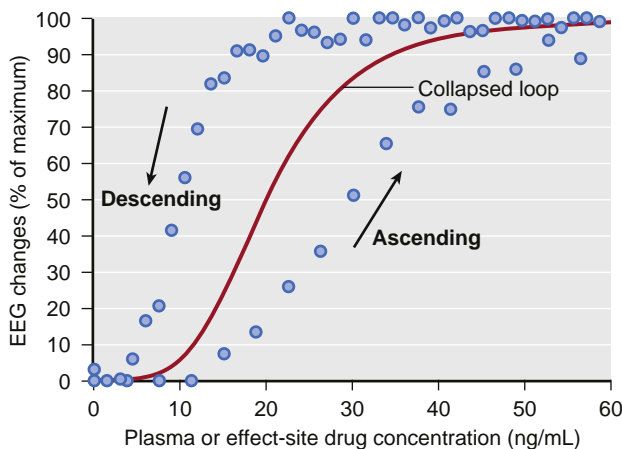


Fig. 18.21 Schematic representation of plasma concentrations versus normalized spectral edge measurements (presented as a percentage of maximal effect) from several individuals (blue circles). The black arrows indicate the ascending and descending arms of a hysteresis loop that coincide with increasing and decreasing drug concentrations. The red line represents the pharmacodynamic model developed from collapsing the hysteresis loop. *EEG*, Electroencephalogram.

required to elicit an effect. The C_{50} is a common parameter used to describe potency. For drugs that have a concentration-versus-effect relationship that is shifted to the left (small C_{50}), the drug is considered to be more potent; the reverse is true for drugs that have a concentration-versus-effect relationship shifted to the right. For example, as illustrated in Fig. 18.23, the analgesia C_{50} for some of the fentanyl congeners ranges from small for sufentanil (0.04 ng/mL) to large for alfentanil (75 ng/mL). Thus, sufentanil is more potent than alfentanil.

Efficacy is a measure of drug effectiveness at producing an effect once it occupies a receptor. Similar drugs that work through the same receptor may have varying degrees of effect despite having the same receptor occupancy. For example, with G-protein coupled receptors, some drugs may bind the receptor in such a way as to produce a more pronounced activation of second messengers causing more of an effect than others. Drugs that achieve maximal effect are known as full agonists, and those that

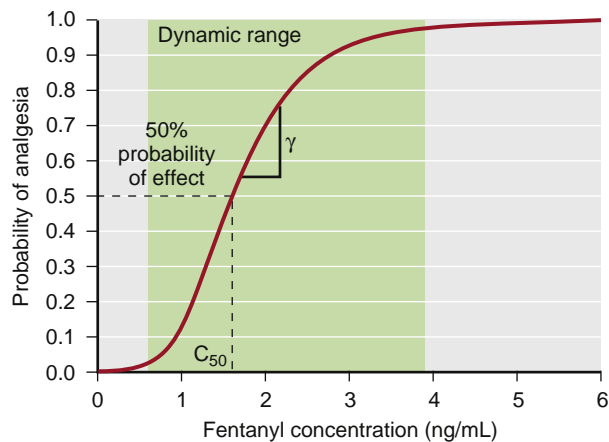


Fig. 18.22 A pharmacodynamic model for the analgesic effect of fentanyl. The green area represents the dynamic range, the concentration range where changes in concentration lead to a change in effect. Concentrations above or below the dynamic range do not lead to changes in drug effect. The C_{50} represents the concentration associated with 50% probability of analgesia. Gamma (γ) represents the slope of the curve in the dynamic range.

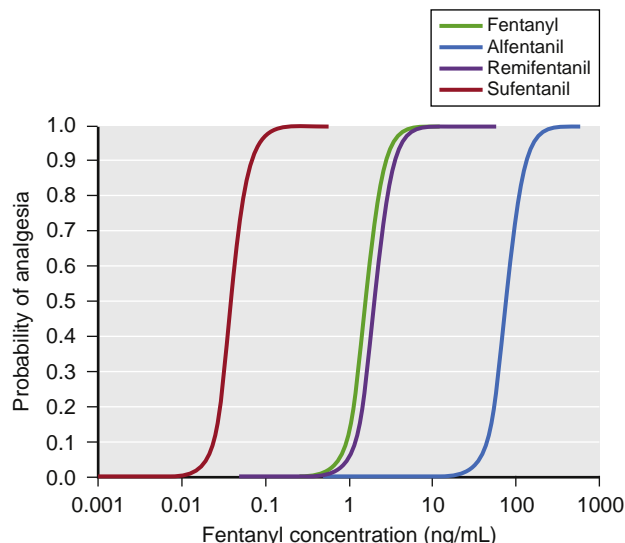


Fig. 18.23 Pharmacodynamic models for fentanyl congeners. The C_{50} for each drug is different, but the slope and maximal effect are similar. (From Egan TD, Muir KT, Hermann DJ, et al. The electroencephalogram (EEG) and clinical measures of opioid potency: defining the EEG-clinical potency relationship ("fingerprint") with application to remifentanil. *Int J Pharmaceut Med*. 2001;15(1):11–19.)

have an effect less than maximal effect are known as partial agonists.

Effective Versus Lethal Doses

A single drug can have multiple effects. The C_{50} concept is used to compare various drug effects for a single drug. For example, as illustrated in Fig. 18.24, fentanyl has a different C_{50} for analgesia (2 ng/mL), ventilatory depression (4 ng/mL), loss of response to laryngoscopy (15 ng/mL), and changes in the EEG (20 ng/mL).⁶

The concentration range where changes in drug effect occur is known as the *dynamic range*. In Fig. 18.22, the

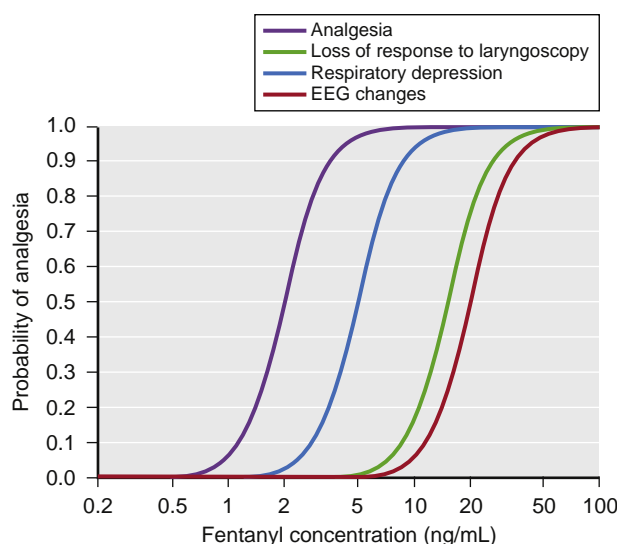


Fig. 18.24 Pharmacodynamic models for various fentanyl effects. *EEG*, Electroencephalogram. (From Egan TD, Muir KT, Hermann DJ, et al. The electroencephalogram (EEG) and clinical measures of opioid potency: defining the EEG-clinical potency relationship ("fingerprint") with application to remifentanil. *Int J Pharmaceut Med*. 2001;15(1):11–19.)

dynamic range is from 0.6 to 3.9 ng/mL to cover a probability of analgesia ranging from 2% to 97%. Concentrations outside the dynamic range do not yield much change in drug effect. Levels below the dynamic range are ineffective, and those above the dynamic range do not provide additional effect.

Like other effects, the concentration-relationship for death is also described with a sigmoid E_{max} curve. The relationship between drug and effect is expressed differently in that the horizontal axis uses dose in place of concentration. Similar to the C_{50} , the ED_{50} is the dose at which there is a 50% probability of effect, and the LD_{50} is the dose with a 50% probability of death. The therapeutic index of a drug is defined as the ratio between the LD_{50} and the ED_{50} (Fig. 18.25). The larger the ratio, the safer the drug is for clinical use.

Anesthetic Drug Interactions

Anesthetics rarely consist of one drug, but rather a combination of drugs to achieve desired levels of hypnosis, analgesia, and muscle relaxation. Hypnotics, analgesics, and muscle relaxants all interact with one another such that rarely does one drug, when administered in the presence of other drugs, behave as if it were administered alone. For example, when administering an analgesic in the presence of a hypnotic, analgesia is more profound with the hypnotic than by itself and hypnosis is more profound with the analgesic than by itself. Thus, anesthesia is the practice of applied drug interactions. This phenomenon is likely a function of each class of drug exerting an effect on different receptors.

Early work by McEwan and associates described interactions between two drugs and is illustrated in Fig. 18.26.⁷ It presents the interaction between isoflurane, a likely GABA agonist, and fentanyl, an opioid receptor agonist. This plot illustrates two key points: First, with a relatively low fentanyl concentration (<2 ng/mL), there is a substantial decrease (>50%) in the end tidal isoflurane concentration necessary

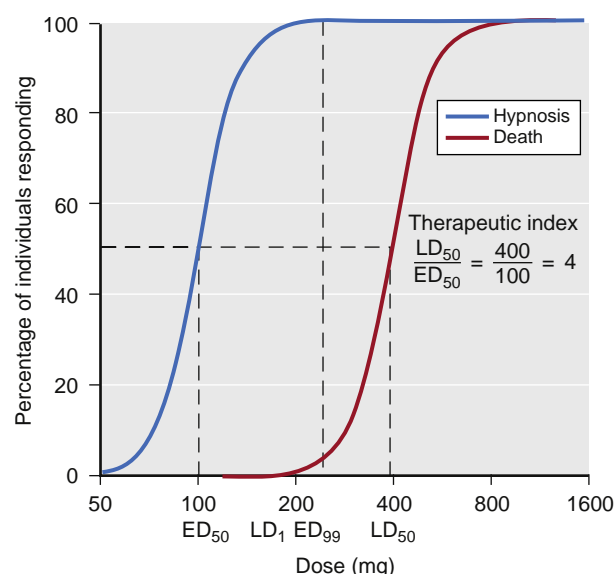


Fig. 18.25 Median effective dose (ED_{50}), median lethal dose (LD_{50}), and the therapeutic index. The blue curve represents the dose-effect relationship for a sedative hypnotic to achieve unresponsiveness. The red curve represents the dose-effect relationship for the same sedative hypnotic to achieve death. The therapeutic index is the ratio of the LD_{50}/ED_{50} , which in this example is 400. Also of interest are the ED_{99} and LD_1 . The ED_{99} is the dose with a 99% probability of unresponsiveness, and the LD_1 is the dose with a 1% probability of death. In this example, the LD_1 is less than the ED_{99} , which is clinically unacceptable.

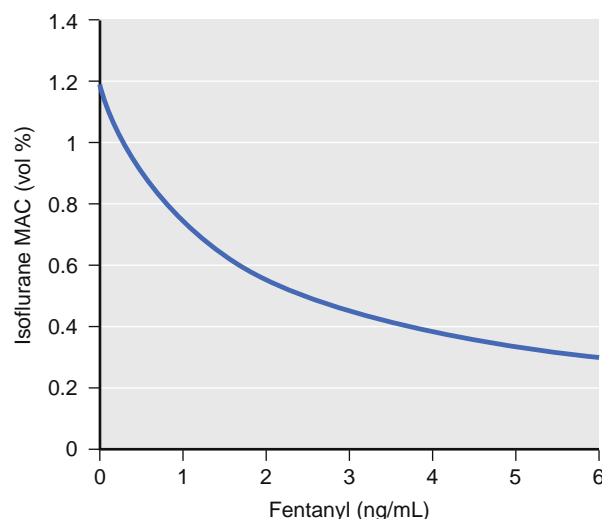


Fig. 18.26 The influence of fentanyl on the isoflurane minimal alveolar concentration (MAC) associated with a 50% probability of movement with skin incision. (Modified from McEwan AI, Smith C, Dyar O. Isoflurane minimum alveolar concentration reduction by fentanyl. *Anesthesiology*. 1993;78:864–869.)

to achieve minimal alveolar concentration (MAC) necessary to avoid movement with skin incision. Second, with fentanyl concentrations above 3 ng/mL, the end tidal concentration of isoflurane to maintain the MAC, although low, does not change much. Thus, there is a ceiling effect indicating that some isoflurane is necessary regardless of the fentanyl concentration to maintain a MAC of anesthesia.

A substantial body of work has been done to explore how anesthetic drugs interact with one another. As illustrated in Fig. 18.27, interactions have been characterized as antagonistic, additive, and synergistic. When drugs that have an

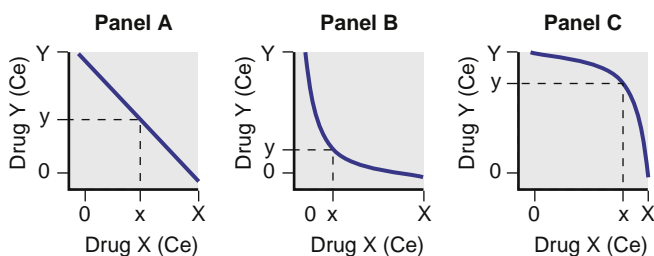


Fig. 18.27 Drug interactions. For two drugs, X and Y, Panel (A) represents additive, Panel (B) represents synergistic, and Panel (C) represents antagonistic interactions.

additive interaction are coadministered, their overall effect is the sum of the two individual effects. With antagonistic interactions, the overall effect is less than if the drug combination were additive; with synergistic interactions, the overall effect is greater than if the drug combination were additive.

A term used to characterize the continuum of drug concentrations across various combinations of drug pairs (X in combination with Y) is the isobole. The isobole is an isoeffect line for a selected probability of effect. A common isobole is the 50% isobole line. It represents all possible combinations of two-drug effect-site concentrations that would lead to a 50% probability of a given effect. Other isoboles are of more clinical interest. For example, the 95% isobole for loss of responsiveness represents the concentration pairs necessary to ensure a 95% probability of unresponsiveness. Similarly, the 5% isobole represents the concentration pairs in which the likelihood of that effect is low (i.e., most patients would be responsive). When formulating an anesthetic dosing regimen, dosing an anesthetic to achieve a probability of effect just above but not far beyond the 95% isobole is ideal (Fig. 18.28).

Hendrickx and colleagues surveyed the literature for work in both humans and animal models that described anesthetic drug interactions for opioids, sedative hypnotics, and inhalation agents for two anesthetic effects: (1) loss of responsiveness (humans) and loss of the righting reflex (animals) and (2) immobility defined as loss of movement in response to noxious stimulus in a non-paralyzed subject.⁸ They found several interesting features of anesthetic drug combinations. First, inhalation agents when combined are strictly additive, suggesting a common mechanism of action, except for nitrous oxide, which has an infra-additive interaction with other inhalation agents. Second, interactions between various intravenous drugs and inhalation agents are synergistic except for nitrous oxide and GABA sedative hypnotics. Third, interactions between different classes of intravenous drugs (e.g., opioids and sedative hypnotics) are also primarily synergistic, except for ketamine and benzodiazepines (Fig. 18.29).

Several researchers have developed mathematical models that characterize anesthetic drug interactions in three dimensions. These models are known as response surface models and include effect-site concentrations for each drug, as well as a probability estimate of the overall effect. Fig. 18.30 presents the propofol-remifentanil interaction for loss of responsiveness as published by Bouillon and

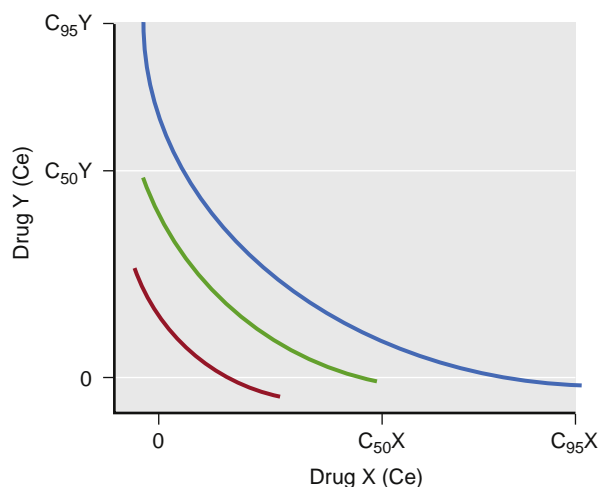


Fig. 18.28 Schematic illustration of iso-effect (isobole) lines. The red, green, and blue lines represent the 50% and 95% isoboles for a synergistic interaction between drugs X and Y. Isoboles represent concentration pairs with an equivalent effect. A set of 5%, 50%, and 95% isoboles can be used to describe the dynamic range of the concentrations for drugs X and Y for a given effect. As with single concentration effect curves, the ideal dosing leads to concentration pairs that are near the 95% isobole.

associates.⁹ The response surface presents the full range of remifentanil-propofol isoboles (0%-100%) for loss of responsiveness. There are two common representations of the response surface model: the three-dimensional plot and the topographical plot. The topographical plot represents a top-down view of the response surface with drug concentrations on the vertical and horizontal axes. Drug effect is represented with selected isobole lines (i.e., 5%, 50%, and 95%).

Response surface models have been developed for a variety of anesthetic effects to include responses to verbal and tactile stimuli, painful stimuli, hemodynamic or respiratory effects, and changes in electrical brain activity. For example, with airway instrumentation, response surface models have been developed for loss of response to placing a laryngeal mask airway,¹⁰ laryngoscopy,^{11,12} tracheal intubation,¹³ and esophageal instrumentation¹⁴ for selected combinations of anesthetic drugs. Although many response surface models exist, there are several gaps in available models covering all common combinations of anesthetic drugs and various forms of stimuli encountered in the perioperative environment.

Recent work characterizing the interaction between sevoflurane and remifentanil has been done for a variety of drug effects to include loss of responsiveness, loss of response to several surrogates of surgical pain such as electrical tetany (up to 50 mA), pressure algometry (50 PSI pressure on the anterior tibial), loss of response to laryngoscopy, and temperature.¹² Using end tidal measures of sevoflurane was found to be inaccurate under non-steady state conditions (i.e., with a change in vaporizer settings). This was because end tidal concentrations did not account for the hysteresis (or time lag) between end tidal and effect-site concentrations. Improved model predictions were achieved when using estimated effect site concentrations.¹⁵ Overall, for sevoflurane-opioid interactions, analgesic effects are

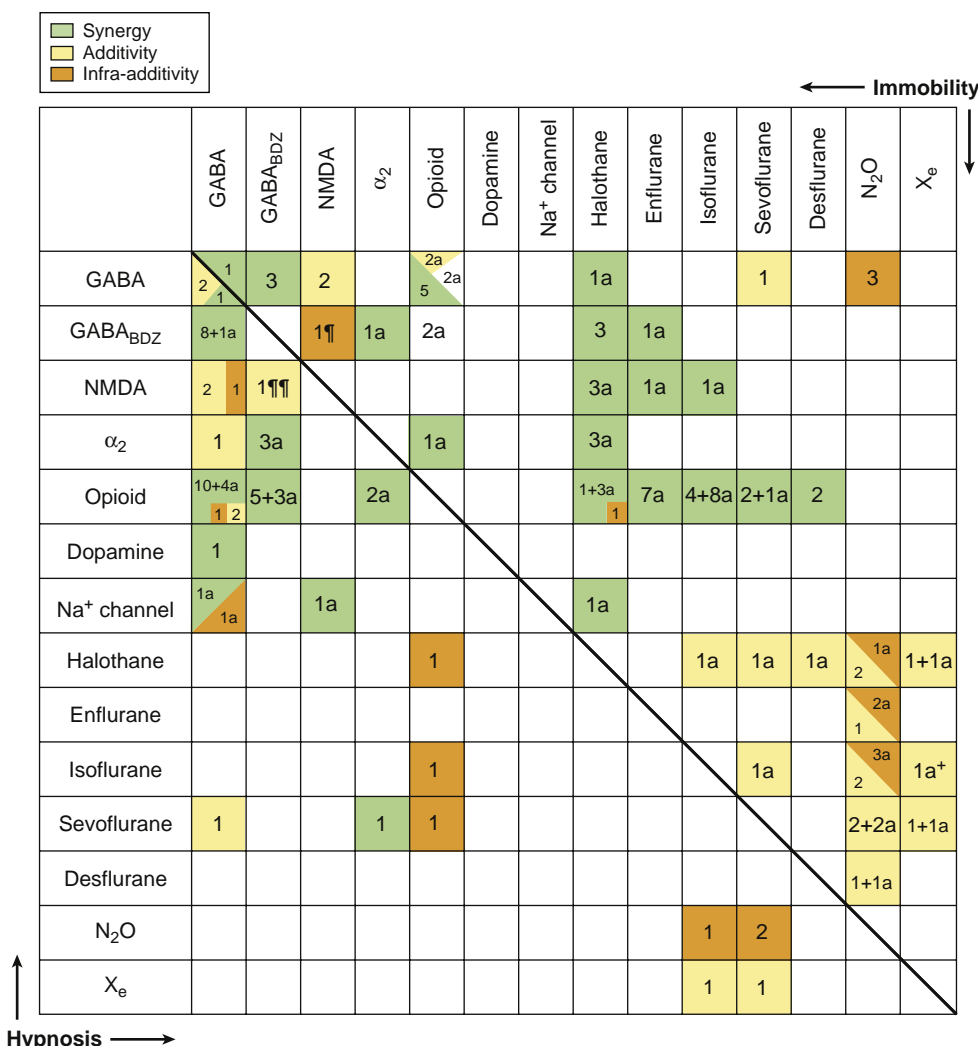


Fig. 18.29 Summary of drug interactions in humans and animals for hypnosis (loss of responsiveness in humans, loss of righting reflex in animals) and immobility (loss of movement in response to a noxious stimulus). The numbers in each cell refer to the number of papers supporting the finding. α_2 Agonists include dexmedetomidine and clonidine. Opioid agonists include morphine, remifentanil, fentanyl, sufentanil, and alfentanil. Dopamine agonists include droperidol and metoclopramide. Na⁺ (sodium) channel antagonists include lidocaine and bupivacaine. The letter "a" indicates the interaction was characterized in an animal model. The thick diagonal line separates studies characterizing drug-drug interactions of hypnosis (bottom half) and immobility (top half). GABA, Gamma aminobutyric acid (GABA agonist drugs include propofol, thiopental, methohexitol, and etomidate; GABA_{BDZ} agonist drugs that work via benzodiazepine binding site include midazolam and diazepam); NMDA, N-methyl-D-aspartate (NMDA receptor antagonists include ketamine) (From Hendrickx J, Eger EI 2nd, Sonner JM, et al. Is synergy the rule? A review of anesthetic interactions producing hypnosis and immobility. *Anesth Analg*. 2008;107:494–506.)

markedly synergistic whereas sedative effects are somewhat synergistic.

Preliminary work has explored the adaptability of the sevoflurane-remifentanil interactions to other potent inhaled agent–opioid combinations using MAC and opioid equivalencies.¹⁶ Predictions from sevoflurane-remifentanil models adapted to isoflurane-fentanyl correlated well with observed effects in patients undergoing elective general surgery procedures. Recent work has also explored the construction of models that characterize the interactions between three or more drugs.¹⁷ For example, Vereecke and associates published a model that accounts for nitrous oxide, sevoflurane, and remifentanil.¹⁸ This is of clinical relevance because most anesthetics consist of more than two anesthetic drugs.

Substantial work has explored interactions between sedative hypnotics and opioids, primarily propofol with

alfentanil¹⁹ or remifentanil^{9,11,14,20,21} for a variety of effects. As with potent inhaled anesthetics and opioids, the interactions between sedative hypnotics and opioids for analgesic effects are markedly synergistic whereas sedative hypnotic effects are somewhat synergistic.

Some work has explored interactions between different types of sedative hypnotics. Two include midazolam combined with propofol^{22,23} and propofol combined with a volatile anesthetic.^{24–26} These interactions were found to be primarily additive.

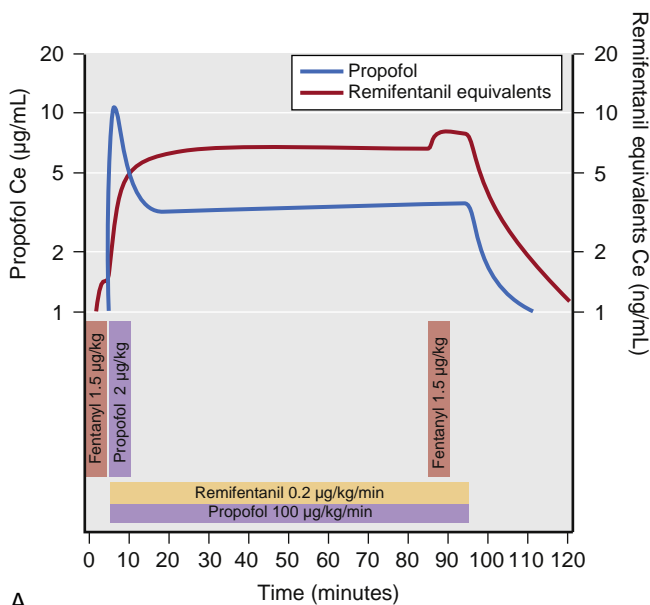
Drug Displays

One major disadvantage to response surface models, as presented in the literature, is that they are complex and difficult to use in a clinical setting. Recent work has adapted these models to drug displays that allow clinicians to use them in real-time patient care settings.

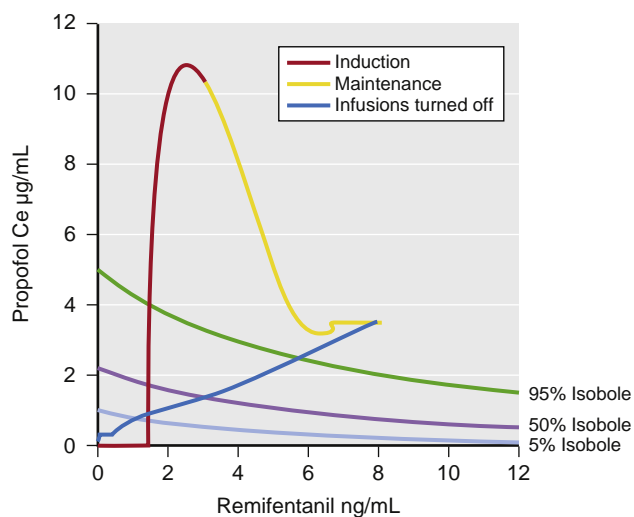
These displays provide estimates of not only drug concentrations (both plasma and effect site) but various drug effects over time such as loss of responsiveness, analgesia, and reduction in response to peripheral train-of-four simulation (i.e., monitoring of muscle relaxant action), among others. With manual entry of patient demographics (age, gender, height, and weight) and drugs administered by syringe, either by bolus or continuous infusion along with automated data collection from an anesthesia machine (end tidal potent inhaled anesthetic concentrations and, in some instances, infusion pump information), drug displays

provide predictions of drug concentration and effects. Drug displays are currently available from several anesthesia machine manufacturers (Navigator Suite from GE Healthcare, Wauwatosa, Wisconsin, USA, and SmartPilot View from Dräger, Lübeck, Germany). An example of a drug display is presented in Fig. 18.30. All drug display examples are based on response surface interaction models.

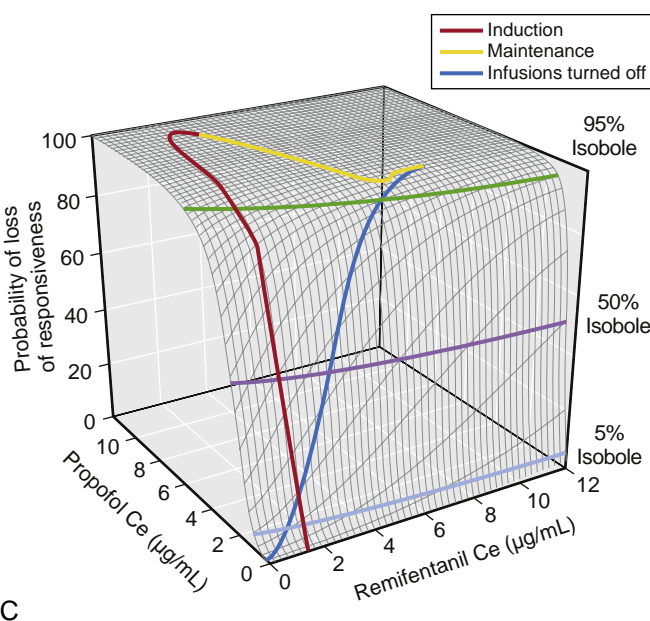
A unique feature of drug displays is that a given dosing regimen can be simulated prior to administration. This information may be useful in identifying the optimal dose in challenging patients, especially when more than one



A



B



C

Fig. 18.30 (A–C) Simulation of a 90-minute total intravenous anesthetic consisting of propofol bolus (2 μg/kg) and infusion (100 μg/kg/min), remifentanil (0.2 μg/kg/min), and intermittent fentanyl boluses (1.5 μg/kg). (A) Resultant effect site concentrations (Ce) are presented. (B) Predictions of loss of responsiveness are presented on a topographical (top-down) view. (C) A three-dimensional response surface is shown. The light blue, purple, and green lines represent the 5%, 50%, and 95% isoboles. Each isobole presents the propofol-remifentanil pairs that yield the same effect. The inward bow of the isoboles indicates that the interaction is synergistic. The isoboles are in close proximity to one another indicating a steep transition from responsive to unresponsive.

drug is used. The drug displays use population models that, although generalizable, may not provide a good “fit” to every patient. For some drug display systems, observed patient responses are used to calibrate predictions of drug effect (Fig. 18.31). For example, with elderly or debilitated patients, smaller doses are often required to achieve a desired effect. Drug displays allow clinicians to identify concentrations that produce a desired response and can be used to titrate additional anesthetic.

There are several other advantages from using drug displays. When titrating an anesthetic, it is often difficult to appreciate when effect-site concentrations are near steady state. Clinicians may be tempted to administer additional drug assuming that drug concentrations have peaked (with bolus dosing) or are near steady-state conditions (with continuous infusions of potent inhaled anesthetics). Clinicians

may also be impatient, assuming that drug concentrations are near zero when in fact they are still increased, even after terminating delivery (e.g., the end tidal potent inhaled agent concentration is 0 mm Hg but there is persistent unresponsiveness).

A second advantage is that drug displays provide a means of delivering passive TCI. Although widely used throughout the world, TCI is not used in the United States because of regulatory barriers.²⁷ TCI uses population pharmacokinetic models to drive infusion pumps. After entering the target plasma or effect-site concentration, a computer identifies the optimal infusion rate to achieve that concentration. With passive TCI, population models are used to display predicted effect-site concentrations and associated effects over time, but the models do not deliver information to drive infusion pumps as with TCI. With this approach,

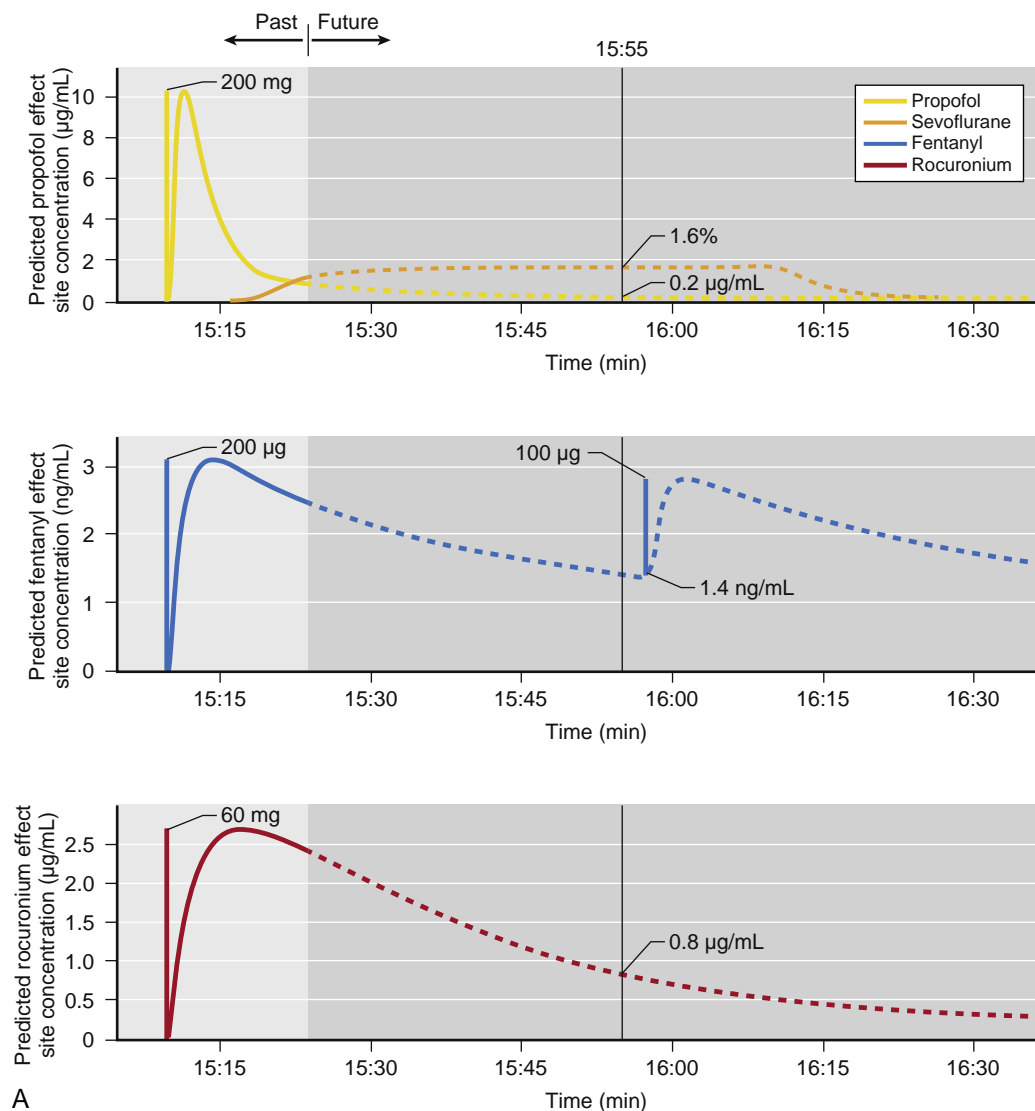


Fig. 18.31 (A) Example of a drug display. This example presents predictions of site effect concentrations (A) and drug effects (B) for a combined technique using fentanyl (2 μg/kg), propofol (2 mg/kg), and rocuronium (0.6 mg/kg) boluses and maintenance with sevoflurane (2%) and fentanyl bolus (1 μg/kg). This simulation assumes a 30-year-old, 100-kg male, 183 cm tall, with normal cardiac output and lung ventilation. (A) Predicted effect site concentrations for propofol (bright yellow line), sevoflurane (dark orange line), fentanyl (blue line), and rocuronium (red line). Bolus doses are represented as vertical lines, with the dose labeled adjacent to the line. Past predictions are solid lines and future predictions are dashed lines. The vertical black line represents a future prediction of effect site concentrations at 15:55 PM. Concentrations are reported.

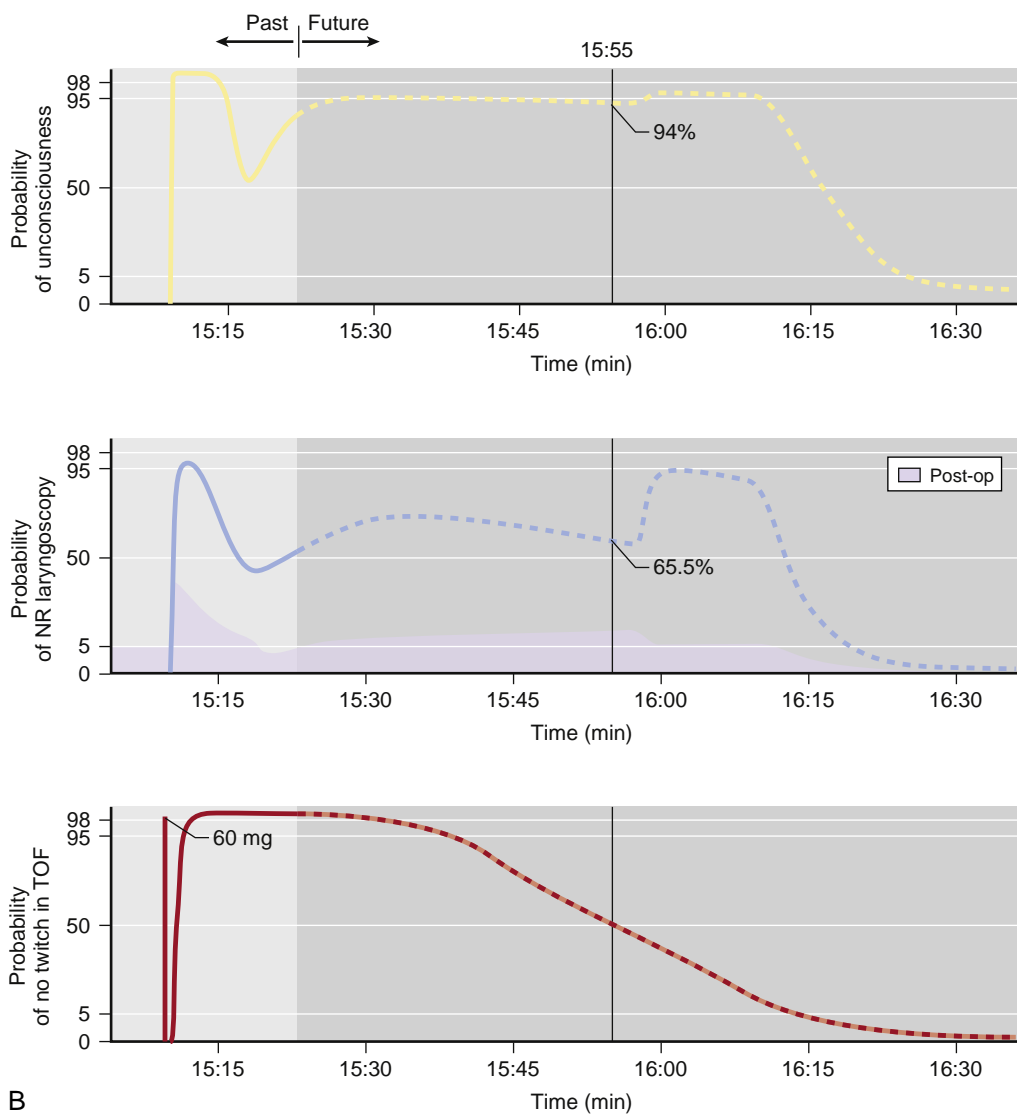


Fig. 18.31 Cont'd (B) Predicted drug effects. Probability of unresponsiveness (yellow line), probability of no response to laryngoscopy (blue line), and probability of loss of train-of-four (red line) from this combined technique. The white horizontal lines represent the 5%, 50%, 95%, and 98% probability of effect. The vertical black line represents a future prediction of drug effects at 15:55 PM. NR, No response to laryngoscopy; TOF, train-of-four. ([A] From Applied Medical Visualizations, Salt Lake City, Utah.)

clinicians can test out dosing regimens (bolus doses and infusion rates) before administering them to confirm they will achieve a desired effect. These features provide for a more consistent approach to drug delivery.

A third advantage is that they provide a better approach to dosing anesthetics. Instead of considering an anesthetic in terms of MAC, where 50% of patients may respond to surgical stimulus, drug displays provide a more refined characterization of anesthetic effect. Clinicians do not titrate an anesthetic to achieve a 50% probability of effect but rather aim for a 95% to 99% probability of effect. With response surfaces, anesthetic dosing regimens necessary to achieve this level of effect are easily visualized. Second, the concept of MAC does not fully embody the three elements of an anesthetic: analgesia, sedation and hypnosis, and muscle relaxation. Drug displays provide a means of visualizing all three effects simultaneously over a full 0% to 100% probability range.

Special Populations

When formulating an anesthetic, many aspects of patient demographics and medical history need to be considered to find the correct dose: age; body habitus; gender; chronic exposure to opioids, benzodiazepines, or alcohol; the presence of heart, lung, kidney, or liver disease; and the extent of blood loss or dehydration. Any of these factors can dramatically affect anesthetic drug kinetics and dynamics. Unfortunately, most studies characterizing anesthetic drug behavior have been conducted in healthy volunteers that rarely represent the general population presenting for surgery. Extensive work has explored how some patient characteristics (e.g., obesity) influence anesthetic drug behavior, whereas other patient characteristics remain difficult to assess (chronic opioid exposure). In addition, not all anesthetics have been studied. Most work has primarily focused on newer anesthetic drugs, such as propofol and

remifentanil. This section will briefly summarize work that has been done to characterize the pharmacokinetics and pharmacodynamics in a few unique special populations.

Influence of Obesity on Anesthetic Drugs

Obesity is a worldwide epidemic, and overweight patients frequently undergo anesthesia and surgery. Furthermore, pharmacologic alterations of anesthetics occur in obese individuals. In general, manufacturer dosing recommendations are on a per-kg basis according to the actual total body weight (TBW). Anesthesia providers rarely use mg/kg dosing in obese patients for fear of administering an excessive dose (e.g., a 136-kg patient does not require twice as much drug as a patient of the same height who weighs 68 kg). To resolve this problem, several weight scalars were developed to avoid excessive dosing or under dosing in this patient population. Some of these include lean body mass (LBM), ideal body weight (IBW), corrected body weight (CBW), and fat-free mass (FFM). Table 18.1 presents the formulas used to estimate these weight scalars. Table 18.2 shows samples of the resultant scaled weight for lean and obese individuals. In general, the aim of weight scalars is to match dosing regimens for obese patients with what is required for normal-size patients. These scaled weights are usually smaller than TBW in obese patients and thus help prevent excessive drug dosing (Fig. 18.32). Scaled weights have been used in place of TBW for both bolus (mg/kg) and infusion (mg/kg/hr) dosing and also for TCI.

This section will discuss the pharmacologic (primarily pharmacokinetic) alterations of select intravenous anesthetic drugs (propofol, remifentanil, and fentanyl) in obese patients, review examples of weight scalars and their shortcomings when used in bolus and continuous infusion dosing, and when data are available, briefly describe pharmacologic models used to drive TCI.

Propofol

Dosing propofol in obese patients can be a challenge. For bolus dosing and continuous infusions, the choice of weight scalar is specific to the dosing technique being used (i.e., one is best for bolus dosing and another for continuous infusions). Furthermore, of the available propofol pharmacokinetic models, the one built from observations in obese patients may be best for TCI.

The influence of obesity on propofol pharmacokinetics is not entirely clear. Generally, in obese patients, the blood distributes more to nonadipose than to adipose tissues. This may result in higher plasma drug concentrations in obese patients with mg/kg dosing than in normal patients with less adipose mass. Furthermore, propofol clearance increases because of the increased liver volume and/or liver blood flow associated with obesity (and increased cardiac output). Distribution likely influences concentration peaks with bolus dosing, and clearance likely influences concentrations during and following infusions.

Dosing Scalars for Propofol. Simulations of an infusion using various weight scalars are presented in Fig. 18.33. The simulations predict propofol effect-site concentrations from a 60-minute infusion (167 μ g/kg/min) in 176-cm (6-ft) males, obese (185 kg), and lean (68 kg). If dosed according to TBW, peak effect-site concentrations in a lean and obese individual are different; their respective peak propofol concentrations

TABLE 18.1 Common Weight Scalars (Modified Added Modified Fat-Free Mass)

Name	Equations
Ideal body weight	Male: 50 kg + 2.3 kg for each 2.54 cm (1 inch) over 152 cm (5 ft) Female: 45.5 kg + 2.3 kg for each 2.54 cm (1 inch) over 152 cm (5 ft)
Corrected body weight	IBW + 0.4 \times (TBW – IBW)
Lean body mass	Male: 1.1 \times TBW – 128 \times (TBW/Ht) ² Female: 1.07 \times TBW – 148 \times (TBW/Ht) ²
Fat-free mass ⁶⁶	Male: (9.27 \times 10 ³ \times TBW)/(6.68 \times 10 ³ + 216 \times BMI) Female: (9.27 \times 10 ³ \times TBW)/(8.78 \times 10 ³ + 244 \times BMI)
Pharmacokinetic mass ^{46,47}	52/[1 + (196.4 e ^{-0.025 TBW} – 53.66)/100] (fentanyl only)
Modified fat-free mass ^{28,36}	FFM + 0.4 \times (TBW – FFM)

BMI, Body mass index; FFM, fat free mass; Ht, height in centimeters; IBW, ideal body weight; LBM, lean body mass; TBW, total body weight in kg.

TABLE 18.2 Dosing Weights Based on Various Dosing Scalars (Values Per K Johnson)

Dosing Scalar	176-cm (6 FT) Male	
	68 kg BMI = 22	185 kg BMI = 66
Total body weight (TBW)	68	185
Ideal body weight (IBW)	72	72
Corrected body weight (CBW)	70	117
Lean body mass (LBM)	56	62
Fat-free mass (FFM)	55	88
Modified fat-free mass (MFFM)	60	127

BMI, Body mass index (kg/m²).

are approximately 5.2 and 7.1 μ g/mL, respectively. If the obese individual is dosed to CBW, the peak concentration is near 4.5 μ g/mL. The other weight scalars lead to much lower concentrations with the infusion.

Of the many available dosing scalars, authors recommend LBM¹² for bolus dosing (i.e., during induction) and TBW or CBW for infusions.^{9,13} For continuous infusions, other weight scalars are likely inadequate (the most worrisome is LBM). When dosing to CBW, plasma concentrations may be lower than concentrations when dosed to TBW.

One concern with using TBW to dose continuous infusions is drug accumulation. Prior work, however, does not support this assumption. Servin and colleagues²⁸ performed pharmacokinetic analyses of propofol administration to normal and obese patients using TBW and CBW. The CBW was defined as the IBW + 0.4 \times (TBW – IBW).²⁹ They found similar concentrations at eye opening in both groups

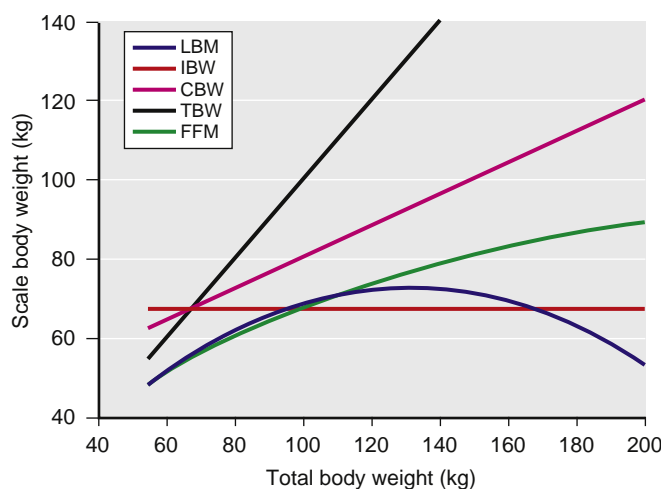


Fig. 18.32 Scaled weights as a function of total body weight (TBW). Key points in this plot: IBW remains the same regardless of the TBW, and LBM starts to decline for weight increases above 127 kg. CBW, Corrected body weight; FFM, fat-free mass; IBW, Ideal body weight; LBM, lean body mass (for a 40-year-old male, 176 cm tall).

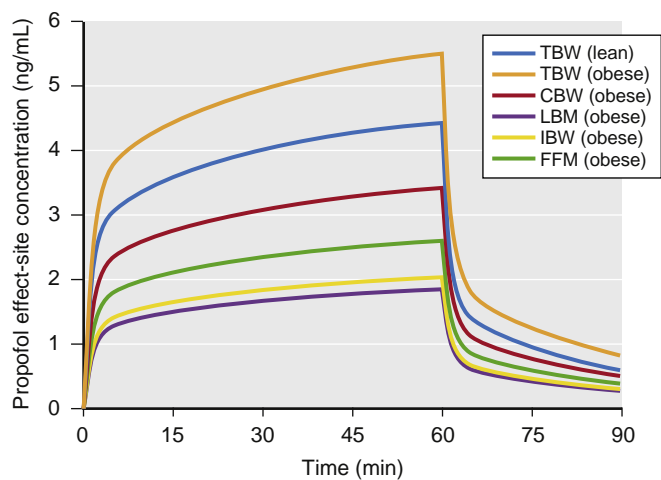


Fig. 18.33 Simulations of propofol effect site concentrations that result from a 60-minute infusion (10 mg/kg/h–167 μ g/kg/min) to a 40-year-old male who is 176 cm tall. Simulations include the following dosing weights: total body weights (TBW) of 68 kg and 185 kg (body mass indices of 22 and 60, respectively) and scaled weights for the 185 kg weight to include Servin's corrected body weight (CBW), lean body mass (LBM), ideal body weight (IBW), and fat-free mass (FFM). Key points: At the 185-kg weight, when dosed to TBW, the infusion leads to high propofol concentrations, whereas when dosed to IBW or LBM, the infusion leads to low propofol concentrations. When the 185-kg individual is dosed using CBW, it best approximates the propofol concentrations that result from TBW in a lean individual. Predictions of propofol effect site concentrations were made using the Eleveld model.

and absence of propofol accumulation in obese patients; in fact, obese patients showed earlier awareness after the termination of propofol infusions than did the normal subjects. Data suggest that dosing infusions according to Servin's CBW may underdose obese patients.³⁰

Propofol Kinetic Models Target-Controlled Infusions. Of the many available models, the two most widely used propofol kinetic models for TCI are those published by Marsh and associates and Schnider and associates.^{31,32} In addition to model selection, as with bolus and continuous

infusion dosing, identifying the ideal weight scalar to use is also important.

The Marsh model, although useful, was built from data collected in a pediatric population. Researchers have explored different dosing weights using this model in morbidly obese patients when coadministered with remifentanil with varied results. Albertin and colleagues²⁹ used CBW to dose a propofol TCI using the Marsh model. They found predicted substantially overestimated measured propofol concentrations and expressed concern for intraoperative awareness when using CBW with the Marsh TCI model. The same group³³ compared the predictive performance of the TCI using CBW versus TBW and found that CBW performed worse than TBW. They concluded that TBW, not CBW, should be used to administer propofol via TCI to morbidly obese patients. In contrast, recently, Cortinez and colleagues³⁴ evaluated the several pharmacokinetic models, and the use of CBW with the Marsh and Schnider models (described later) showed acceptable prediction performances. They stated that with both models using CBW is one of the best options for propofol TCI in obese patients, as their opinion. In any case, electroencephalographic monitoring is recommended to avoid the risk of awareness.

The Schnider model, although built from data collected in adults over a range of weights, heights, and ages, does not specifically include obese patients. This model uses the weight scalar LBM, which has limited application in morbidly obese patients.³²

For comparison, the Marsh or the Schnider model has been applied on morbidly obese patients. Echevarria and colleagues³⁵ reported differences in effect-site propofol concentrations with a BIS of less than 60 between the two pharmacokinetic models when used for induction in morbidly obese patients. To achieve a 95% probability of effect, target concentrations of 4.2 and 5.5 μ g/mL were required for the Marsh and Schnider models, respectively. This difference occurred because of the potential prediction errors in each pharmacokinetic model that was used (the actual drug concentrations in each patient are unknown).

Cortinez and colleagues used an international data repository called Open TCI (<http://www.opentci.org>) to build a model using propofol concentrations from a wide range of body weights.³⁶ They built a propofol kinetic model that scales normal-size to obese individuals using an empirically derived formula that uses allometric scaling. In this formula, TBW accounts for differences in distribution and clearances in obese patients. TBW is divided by a standard patient size (70 kg) and raised to the power of 1 for distribution volumes and by the power of 0.75 for clearances. Van Kralingen and colleagues³⁷ further modified this approach and reported better model performance with exponents of 0.71 for clearance. Eleveld and colleagues³⁸ constructed a general purpose allometric pharmacokinetic model for propofol using a large dataset containing data from young children, children, adults, elderly, and obese individuals (pharmacokinetic parameter estimates can be calculated by entering patient demographics at http://www.eurosi va.eu/tivatrainer/modeltranslate/calc_compartments.h tml; last accessed 2018/01/05). Cortinez and colleagues³⁴ evaluated the predictive performances of the five foregoing models (i.e., Marsh, Schnider, Cortinez, Van Kralingen, and Eleveld models) in data from obese patients and found that

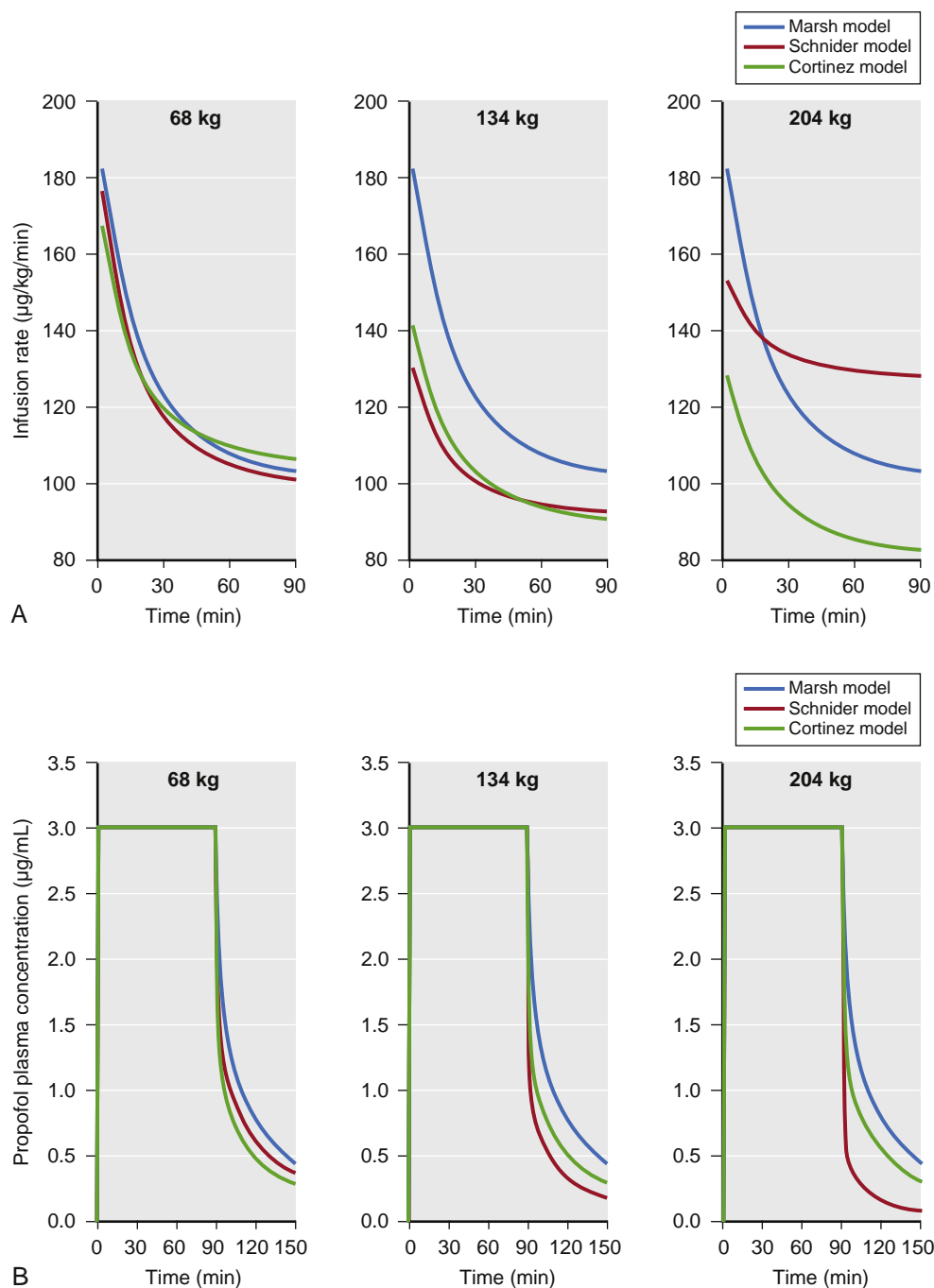


Fig. 18.34 Simulations of a 90-minute propofol target-controlled infusion set to achieve and maintain a plasma concentration (C_p) of 3 $\mu\text{g}/\text{mL}$ using four different published propofol pharmacokinetic models: Marsh and associates,³¹ Schnider and associates,³² Cortinez and associates,³⁶ and Eleveld and associates.^{36,38} Simulations assumed 40-year-old males who are 176 cm tall and weigh 68, 134, or 204 kg. (A) Propofol infusion rates for each model at each weight. (B) Propofol plasma concentrations predicted by each model for each weight.

the Eleveld allometric pharmacokinetic model performed best. They stated that the Eleveld model using TBW is one of the best options for propofol TCI in obese patients.

Fig. 18.34 presents a simulation of propofol infusion rates and associated plasma concentrations using the Marsh, Schnider, Cortinez, and Eleveld models to drive a TCI to achieve a concentration of 3 $\mu\text{g}/\text{mL}$. Key points from this simulation include: TCI infusions based on the Marsh model are linear to TBW such that the infusion rates and plasma concentrations are identical across weights. With an increase in body weights, the degree of increase in total

propofol amounts for TCI administrations is smaller with the Cortinez and Eleveld models than with the Marsh and Schnider models.

For propofol, the Eleveld model may be best suited for TCI in obese and morbidly obese patients. Unfortunately, this model is not yet available in many commercial TCI pumps. One caveat that is important to consider is that model differences are likely overshadowed by inter-individual variability. In sum, any one of the four models will likely yield similar clinical results if titrated to effect in conjunction with processed EEG monitoring.

Other Sedatives. Only limited information is available on the behavior of other sedatives (i.e., midazolam, ketamine, etomidate, dexmedetomidine, and barbiturates) in obese patients. In a study by Greenblatt and associates, the volume of distribution even when normalized to weight (e.g., L/kg) was larger in obese patients, suggesting that lean tissue may take up less midazolam than adipose tissue.³⁹ Thus, midazolam's distribution volume follows the TBW: as patient size increases, so does the distribution volume. In addition, midazolam elimination was the same in all study subjects (lean or obese). This suggests that regardless of dose, hepatic metabolism of midazolam is fixed and elimination will require more time in obese patients. Another interesting finding was that time to peak concentration and peak plasma drug concentrations were the same when administered in a weight-normalized fashion regardless of body habitus.

Although not clinically validated in obese patients, the authors recommend that bolus doses should be scaled to TBW and other dosing scalars may lead to inadequate effect. On the other hand, with a fixed elimination, continuous infusion rates should be dosed to IBW.³⁹

Cortinez and colleagues⁴⁰ characterized the influence of obesity on pharmacokinetics of dexmedetomidine and found that fat mass is not related to a proportional increase in distribution volume and is associated with the impairment of clearance. Xu and colleagues⁴¹ performed noncompartment pharmacokinetic analysis of dexmedetomidine with dosing calculated on TBW. In obese patients, higher initial concentrations and lower clearance per kg, and deeper sedation with lower SpO_2 values were observed. These results suggest that dosing of dexmedetomidine, which is calculated using TBW, can be overdosing in these populations.

OPIOIDS

With the exception of remifentanil, minimal work has explored the implication of obesity on the kinetic and dynamic behavior of opioids.

Remifentanil

In obese patients, largely due to its rapid metabolism by nonspecific esterases, the distribution volume and clearance of remifentanil are similar in lean and obese patients.⁴² As with propofol, researchers have explored several scaled weights in an effort to optimize bolus dosing, continuous infusions, and TCIs.

Dosing Scalars

As previously noted with propofol, simulation is used to present the predicted remifentanil effect-site concentrations and analgesic effect for a variety of scaled weights in individuals 174 cm in height, some obese (185 kg, BMI of 60) and lean (68 kg, BMI of 22) (Fig. 18.35). Several key points are illustrated in these simulations:

1. For an obese patient, dosing scaled to FFM resulted in almost identical remifentanil effect-site concentrations as in the lean patient dosed according to TBW. Unlike propofol, dosing remifentanil to CBW (red line) leads to higher plasma concentrations compared with levels achieved when dosing to TBW in a lean individual.
2. Dosing scaled to LBM in the obese individual resulted in lower effect-site concentrations than those in a lean individual dosed according to TBW.

Remifentanil Kinetic Models for Target-Controlled Infusions

For remifentanil TCI, there is one available pharmacokinetic model published by Minto and associates.⁴³ Although built from data collected in adults over a range of weights, heights, and ages, obese patients and morbidly obese patients were not included. Many of the model parameters are scaled to LBM. As previously discussed, this may limit the application of this model in the morbidly obese. Kim and colleagues⁴⁴ developed a new population pharmacokinetic model for remifentanil that characterize the influence of

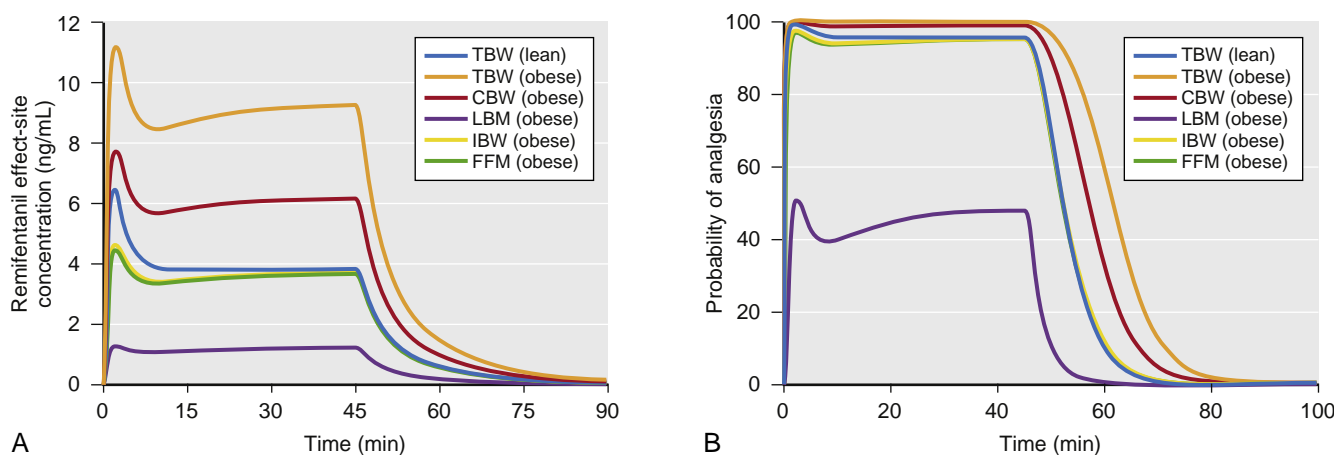


Fig. 18.35 (A and B) Simulations of remifentanil effect-site concentrations (A) and analgesic effect (B) that result from a 1 $\mu\text{g}/\text{kg}$ bolus and a 60-minute infusion at a rate of 0.15 $\mu\text{g}/\text{kg}/\text{min}$ to a 40-year-old male who is 176 cm tall. Simulations include the following dosing weights: total body weights (TBW) of 68 kg and 185 kg (body mass indices of 22 and 60, respectively) and scaled weights for the 185-kg weight to include Servin's corrected body weight (CBW), lean body mass (LBM), ideal body weight (IBW), and fat free mass (FFM). Remifentanil effect-site concentrations and estimates of analgesic effect were estimated using published pharmacokinetic models. (From Minto CF, Schnider TW, Egan TD, et al. Influence of age and gender on the pharmacokinetics and pharmacodynamics of remifentanil. I. Model development. *Anesthesiology*. 1997;86(1):10–23.)

body weight using allometric body mass scaling in the general adult population.

Fig. 18.36 presents a simulation of the predicted remifentanil plasma concentrations based on the Minto and Kim models. The Minto model overestimates remifentanil concentrations with increasing weight. This is likely due to the use of LBM when estimating pharmacokinetic parameters.

In summary, available models (Minto or Kim) are appropriate for TCI in this patient group but will administer different amounts of remifentanil and require titration to achieve desired yet avoid adverse clinical effects.

FENTANYL

Despite widespread use in the clinical arena, relatively little work has explored how obesity impacts fentanyl pharmacokinetics. Published fentanyl pharmacokinetic models⁴⁵ tend to overestimate fentanyl concentrations as TBW increases. A fentanyl kinetic model based on data collected in obese subjects has not (yet) been published. Shibutani and colleagues^{46,47} explored ways to improve predictions using published models by modifying demographic data (e.g., either height or weight). They characterized a nonlinear relationship between fentanyl clearance and TBW and recommended the use of a modified weight, called the pharmacokinetic mass, to improve the predictive performance of one of the many available fentanyl kinetic models, a model published by Shafer and colleagues. They explored the use of pharmacokinetic mass when dosing obese patients with fentanyl in a postoperative setting. They found that dosing based on TBW may be excessive.³⁶

Other Opioids

Even less information regarding the impact of obesity on drug behavior is available for opioids other than remifentanil and fentanyl. Sufentanil has been studied in obese

patients, where its volume of distribution increases linearly with TBW⁴⁸ and clearance was similar between lean and obese individuals. It was recommended that bolus dosing use TBW and “prudently reduced” dosing for continuous infusions. For TCI, Slepchenko and colleagues found model estimates of sufentanil concentrations accurately predicted measured concentrations in morbidly obese patients⁴⁹ using a previously published model of sufentanil kinetics by Gepts and associates.⁵⁰ This is likely due to the fact that the kinetic model was built from measured concentrations in patients with a weight range of 47 to 94 kg. de Hoogd and colleagues⁵¹ performed a population pharmacokinetic analysis of intravenous morphine in morbidly obese individuals. They found that morphine pharmacokinetics were comparable to those of healthy volunteers. They concluded that no weight-based dosing adjustments were necessary. However, they also found that the elimination of pharmacologically active metabolite was decreased, resulting in an increased exposure to active metabolite with prolonged administrations. They concluded that the clinical relevance of this phenomenon was not clear.

INHALED ANESTHETICS

The perception of volatile anesthetics is that they accumulate more in obese than in lean patients and that this leads to prolonged emergence. Studies on inhalation anesthetics in obese individuals, however, have not confirmed this perception.⁵² Two phenomena contribute to this observation: first, blood flow to adipose tissue *decreases* with increasing obesity,⁵³ and second, the time required to fill adipose tissue with volatile anesthetics is long. The time required to achieve 63% of the final equilibrium within adipose tissue for desflurane and isoflurane are longer than 22 and 35 hours, respectively.^{54,55}

INFLUENCE OF AGE ON ANESTHETIC DRUG PHARMACOLOGY

Clinicians are often faced with anesthetizing elderly adults and have long recognized that they usually require a smaller dosage of most anesthetics to produce the desired therapeutic effect while minimizing adverse effects. Age is one of the most valuable covariates to consider when developing an anesthetic plan. The influence of age on pharmacokinetics and pharmacodynamics of many anesthetics has been well described. As with obesity, both remifentanil and propofol can serve as prototypes to understand how age influences anesthetic drug behavior. Studies specifically designed to assess the influence of age on remifentanil and propofol have characterized the influence of age in quantitative terms.^{32,38,43,44,56,57}

With remifentanil, elderly patients require less drug to produce an opioid effect. Reduced doses are primarily a function of changes in pharmacodynamics, but may involve pharmacokinetic changes as well.⁴³ The concentration required to produce electroencephalographic changes is decreased. Based on previously published pharmacokinetic and pharmacodynamic models built from measurements over a wide age range,^{32,43,56,57} simulations can be performed to explore how age may influence dosing. For

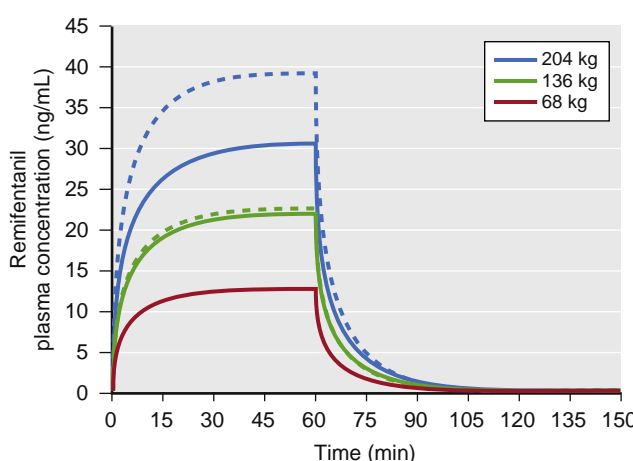


Fig. 18.36 Simulations of remifentanil plasma concentrations that result from a 60-minute infusion (0.5 μ g/kg/min) in a 40-year-old male, 176 cm tall. The simulations include three total body weights: 68, 136, and 204 kg with body mass indices of 22, 44, and 66, respectively. Simulations were performed using pharmacokinetic parameters published by Minto and associates⁴³ (dashed lines) and Kim and colleagues⁴⁴ (solid lines). In an extremely obese (204 kg) individual, Minto's model predicts very high remifentanil concentrations.

example, to achieve equipotent doses in 20- and 80-year-olds, the dose for the 80-year-old should be reduced by 55%. A similar analysis for propofol recommends that the dose for an 80-year-old should be reduced by 65% compared to that of a 20-year-old.

The mechanisms for these changes are not clear, especially for pharmacodynamic changes. One possible source of change in pharmacokinetic behavior may be due to decreased cardiac output. Lower cardiac output in the elderly⁵⁸ results in slower circulation and subsequent changes in drug distribution and redistribution. This may lead to high peak concentrations^{58,59} and decreased drug delivery to metabolic organs and reduced clearance. This is consistent with what has been reported for many intravenous anesthetics (propofol, thiopental, and etomidate), which have slower clearance and a smaller volume of distribution.^{32,60–62} Beyond age-related changes in cardiac output, it is important to consider comorbidities that may reduce cardiovascular function.⁶³ Taking this into account, anesthesiologists often consider a patient's "physiologic" age instead of solely relying on actual age.^{64,65} For some older adult patients, such as those with no significant coexisting disease, normal body habitus, and good exercise tolerance, a substantial reduction in dose may not be warranted.

Summary

This chapter reviewed basic principles of clinical pharmacology used to describe anesthetic drug behavior: pharmacokinetics, pharmacodynamics, and anesthetic drug interactions. These principles provide the information needed to make rational decisions about the selection and administration of anesthetics. From a practical aspect, these principles characterize the magnitude and time course of drug effect, but because of complex math requirements, they have limited clinical utility in everyday practice. Advances in computer simulation, however, have brought this capability to the point of real-time patient care. Perhaps one of the most important advances in our understanding of clinical pharmacology is the development of interaction models that describe how different classes of anesthetic drugs influence one another. This is especially relevant to anesthesiologists, given that they rarely use just one drug when providing anesthesia.

 Complete references available online at expertconsult.com.

References

- Wilkinson GR, Shand DG. *Clin Pharmacol Ther*. 1975;18:377.
- Ebling WF, Wada DR, Stanski DR. *J Pharmacokinet Biopharm*. 1994;22:259.
- Youngs EJ, Shafer SL. Basic pharmacokinetic and pharmacodynamic principles. In: White PF, ed. *Textbook of Intravenous Anesthesia*. Baltimore: William & Wilkins; 1997.
- Krejcie TC, Avram MJ, Gentry WB. *J Pharmacokinet Biopharm*. 1997;25:169.
- Hughes MA, et al. *Anesthesiology*. 1992;76(3):334.
- Egan TD, et al. *Int J Pharm Med*. 2001;15(1):11.
- McEwan AI, Smith C, Dyar O. *Anesthesiology*. 1993;78:864.
- Hendrickx J, et al. *Anesth Analg*. 2008;107:494.
- Bouillon TW, et al. *Anesthesiology*. 2004;100(6):1353.
- Heyse B, et al. *Anesthesiology*. 2012;116(2):311.
- Kern SE, et al. *Anesthesiology*. 2004;100(6):1373.
- Manyam SC, et al. *Anesthesiology*. 2006;105(2):267.
- Mertens MJ, et al. *Anesthesiology*. 2003;99(2):347.
- LaPierre CD, et al. *Anesth Analg*. 2011;113(3):490.
- Johnson KB, et al. *Anesth Analg*. 2010;111(2):387.
- Syroid ND, et al. *Anesth Analg*. 2010;111(2):380.
- Minto CF, Schnider TW. *Anesthesiology*. 2000;92:1603.
- Vereecke HE, et al. *Anesthesiology*. 2013.
- Vuyk J, Lim T, Engbers FH. *Anesthesiology*. 1995;83(8).
- Johnson KB, et al. *Anesth Analg*. 2008;106(2):471.
- Zanderigo E, et al. *Anesthesiology*. 2006;104(4):742.
- Fidler M, Kern SE. *Anesthesiology*. 2006;105(2):286.
- Vinik HR, et al. *Anesth Analg*. 1994;78(2):354.
- Harris RS, et al. *Anesthesiology*. 2006;104(6):1170.
- Schumacher PM, et al. *Anesthesiology*. 2009;111(4):790.
- Sebel LE, et al. *Anesthesiology*. 2006;104(6):1176.
- Egan TD, Shafer SL. *Anesthesiology*. 2003;99(5):1039.
- Servin F, et al. *Anesthesiology*. 1993;78(4):657.
- Albertin A, et al. *Br J Anaesth*. 2007;98(1):66.
- Igarashi T, et al. *Masui*. 2002;51(11):1243.
- Marsh B, et al. *Br J Anaesth*. 1991;67(1):41.
- Schnider TW, et al. *Anesthesiology*. 1998;88(5):1170.
- La Colla L, et al. *Eur J Anaesthesiol*. 2009;26(5):362.
- Cortinez LI, et al. *Anesth Analg*. 2014;119(2):302.
- Echevarria GC, et al. *Anesth Analg*. 2012;115(4):823.
- Cortinez LI, et al. *Br J Anaesth*. 2010;105(4):448.
- van Kralingen S, et al. *Br J Clin Pharmacol*. 2011;71(1):34.
- Elefeldt DJ, et al. *Anesth Analg*. 2014;118(6):1221.
- Greenblatt DJ, et al. *Anesthesiology*. 1984;61(1):27.
- Cortinez LI, et al. *Eur J Clin Pharmacol*. 2015;71(12):1501.
- Xu B, et al. *J Anesth*. 2017;31(6):813.
- Egan TD, et al. *Anesthesiology*. 1998;89:562–573.
- Minto CF, et al. *Anesthesiology*. 1997;86(1):10.
- Kim TK, et al. *Anesthesiology*. 2017;126(6):1019.
- Shafer SL, et al. *Anesthesiology*. 1990;73:1091–1102.
- Shibutani K, et al. *Anesthesiology*. 2004;101(3):603.
- Shibutani K, et al. *Br J Anaesth*. 2005;95(3):377.
- Schwartz AE, et al. *Anesth Analg*. 1991;73(6):790.
- Slepchenko G, et al. *Anesthesiology*. 2003;98(1):65.
- Gepts E, et al. *Anesthesiology*. 1995;83(6):1194.
- de Hoogd S, et al. *Clin Pharmacokinet*. 2017;56(12):1577.
- Cortinez LI, et al. *Anesth Analg*. 2011;113(1):70.
- Lesser GT, Deutscher S. *J Appl Physiol*. 1967;23(5):621.
- Eger EJ, et al. *Anesthesiology*. 1971;35(4):365.
- Wahrenbrock EA, et al. *Anesthesiology*. 1974;40(1):19.
- Minto CF, et al. *Anesthesiology*. 1997;86(1):24.
- Schnider TW, et al. *Anesthesiology*. 1999;90(6):1502.
- Upton RN, et al. *Anesth Analg*. 1999;89(3):545.
- Krejcie TC, Avram MJ. *Anesth Analg*. 1999;89(3):541.
- Arden JR, et al. *Anesthesiology*. 1986;65(1):19.
- Homer TD, Stanski DR. *Anesthesiology*. 1985;62:714.
- Stanski DR, Maitre PO. *Anesthesiology*. 1990;72(3):412.
- Rodeheffer RJ, et al. *Circulation*. 1984;69(2):203.
- Avram MJ, et al. *Anesthesiology*. 1990;72(3):403.
- Williams TF. *Clin Pharmacol Ther*. 1987;42(6):663.
- Janmehasatian S, et al. *Clin Pharmacokinet*. 2005;44(10):1051.
- Doufas AG, et al. *Anesthesiology*. 2004;101:1112.
- Lee S, et al. *J Clin Pharm Ther*. 2012;37:698.
- Scott JC, Stanski DR. *J Pharmacol Exp Ther*. 1987;240:159.
- Hudson RJ, et al. *Anesthesiology*. 1989;70:426.

References

1. Wilkinson GR, Shand DG. Commentary: a physio-logical approach to hepatic drug clearance. *Clin Pharmacol Ther.* 1975;18:377–390.
2. Ebliing WF, Wada DR, Stanski DR. From piecewise to full physiologic pharmacokinetic modeling: applied to thiopental disposition in the rat. *J Pharmacokinet Biopharm.* 1994;22:259–292.
3. Youngs EJ, Shafer SL. Basic pharmacokinetic and pharmacodynamic principles. In: White PF, ed. *Textbook of Intravenous Anesthesia*. Baltimore: Williams & Wilkins; 1997.
4. Krejcie TC, Avram MJ, Gentry WB. A recirculatory model of the pulmonary uptake and pharmacokinetics of lidocaine based on analysis of arterial and mixed venous data from dogs. *J Pharmacokinet Biopharm.* 1997;25:169–190.
5. Hughes MA, Glass PS, Jacobs JR. Context-sensitive half-time in multicompartment pharmacokinetic models for intravenous anesthetic drugs. *Anesthesiology.* 1992;76(3):334–341.
6. Egan TD, et al. The electroencephalogram (EEG) and clinical measures of opioid potency: defining the EEG-clinical potency relationship ('fingerprint') with application to remifentanil. *Int J Pharmaceut Med.* 2001;15(1):11–19.
7. McEwan AI, Smith C, Dyrar O. Isoflurane minimum alveolar concentration reduction by fentanyl. *Anesthesiology.* 1993;78:864–869.
8. Hendrickx J, et al. Is synergy the rule? A review of anesthetic interactions producing hypnosis and immobility. *Anesth Analg.* 2008;107:494–506.
9. Bouillon TW, et al. Pharmacodynamic interaction between propofol and remifentanil regarding hypnosis, tolerance of laryngoscopy, bispectral index, and electroencephalographic approximate entropy. *Anesthesiology.* 2004;100(6):1353–1372.
10. Heyse B, et al. Sevoflurane remifentanil interaction: comparison of different response surface models. *Anesthesiology.* 2012;116(2):311–323.
11. Kern SE, et al. A response surface analysis of propofol-remifentanil pharmacodynamic interaction in volunteers. *Anesthesiology.* 2004;100(6):1373–1381.
12. Manyam SC, et al. Opioid-volatile anesthetic synergy: a response surface model with remifentanil and sevoflurane as prototypes. *Anesthesiology.* 2006;105(2):267–278.
13. Mertens MJ, et al. Predictive performance of computer-controlled infusion of remifentanil during propofol/remifentanil anaesthesia. *Br J Anaesth.* 2003;90(2):132–141.
14. LaPierre CD, et al. An exploration of remifentanil-propofol combinations that lead to a loss of response to esophageal instrumentation, a loss of responsiveness, and/or onset of intolerable ventilatory depression. *Anesth Analg.* 2011;113(3):490–499.
15. Johnson KB, et al. An evaluation of remifentanil-sevoflurane response surface models in patients emerging from anesthesia: model improvement using effect-site sevoflurane concentrations. *Anesth Analg.* 2010;111(2):387–394.
16. Syroid ND, et al. Response surface model predictions of emergence and response to pain in the recovery room: an evaluation of patients emerging from an isoflurane and fentanyl anesthetic. *Anesth Analg.* 2010;111(2):380–386.
17. Minto CF, Schnider TW, Short TG. Response surface model for anesthetic drug interactions. *Anesthesiology.* 2000;92:1603–1616.
18. Vereecke HE, et al. Interaction between nitrous oxide, sevoflurane, and opioids: a response surface approach. *Anesthesiology.* 2013.
19. Vuyk J LT, Engbers FH. The pharmacodynamic interaction of propofol and alfentanil during lower abdominal surgery in women. *Anesthesiology.* 1995;83:8–22.
20. Johnson KB, et al. An evaluation of remifentanil propofol response surfaces for loss of responsiveness, loss of response to surrogates of painful stimuli and laryngoscopy in patients undergoing elective surgery. *Anesth Analg.* 2008;106(2):471–479. table of contents.
21. Zanderigo E, et al. The well-being model: a new drug interaction model for positive and negative effects. *Anesthesiology.* 2006;104(4):742–753.
22. Fidler M, Kern SE. Flexible interaction model for complex interactions of multiple anesthetics. *Anesthesiology.* 2006;105(2):286–296.
23. Vinik HR, Bradley EL, Kissin I. Triple anesthetic combination: propofol-midazolam-alfentanil. *Anesth Analg.* 1994;78(2):354–358.
24. Harris RS, et al. Interaction of propofol and sevoflurane on loss of consciousness and movement to skin incision during general anesthesia. *Anesthesiology.* 2006;104(6):1170–1175.
25. Schumacher PM, et al. Response surface modeling of the interaction between propofol and sevoflurane. *Anesthesiology.* 2009;111(4):790–804.
26. Sebel LE, et al. Additive effects of sevoflurane and propofol on gamma-aminobutyric acid receptor function. *Anesthesiology.* 2006;104(6):1176–1183.
27. Egan TD, Shafer SL. Target-controlled infusions for intravenous anesthetics: surfing USA not! *Anesthesiology.* 2003;99(5):1039–1041.
28. Servin F, et al. Propofol infusion for maintenance of anesthesia in morbidly obese patients receiving nitrous oxide. A clinical and pharmacokinetic study. *Anesthesiology.* 1993;78(4):657–665.
29. Albertin A, et al. Predictive performance of 'Servin's formula' during BIS-guided propofol-remifentanil target-controlled infusion in morbidly obese patients. *Br J Anaesth.* 2007;98(1):66–75.
30. Igarashi T, et al. [Two cases of intraoperative awareness during intravenous anesthesia with propofol in morbidly obese patients]. *Masui.* 2002;51(11):1243–1247.
31. Marsh B, et al. Pharmacokinetic model driven infusion of propofol in children. *Br J Anaesth.* 1991;67(1):41–48.
32. Schnider TW, et al. The influence of method of administration and covariates on the pharmacokinetics of propofol in adult volunteers. *Anesthesiology.* 1998;88(5):1170–1182.
33. La Colla L, et al. No adjustment vs. adjustment formula as input weight for propofol target-controlled infusion in morbidly obese patients. *Eur J Anaesthesiol.* 2009;26(5):362–369.
34. Cortinez LI, et al. Performance of propofol target-controlled infusion models in the obese: pharmacokinetic and pharmacodynamic analysis. *Anesth Analg.* 2014;119(2):302–310.
35. Echevarria GC, et al. The effective effect-site propofol concentration for induction and intubation with two pharmacokinetic models in morbidly obese patients using total body weight. *Anesth Analg.* 2012;115(4):823–829.
36. Cortinez LI, et al. Influence of obesity on propofol pharmacokinetics: derivation of a pharmacokinetic model. *Br J Anaesth.* 2010;105(4):448–456.
37. van Kralingen S, et al. Comparative evaluation of atracurium dosed on ideal body weight vs. total body weight in morbidly obese patients. *Br J Clin Pharmacol.* 2011;71(1):34–40.
38. Eleveld DJ, et al. A general purpose pharmacokinetic model for propofol. *Anesth Analg.* 2014;118(6):1221–1237.
39. Greenblatt DJ, et al. Effect of age, gender, and obesity on midazolam kinetics. *Anesthesiology.* 1984;61(1):27–35.
40. Cortinez LI, Anderson BJ, Penna A, et al. Influence of obesity on propofol pharmacokinetics: derivation of a pharmacokinetic model. *Br J Anaesth.* 2010;105(4):448–456.
41. Xu B, et al. Pharmacokinetic and pharmacodynamics of intravenous dexmedetomidine in morbidly obese patients undergoing laparoscopic surgery. *J Anesth.* 2017;31(6):813–820.
42. Egan TD, et al. The pharmacokinetics of the new short-acting opioid remifentanil (GI87084B) in healthy adult male volunteers. *Anesthesiology.* 1993;79(5):881–892.
43. Minto CF, et al. Influence of age and gender on the pharmacokinetics and pharmacodynamics of remifentanil. I. Model development. *Anesthesiology.* 1997;86(1):10–23.
44. Kim TK, et al. Disposition of remifentanil in obesity: a new pharmacokinetic model incorporating the influence of body mass. *Anesthesiology.* 2017;126(6):1019–1032.
45. Shafer SL, et al. Pharmacokinetics of fentanyl administered by computer-controlled infusion pump. *Anesthesiology.* 1990;73(6):1091–1102.
46. Shibutani K, et al. Accuracy of pharmacokinetic models for predicting plasma fentanyl concentrations in lean and obese surgical patients: derivation of dosing weight ("pharmacokinetic mass"). *Anesthesiology.* 2004;101(3):603–613.
47. Shibutani K, et al. Pharmacokinetic mass of fentanyl for postoperative analgesia in lean and obese patients. *Br J Anaesth.* 2005;95(3):377–383.
48. Schwartz AE, et al. Pharmacokinetics of sufentanil in obese patients. *Anesth Analg.* 1991;73(6):790–793.
49. Slepchenko G, et al. Performance of target-controlled sufentanil infusion in obese patients. *Anesthesiology.* 2003;98(1):65–73.
50. Gepts E, et al. Linearity of pharmacokinetics and model estimation of sufentanil. *Anesthesiology.* 1995;83(6):1194–1204.
51. de Hoogd S, et al. Influence of morbid obesity on the pharmacokinetics of morphine, morphine-3-glucuronide, and morphine-6-glucuronide. *Clin Pharmacokinet.* 2017;56(12):1577–1587.

52. Cortinez LI, et al. Obesity does not influence the onset and offset of sevoflurane effect as measured by the hysteresis between sevoflurane concentration and bispectral index. *Anesth Analg*. 2011;113(1):70–76.
53. Lesser GT, Deutsch S. Measurement of adipose tissue blood flow and perfusion in man by uptake of 85Kr. *J Appl Physiol*. 1967;23(5):621–630.
54. Eger EIn, Bahlman SH, Munson ES. The effect of age on the rate of increase of alveolar anesthetic concentration. *Anesthesiology*. 1971;35(4):365–372.
55. Wahrenbrock EA, et al. Anesthetic uptake—of mice and men (and whales). *Anesthesiology*. 1974;40(1):19–23.
56. Minto CF, Schnider TW, Shafer SL. Pharmacokinetics and pharmacodynamics of remifentanil. II. Model application. *Anesthesiology*. 1997;86(1):24–33.
57. Schnider TW, et al. The influence of age on propofol pharmacodynamics. *Anesthesiology*. 1999;90(6):1502–1516.
58. Upton RN, et al. Cardiac output is a determinant of the initial concentrations of propofol after short-infusion administration. *Anesth Analg*. 1999;89(3):545–552.
59. Krejcie TC, Avram MJ. What determines anesthetic induction dose? It's the front-end kinetics, doctor! *Anesth Analg*. 1999;89(3):541–544.
60. Arden JR, Holley FO, Stanski DR. Increased sensitivity to etomidate in the elderly: initial distribution versus altered brain response. *Anesthesiology*. 1986;65(1):19–27.
61. Homer TD, Stanski DR. The effect of increasing age on thiopental disposition and anesthetic requirement. *Anesthesiology*. 1985;62:714–724.
62. Stanski DR, Maitre PO. Population pharmacokinetics and pharmacodynamics of thiopental: the effect of age revisited. *Anesthesiology*. 1990;72(3):412–422.
63. Rodeheffer RJ, et al. Exercise cardiac output is maintained with advancing age in healthy human subjects: cardiac dilatation and increased stroke volume compensate for a diminished heart rate. *Circulation*. 1984;69(2):203–213.
64. Avram MJ, Krejcie TC, Henthorn TK. The relationship of age to the pharmacokinetics of early drug distribution: the concurrent disposition of thiopental and indocyanine green. *Anesthesiology*. 1990;72(3):403–411.
65. Williams TF. Aging or disease? *Clin Pharmacol Ther*. 1987;42(6):663–665.
66. Janmahasatian S, et al. Quantification of lean bodyweight. *Clin Pharmacokinet*. 2005;44(10):1051–1065.
67. Doufas AG, et al. Induction speed is not a determinant of propofol pharmacodynamics. *Anesthesiology*. 2004;101:1112–1121.
68. Lee S, Kim BH, Lim K, et al. Pharmacokinetics and pharmacodynamics of intravenous dexmedetomidine in healthy Korean subjects. *J Clin Pharm Ther*. 2012;37:698–703.
69. Scott JC, Stanski DR. Decreased fentanyl and alfentanil dose requirements with age. A simultaneous pharmacokinetic and pharmacodynamic evaluation. *J Pharmacol Exp Ther*. 1987;240:159–166.
70. Hudson RJ, Bergstrom RG, Thomson IR, et al. Pharmacokinetics of sufentanil in patients undergoing abdominal aortic surgery. *Anesthesiology*. 1989;70:426–431.

MISHA PEROUANSKY, ROBERT A. PEARCE, HUGH C. HEMMINGS, and NICHOLAS P. FRANKS

KEY POINTS

- Anesthesia consists of separable and independent components, each of which involves distinct, but possibly overlapping, mechanisms at different sites in the central nervous system.
- The potencies of general anesthetics correlate with their solubility in oil, indicating the importance of interactions with predominantly hydrophobic targets.
- General anesthetics act by binding directly to amphiphilic cavities in proteins. Binding sites have been identified by a combination of site-directed mutagenesis and high-resolution structural analysis of anesthetic binding.
- Mutations made to render putative protein targets insensitive to inhaled anesthetics have been expressed in mice but have not generated breakthroughs analogous to the success of this strategy with intravenous anesthetics.
- The effects of inhaled anesthetics cannot be explained by a single molecular mechanism. Rather, several targets contribute to the component actions comprising the anesthetic effects of each anesthetic. However, these effects do converge on a limited number of states underlying the behavioral effects.
- The immobilizing effect of inhaled anesthetics involves actions in the spinal cord, whereas sedation/hypnosis and amnesia involve supraspinal mechanisms that interact with endogenous memory, sleep, and consciousness pathways and networks.
- Volatile inhaled anesthetics enhance inhibitory synaptic transmission postsynaptically by potentiating ligand-gated ion channels activated by γ -aminobutyric acid (GABA) and glycine, extrasynaptically by enhancing GABA receptors, and presynaptically by enhancing basal GABA release.
- Inhaled anesthetics suppress excitatory synaptic transmission presynaptically by reducing glutamate release (volatile anesthetics) and postsynaptically by inhibiting excitatory ionotropic receptors activated by glutamate (gaseous and to some extent volatile anesthetics).
- Inhaled anesthetics directly activate certain two-pore-domain potassium channels, which is likely to result in both pre- and post-synaptic effects.
- There is as yet no comprehensive theory of anesthesia that describes the sequence of events leading from the interaction between an anesthetic molecule and its targets to the behavioral effects.

Despite the widespread clinical use of general anesthetics, our current understanding of their molecular, cellular, and network mechanisms is incomplete. This critical gap in the pharmacology of one of medicine's most important drug classes not only impedes rational use of available anesthetics but also hinders the development of newer anesthetics that might selectively achieve the desirable end points of anesthesia with fewer adverse cardiovascular, respiratory, and possibly neuropathologic side effects. Although major progress has been made in understanding the pharmacology of the intravenous anesthetics by molecular genetic approaches, the actions of the inhaled anesthetics at the molecular and cellular levels are more

enigmatic. It is still not possible to trace precisely the sequence of events that leads from inhaled anesthetic-target interactions, through ascending levels of biologic complexity, to the various behavioral effects that characterize the composite state of clinical anesthesia in humans. Nevertheless, investigations continue to reveal fundamental principles of action and have led to a framework for understanding anesthetic effects at different organizational levels.

The focus of this chapter is on the mechanisms involved in the principal therapeutic effects (anesthesia) and on the side effects of the inhaled anesthetics (Fig. 19.1), a chemically and pharmacologically diverse group that includes

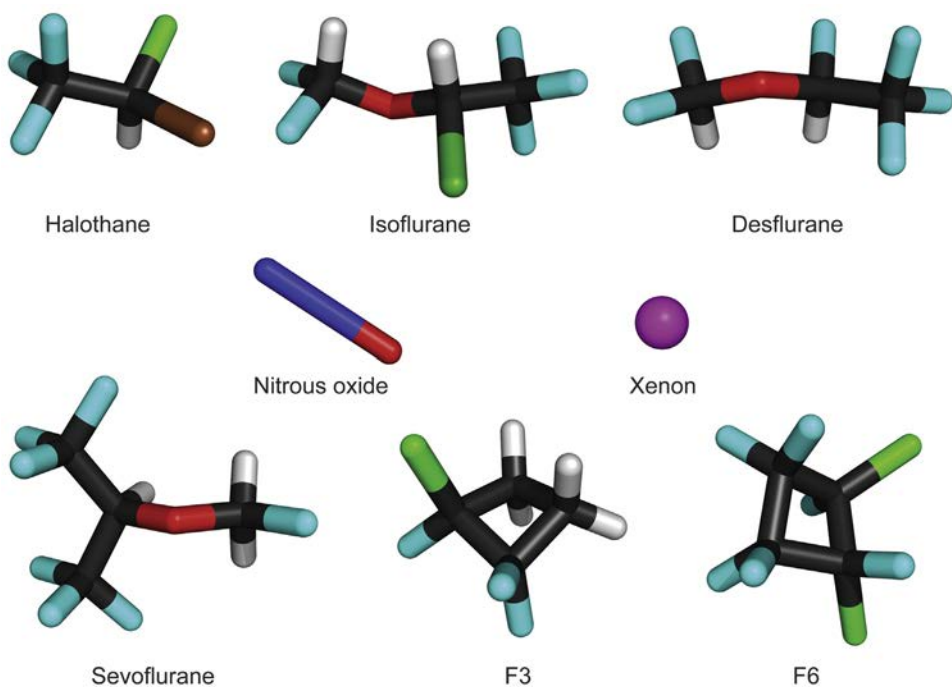


Fig. 19.1 Structures of some representative general anesthetics and a nonimmobilizer (F6). The colors are bromine (brown), carbon (black), chlorine (green), fluorine (cyan), hydrogen (gray), oxygen (red), and xenon (magenta). Note that halothane, isoflurane, desflurane, and F3 all contain a chiral carbon; therefore each exists as two mirror-image enantiomers (only one enantiomer is shown). Also, the nonimmobilizer F6 contains two chiral carbons and exists as two trans enantiomers and one cis stereoisomer (only one of the enantiomers is shown).

the potent halogenated ether (isoflurane, sevoflurane, desflurane, enflurane) and alkane (halothane) volatile anesthetics and the inorganic gaseous anesthetics (nitrous oxide and xenon). This critical summary of the current state of knowledge begins with an historical overview and a review of the behavioral end points of anesthesia. We then trace, where possible, inhaled anesthetic effects through ascending levels of organization from molecules, cells, circuits, networks, and organs to mammalian behavior. We also briefly address studies of anesthetic effects in very simple model organisms, with anesthetic end points being identified that as yet bear uncertain relationships to those in mammals.¹

History

THE UNIFIED PARADIGM OF ANESTHETIC THEORIES

The first monograph reporting experimental work on anesthetic mechanisms, proposing a soon-to-be discredited lipid-elution theory of anesthetic action, was published only 6 months after Morton's public demonstration of ether anesthesia in Boston's Ether Dome. For decades thereafter, the phenomenon of anesthesia puzzled, inspired, and awed those who tried to understand it. An influential paradigm of anesthetic action formulated by Claude Bernard in the 1870s posited that anesthesia was a "unified" phenomenon—a unitary mechanism applicable to all forms of life. Although the anesthetized state could be brought about by a variety of agents, its essence was the same in all living creatures. In fact, Bernard thought that life itself was defined by

susceptibility to anesthesia. Bernard also proposed a more specific theory of anesthesia, coagulation of protoplasm, which competed with a number of coexisting theories entertained by the scientific community. In a major work published in 1919, Hans Winterstein² summarized the perplexing diversity of anesthetic theories by listing more than 600 references, the majority to original laboratory work—a convincing testimony to the interest of the scientific world in this phenomenon. Of note, the work of Meyer and Overton at the end of the nineteenth century had only a limited effect on the trajectory of research until the 1960s. Only then was the striking simplicity of the Meyer-Overton correlation (Fig. 19.2A) of anesthetic potency with solubility in olive oil interpreted by the majority of researchers to indicate that lipids are likely to be the anesthetic target. This interpretation focused attention on anesthetic effects on the bulk physical properties of cell membranes, which were known to consist primarily of lipid molecules. Such non-specific or "lipoid-based" anesthetic theories dominated the field from the 1960s to the 1980s.

MINIMUM ALVEOLAR CONCENTRATION—A BRIDGE BETWEEN PAST AND PRESENT

The potencies of inhaled anesthetics for immobilization were established in the classic studies in the 1960s of Eger and colleagues,^{3,4} who defined the *minimum alveolar concentration* (MAC) as the inhaled anesthetic atmospheric pressure required to prevent movement in response to a defined noxious stimulus in 50% of subjects. The concept of MAC evolved within a unitary paradigm of anesthetic action and also reflected the priorities of clinical practice. As a result, prevention of movement (immobility) became a

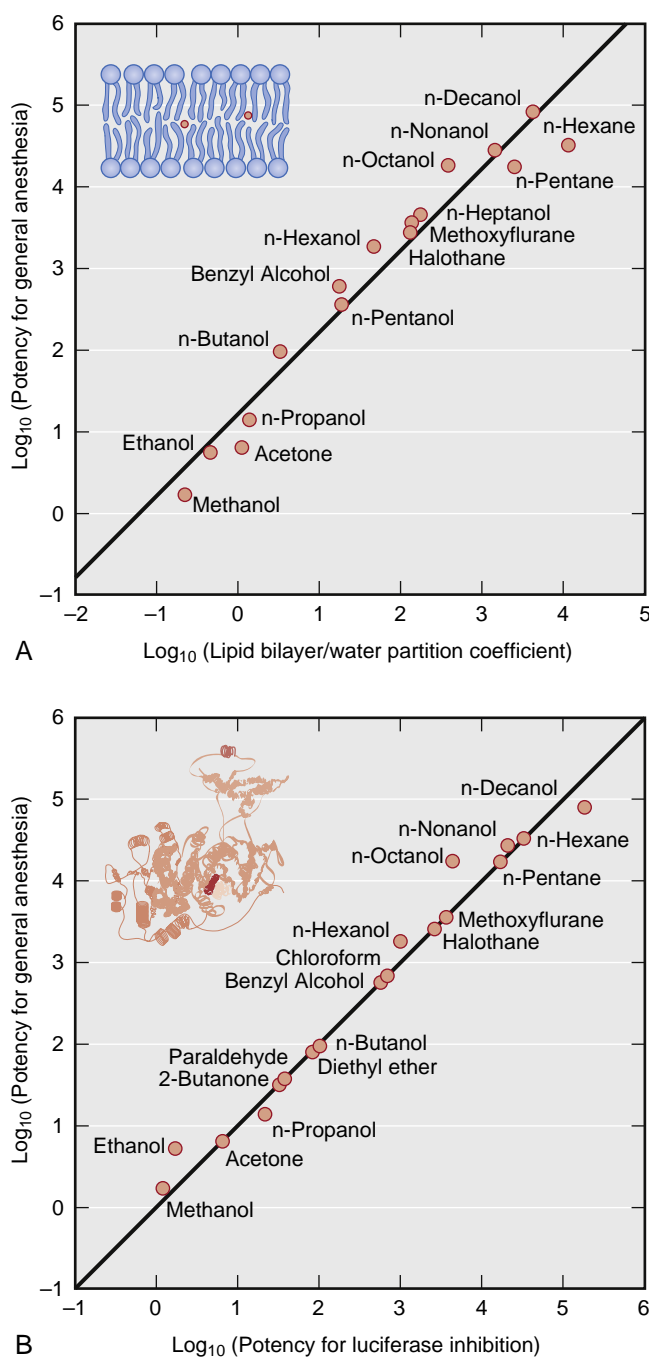


Fig. 19.2 General anesthetics act by binding directly to proteins. (A) The iconic Meyer-Overton correlation (c.1900) between anesthetic potency and the lipid-water partition coefficient was initially interpreted as evidence that lipids of nerve membranes were the principal anesthetic target sites. (B) Progress in the 20th century showed that general anesthetic potencies correlate equally well with their ability to inhibit activity of the soluble firefly enzyme luciferase, which is not a physiologically relevant anesthetic target itself but serves as a lipid-free model protein for anesthetic binding. *Inset*, The crystal structure of luciferase¹¹⁰ with bound anesthetic (red). (Reprinted with permission from Franks NP, Lieb WR. Molecular and cellular mechanisms of general anesthesia. *Nature*. 1994;367:607–614.)

universal yardstick for anesthetic effects, presumed to occur in the brain. Moreover, the simple elegance of the relationship between anesthetic potency and lipid solubility (see Fig. 19.2A) graphically illustrated Meyer and Overton's

conclusion that "All chemically indifferent substances that are soluble in fat are anesthetics. Their relative potency as anesthetics will depend on their affinity to fat on the one hand and water on the other hand, that is, on the fat/water partition coefficient."¹ This was interpreted as favoring lipids as the primary targets of anesthetics and a single non-specific theory to explain anesthesia. The appeal of a single unified mechanism to explain anesthesia was (and remains) intellectually appealing. This focused the bulk of research efforts on delineating how anesthetic interactions with lipid membranes might lead to the behavioral changes observed under anesthesia—the nonspecific lipid theory.

Because inhaled anesthetic concentrations reflect concentrations in the tissues after equilibration, which is most rapidly achieved for well-perfused organs such as the brain and heart, MAC is analogous to the plasma concentration for 50% effect (EC_{50}) for intravenous anesthetics. In clinical applications, MAC is usually expressed as volume percent (vol%), which varies considerably with temperature owing to the large temperature dependence of partitioning between the gas phase and condensed phases (be they water, lipids, or proteins), whereas the equivalent condensed-phase molar concentrations are much less dependent on temperature.⁵ The MAC concept provided researchers and clinicians with a universal standard whereby to measure a defined anesthetic end point (immobility), making meaningful comparisons of experimental results possible and accelerating clinical and laboratory research into anesthetic mechanisms. Today, a more nuanced understanding of MAC considers the structural and functional diversity of the physiologic targets for the different components of the anesthetic state.

SHIFT FROM LIPID- TO PROTEIN-CENTERED MECHANISMS

Lipid-centered mechanisms of anesthesia prevailed in the two decades after definition of the MAC concept. Alternative targets were occasionally proposed but largely neglected by the scientific mainstream. Experimental inconsistencies of lipid targets,^{6–8} as well as evidence compatible with proteins as primary sites of action,^{9,10} were largely ignored. A shift from lipid- to protein-centered mechanisms, however, began in the late 1970s, owing largely to the discoveries of Franks and Lieb,^{11–15} who in an influential series of publications demonstrated that not only were lipids implausible targets but that protein targets were also compatible with the Meyer-Overton correlation (see Fig. 19.2B)—a proof of concept that, within a few years, redirected the bulk of research efforts toward proteins. As a corollary of this reorientation, evidence against lipid-based theories was recognized. Examples include the cutoff in anesthetic potency in homologous series of long-chain anesthetic alcohols^{15,16} and the identification of hydrophobic drugs that do not obey the Meyer-Overton correlation.^{1,17} The enantiomeric selectivity of several anesthetics further strengthened the case for specific binding sites on proteins because stereoselectivity is difficult to reconcile with lipid targets.^{18–20} Today, there is widespread acceptance of the notion that lipid bilayers remain essentially unaffected by general anesthetics^{11,21} and that critical signaling proteins (e.g., ion channels or ligand-gated receptors) are the relevant

molecular targets of anesthetic action.²² The exact identity of proteins contributing to specific anesthetic end points continues to be sought, with research addressing not only the “where” (target) but also the “how” (process) of anesthetic mechanisms.

DIVERSITY OF POTENTIAL ANESTHETIC TARGETS

At high concentrations *in vitro*, most inhaled anesthetics affect the functions of multiple proteins, several of which might be plausibly connected to the components of the anesthetic state or anesthetic side effects. However, when a specific anesthetic end point is considered, anesthetics are effective *in vivo* over a very narrow concentration range. This makes the concentration at which a relevant anesthetic effect is observed a critical consideration for deciding potential relevance. The mechanistic relevance of small effects observed *in vitro* at relevant concentrations is less clear; that is, what effect is too small to be considered relevant to anesthesia?²³⁻²⁵

Whether anesthesia results from the sum of minor perturbations at multiple sites or from substantial effects on a small number of targets remains to be determined. This should be resolved as more sophisticated molecular genetics experimental techniques are applied to test the relevance of putative targets. There are two reasons for believing that the number of relevant targets may be small. First, the extreme steepness of anesthetic concentration-response curves means that, for a given end point, substantial effects on two or three targets would be sufficient to account entirely for the *in vivo* effect. Second, the stereoselectivity observed *in vivo*²⁶ is comparable to the largest effects seen in putative targets *in vitro*,^{18,20} suggesting that only a small number of targets are likely to be involved. Set against this logic is the experimental evidence that a rather large number of plausible target proteins are affected, albeit usually to small extents, and determining which of these are relevant to the various anesthetic end points remains a challenge.

ANESTHESIA: A COMPOSITE NEUROPHARMACOLOGIC STATE

Along with progress in identifying the molecular mechanisms of anesthesia, our understanding of the nature of the anesthetic state has evolved. Whereas a drug-induced coma-like state of general anesthesia can be induced by inhaled anesthetics administered at appropriate concentrations (approximately 1.3 times MAC, equivalent to the EC₉₅ of an intravenous anesthetic), the use of such high concentrations can lead to short- and possibly long-term side effects. It is now clear that anesthesia consists of separable and at least partially independent components or substates, each of which involves distinct but possibly overlapping mechanisms in different regions of the central nervous system (CNS) and with variations in relative potencies between specific agents.²⁷ Immobilization, the core measure of MAC, is mediated largely at the level of the spinal cord by inhaled anesthetics^{28,29} but not by barbiturates.³⁰ On the other hand, the spinal cord is clearly not the primary site of such phenomena as

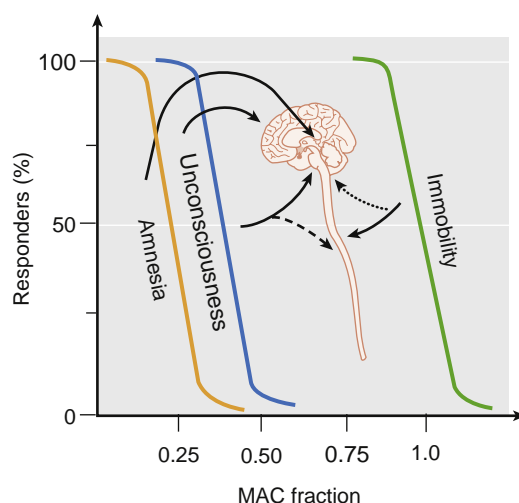


Fig. 19.3 Several behavioral end points and sites of action underlie inhaled anesthetic action. Amnesia, the most sensitive anesthetic end point, probably involves the hippocampus, amygdala, mediotemporal lobe, and other cortical structures. Unconsciousness likely involves the cerebral cortex, thalamus, and neuronal pathways of sleep and arousal. Sedation and hypnosis (loss of responsiveness) are part of the consciousness-unconsciousness continuum and are not shown. Immobility occurs by anesthetic action in the spinal cord, although supraspinal effects (dotted arrow) are likely to be important for some anesthetics. Anesthetic action in the spinal cord blunts ascending impulses arising from noxious stimulation and might indirectly contribute to anesthetic-induced unconsciousness and amnesia (dashed arrow). Cardiovascular responses occur at even greater MAC fractions (not shown). (Courtesy Joseph Antognini, University of California, Davis, CA.)

amnesia, sedation, and unconsciousness, which rather are produced by anesthetic effects on cerebral cortical function (Fig. 19.3). A functional separation between amnesia and sedation has been demonstrated for intravenous anesthetics,³¹ and it seems likely that this will apply to inhaled anesthetics as well. The state commonly referred to as “unconsciousness” is in itself heterogeneous, with evidence for distinct states of unresponsiveness and unconsciousness.³² These and similar findings have led to the concept that general anesthesia consists of multiple independent components that can be resolved experimentally and clinically.

In principle, each component of anesthesia can be preferentially induced in a concentration- and agent-specific manner using individual cellular/molecular pathways in various regions of the CNS. For example, injections of pentobarbital into discrete sites in the mesopontine tegmentum induce a comatose state,^{33,34} whereas sedation induced by systemic administration of propofol can be reversed by microinjections of γ -aminobutyric acid (GABA)_A receptor antagonists into the tuberomammillary nucleus, a sleep-regulating nucleus in the hypothalamus.³⁵ Thus general anesthetics produce separate identifiable anesthetic substates via agent-specific actions at discrete anatomic sites in the CNS through different molecular targets. An important consequence of this complexity is that MAC, which is based exclusively on a motor response, might not proportionately reflect other components of anesthesia. Although this heterogeneity of anesthetic actions complicates a mechanistic understanding, it does open the possibility of developing substate-specific drugs.

Integrated Effects on Central Nervous System Function

IMMOBILITY

Electroencephalography as a monitor of brain activity has been applied both to the study of anesthetic mechanisms and as a monitor of the anesthetic state. Failure to find a correlation between quantitative electroencephalographic activity and immobility in response to noxious stimulation led to the somewhat radical (at the time) hypothesis that immobility was not a cerebral cortex-mediated phenomenon.³⁶ Experimental demonstration that volatile anesthetics act on the spinal cord to suppress movement^{28,29} supported this hypothesis and was a major factor leading to the contemporary separation of anesthetic substates, of which immobility requires the highest drug concentrations (see Fig. 19.3). Taking advantage of the atypical blood supply of goat CNS, which allows separate experimental perfusion of the brain and spinal cord, Antognini and colleagues^{28,37} showed that immobility involves anesthetic effects at the spinal level because selective delivery of isoflurane or halothane only to the brain required 2.5-fold to 4-fold higher concentrations compared with delivery to the whole CNS. At the same time, experiments by Rampil and colleagues²⁹ that used surgical separation of the forebrain and midbrain from the spinal cord in rats led to the conclusion that immobilization involves primarily suppression of the nocifensive withdrawal reflex arc at the level of the spinal cord (Fig. 19.4).

In the 25 years since the identification of the spinal cord as the site of anesthetic-induced immobility, research has centered on pharmacologic, genetic, and complex network approaches. The conventional pharmacologic approach (“bulk” administration of agonists and antagonists into the CNS) to identify receptor-level contributions to isoflurane-induced immobility (isoflurane being the standard potent ether for experimental purposes) has severe limitations in the complex networks of the CNS. Nevertheless, it yielded at least one surprising insight—that actions at GABA_A receptors appear not to be important for the end point of immobility, at least where inhalational agents are concerned.³⁸ Anesthetic-resistant transgenic mice confirmed that GABA_A receptors containing $\alpha 1$ - or $\alpha 3$ -subunits do not contribute to the immobilizing action of isoflurane.^{39,40} Perhaps less surprisingly, inhibition of central nicotinic acetylcholine receptors also plays no role in immobilization.⁴¹ A role for voltage-gated sodium (Na⁺) channels was suggested by the finding that intrathecal administration of a selective inhibitor of Na⁺ channels potentiates anesthetic immobility (reduces MAC), whereas an enhancer of Na⁺ channel activity does the opposite.⁴²

In contrast, work in mutant mice suggests a potential role for tandem-pore domain potassium channels (K_{2P}) in anesthetic-induced immobility. Global knockout mice lacking the TASK-1, TASK-3, and TREK-1 K_{2P} channels are less sensitive to volatile but not intravenous anesthetics,⁴³⁻⁴⁶ indicating a role for these channels possibly by a presynaptic mechanism.⁴⁷ An important limitation is that global knockout results almost invariably in wide-ranging compensatory changes in the molecular landscape of the

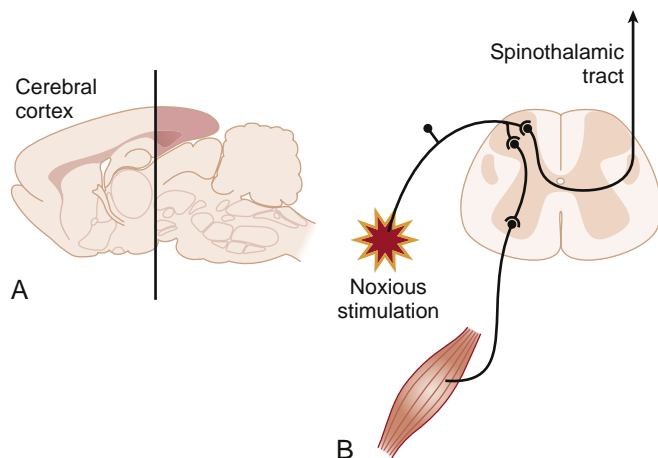


Fig. 19.4 Inhaled anesthetics produce immobility at the spinal level. (A) Decerebration by removal of the forebrain rostral to the black line does not alter the minimum alveolar concentration of isoflurane in rats, indicating that volatile anesthetic immobilization does not depend on the cerebral cortex.^{28,29} (B) Anesthetics suppress the nocifensive withdrawal reflex response to noxious stimulation transmitted to the dorsal horn by sensory nerves at the spinal level. Current efforts are focused on identifying the molecular, cellular, and anatomic substrates for this effect.

organism with unpredictable consequences for the phenomenon under investigation.

Work with ex vivo preparations that attempt to preserve parts of the complex spinal cord circuitry suggests that anesthetic inhibition of afferent (noxious sensory) input to the dorsal horn plays a subordinate role to the suppression of the efferent (motor) output from the ventral horn, although this may vary by specific agent. This motor output is coordinated by neuronal networks organized in so-called central pattern generators that control the activity of cholinergic motoneurons.⁴⁸ Not unlike understanding the anesthetic effects on higher cognitive function, the key to understanding immobility will likely lie in resolving the effect of anesthetics on integrated spinal network activity after understanding the circuit physiology.

UNCONSCIOUSNESS

Compared with the other end points of anesthesia, research into the biologic basis of anesthetic-induced unconsciousness is relatively recent, but it has become an area of active investigation. Research is being conducted in animal models and human subjects and commercial interests are working to develop effective depth-of-anesthesia monitors. These efforts reflect increasing interest, and progress, in “consciousness science” in general.^{49,50} Moreover, anesthetics are themselves being used as research tools to help unravel the neuronal underpinnings of consciousness.

Loss of consciousness (or hypnosis) is a hallmark of the onset of anesthesia. However, what is commonly referred to as *unconsciousness under anesthesia* might be more accurately described as *unresponsiveness*, a condition that could also encompass states of self-awareness without environmental awareness (as in dreaming) or environmental awareness without recall (e.g. conscious amnesia combined with neuromuscular paralysis during induction of anesthesia).^{32,51}

Numerous theories have been advanced to explain anesthetic-induced unconsciousness. They can generally be divided into those that address “bottom-up” changes in the brain stem circuitry that controls arousal,^{52,53} versus “top-down” changes in the thalamocortical circuits that integrate information.⁵⁴ Indeed, this distinction formed the basis for a recent suggestion that the *level* of consciousness reflects bottom-up processes whereas the *content* of consciousness reflects top-down processes—a notion with intuitive appeal.⁵⁵

One of the most influential theories has been the “integrated information theory of consciousness (IITC)” of Tononi,⁵⁶ which emphasizes the need for simultaneous differentiation between brain states and their integration into a coherent whole.⁵⁷ Drugs or diseases that suppress consciousness could act through either process. Other information-based approaches use symbolic analysis,⁵⁸ transfer entropy,⁵⁹ chaos theory,⁶⁰ and more. The rich connectivity of the cerebral cortex and its hierarchical organization are especially suited to enable high levels of information integration in the human brain. Some brain areas present a “rich club” organization (i.e., highly connected nodes tend to be preferentially connected to other highly connected nodes), which has been suggested to be optimal for information integration.^{61,62} These hubs are promising targets for the hypnotic action of general anesthetic drugs.

Anesthetics might act by interfering with the operational synchronicity and coherence of corticothalamic networks. Consequent disruption of functional and effective connectivity has been observed during natural slow-wave⁶³ and midazolam-induced loss of responsiveness.⁶⁴ This breakdown of cortical connectivity, rather than pharmacologic deafferentation from the environment, could underlie loss of consciousness.⁶⁵ Unconsciousness would then be characterized not by the absence but by the fragmentation of cortical processing.

Although the mechanism of “binding” (i.e., creating the unity of perception) is uncertain, synchronicity of neuronal activity in the 40- to 90-Hz range across functionally connected cortical areas (commonly referred to as 40-Hz- or γ -rhythm) is a viable candidate. Animal^{66,67} and human⁶⁸ data implicate activity in the γ -band throughout the cortex as a network-level target of general anesthetics. Anesthetic actions on cortical information processing probably consist not merely of suppression of responses but of reduced complexity and variability reflected counterintuitively in the increased reliability and precision of evoked responses.^{69,70}

A consistent and intriguing observation has been that anesthetics suppress descending more than ascending neural connectivity.^{59,71} Within the framework of predictive coding,⁷² this indicates that unconsciousness is associated with a reduction in internally generated predictions more than a suppression of incoming sensory information. The molecular and cellular mechanisms underlying this effect remain undefined, but the preferential suppression by isoflurane of cortico-cortical responses in brain slices *in vitro*^{73,74} supports a top-down mechanism wherein the anesthetic acts directly on the thalamocortical circuitry.

By contrast, “bottom-up” theories attribute changes in consciousness to anesthetic modulation of subcortical arousal nuclei. An interesting theme has emerged from

this line of research. There is substantial overlap between the centers whose activity is altered during natural slow-wave sleep and the state of general anesthesia.^{35,75-77} That is, many anesthetics may induce unconsciousness, at least in part, by “hijacking” neural sleep^{78,79} or arousal⁸⁰ pathways.

Thalamic theories of anesthetic-induced unconsciousness^{81,82} incorporate aspects of both top-down and bottom-up mechanisms, reflecting not only the intermediate position of this structure in the hierarchical organization of the brain but also the different connection patterns of “sensory relay” versus higher-order “nonspecific” thalamic nuclei.⁸³

LEARNING AND MEMORY

Anterograde amnesia, one of the core desirable anesthetic end points, is achieved at lower anesthetic concentrations (\sim 0.25 MAC) than those required for unconsciousness (\sim 0.5 MAC). Perhaps the closest analogue in rodents to explicit memory in humans is medial temporal lobe-dependent learning of temporal and spatial sequences known as *hippocampus-dependent spatial learning*. Other learning paradigms, such as fear conditioning to tone, are by contrast independent of the hippocampus. Spatial learning can be tested by a variety of experimental paradigms, including fear conditioning to context (Fig. 19.5). Isoflurane and the nonimmobilizer F6 both inhibit hippocampus-dependent learning at about half the concentration necessary for disrupting hippocampus-independent learning.⁸⁴ Similarly, anesthetic concentrations that inhibit explicit memory in humans (memory that can be explicitly recalled as opposed to motor learning, classical conditioning, and so on) are similarly lower than concentrations that impair implicit memory (not subject to willful recollection).⁸⁵ Taken together, these findings implicate effects on function of the medial temporal lobe, including the hippocampus, in the suppression of explicit memory by anesthetics. Effects on other structures, such as the amygdala, may be relevant to anesthetic impairment of implicit or other types of memory.⁸⁶

Because inhaled anesthetics affect multiple cellular targets even at amnesic concentrations, it is likely that anesthetic-induced amnesia arises from multiple cellular-level changes. A quantitative comparison of the degree of change in synaptic inhibition in the hippocampus produced by equiamnestic concentrations of isoflurane versus etomidate indicated that the enhancement of GABAergic inhibition can account for a substantial portion of isoflurane’s effect on memory.⁸⁷ Other contributing targets may include nAChRs,⁸⁸ HCN1 channels,⁸⁹ and excitatory glutamatergic synapses.⁹⁰ Conversely, it is also likely that suppression of learning and memory by drugs known to have different receptor affinities share common mechanisms at some level of integration. For example, θ -rhythms (4-12 Hz) are clearly important for hippocampus-dependent learning and memory.⁹¹ Benzodiazepines⁹² and cannabinoids⁹³ slow and suppress hippocampal θ -rhythms in proportion to their ability to impair hippocampus-dependent learning. Isoflurane and the nonimmobilizer F6 have comparable effects on θ -rhythms at amnesic concentrations while having different receptor-level profiles and opposite effects on sedation.⁹⁴ Thus alterations in neuronal synchrony may

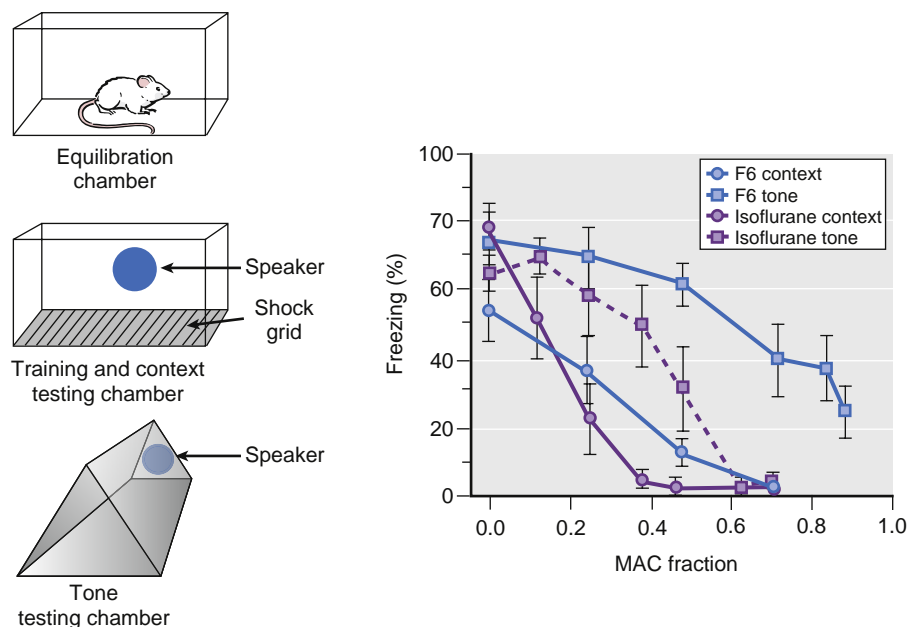


Fig. 19.5 Differential sensitivity of different types of learning to anesthetics and nonimmobilizers. Freezing in anticipation of a noxious stimulus is a measure of learning in rats; less freezing indicates less learning. *Left*, the learning protocol involves preequilibration of rats in the equilibration chamber to isoflurane or the nonimmobilizer F6 at the desired concentration before placement into the training chamber. For testing of memory to context, the training and test chamber are identical. For testing of memory to tone, training and testing take place in different chambers. *Right*, hippocampus-dependent learning (fear conditioning to context, *closed symbols*) is inhibited by isoflurane (*purple circles*) at lower concentrations than hippocampus-independent learning (fear conditioning to tone, *purple squares*). This differential sensitivity is mirrored by the nonimmobilizer F6 (*blue circles* and *blue squares* for context and tone, respectively). (*Left panel* adapted with permission from Eger EI 2nd, Xing Y, Pearce R, et al. Isoflurane antagonizes the capacity of flurothyl or 1,2-dichlorohexafluorocyclobutane to impair fear conditioning to context and tone. *Anesth Analg*. 2003;96:1010–1018; *right panel* data points reconstructed from Dutton RC, Maurer AJ, Sonner JM, et al. Short-term memory resists the depressant effect of the nonimmobilizer 1,2-dichlorohexafluorocyclobutane (2N) more than long-term memory. *Anesth Analg*. 2002;94:631–639; and Dutton RC, Maurer AJ, Sonner JM, et al. The concentration of isoflurane required to suppress learning depends on the type of learning. *Anesthesiology*. 2001;94:514–519.)

provide a common network-level substrate for memory impairment. The synchronization between amygdalar and hippocampal θ -rhythms that occurs during fear memory retrieval indicates that this principle might also apply to other forms of memory and their impairment by anesthetics.⁹⁵ As with other components of the anesthetic state, the precise mechanisms of memory impairment by anesthetics and of memory itself remain to be fully elucidated.

SEDATION

Sedation (defined as a decrease in activity, alertness, arousal, and/or vigilance), which is on a behavioral continuum leading to hypnosis, is achieved at anesthetic doses similar to those that produce amnesia (<0.5 MAC). There is no clear mechanistic or clinical separation between sedation and hypnosis. By contrast, even though sedation can be difficult to separate from amnesia, for intravenous anesthetics there may be separate but overlapping substrates for these two end points.³¹ The mechanisms involved in these behavioral effects are likely to resemble those of less promiscuous drugs, for which genetic approaches have been informative. An amino acid knockin mutation (H101R) in mice that renders the α_1 GABA_A receptor subunit insensitive to modulation by benzodiazepines produces resistance to the sedative and amnesic effects of benzodiazepines while maintaining other behavioral effects, among them anxiolysis.⁹⁶ The α_1 subunit is abundantly expressed in the CNS, mainly in the cortical areas and thalamus. Volatile anesthetics have qualitatively similar effects on α_1 -containing

GABA_A receptors (but also those containing other subunits) at low concentrations. The observation that the nonimmobilizer F6, which is devoid of sedative properties,⁹⁴ is amnesic⁹⁷ but does not modulate benzodiazepine-sensitive α_1 -containing GABA_A receptors,^{98,99} is compatible with a role for α_1 -containing receptors in volatile anesthetic-induced sedation, because few other targets are affected at purely sedative concentrations. Possible targets for the sedative effects of the gaseous anesthetics nitrous oxide and xenon, which do not affect GABA_A receptors, include N-methyl-D-aspartate (NMDA) receptor antagonism¹⁰⁰ and K_{2P} channel activation.¹⁰¹ Consistent with this distinct pharmacologic profile, nitrous oxide has strikingly different effects from those of benzodiazepines in behavioral tests aimed at evaluating sedation in mice.¹⁰²

Recognizing that there may be more than a superficial similarity between natural sleep and anesthetic-induced sedation and hypnosis, the effects of some anesthetics apparently share natural sleep mechanisms by directly activating discrete sleep-promoting nuclei in the hypothalamus.³⁵ Indeed, the same neurons, or at least overlapping populations of neurons, that are activated by sleep deprivation are also activated during dexmedetomidine-induced sedation.¹⁰³ Electroencephalographic patterns during natural slow-wave sleep and anesthesia show similarities,¹⁰⁴ and recovery from sleep deprivation can occur under propofol^{105,106} and inhalational anesthesia, supporting this concept. Anesthetic effects on other cortical¹⁰⁷ and subcortical structures³² may also contribute to anesthetic-induced sedation and hypnosis.

Identification of Molecular Sites of Anesthetic Action

CRITERIA FOR IDENTIFYING SITES RELEVANT TO ANESTHESIA

Specific criteria have been proposed to evaluate the relevance of the many potential molecular targets of anesthetics.¹⁰⁸ These criteria include the following:

1. *Reversible alteration of target function at clinically relevant concentrations.* This criterion requires comparable in vivo and in vitro sensitivities and depends on the anesthetic end point under consideration. For example, targets involved in immobility must be sensitive to anesthetics near MAC, whereas targets mediating amnesia must be affected at a fraction of MAC. Recent evidence for persistent effects of inhaled anesthetics demonstrable in the absence of continued anesthetic exposure is challenging the notion of reversibility for certain effects.
2. *Expression of the target in appropriate anatomic locations to mediate the specific anesthetic end point.* For example, immobilization by inhaled agents appears to involve primarily actions in the spinal cord independent of actions in the brain.
3. *Concordant stereoselectivity of anesthetic effects in vivo and on the target in vitro.* Without a specific pharmacologic antagonist of anesthesia, correlation between the stereoselective actions of general anesthetics in vivo and in vitro is a useful test of pharmacologic relevance of putative molecular targets. Stereoselectivity data correlating in vivo potency and in vitro receptor actions implicate GABA_A receptors as a target for the anesthetic actions of etomidate, pentobarbital, neurosteroid anesthetics, and isoflurane.
4. *Appropriate sensitivity or insensitivity to anesthetic and nonanesthetic compounds.* Anesthetic halogenated cyclobutanes together with structural analogs that do not produce anesthesia at concentrations predicted to be anesthetic by the Meyer-Overton correlation (nonimmobilizers) can be used to discriminate relevant volatile anesthetic targets in vitro. For example, the anesthetic F3 (1-chloro-1,2,2-trifluorocyclobutane), but not the structurally similar nonanesthetic F6 (1,2-dichlorohexafluorocyclobutane), affect GABA_A, glycine, AMPA (α -amino-3-hydroxy-5-methyl-4-isoxazolepropionic acid), kainate, and 5-HT₃ receptors; and Na⁺ channels, consistent with possible roles in immobility, whereas both F3 and F6 affect neuronal nicotinic, M1 muscarinic, 5-HT_{2C}, and mGluR5 receptors, indicating that these targets are not involved in immobility. F6 is interesting in that it lacks sedative and immobilizing effects but does possess amnesic effects, hence use of the more accurate term *nonimmobilizer*, making it a useful pharmacologic tool for discriminating targets for these actions.
5. *Predictable effects of genetic manipulations targeted to putative molecular targets.* The effects of targeted deletion of specific molecules implicated as anesthetic targets (knockout mutations) or genetic engineering to introduce specific mutations that modify anesthetic

sensitivity (knockin mutations) in model organisms provide powerful approaches to test the roles of putative molecular targets of anesthetic action. This approach has been particularly successful in implicating specific GABA_A receptor subtypes in the effects of the GABAergic intravenous anesthetics propofol and etomidate, where single amino acid substitutions in specific receptor subtypes eliminate anesthetic effects both in vitro and in vivo.¹⁰⁹ Targeted mutations of putative anesthetic targets provide a bridge between in vitro observations and whole-animal experiments essential for demonstrating anesthetic end points. The existence of multiple targets and redundancy among ion channel subtypes makes this a more challenging experimental approach for inhaled anesthetics compared with intravenous anesthetics (discussed later).

PHYSICOCHEMICAL PROPERTIES OF ANESTHETIC BINDING SITES

A convergence of x-ray crystallography, molecular modeling, and structure-function studies indicates that inhaled anesthetics bind in the hydrophobic cavities formed within proteins.²² The lipophilic (or hydrophobic) nature of these binding sites explains their adherence to the Meyer-Overton correlation. An element of amphiphilicity (possessing both polar and nonpolar characteristics) is also required for effective interaction with these cavities, as indicated by improvements in the Meyer-Overton correlation with more amphipathic solvents (possessing both hydrophobic and hydrophilic properties).⁷

FROM MODEL PROTEINS TO RECEPTORS

Identifying inhaled anesthetic binding sites on plausible target proteins is difficult because of their low-affinity interactions, the paucity of atomic resolution structures of pharmacologically relevant target proteins, and the lack of specific antagonists. Consequently most anesthetic binding sites have been identified in well-characterized model proteins for which three-dimensional atomic resolution structures—such as luciferase¹¹⁰ and serum albumin¹¹¹—are available but are not themselves relevant to anesthesia. These studies indicate that anesthetics bind in pockets with both nonpolar and polar noncovalent chemical interactions.^{23,112} Binding involves weak hydrogen bond interactions with polar amino acid residues and water molecules, nonpolar van der Waals interactions, and a polarizing effect of the amphiphilic binding cavity on the relatively hydrophobic anesthetic molecules. Occupation of a site, or sites, by an anesthetic provides a plausible mechanism for alteration of receptor and ion channel function by selectively binding to a particular conformation (e.g., an open or inactivated state of an ion channel).²² Studies of glycine, GABA_A, and NMDA receptors provide convincing evidence for the existence of anesthetic binding sites in critical neuronal signaling proteins.¹¹³ It is likely that before long, high-resolution crystal structures of these receptors will be determined with inhaled anesthetic bound. However, because anesthetics act by binding only to certain transient conformational states, the relevance of necessarily static crystal structures will have to be assessed with care.

Structural studies using the more accessible prokaryotic homologues of eukaryotic ion channels have provided a powerful tool for the study of anesthetic binding sites in biologically plausible proteins. For example, both propofol and desflurane have been cocrystallized with *Gloebacter violaceus*, a bacterial homologue of eukaryotic inhibitory ligand-gated ion channels (glycine and GABA_A receptors).

Both anesthetics bind to a common preexisting site in the upper part of the transmembrane domain between the transmembrane segments of a single subunit (Fig. 19.6).¹¹⁴ Molecular modeling based on structurally homologous proteins has also been used to identify putative anesthetic binding sites in the transmembrane domains of vertebrate GABA_A and glycine receptors (Fig. 19.7). These models

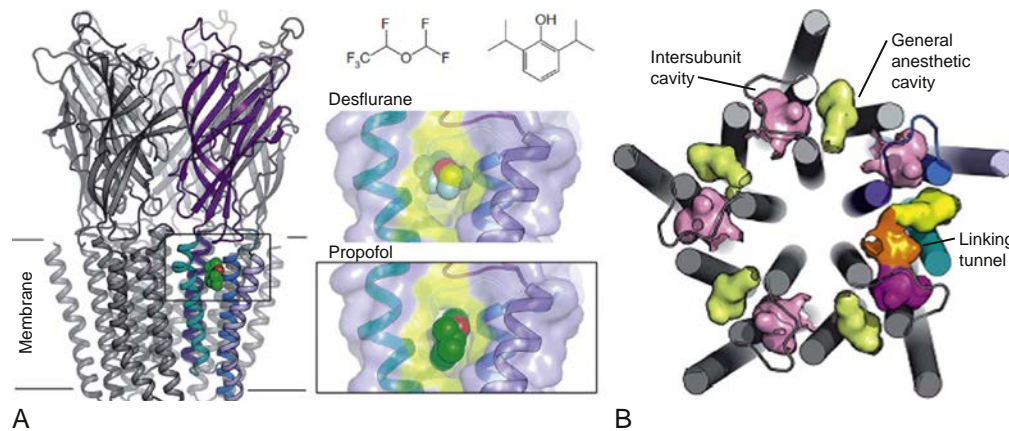


Fig. 19.6 X-ray structures of propofol and desflurane bound to a pentameric ligand-gated ion channel. (A) Cartoon of membrane-plane view of the bacterial homologue of mammalian pentameric ligand-gated ion channels (*Gloebacter violaceus*) with a bound general anesthetic molecule. (B) Molecular surface of the general anesthetic intrasubunit cavities (yellow) and neighboring intersubunit cavities (pink) of the whole pentameric channel. (Modified from Nury H, Van Renterghem C, Weng Y, et al. X-ray structure of general anaesthetics bound to a pentameric ligand-gated ion channel. *Nature*. 2011;469:428–433.)

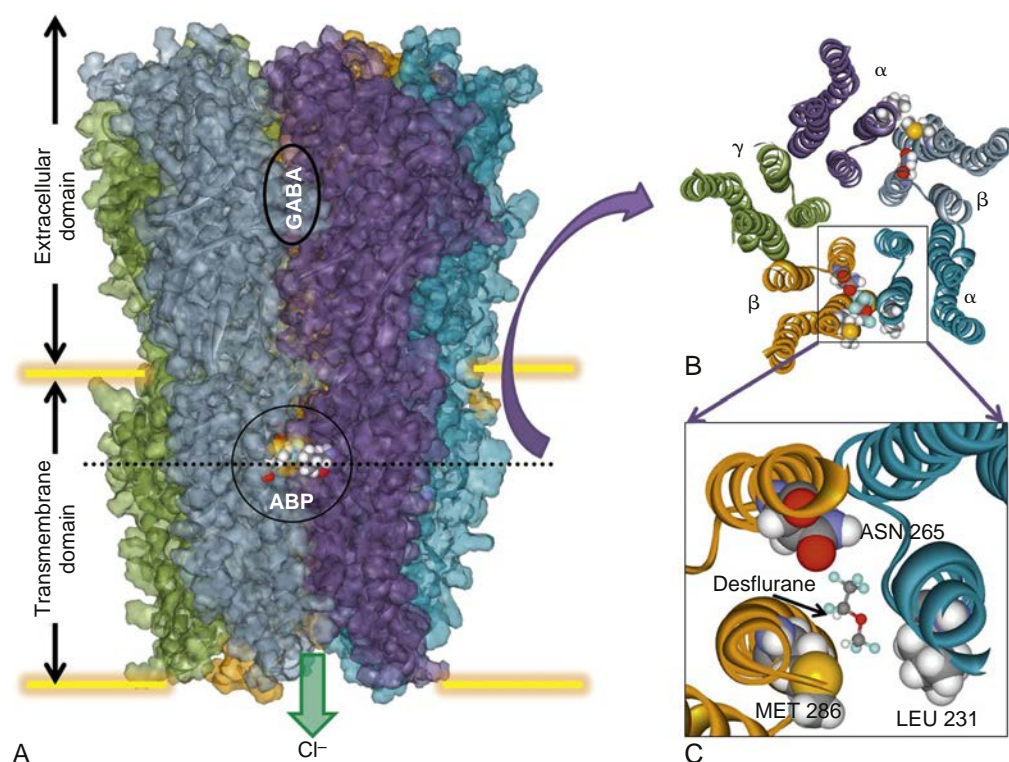


Fig. 19.7 Putative anesthetic binding sites on gamma-aminobutyric acid (GABA_A) receptors identified by molecular modeling. (A) Molecular model of the mouse GABA_A receptor built using homology modeling techniques with computational chemistry optimizations and molecular dockings. The amino acid backbone is displayed in ribbon format and outlined by the transparent solvent-accessible molecular surface. Each of the five subunits is colored uniquely. The GABA binding site is noted in the extracellular domain, whereas the putative anesthetic binding pocket (ABP) for potentiation is noted in the outer third of the transmembrane domain between the α and β subunits. Two binding sites are shown but only one has computationally docked desflurane. (B) A cross-section at the dotted line level in A showing orientation of subunits with pentameric symmetry about a central ion pore. (C) Magnified region of intersubunit anesthetic binding site derived from region in B showing relevant amino acid positions (in space-filling format) interacting with desflurane (in ball-and-stick format at the same scale). (Courtesy the Bertaccini laboratory, Stanford University, Stanford, CA.)

suggest that different drugs may either bind in different orientations within a single amphiphilic cavity or occupy different cavities within the protein, causing similar functional effects. Refinement of these molecular models will continue to provide new insights in the molecular basis for general anesthetic action that can be experimentally tested. For example, potential sites of interaction of xenon and isoflurane with the NMDA receptor have also been identified using this approach. One site, which can contain up to three xenon atoms or one molecule of isoflurane, overlaps the known binding site for the coagonist glycine in the NR1 subunit.¹¹⁵ This suggests that two chemically dissimilar inhaled anesthetics inhibit NMDA receptors by direct competitive inhibition of coagonist binding.

Molecular Targets of Inhaled Anesthetics

Ion channels have emerged as the most promising molecular targets for inhaled anesthetics. Neurotransmitter-gated ion channels—in particular GABA_A, glycine, and NMDA-type glutamate receptors—are leading candidates owing to their appropriate CNS distributions, essential physiologic roles in inhibitory and excitatory synaptic transmission, and sensitivities to clinically relevant concentrations of anesthetics.^{22,27,108,116} Other ion channels that are sensitive to inhaled anesthetics include the hyperpolarization-activated cyclic nucleotide (HCN)-gated family of channels that give rise to pacemaker currents¹¹⁶ and regulate dendritic excitability, two-pore domain (K_{2P}) “leak” K⁺ channels that maintain resting membrane potential in many cells,^{117,118} and voltage-gated Na⁺ and Ca²⁺ channels.¹¹⁶

LIGAND-GATED ION CHANNELS

Potentiation of Inhibitory GABA_A and Glycine Receptors

The ether anesthetics (including isoflurane, sevoflurane, and desflurane), the alkane anesthetic halothane, most intravenous anesthetics (including propofol, etomidate, barbiturates), and the neurosteroid anesthetics enhance GABA_A and glycine receptor (GlyR) function. GABA_A and GlyRs are members of the same cys-loop ligand-gated ion channel superfamily that also includes the cation-permeable nicotinic acetylcholine and 5HT₃ receptors. GABA_A receptors are the principal transmitter-gated Cl⁻ channels in the neocortex and allocortex, whereas GlyRs fulfill this function in the spinal cord, with some overlap in the diencephalon and brain stem. Activated receptors conduct chloride ions, driving the membrane potential toward the Cl⁻ equilibrium potential. Both receptors are inhibitory (except in some cases during development) because the Cl⁻ equilibrium potential is usually more negative than the normal resting potential. Channel opening also reduces membrane resistance and “shunts” excitatory responses. Most functional GABA_A and GlyRs are heteropentamers, typically consisting of three different GABA_A subunits (e.g., two α , two β , and one γ or δ)¹¹⁹ or two different GlyR subunits (three α and two β).¹²⁰ The subunit composition of GABA_A receptors determines their physiologic and pharmacologic properties and varies between and within brain areas as well as between different compartments of individual neurons. Examples are the preferential expression of the α_5 subunit in the dendritic field of the hippocampal CA1 area (a region important for

memory formation), of the α_4 subunit in the thalamus, and of the α_6 subunit in the cerebellum. Presence of a γ subunit is required for benzodiazepine modulation of GABA_A receptors and can also influence modulation by inhaled anesthetics. Although the molecular mechanisms of receptor modulation by inhaled anesthetics are not clear, these receptors have been key to our understanding of anesthetic-receptor interactions. Using chimeric receptor constructs between anesthetic-sensitive GABA_A and insensitive GlyR subunits, specific amino acid residues in transmembrane domains 2 and 3 critical to the action of inhaled anesthetics have been identified.¹²¹ This laid the groundwork for the construction of anesthetic-resistant GABA_A receptors and the generation of transgenic mice with altered anesthetic sensitivity (discussed later).

The related cation-permeable 5-hydroxytryptamine (serotonin)-3 (5HT₃) receptors are similarly potentiated by volatile anesthetics.^{122,123} 5HT₃ receptors are involved with autonomic reflexes and also probably contribute to the emetogenic properties of volatile anesthetics.

Inhibition of Excitatory Acetylcholine and Glutamate Receptors

Neuronal nicotinic acetylcholine receptors (nnAChRs), like the other members of the cys-loop family, are heteropentameric ligand-gated ion channels but are cation-selective. They are composed of α and β subunits but functional homomeric receptors can be formed by certain α subunits. In the CNS, nnAChRs are localized primarily presynaptically.¹²⁴ Homomeric α_7 receptors have high permeability to Ca²⁺, which can exceed that of NMDA receptors.¹²⁴ In contrast to GABA_A and GlyRs, nnAChRs pass cations when activated and therefore depolarize the membrane potential. Receptors containing $\alpha_4\beta_2$ subunits are very sensitive to block by isoflurane.^{125,126} Relevance of nnAChR block to immobilization, sedation, and unconsciousness by inhaled anesthetics is unlikely because nnAChRs are also blocked by nonimmobilizers, although it is possible that they do contribute to amnesia.

NMDA receptors are a major postsynaptic receptor subtype of inotropic receptors for glutamate, the principal excitatory neurotransmitter in the mammalian CNS.¹²⁷ Typical NMDA receptors, defined pharmacologically by their selective activation by the exogenous agonist NMDA, are heteromers consisting of an obligatory GluN1 subunit and modulatory GluN2 subunits. Channel opening requires glutamate (or another synthetic agonist such as NMDA) binding to the GluN2 subunit while the endogenous coagonist glycine binds to the GluN1 subunit. NMDA receptors also require membrane depolarization to relieve voltage-dependent block by Mg²⁺. Depolarization is typically provided by the binding of glutamate to non-NMDA glutamate receptors (discussed later). Because of this requirement for both presynaptic transmitter release and postsynaptic depolarization, synaptic NMDA receptors function as coincidence detectors, and this characteristic is thought to be central to their role in learning and memory. NMDA receptors are also involved in the development of chronic pain, perhaps because of mechanisms similar to those underlying synaptic plasticity, and in ischemia-induced excitotoxicity by virtue of their capacity to allow entry of the ubiquitous intracellular signal Ca²⁺. The nonhalogenated inhaled

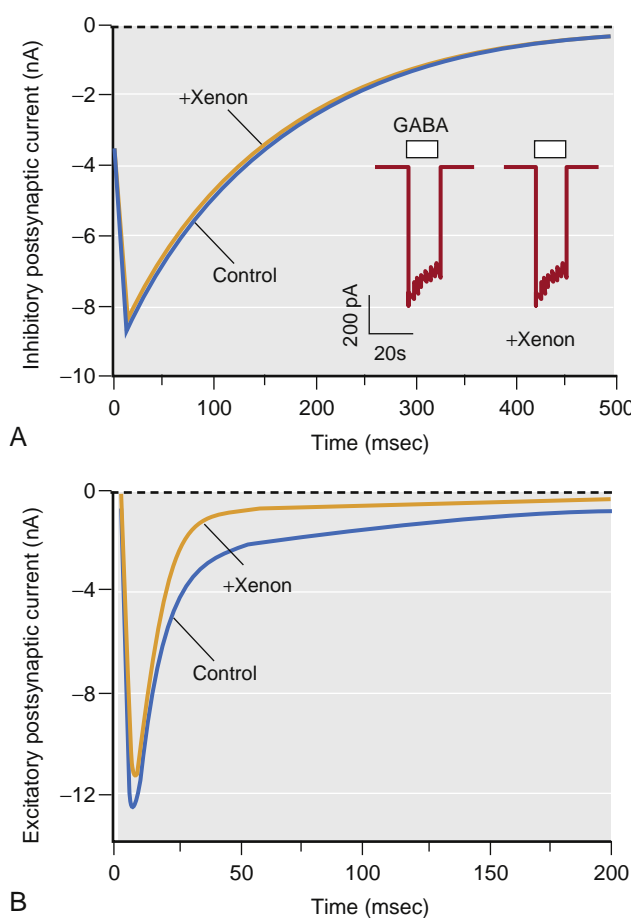


Fig. 19.8 The actions of xenon on inhibitory GABAergic and excitatory glutamatergic synapses in cultured rat hippocampal neurons. Xenon (3.4 mM, or 1 minimum alveolar concentration [MAC]) has no significant effect on the inhibitory postsynaptic current (A) but depresses the excitatory glutamatergic synaptic current, almost exclusively the slow *N*-methyl-D-aspartate receptor-mediated component of the current (B). In contrast, the principal effects of 1 MAC isoflurane are a prolongation in the inhibitory current decay and a reduction in excitatory current peak height, with little change in time course (not shown, see Fig. 19.10). (Reprinted in modified form by permission from de Sousa SLM, et al. Contrasting synaptic actions of the inhalational general anesthetics isoflurane and xenon. *Anesthesiology*. 2000;92:1055–1066.)

anesthetics xenon, nitrous oxide, and cyclopropane have minimal effects on GABA_A receptors but depress excitatory glutamatergic synaptic transmission postsynaptically via NMDA glutamate receptor blockade (Fig. 19.8).^{128,129} Volatile anesthetics can also inhibit isolated NMDA receptors at higher concentrations.¹³⁰ Along with presynaptic inhibition of glutamate release, this might contribute to their depression of NMDA receptor-mediated excitatory transmission.

A second class of inotropic glutamate receptors includes the non-NMDA receptors, which are subdivided into AMPA and kainate receptors based again on their sensitivities to selective exogenous agonists.¹²⁷ Inhaled anesthetics only weakly inhibit AMPA receptors; hence this action is unlikely to be important in their actions.¹³¹ Interestingly, kainate receptors are enhanced by inhaled anesthetics, but this is unlikely to be involved in immobility because MAC is not altered in mice deficient in the GluR6 receptor subunit.¹³² Most evidence suggests that the principal mechanism for

depression of glutamatergic transmission by volatile anesthetics is presynaptic, with minor contributions from postsynaptic receptor blockade^{133–135} (see section on “Cellular Mechanisms”).

VOLTAGE-GATED AND OTHER ION CHANNELS

Volatile anesthetics have diverse effects on a wide variety of ion channels that are critically involved in their neurophysiologic, cardiovascular, and respiratory actions. A detailed understanding of these interactions is crucial to a pharmacologic description of this essential drug class.

Na⁺ Channels

Voltage-gated Na⁺ channels are critical to axonal conduction, synaptic integration, and neuronal excitability. In contrast to findings in invertebrate giant axons,¹³⁶ axonal conduction in small (0.1–0.2 μ m) unmyelinated hippocampal axons is depressed by volatile anesthetics,^{137,138} and small reductions in preterminal action potential amplitude significantly depress transmitter release and hence postsynaptic responses at a mammalian synapse.¹³⁹ Heterologously expressed mammalian voltage-gated Na⁺ channels are sensitive to clinically relevant concentrations of volatile anesthetics. The Na⁺ channel family consists of nine homologous pore-forming α subunits with distinct cellular and subcellular distributions.^{140,141} Isoflurane and other volatile anesthetics inhibit the major mammalian Na⁺ channel isoforms, including neuronal (Na_v1.2), skeletal muscle (Na_v1.4), cardiac (Na_v1.5), and peripheral (Na_v1.8) isoforms.¹⁴² Volatile anesthetics but not nonimmobilizers also inhibit native neuronal and nerve terminal Na⁺ channels,^{141,143–146} lending support to the notion that Na⁺ channel blockade contributes to the depression of synaptic neurotransmitter release.¹⁴⁷ In contrast, xenon has no detectable effect on Na⁺, Ca²⁺, or K⁺ channels in isolated cardiomyocytes.¹⁴⁸ The demonstration that NaChBac, a prokaryotic homologue of voltage-gated Na⁺ channels, is also inhibited by volatile anesthetics opens the way for structure-function studies of these channels.¹⁴⁵ These studies suggest that volatile anesthetics affect channel gating, probably via at least two drug binding sites.^{149–151}

Ca²⁺ Channels

Multiple cellular functions depend on the tightly controlled concentration of intracellular free Ca²⁺ ([Ca²⁺]_i), which is determined by the integrated activities of voltage-gated Ca²⁺ channels, capacitative Ca²⁺ channels, plasma membrane and sarcoplasmic/endoplasmic reticulum (ER) Ca²⁺-adenosine triphosphatases (pumps), Na⁺/Ca²⁺ exchangers, mitochondrial Ca²⁺ sequestration, and cytoplasmic Ca²⁺-binding proteins. Alteration of any of these mechanisms can affect the many cellular processes regulated by the second-messenger actions of Ca²⁺, including synaptic transmission, gene expression, cytotoxicity, and muscle excitation-contraction coupling. Excitable cells translate their electrical activity into action by Ca²⁺ fluxes mediated primarily by voltage-gated Ca²⁺ channels in the plasma membrane. Distinct Ca²⁺ channel subtypes are expressed in various cells and tissues, and are classified pharmacologically and functionally by the degree of depolarization required to gate the channel as low voltage-activated

(LVA; T-type) or high voltage-activated (HVA; L-, N-, R-, and P/Q-type) channels. Cloning and sequencing to identify their pore-forming α subunits has allowed molecular classification of these functionally identified channel subtypes.¹⁴¹ Considerable evidence indicates that volatile anesthetics inhibit certain Ca^{2+} channel isoforms but not others.

Inhibition of presynaptic voltage-gated Ca^{2+} channels coupled to transmitter release has been proposed as a mechanism by which volatile anesthetics reduce excitatory transmission.^{152,153} Indeed, N-type ($\text{Ca}_v2.2$) and P-type ($\text{Ca}_v2.1$) channels, which mediate Ca^{2+} entry coupled to neurotransmitter release, are modestly sensitive to volatile anesthetics^{154,155} but not in all neuron types,¹⁵⁶ suggesting the importance of auxiliary subunits, posttranslational modification, or other potential modulators of anesthetic sensitivity. A modest contribution of R-type Ca^{2+} channels ($\text{Ca}_v2.3$) to anesthesia is suggested by their sensitivity to volatile anesthetics and a small increase in MAC produced by genetic deletion in mice.¹⁵⁷ T-type Ca^{2+} channels are particularly sensitive to volatile anesthetics¹⁵⁸ and nitrous oxide.¹⁵⁹ However, mutant mice lacking a major neuronal T-type Ca^{2+} channel isoform ($\text{Ca}_v3.1$) have normal volatile anesthetic sensitivity, although the onset of anesthesia is delayed.¹⁶⁰ Thus the role that inhibition of these or other Ca^{2+} channels plays in the CNS effects of inhaled anesthetics is unclear.

At higher doses, a role for Ca^{2+} channel inhibition in the negative inotropic effects of volatile anesthetics is well established. The force of myocardial contraction is determined by the magnitude of cytosolic Ca^{2+} increase after electrical excitation, the responsiveness of the contractile proteins to Ca^{2+} , and sarcomere length. Negative inotropic effects of volatile anesthetics are mediated by reductions in Ca^{2+} availability, Ca^{2+} sensitivity of the contractile proteins, and rate of cytosolic Ca^{2+} clearance. Volatile anesthetics reduce the Ca^{2+} transient and shorten action potential duration in cardiomyocytes primarily by inhibiting L-type ($\text{Ca}_v1.2$) Ca^{2+} currents, resulting in a negative inotropic effect and arrhythmogenicity.¹⁶¹⁻¹⁶³ In contrast, xenon does not depress myocardial function or inhibit L-type Ca^{2+} , Na^+ , or K^+ currents in isolated cardiomyocytes.^{164,165} Inhibition of trans-sarcolemmal Ca^{2+} influx through cardiac L-type Ca^{2+} channels plays a major role in the negative inotropic effects of volatile anesthetics—greatest for halothane—along with contributions from effects on myofilament Ca^{2+} sensitivity and sarcolemmal Ca^{2+} release.^{162,166}

In contrast to voltage-gated Ca^{2+} channels that regulate the influx of extracellular Ca^{2+} , intracellular Ca^{2+} channels regulate Ca^{2+} release from intracellular stores, particularly the ER and sarcoplasmic reticulum (SR). These include 1,4,5-inositol triphosphate receptors (IP₃Rs), regulated by the second messenger IP₃, and ryanodine receptors (RyRs); the latter mediate the release of SR Ca^{2+} , which is critical to excitation-contraction coupling in muscle. Volatile anesthetic-induced Ca^{2+} leak occurs by effects on both IP₃R and RyR channels, which leads to depletion of intracellular Ca^{2+} stores from the SR and ER. In brain, volatile anesthetic activation of IP₃Rs has been proposed as a mechanism for anesthetic neurotoxicity.¹⁶⁷ This blunts changes in intracellular Ca^{2+} in response to stimulation and contributes to the smooth muscle-relaxing properties of volatile anesthetics that underlie bronchodilation and vasodilation.¹⁶⁸

Malignant hyperthermia is a pharmacogenetic disorder that manifests as a potentially fatal hypermetabolic crisis triggered by volatile anesthetics, particularly halothane. It is often associated with mutations in RyR1 and the physically associated L-type Ca^{2+} channel ($\text{Ca}_v1.1$), which functions as the voltage sensor.¹⁶⁹ Volatile anesthetics activate the mutated RyRs, resulting in uncontrolled intracellular Ca^{2+} release from the SR, muscle contraction, and hypermetabolic activity.¹⁷⁰

K⁺, HCN, and TRP Channels

Potassium (K⁺) channels are members of an extremely diverse ion channel family noted for their varied modes of activation. They regulate electrical excitability, muscle contractility, and neurotransmitter release. They are important in determining input resistance and in driving repolarization after action potentials; thus they determine excitability and action potential duration. Given the large diversity in K⁺ channel structure, function, and anesthetic sensitivity, it is not surprising that there is considerable diversity in their sensitivity and response to inhaled anesthetics,¹⁷¹ from relatively insensitive (voltage-gated K⁺ channels K_v1.1, K_v3)¹⁷² to sensitive (some members of the K_{2P} family), resulting in either inhibition, activation, or no effect on K⁺ currents.

Volatile anesthetic activation of certain “leak” K⁺ channels was first observed in the snail *Lymnaea*,¹⁷³ although the molecular identity of the affected ion channels was unknown. Activation of K_{2P} channels by volatile and gaseous anesthetics—including xenon, nitrous oxide, and cyclopropane—was subsequently observed in mammals.¹¹⁸ Increased K⁺ conductance can hyperpolarize neurons, reducing responsiveness to excitatory synaptic input and possibly altering network synchrony. Targeted deletion of the TASK-1, TASK-3, and TREK-1 K_{2P} channels in mice reduces sensitivity to immobilization by volatile anesthetics in an agent-specific manner, implicating these channels as contributory anesthetic targets *in vivo*.⁴⁴⁻⁴⁷ The K⁺ channel TREK-1 also contributes to the neuroprotective effects of xenon¹⁷⁴ and sevoflurane.¹⁷⁵

Progress has recently been made in identifying anesthetic binding sites to K⁺ channels using photoaffinity labeling, which has identified a sevoflurane binding site in the K_v1.2 channel; this is widely expressed in brain and positively modulated by volatile anesthetics.¹⁷⁶ Molecular modeling has also been used to identify likely binding sites in K_{2P} channels.¹⁷⁷

The recognition that inherited channelopathies are arrhythmogenic and constitute an important contributor to sudden cardiac death,¹⁷⁸ particularly in young children,¹⁷⁹ highlights the importance of analyzing anesthetic modulation of cardiac ion channels. Recombinant hERG (human ether-a-go-go-related) channels are moderately inhibited by halothane, and their depression likely contributes to arrhythmogenic effects of volatile anesthetics^{162,180}; they are also involved in acquired (drug-induced) and inherited long QT syndrome. Cardiac inward-rectifying (K_{IR}), voltage-gated (K_v), and Ca^{2+} -activated K⁺ channels are generally relatively insensitive to clinical concentrations of volatile anesthetics and xenon.^{162,164,181} In contrast, volatile anesthetics and xenon activate cardiac mitochondrial and sarcolemmal K_{ATP} channels,¹⁸² which might contribute

to anesthetic preconditioning to cardiac ischemia. Direct electrophysiologic effects of anesthetics with preconditioning properties have been demonstrated on both mitochondrial and sarcolemmal K_{ATP} channels, although the precise mechanisms remain to be clarified. The large conductance (BK) mitochondrial K^+ channel Slick of the *Slo2* gene family has been shown to be important for volatile anesthetic preconditioning *in vivo*.¹⁸³

Volatile anesthetics also inhibit HCN pacemaker channels, reducing the rate of rise of pacemaker potentials and the bursting frequency of certain neurons that show autorhythmicity. They decrease the I_h conductance in neurons¹⁸⁴ and modulate recombinant HCN1 and HCN2 channel isoforms at clinically relevant concentrations.¹⁸⁵ Because HCN channels contribute to resting membrane potential, control action potential firing, dendritic integration, neuronal automaticity, and temporal summation, and also determine periodicity and synchronization of oscillations in many neuronal networks,¹⁸⁶ anesthetic modulation of these channels could play an important role in anesthetic effects on neuronal integrative functions. Selective knockout of HCN1 in mouse forebrain shows a role for these channels in the amnestic and hypnotic but not immobilizing effects of volatile anesthetics.¹⁸⁹

INTRACELLULAR SIGNALING MECHANISMS

Cell signaling mechanisms are critical to all phases of organ and cellular function, which has made them attractive targets for producing the broad effects of general anesthetics on multiple organs. Anesthetics have complex actions on intracellular cell signaling pathways, which include processes downstream from cell surface receptors and ion channels, including effects on second messengers, protein phosphorylation pathways, and other regulatory mechanisms.¹⁸⁷

G-Protein-Coupled Receptors

A variety of signals—including hormones, neurotransmitters, cytokines, pheromones, odorants, and photons—produce their intracellular actions by interactions with metabotropic receptors that activate heterotrimeric guanine nucleotide-binding proteins (G proteins). In contrast to inotropic receptors that directly couple to ion-selective channels, G proteins act as indirect molecular switches to relay information from activated plasma membrane receptors to appropriate intracellular targets.

Heterotrimeric G proteins consist of a large α -subunit and a smaller β/γ -subunit dimer, each expressed as multiple isoforms with distinct properties and downstream targets. G proteins regulate a plethora of downstream effectors to control the levels of cytosolic second messengers such as Ca^{2+} , cyclic adenosine monophosphate, and inositol triphosphate. These, in turn, regulate effector proteins such as ion channels and enzymes, either directly or via second messenger-regulated protein phosphorylation pathways. Ca^{2+} is a ubiquitous second messenger that regulates a number of downstream effectors, often mediated by the multifunctional Ca^{2+} -binding protein calmodulin. As volatile anesthetics have profound effects on intracellular Ca^{2+} concentrations via their effects on both plasma membrane and intracellular Ca^{2+} channels, transporters,

and exchangers (see the section on ion channels earlier), many of the downstream effects of anesthetics are ultimately mediated by changes in the second-messenger actions of Ca^{2+} .

Drugs that act through G protein-coupled receptors (GPCRs) such as agonists for μ -opioid and α_2 -adrenergic receptors can affect anesthetic sensitivity (reduce MAC). Inhaled anesthetics can also directly affect signaling via GPCRs.¹⁸⁸ For example, volatile anesthetics activate multiple olfactory GPCRs in the rat *in vivo* in a receptor- and agent-selective manner.¹⁸⁹ Analogous effects on related GPCRs more relevant to critical anesthetic end points are possible but remain to be demonstrated. The observation that both volatile anesthetics and nonimmobilizers inhibit mGluR5 glutamate receptors, 5-HT_{2A} serotonin receptors, and muscarinic acetylcholine receptors suggests that these GPCR effects do not contribute to anesthetic immobilization.¹⁹⁰⁻¹⁹²

Protein Phosphorylation

Phosphorylation of proteins on specific serine, threonine, or tyrosine hydroxyl groups, a posttranslational modification involved in the regulation of many anesthetic-sensitive receptors and ion channels, is pivotal to synaptic plasticity (e.g., long-term potentiation [LTP]). Phosphorylation is controlled by the balance of activity between protein kinases and phosphatases, several of which are plausible anesthetic targets. The protein kinase C (PKC) family of multifunctional protein kinases is activated by the lipid-signaling molecule diacylglycerol and is involved in the regulation of many ion channels and receptors. Halothane¹⁹³ and sevoflurane¹⁹⁴ enhance the activity of some PKC isoforms and stimulate phosphorylation of specific PKC substrates. Structural studies have identified a potential binding site in the diacylglycerol binding domain of PKC δ , consistent with the ability of certain anesthetics to mimic this natural regulator by binding to the activating site.¹⁹⁵ A specific role for a direct pharmacologically relevant effect related to general anesthesia mediated by anesthetic activation of PKC or of any other kinase has yet to be demonstrated. Intrathecal injection of isoform-specific inhibitors of PKC does not affect sensitivity to halothane *in vivo*.¹⁹⁶ Knockout mice lacking the PKC γ isoform show normal sensitivity to halothane and desflurane while isoflurane MAC was increased,¹⁹⁷ suggesting that PKC is not critical to volatile anesthetic immobilization.

An important role for effects of volatile anesthetics and xenon on cell signaling mechanisms has been discovered for anesthetic-induced preconditioning in the heart and brain against ischemic damage.¹⁹⁸⁻²⁰² Anesthetic-induced and ischemic cardiac preconditioning share critical signaling mechanisms, including activation of multiple GPCRs (e.g., adenosine, opioid, adrenergic) and protein kinases (e.g., src kinase, PKC δ , PKC ϵ , Akt, mitogen-activated protein kinases [MAPKs]), and their downstream targets, particularly sarcolemmal and/or mitochondrial K_{ATP} channels, possibly initiated by changes in reactive oxygen species as the critical second messenger.^{203,204} Volatile anesthetics and xenon share cardioprotective and neuroprotective effects involving these signaling pathways.^{202,205}

The effects of anesthetics on the phosphorylation of individual residues in specific substrates can be studied using

phosphorylation state-specific antibodies that are able to detect the phosphorylated forms of kinase substrates. A comparison of the effects of three mechanistically diverse anesthetics (isoflurane, propofol, and ketamine) on critical intracellular protein phosphorylation signaling pathways that are known to integrate multiple second messenger systems reveals both shared and agent-specific actions *in vivo*.²⁰⁶ All three anesthetics reduce phosphorylation of activating sites on NMDA and AMPA glutamate receptors and of the downstream extracellular signal-regulated kinase ERK2, all of which are known to be involved in synaptic plasticity, consistent with depression of normal glutamatergic synaptic transmission in the anesthetized mouse cerebral cortex. These effects are somewhat selective in that several other protein kinase A (PKA) substrates examined are not affected, indicating substrate-specific effects rather than a general inhibition of PKA activity.²⁰⁷ Additional studies will be required to determine which anesthetic effects on kinase pathways represent direct effects, as occurs with PKC, and which are indirect because of anesthetic-induced alterations in signaling molecules known to regulate protein kinase and phosphatase activity such as Ca^{2+} and other second messengers.

Gene Expression

The ability of general anesthetics to alter gene expression in the brain was first observed for the highly reactive immediate early genes *c-fos* and *c-jun*.²⁰⁸ Anesthetic effects on gene expression have since been observed for multiple anesthetics and organs.²⁰⁹ In the hippocampus of aged rats, changes in gene expression persisted for up to 2 days in rats exposed to isoflurane and nitrous oxide,²¹⁰ and changes in protein expression have been observed 3 days after exposure to desflurane.²¹¹ The significance of these changes in gene and protein expression persisting after recovery from the classic signs of anesthesia remains to be established (see review²¹²). Recent findings suggest that certain anesthetic effects are mediated by epigenetic mechanisms involving specific posttranslational modifications of DNA-binding histone proteins by acetylase and deacetylase enzymes. For example, exposure of neonatal rats to general anesthesia led to reduced histone 3 acetylation and delayed cognitive deficits that could be reversed by a histone deacetylase inhibitor.²¹³

Cellular Mechanisms

NEURONAL EXCITABILITY

Neuronal excitability is determined by resting membrane potential, threshold for action potential initiation, and input resistance (an indication of overall channel activity). Considerable diversity exists for each of these factors in different types of neurons, and membrane properties differ not only between neurons but also between compartments (e.g., soma versus dendrite). Moreover, anesthetic effects vary with the state of the individual neuron—that is, whether it is hyperpolarized or depolarized, stimulated by synaptic inputs, or quiescent. Therefore results obtained using model systems or reduced preparations (e.g. cultured neurons and brain slices) incompletely reflect anesthetic

effects *in vivo*. Nevertheless much valuable information has been obtained using these approaches because they allow changes in neuronal activity to be attributed to specific cellular and molecular targets.

The intrinsic excitability of spinal motoneurons was reported to be little affected by halothane,²¹⁴ but changes in hippocampal pyramidal neuron excitability were shown to be substantial and complex. Threshold can be increased or decreased, and regional differences and dose-dependent effects on firing patterns have been observed.^{215,216} Neurons in the ventral-posterior nucleus of the thalamus (possibly thalamic relay neurons) hyperpolarize in the presence of isoflurane and are less likely to fire action potentials because of a decrease in input resistance (increased shunting)—an effect that has been attributed to increased K^+ conductance.²¹⁷ Similar effects are observed in hypoglossal motoneurons and neurons from the locus coeruleus, where a TASK-type $\text{K}_{2\text{P}}$ channel has been causally implicated.²¹⁸

GABA_A receptors located at extrasynaptic sites can also influence excitability by increasing membrane conductance and thereby “shunting” excitatory currents. These receptors have a high affinity for GABA; they are continually exposed to low ambient GABA concentrations and desensitize slowly.²¹⁹ Their importance to anesthesia, however, may hinge on exactly what these ambient concentrations are.²²⁰ Tonic current in hippocampal pyramidal neurons arises primarily from α_5 subunit-containing GABA_A receptors, which are highly sensitive to etomidate, propofol, midazolam, and isoflurane.²²¹⁻²²⁴ Thus they provide a potential substrate for the amnesic properties of anesthetics. These same receptors also contribute to slow phasic (synaptic) currents, which are produced by spillover of GABA from synapses.²²⁵ Their slow time course and location, matching those of synaptic NMDA receptors, place them in an ideal position to modulate synaptic plasticity. Indeed, reducing or eliminating $\alpha_5\text{-GABA}_A$ receptors by pharmacologic or genetic means attenuates the amnestic properties of the GABA_A receptor-selective anesthetic etomidate. However, since elimination of $\alpha_5\text{-GABA}_A$ receptors from pyramidal neurons does not reproduce this effect,²²⁶ modulation of other cell types (interneurons or glia) may also play a role in anesthetic-induced amnesia and other anesthetic end points.

PRESYNAPTIC VERSUS POSTSYNAPTIC EFFECTS ON SYNAPTIC TRANSMISSION

General anesthetics have potent and specific effects on synaptic transmission, including presynaptic actions (by altering transmitter release) and postsynaptic actions (by altering the postsynaptic responses of neurons to specific transmitters). The relative contributions of presynaptic compared with postsynaptic anesthetic effects on synaptic transmission have been difficult to resolve, probably because the effects are transmitter- and synapse-specific. The net effect of anesthetics on synaptic transmission is determined by the relative magnitude and direction of both their presynaptic and postsynaptic effects. The general effects of inhaled anesthetics are to increase inhibitory synaptic transmission and to inhibit excitatory synaptic transmission (Fig. 19.9).

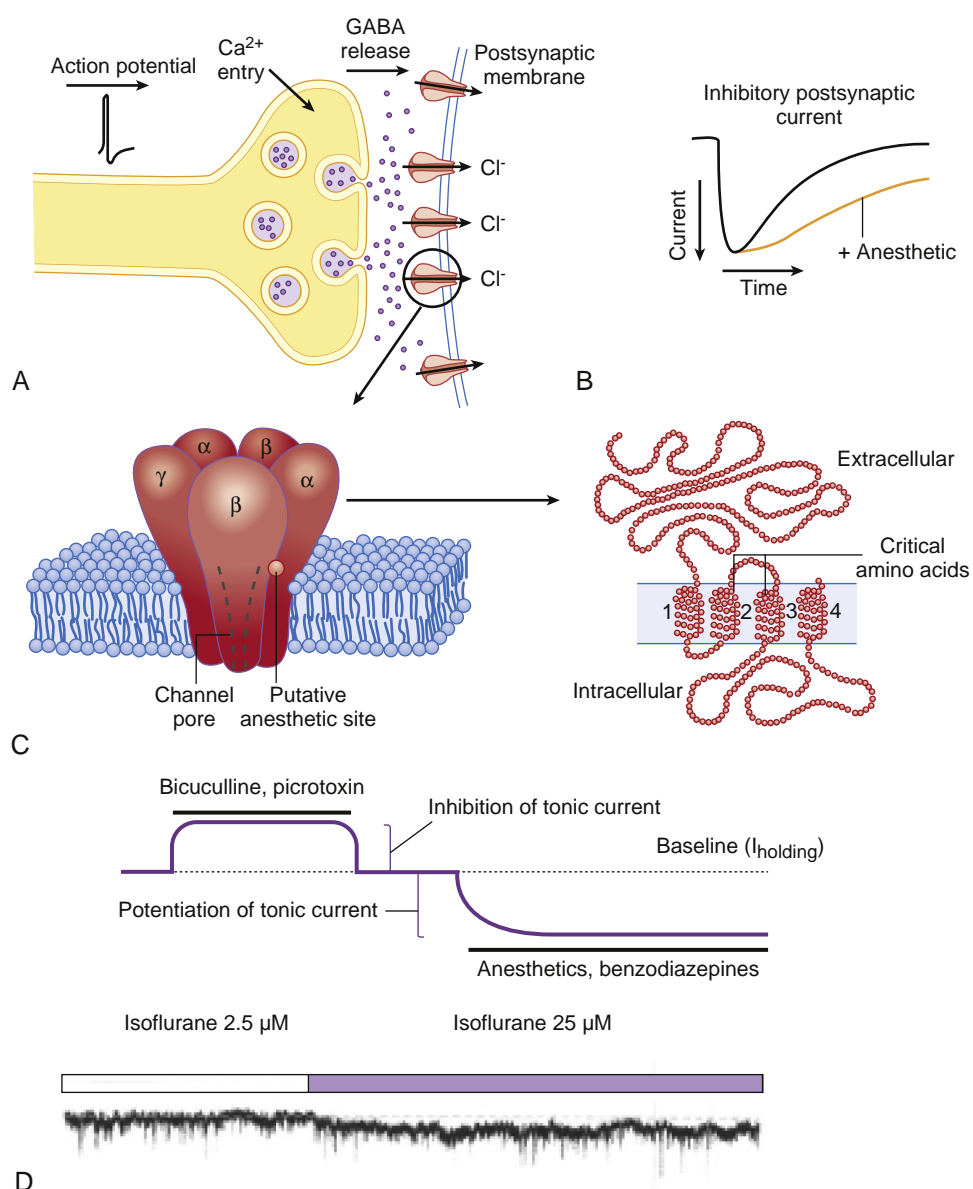


Fig. 19.9 Synaptic and extrasynaptic γ -aminobutyric acid (GABA_A) receptors are targets for inhaled anesthetics. (A) On binding of GABA to the GABA_A receptor, its chloride-permeable channel opens, usually leading to hyperpolarization. Volatile anesthetics have a relatively low potency but high efficacy at synaptic GABA_A receptors and a high potency and low efficacy at extrasynaptic GABA_A receptors. (B) General anesthetics prolong channel opening and increase postsynaptic inhibition. The cartoon illustrates the prolongation of miniature inhibitory synaptic currents by the slowing of current decay. (C) A pentameric GABA_A receptor complex in the lipid bilayer membrane (left), with a blowup of a single subunit showing the location of residues critical to anesthetic efficacy in the second and third transmembrane domains (right). (D) A tonic inhibitory conductance is revealed by the application of a GABA_A receptor antagonist (bicuculline or picrotoxin), as shown by the upward shift in the baseline current. Anesthetics and benzodiazepines increase the tonic conductance, as indicated by the inward shift in the current. (Modified from Hemmings HC Jr, Akabas MH, Goldstein PA, et al. Emerging molecular mechanisms of general anesthetic action. *Trends Pharmacol Sci*. 2005;26:503–510.)

Excitatory synaptic excitation is generally decreased by volatile anesthetics (Fig. 19.10). Experiments in various slice preparations indicate that reduced excitation is primarily caused by presynaptic mechanisms.^{87,133,214,227–229} A postsynaptic mechanism is also involved because the response to directly applied glutamate is reduced to some degree.^{229–231} Volatile anesthetics have inconsistent effects on cloned AMPA or NMDA glutamate receptors, but they potentiate kainite receptors,^{115,129,232,233} consistent with a predominantly presynaptic mechanism for glutamatergic synapses. By contrast, the effects of the nonhalogenated inhaled anesthetics (xenon, nitrous oxide, cyclopropane)

appear to be mediated primarily by inhibition of postsynaptic NMDA receptors (discussed earlier). Under some circumstances, such as in patients with defects in mitochondrial complex 1²³⁴ and in mice carrying mutations in mitochondrial complex 1,²³⁵ inhaled agents suppress glutamate release by interfering with the energy-intensive glutamate recycling pathways,²³⁶ thereby leading to extreme anesthetic sensitivity. Recent evidence from conditional knockout mice indicates this mechanism may contribute to various end points even in nonpathogenic states.²³⁷

Augmentation of GABAergic inhibition by most general anesthetics is mediated by both presynaptic and postsynaptic

mechanisms. Enhancement of postsynaptic and extrasynaptic GABA_A receptors is well recognized.¹¹⁶ Volatile anesthetics increase spontaneous GABA release and inhibitory postsynaptic current (IPSC) frequency^{238–242}—that is, their presynaptic effects at GABAergic terminals are distinct from those at glutamatergic synapses.

The mechanisms for the presynaptic effects of inhaled anesthetics, like those for their postsynaptic effects, are complex and involve multiple targets. Although a synapse-specific contribution of presynaptic Ca²⁺ channels is likely,²⁴³ presynaptic Na⁺ channels are more sensitive than the Ca²⁺ channels coupled to glutamate release. This finding is consistent with observations that the predominant Ca²⁺ channel coupled to neurotransmitter release at hippocampal glutamatergic synapses (P/Q-type) is insensitive to isoflurane.¹⁵⁶ Other presynaptic mechanisms have been proposed, including actions on the vesicle fusion process, as demonstrated in the model organism *Caenorhabditis elegans*.^{244,245} However, isoflurane effects on exocytosis in rat hippocampal neurons occur primarily upstream of vesicle fusion.^{139,246}

Simple Circuits and Complex Networks

SIMPLE CIRCUIT PHENOMENA

The development of a mechanistic understanding of phenomena involving complex circuits has been greatly facilitated by the study of anatomically reduced (in vitro) or physiologically simplified (in vivo) preparations complemented by computer simulations (in silico). These approaches are essential for integrating reductionist observations of the multiple molecular effects of anesthetics into functional models relevant to behavioral end points. Anesthetic effects have been studied in acute brain slice preparations from various regions of the CNS (hippocampus, amygdala, cortex, thalamus, brain stem, and spinal cord)—most often from rodents. Brain slices preserve native connections but usually lack natural inputs and outputs. Slices

from developing mammalian brain can also be cultured in vitro. These “organotypic slice cultures” preserve a high degree of synaptic connectivity and display spontaneous network activity, typically absent from “acute slices.” Simplified in vivo preparations involve phenomena (typically evoked responses) with relatively well-understood circuitry. Computer models and simulations can assist in generating hypotheses for experimental testing and developing hypotheses based on experimental data.

Synaptic Plasticity

Paired-pulse depression and paired-pulse facilitation are examples of short-term plasticity in response to external stimulation. Synaptic inhibition is prolonged by volatile anesthetics in vivo²⁴⁷ and in vitro,²⁴⁸ in general agreement with the notion that anesthetics enhance functional inhibition in the CNS. Enhancement of paired-pulse facilitation has been attributed to the presynaptic depressant effect of volatile agents (Fig. 19.11).^{133,228}

LTP, a cellular model of learning and memory, is a use-dependent strengthening of glutamatergic excitatory synaptic connections. Volatile anesthetic effects on LTP depend on the experimental preparation. Halothane, enflurane, and isoflurane do not block LTP induction in vivo, whereas ketamine and the NMDA antagonist CPP do.^{247,249} By contrast, isoflurane blocks LTP in the hippocampal slice by enhancing GABA_A receptor-mediated inhibition (Fig. 19.12)²⁵⁰ or blocking neuronal nicotinic receptors.⁸⁸ Long-term depression, a use-dependent weakening of excitatory connections that is effectively a homeostatic counterpart of LTP, is also blocked by isoflurane in vitro.²⁵⁰ The discrepancy between findings in vivo and in vitro remains unexplained.

Spontaneously Active Circuits

Spontaneous neuronal activity is decreased by volatile anesthetics both in vivo and in cortical brain slices. This effect is largely GABA_A receptor-dependent and marked even at low sedative concentrations.¹⁰⁷ Because the cortical brain slices lack subcortical input, these results suggest that volatile anesthetics can cause some effects (e.g., sedation)

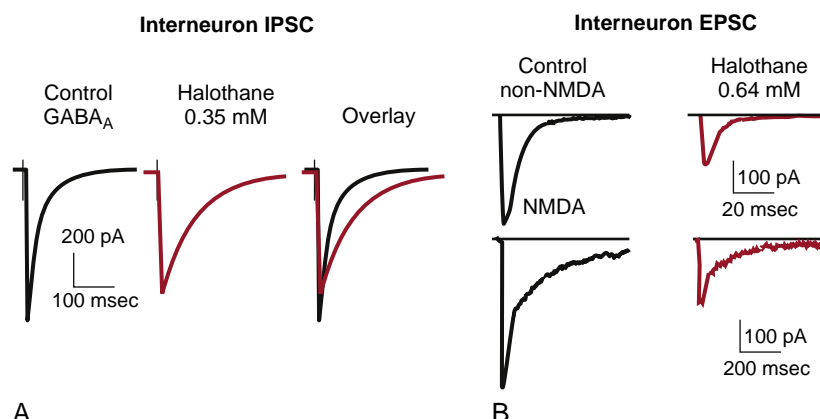


Fig. 19.10 Halogenated anesthetics enhance inhibitory and depress excitatory synaptic transmission. Halothane slows the decay of GABA_A receptor-mediated inhibitory postsynaptic currents (IPSCs) (A) and depresses the amplitude of glutamatergic excitatory postsynaptic currents (EPSCs) without affecting the decay (B) in hippocampal interneurons. (A) Redrawn with permission from Nishikawa K, MacLver MB. Membrane and synaptic actions of halothane on rat hippocampal pyramidal neurons and inhibitory interneurons. *J Neurosci*. 2000;20:5915–5923. (B) Redrawn with permission from Perouansky M, Baranov D, Salman M, Yaari Y. Effects of halothane on glutamate receptor-mediated excitatory postsynaptic currents. A patch-clamp study in adult mouse hippocampal slices. *Anesthesiology*. 1995;83:109–119.

via direct cortical action. However, changes in raw neuronal firing rates do not provide a precise quantitative measure of higher cognitive function, which is better reflected by the relationship of firing patterns to the strength and phase of ongoing cortical rhythms (see next section). Anesthetic effects have also been tested on the circuitry underlying locomotion, a well-studied central pattern generator. Effects of isoflurane on *in vitro* lamprey and rat spinal cord preparations support the spinal cord as the primary target for volatile anesthetic-induced immobility.^{251,252}

RHYTHMS AND SIMULATIONS

The brain perpetually generates complex electrical rhythms (oscillations in extracellular field potentials) that range in

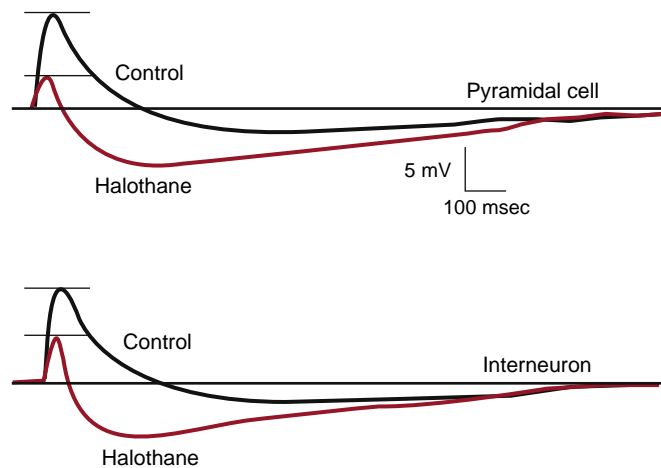


Fig. 19.11 Anesthetics affect excitation and inhibition simultaneously in opposite directions. Halothane depresses the excitatory depolarization and augments the inhibitory hyperpolarization in both hippocampal pyramidal cells and interneurons. The net result will depend on the underlying neuronal state as well as the neuronal network and its function. (Redrawn with permission from Nishikawa K, MacIver MB. Membrane and synaptic actions of halothane on rat hippocampal pyramidal neurons and inhibitory interneurons. *J Neurosci*. 2000;20:5915–5923.)

frequency from fractions to hundreds of Hertz (Hz; cycles per second), as recorded on the surface of the scalp as the electroencephalogram (EEG; the higher-frequency oscillations cannot be resolved in surface recordings). All oscillations are behavioral state-dependent and multiple oscillations coexist throughout the sleep-wake cycle. Lower-frequency rhythms allow for integration over longer time periods and typically engage larger areas of the brain. By contrast, higher-frequency rhythms allow for higher temporal resolution on local scales. Cross-frequency modulation allows for integration of both aspects of information processing. Although their physiologic roles are not clear, brain rhythms reflect, subserve, and/or constitute fundamental higher-order processing such that their modulation by anesthetics is of great interest. The current nomenclature of brain rhythms reflects historical conventions and is not based on underlying mechanisms.

δ-Rhythms and Other Slow Rhythms

Oscillations with EEG frequencies from 1.5 to 4 Hz are generally referred to as δ-rhythms, and these oscillations are characteristic of deep sleep and are commonly observed under general anesthesia. Even slower rhythms (below 1 Hz) occur during non-rapid eye movement (NREM) sleep and appear at loss of consciousness induced by propofol²⁵³ and sevoflurane.²⁵⁴ During natural NREM sleep, δ-rhythms and sleep spindles are phase related to a slower oscillation, suggesting functional interaction.²⁵⁵ Paroxysmal spindle-like waxing and waning oscillations overriding slower rhythms are also present in the cortical EEG under anesthesia. A change in δ-α phase relationships has been proposed as a “signature” of propofol-induced unconsciousness,²⁵⁶ but how this comes about, whether similar changes occur for a wider range of anesthetics, and the underlying physiology and functional significance are unknown.

θ-Rhythms

θ-Rhythms, present in various cortical structures but most prominent in the hippocampus, are thought to signal the “online state.” They are associated with sensorimotor and

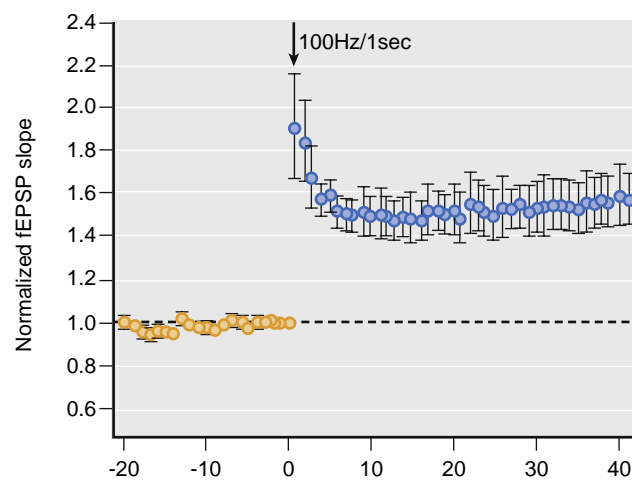
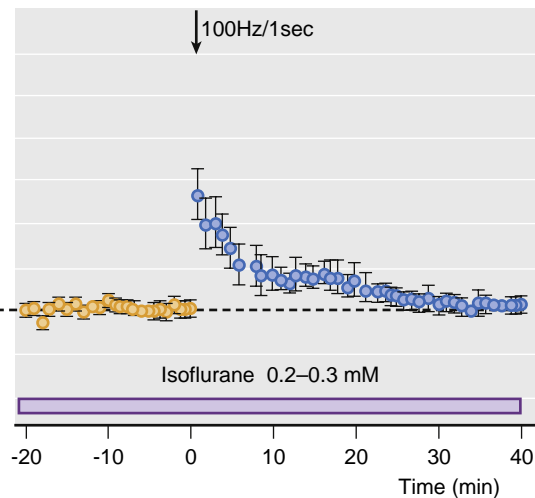


Fig. 19.12 Isoflurane blocks the induction of synaptic plasticity *in vitro* (a model of learning and memory). Long-term potentiation (an increase in normalized excitatory postsynaptic potential (EPSP) slope, in hippocampal slices evoked by tetanic stimulation of excitatory synapses is blocked by 0.2 to 0.3 mM isoflurane. (Redrawn with permission from Simon W, Hapfelmeier G, Kochs E, et al. Isoflurane blocks synaptic plasticity in the mouse hippocampus. *Anesthesiology*. 2001;94:1058–1065.)



mnemonic functions during waking behavior.²⁵⁷ One component of the θ -rhythm (type I or atropine-resistant) can be affected by amnestic concentrations of isoflurane as well as by the amnestic nonimmobilizer F6,⁹⁴ indicating a potential network-level signature effect for anesthetic-induced amnesia. Type II θ -rhythm (atropine-sensitive) can be evoked under anesthesia and is slowed and potentiated by halothane.²⁵⁸ Interestingly, this halothane-induced oscillation disappears in TASK-3 knockout mice.⁴⁶

γ -Rhythms

This designation includes an extremely broad and probably functionally and mechanistically heterogeneous spectrum of rhythms. It is frequently subdivided into slow γ (30-50 Hz; i.e., the spectrum above β -rhythms); γ (50-90 Hz), and fast-, ultra- γ , or ϵ -rhythms (>90 and up to hundreds of Hz). Fast GABA_A ergic synaptic inhibition and the intrinsic resonant properties of neurons play important roles in γ -physiology, making these obvious candidates for anesthetic modulation. Isoflurane slows the frequency of evoked γ -oscillations (30-90 Hz, also known as “40-Hz rhythms”) in humans.^{259,260} Studies of γ -oscillations in vitro suggest that their frequency depends on the time constant of decay of GABA_A receptor-mediated synaptic currents in inhibitory networks.²⁶¹ Isoflurane slows γ -rhythms in hippocampal²⁶² and neocortical slices²⁶³ to a comparable degree as it does in humans,²⁵⁹ providing a tentative link between receptor and circuit-level effects. However, the interaction between anesthetics and behaviorally relevant network effects is likely to be complex because flash-evoked γ -oscillations in the primary visual cortex are not affected by inhaled agents,⁶⁷ whereas feedback information transfer at γ -frequencies between the visual and frontal cortices is disrupted.^{59,67} Moreover, many brain rhythms are interlinked (e.g., θ -rhythm modulates γ -oscillations (θ - γ nesting)). The nature of their modulation by anesthetics as well as its relevance are far from clear.

Models and Simulations

On the macroscopic scale, computer simulations can provide an integrated picture of modulation of dynamic neuronal and network activity. “Bottom-up” neuron-by-neuron approaches are based on computational models of individual neurons, known *anesthetic effects* on intrinsic and synaptic membrane conductances, and simple network models. Computer simulations of anesthetic effects on integrated outputs can thereby be generated (e.g., the ring of pacemaker neurons).²⁶⁴ These models obviously rely on the accuracy of the derived characteristics of real neurons and networks as well as knowledge of the effects of anesthetics; the scale of simulations is limited by the complexity of its elements.²⁶⁵ An alternative is a “top-down” approach, such as mean-field modeling, in which molecular and cellular individual accuracy detail is sacrificed in favor of global dynamics. For example, global cortical phenomena, such as anesthetic-induced seizures, have been modeled as phase transitions based on mean interactions between populations of averaged neurons (analogous to the EEG signal that also averages the signals of neuronal populations).²⁶⁶ This approach can be extended to other global cortical phenomena such as consciousness.²⁶⁷ Neuronal modeling and

computer simulations may gain importance in the future as bridges between theoretical and experimental studies of anesthesia.

Research Strategies for the Future

The search for anesthetic mechanisms is driven by advances in the basic sciences. Some strategies that should facilitate understanding of anesthetic mechanisms include use of agonists or antagonists *in vivo*, nonanesthetics or nonimmobilizers, high-resolution imaging of the functioning brain, transgenic animals, and the application of the latest techniques of molecular genetics.

PHARMACOLOGIC APPROACHES

Agonists, Antagonists, and Experimental Anesthetics

Use of receptor-specific agonists and antagonists provides a pharmacologic method for bridging *in vitro* with *in vivo* studies. In this approach, a receptor may be tested for its contribution to a specific end point (e.g., immobility) according to the criteria presented earlier. This approach was used to exclude an important role for NMDA receptor block in the immobilizing action of volatile anesthetics but did not yield conclusive results for the roles of GABA_A and GlyR for immobilization,^{267,268} probably owing to the intricacies of drug-receptor interactions on different levels of integration in complex networks like the spinal cord. A complementary pharmacologic approach using experimental anesthetics that inhibit NMDA receptors *in vitro* with different potencies supports the conclusion that NMDA receptor blockade does not contribute significantly to immobility by conventional volatile anesthetics.²⁶⁹ Refinement of this strategy involves the anatomically discrete application of drugs to nuclei with known function. For example, the tuberomamillary nucleus (part of the endogenous sleep pathway) mediates the sedative component of anesthesia for some intravenous anesthetics (e.g., propofol).³⁵ A discrete site of general anesthetic action for GABAergic drugs in the mesopontine tegmentum has also been proposed based on this strategy.^{33,34} However, these approaches suffer from the fact that, invariably, high concentrations of drugs have to be injected locally to observe pharmacologic effects (because of rapid redistribution), so that such observations need to be substantiated using more sophisticated approaches, such as genetic manipulations (see later).

Nonimmobilizers

Nonimmobilizers are compounds with physicochemical characteristics similar to those of conventional inhaled anesthetics, but their predicted anesthetizing concentrations (based on their lipid solubility and the Meyer-Overton correlation [MAC_{pred}]) do not induce immobility.¹⁷ Initially termed *nonanesthetics*, the terminology was revised when it was discovered that at least some of them cause amnesia at similar MAC_{pred} fractions to classic volatile anesthetics.⁹⁸ If a molecular or cellular process is affected in similar ways by an anesthetic and a nonimmobilizer, that process is not relevant for the anesthetic state, with the notable exception of amnesia. Despite this elegant rationale, only

a limited number of receptors have been excluded because, compared with volatile anesthetics, nonimmobilizers are relatively target selective. These compounds have the potential to provide insights beyond the initially envisaged receptor-level studies by allowing the separation of sedation from amnesia for the study of underlying network activity *in vivo*.⁹⁵

Photoreactive Anesthetics

An approach that has proven to be very successful with intravenous drugs²⁷⁰ is one in which an analog of an anesthetic is synthesized that bears a photoreactive group (often a tri-fluoro-diazirine) which, when irradiated at a wavelength of around 300 nm, reacts irreversibly with some amino acids in the anesthetic binding site. This approach, of course, requires that the pharmacologic profile of the analog is very similar to that of the parent compound, so that the relevant binding site is identified. Photoreactive analogs of inhaled anesthetics have been synthesized and four putative sites on GABA_A receptors have been identified.²⁷¹ One advantage of this approach over x-ray crystallography is that anesthetic binding to different conformational states of the receptor are, at least in principle, more accessible to analysis.

GENETIC APPROACHES

Whole-Organism Genetics

Genetic strategies on whole organisms take two forms: forward and reverse.²⁷² The reverse genetic approach focuses on a particular gene chosen because there are reasons to hypothesize that its product may be important to anesthesia. Examples of this strategy are targeted mutations that alter the sensitivity of specific neurotransmitter receptors to anesthetics.¹²¹ Initially, these mutations were used to identify anesthetic binding sites. Subsequently, transgenic animals rendered resistant to anesthetics, either by deletion of a putative target protein from the genome or by expressing a target receptor engineered to be insensitive to an anesthetic, were used to test behavioral relevance of the altered gene product for the production of anesthesia. Forward genetics, by contrast, is a discovery process that involves the study of randomly generated mutations (either experimentally induced or naturally occurring polymorphisms) that affect the phenotype of interest (i.e., anesthetic end points) in a population. This approach, however, has not been widely used.

Molecular Genetics

A third genetic approach that is playing an increasing role in neuroscience is the selective modification of neuronal function using molecular genetics. Many different approaches are used, ranging from the selective knock-down of specific receptor populations using microRNA (a small noncoding piece of RNA that can selectively reduce protein expression), the block of neurotransmitter release from a population of neurons using tetanus toxin light chain, and the selective activation or inhibition of neuronal networks using optogenetics²⁷³ or pharmacogenetics.²⁷⁴ A powerful complement to these techniques is the ability to deliver artificial transgenes to defined neuronal populations using adeno-associated virus (AAV), and mouse lines

that express Cre recombinase in particular cell types, which allow the selective expression of those genes in those specific cells. These approaches are only just beginning to be used to identify neuronal pathways that are involved in anesthetic action. For example, it has recently been shown that the sedative effects of propofol require the activation of the lateral habenula, an excitatory nucleus that lies close to the thalamus.²⁷⁵ These approaches are likely to have an increasing impact on our understanding of the mechanisms of inhaled general anesthetics.

Knockout and Knockin Animals

In the knockout approach, expression of the gene encoding a protein of interest is disrupted by a specific deletion or insertion. Nearly all such studies have been carried out in mice. A well-recognized problem with the global knockout approach is that extensive compensatory changes can be induced, from anomalies that are lethal *in utero* to insidious (but experimentally confounding) influences that might be expressed only at maturity. A complementary strategy is the conditional knockout, in which the genetic deletion is restricted either anatomically (limited to certain brain regions) or temporally (at a known point in time). These strategies can minimize developmental anomalies and reduce the likelihood of compensatory changes. In the knockin approach, a mutation, usually of a single amino acid residue, is targeted to produce a protein with altered sensitivity to a drug of interest. Ideally, this mutation remains completely silent in the absence of the drug; that is, it does not perturb the normal expression and function of the protein of interest or alter the expression of other genes.

GABA_A receptors. Results from transgenic animals illustrate both the utility and the difficulties of the genetic approach with respect to inhaled agents. The conditional forebrain-restricted GABA_A receptor α_1 -subunit knockout mouse was found to be less sensitive to isoflurane-induced amnesia than wild-type mice, which led to the conclusion that action at these receptors contributes to isoflurane's amnesic effects.²⁷⁶ By contrast, a mouse harboring a mutation of the GABA_A receptor α_1 subunit that renders the receptor insensitive to isoflurane *in vitro* did not show reduced sensitivity to either the amnesic or the immobilizing effects of isoflurane, leading to the conclusion that this subunit does not mediate the impairment of learning and memory by isoflurane.⁴⁰ Similar experiments indicate that action at the GABA_A receptor β_3 subunit does not mediate immobility or amnesia by isoflurane.³⁹ This bottom-up genetic approach is a work-intensive but powerful tool that has yielded clear results with the receptor-specific intravenous anesthetics,²⁷ but it has proved challenging to apply it to the more promiscuous inhaled agents.

Glycine $\alpha 1$ -containing receptors. Pharmacologic studies supported the notion that glycinergic neurotransmission might be the effector for the immobilizing action of inhaled anesthetics in the spinal cord, where glycine replaces GABA as the principal inhibitory transmitter. However, mice harboring mutations that render α_1 subunit-containing glycine receptors largely insensitive to alcohol and inhaled ether anesthetics did not demonstrate a concordant change

in MAC values. Because α_1 is the most widely expressed subunit in adult animals, it is unlikely that action at glycine receptors plays an important part in the immobilizing action of inhaled anesthetics.²⁷⁶

Two-pore domain K⁺ channels. Use of mice harboring knockout mutations of several two-pore domain K⁺ channel (K_{2P}) family members (TASK-1, TASK-3, TREK-1) has demonstrated a role for these channels in volatile anesthesia.^{44,45,47} For example, TREK-1 knockout mice are partially resistant to all volatile anesthetics tested with respect to both loss of righting reflex (a surrogate measure of consciousness) and immobility, but anesthesia can still be induced, albeit at higher anesthetic concentrations. Interestingly, responses to pentobarbital are unaffected, indicating that the mutation does not cause a generalized resistance to anesthesia.

FORWARD AND POPULATION GENETICS

The nematode *C. elegans* and the fruit fly *Drosophila melanogaster*, with 302 and 100,000 neurons, respectively, have also been used as model organisms in anesthesia research.²⁷⁷ Mutations in a number of *C. elegans* genes affect sensitivity to volatile anesthetics,²⁷⁸ most notably *unc-1*,²⁷⁹ a close homologue of the mammalian protein stomatin.²⁸⁰ Yeasts have also been used as model organisms, with even more obvious limitations with respect to identification of appropriate anesthetic end points.

Sensitivity to anesthetics is a quantitative trait (varying continuously in a population). Quantitative genetics is the study of the heritability of continuous traits. These traits are controlled by genes represented in quantitative trait loci (QTLs). A top-down population-based approach has been used to localize QTLs that govern susceptibility of individuals to anesthetics, in higher and lower organisms. Starting from the observation that inbred mouse strains vary in their sensitivity to isoflurane, microsatellite-based linkage analysis and, alternatively, single-nucleotide polymorphism-based analysis of genetic variation localized a QTL for isoflurane immobilization to the proximal part of mouse chromosome 7.²⁸¹ Genetic variability in the sensitivity of *D. melanogaster* to inhaled anesthetics has also been demonstrated.²⁸² This type of analysis promises to assist in defining the genetic basis for variability in the susceptibility to both primary anesthetic end points and side effects.

FUNCTIONAL IMAGING AND HIGH-DENSITY ELECTROENCEPHALOGRAPHY

Identification of the anatomic and functional substrates for anesthetic effects on consciousness, memory, and immobility is now approachable with improved imaging techniques. Imaging is based on mapping of either metabolic or hemodynamic changes as surrogate measures of neuronal activity, as in positron emission tomography (PET) and functional magnetic resonance imaging, or on mapping electrical activity with high-density EEG, magnetoencephalography, and low-resolution brain electromagnetic tomography. Properties of receptors can also be probed with radioactive ligands by PET. These techniques have the capacity to identify neuroanatomic substrates of drug

action with method-specific limitations. Results from functional PET imaging suggest that propofol suppresses episodic memory by targeting the prefrontal and posterior parietal cortex as opposed to the medial temporal lobe²⁸³ and that suppression of consciousness is caused by anesthetic action in the thalamus, parts of the medial and posterior parietal cortex, and/or the posterior cingulate and medial parietal cortex.²⁸⁴ Although observations of regionally specific and global suppressive effects of anesthetics on metabolic activity are unlikely to provide a definitive mechanistic understanding, such information can facilitate hypotheses and experimentally testable predictions.

Advanced analytical approaches based on theories from mathematical and statistical sciences are being increasingly applied to enhance the power of existing technologies. Magnetic resonance images and high-density EEG recordings of the brain reveal strong interregional connections, but the considerable potential of this connectivity information to better understand the brain's response to anesthesia has only recently begun to be tapped. The growing use of invasive recording techniques (e.g., brain surface electrode grids and microelectrodes implanted deep into the brain for functional neurosurgical therapies) is also advancing the frontiers of neuroscience in general and the understanding of anesthetic mechanisms in particular.

Summary

The mechanisms of inhaled anesthetics have proved more difficult to explain than was envisaged a generation ago, when the paradigm shifted from lipids to amphiphilic cavities in proteins as targets for anesthetics. Despite a remarkable accumulation of information, a comprehensive theory of general anesthetic action has yet to be formulated. Progress toward this goal has been difficult for several reasons. Important pharmacologic characteristics of inhaled anesthetics that have impeded identification of their relevant molecular targets are their low potency (micromolar range), activity at multiple targets, lack of specific antagonists, and limitations in the neuroscience of memory and consciousness. This contrasts with the situation for intravenous anesthetics, which exhibit more conventional receptor pharmacology. Moreover, accumulating evidence indicates that no universal target exists to explain the actions of every general anesthetic or even of a single anesthetic agent. It is now clear that the composite state of anesthesia and its core components (amnesia, sedation/unconsciousness, immobility) are separable behavioral states *in vivo*. Resolution of these phenomena at the molecular and cellular levels represents the cutting edge of contemporary neuroscience. Of the multiple molecular and cellular anesthetic effects identified, it is unclear which are critical for the desired behavioral end points, which are harmless or beneficial side effects (e.g., preconditioning), and which, if any, could have long-lasting or delayed undesirable consequences (e.g., cell death, cognitive dysfunction). Progress in identifying the molecular targets of general anesthetics provides a foundation for identification of the network- and systems-level effects relevant to their behavioral and peripheral end points. As the biologic foundations of behaviors once thought to be exclusively the

realm of psychology are unraveled, for which anesthetics provide a valuable investigative tool, a comprehensive theory of anesthesia will also develop.

Complete references available online at expertconsult.com.

References

- Perouansky M. *Anesthesiology*. 2012;117:465.
- Winterstein H. *Die Narkose in ihrer Bedeutung für die Allgemeine Physiologie*. Springer; 1919.
- Eger EI, et al. *Anesthesiology*. 2002;96:238–239.
- Eger EI, et al. *Anesthesiology*. 1965;26:756–763.
- Franks NP, Lieb WR. *Anesthesiology*. 1996;84:716–720.
- Boggs JM, et al. *Mol Pharmacol*. 1976;12:127–135.
- Franks NP, Lieb WR. *Nature*. 1978;274:339–342.
- Franks NP, Lieb WR. *J Mol Biol*. 1979;133:469–500.
- Featherstone RM, et al. *Anesthesiology*. 1961;22:977–981.
- Ueda I, Kamaya H. *Anesthesiology*. 1973;38:425–436.
- Franks NP, Lieb WR. *Nature*. 1982;300:487–493.
- Franks NP, Lieb WR. *Nature*. 1984;310:599–601.
- Franks NP, Lieb WR. *Anesthesiology*. 2004;101:235–237.
- Franks NP, Lieb WR. *Nature*. 1981;292:248–251.
- Franks NP, Lieb WR. *Nature*. 1985;316:349–351.
- Franks NP, Lieb WR. *Proc Natl Acad Sci U S A*. 1986;83:5116–5120.
- Koblin DD, et al. *Anesth Analg*. 1994;79:1043–1048.
- Hall AC, et al. *Br J Pharmacol*. 1994;112:906–910.
- Dickinson R, et al. *Biophys J*. 1994;66:2019–2023.
- Franks NP, Lieb WR. *Science*. 1991;254:427–430.
- Herold KF, et al. *Proc Natl Acad Sci U S A*. 2017;114:3109–3114.
- Franks NP. *Nat Rev Neurosci*. 2008;9:370–386.
- Eckenhoff RG. *Mol Interv*. 2001;1:258–268.
- Eckenhoff RG, Johansson JS. *Anesthesiology*. 2001;95:1537–1539.
- Eger 2nd EI, et al. *Anesthesiology*. 2001;94:915–921.
- Dickinson R, et al. *Anesthesiology*. 2000;93:837–843.
- Rudolph U, Antkowiak B. *Nat Rev Neurosci*. 2004;5:709–720.
- Antognini JF, Schwartz K. *Anesthesiology*. 1993;79:1244–1249.
- Rampil IJ, et al. *Anesthesiology*. 1993;78:707–712.
- Stabernack C, et al. *Anesth Analg*. 2005;100:128–136.
- Veselis RA, et al. *Anesthesiology*. 2001;95:896–907.
- Sanders RD, et al. *Anesthesiology*. 2012;116:946–959.
- Devor M, Zalkind V. *Pain*. 2001;94:101–112.
- Minert A, et al. *J Neurosci*. 2017;37:9320–9331.
- Nelson LE, et al. *Nat Neurosci*. 2002;5:979–984.
- Rampil IJ, Lester MJ. *Anesthesiology*. 1992;77:920–925.
- Antognini JF, et al. *Anesthesiology*. 2002;96:980–986.
- Zhang Y, et al. *Anesth Analg*. 2004;99:85–90.
- Liao M, et al. *Anesth Analg*. 2005;101:412–418.
- Sonner JM, et al. *Anesthesiology*. 2007;106:107–113.
- Raines DE, et al. *Anesth Analg*. 2002;95:573–577.
- Zhang Y, et al. *Br J Pharmacol*. 2010;159:872–878.
- Heurteaux C, et al. *EMBO J*. 2004;23:2684–2695.
- Linden AM, et al. *J Pharmacol Exp Ther*. 2006;317:615–626.
- Linden AM, et al. *J Pharmacol Exp Ther*. 2007;323:924–934.
- Pang DS, et al. *Proc Natl Acad Sci U S A*. 2009;106:17546–17551.
- Westphalen RI, et al. *Br J Pharmacol*. 2007;152:939–945.
- Jinks SL, et al. *Anesthesiology*. 2008;108:1016–1024.
- Koch C, et al. *Nat Rev Neurosci*. 2016;17:307–321.
- Mashour GA, Hudetz AG. *Trends Neurosci*. 2018;41:150–160.
- Sanders RD, et al. *Anesthesiology*. 2017;126:214–222.
- Leung LS, et al. *Prog Neurobiol*. 2014;122:24–44.
- Brown EN, et al. *Annu Rev Neurosci*. 2011;34:601–628.
- Mashour GA. *Front Syst Neurosci*. 2014;8:115.
- Mashour GA, Hudetz AG. *Front Neural Circuits*. 2017;11:44.
- Tononi G. *Biol Bull*. 2008;215:216–242.
- Tononi G, et al. *Nat Rev Neurosci*. 2016;17:450–461.
- Lee U, et al. *Philos Trans A Math Phys Eng Sci*. 2015;373.
- Imas OA, et al. *Neurosci Lett*. 2005;387:145–150.
- MacIver MB, Bland BH. *Front Syst Neurosci*. 2014;8:203.
- Bullmore E, Sporns O. *Nat Rev Neurosci*. 2012;13:336–349.
- van den Heuvel MP, Sporns O. *J Neurosci*. 2011;31:15775–15786.
- Massimini M, et al. *Science*. 2005;309:2228–2232.
- Ferrarelli F, et al. *Proc Natl Acad Sci U S A*. 2010;107:2681–2686.
- Alkire MT, et al. *Science*. 2008;322:876–880.
- Imas OA, et al. *Anesthesiology*. 2005;102:937–947.
- Imas OA, et al. *Neurosci Lett*. 2006;402:216–221.
- John ER, et al. *Conscious Cogn*. 2001;10:165–183.
- Burlingame RH, et al. *Anesthesiology*. 2007;106:754–762.
- Ter-Mikaelian M, et al. *J Neurosci*. 2007;27:6091–6102.
- Lee U, et al. *Anesthesiology*. 2013;118:1264–1275.
- Wacongne C, et al. *Proc Natl Acad Sci U S A*. 2011;108:20754–20759.
- Raz A, et al. *Front Syst Neurosci*. 2014;8:191.
- Hentschke H, et al. *Br J Anaesth*. 2017;119:685–696.
- Kelz MB, et al. *Proc Natl Acad Sci U S A*. 2008;105:1309–1314.
- Moore JT, et al. *Curr Biol*. 2012;22:2008–2016.
- McCarren HS, et al. *J Neurosci*. 2014;34:16385–16396.
- Solt K. *Curr Biol*. 2012;22:R918–R919.
- Scharf MT, Kelz MB. *Curr Anesthesiol Rep*. 2013;3:1–9.
- Taylor NE, et al. *Proc Natl Acad Sci U S A*. 2016.
- Alkire MT, et al. *Conscious Cogn*. 2000;9:370–386.
- Baker R, et al. *J Neurosci*. 2014;34:13326–13335.
- Saalmann YB. *Front Syst Neurosci*. 2014;8:83.
- Dutton RC, et al. *Anesthesiology*. 2001;94:514–519.
- Brown EN, et al. *N Engl J Med*. 2010;363:2638–2650.
- Alkire MT, Nathan SV. *Anesthesiology*. 2005;102:754–760.
- Dai S, et al. *Anesthesiology*. 2012;116:816–823.
- Piao MH, et al. *Ann Fr Anesth Reanim*. 2013;32:e135–e141.
- Zhou C, et al. *Anesth Analg*. 2015;121:661–666.
- Kuo MC, Leung LS. *Anesthesiology*. 2017;127:838–851.
- Vertes RP. *Hippocampus*. 2005;15:923–935.
- Pan WX, McNaughton N. *Brain Res*. 1997;764:101–108.
- Robbe D, et al. *Nat Neurosci*. 2006;9:1526–1533.
- Perouansky M, et al. *Anesthesiology*. 2007;106:1168–1176.
- Seidenbecher T, et al. *Science*. 2003;301:846–850.
- Rudolph U, et al. *Nature*. 1999;401:796–800.
- Kandel L, et al. *Anesth Analg*. 1996;82:321–326.
- Mihic SJ, et al. *Mol Pharmacol*. 1994;46:851–857.
- Zarnowska ED, et al. *Anesth Analg*. 2005;101:401–406.
- Jevtic-Todorovic V, et al. *Nat Med*. 1998;4:460–463.
- Gruss M, et al. *Mol Pharmacol*. 2004;65:443–452.
- Gries DA, et al. *Life Sci*. 2005;76:1667–1674.
- Zhang Z, et al. *Nat Neurosci*. 2015;18:553–561.
- Murphy M, et al. *Sleep*. 2011;34:283–291A.
- Tung A, et al. *Anesthesiology*. 2004;100:1419–1426.
- Nelson AB, et al. *Sleep*. 2010;33:1659–1667.
- Hentschke H, et al. *Eur J Neurosci*. 2005;21:93–102.
- Franks NP, Lieb WR. *Nature*. 1994;367:607–614.
- Zeller A, et al. *Handb Exp Pharmacol*. 2008;31–51.
- Franks NP, et al. *Biophys J*. 1998;75:2205–2211.
- Bhattacharya AA, et al. *J Biol Chem*. 2000;275:38731–38738.
- Bertaccini EJ, et al. *Anesth Analg*. 2007;104:318–324.
- Howard RJ, et al. *Pharmacol Rev*. 2014;66:396–412.
- Nury H, et al. *Nature*. 2011;469:428–431.
- Dickinson R, et al. *Anesthesiology*. 2007;107:756–767.
- Hemmings HC, et al. *Trends Pharmacol Sci*. 2005;26:503–510.
- Patel AJ, et al. *Nat Neurosci*. 1999;2:422–426.
- Franks NP, Honore E. *Trends Pharmacol Sci*. 2004;25:601–608.
- Sieghart W. *Adv Pharmacol*. 2015;72:53–96.
- Lynch JW. *Physiol Rev*. 2004;84:1051–1095.
- Mihic SJ, et al. *Nature*. 1997;389:385–389.
- Solt K, et al. *J Pharmacol Exp Ther*. 2005;315:771–776.
- Jenkins A, et al. *Br J Pharmacol*. 1996;117:1507–1515.
- Role LW, Berg DK. *Neuron*. 1996;16:1077–1085.
- Flood P, et al. *Anesthesiology*. 1997;86:859–865.
- Violet JM, et al. *Anesthesiology*. 1997;86:866–874.
- Dingledine R, et al. *Pharmacol Rev*. 1999;51:7–61.
- Franks NP, et al. *Nature*. 1998;396:324.
- de Sousa SL, et al. *Anesthesiology*. 2000;92:1055–1066.
- Solt K, et al. *Anesth Analg*. 2006;102:1407–1411.
- Harris RA, et al. *FASEB J*. 1995;9:1454–1462.
- Sonner JM, et al. *Anesth Analg*. 2005;101:143–148.
- MacIver MB, et al. *Anesthesiology*. 1996;85:823–834.
- Perouansky M, et al. *Anesthesiology*. 2004;100:470–472.
- Winegar BD, MacIver MB. *BMC Neurosci*. 2006;7:5.
- Haydon DA, Urban BW. *J Physiol*. 1983;341:429–439.
- Berg-Johnsen J, Langmoen IA. *Acta Physiol Scand*. 1986;127:87–93.
- Mikulec AA, et al. *Brain Res*. 1998;796:231–238.
- Wu XS, et al. *Anesthesiology*. 2004;100:663–670.
- Yu FH, Catterall WA. *Sci STKE*. 2004;2004:re15.
- Catterall WA. *Annu Rev Cell Dev Biol*. 2000;16:521–555.

142. Herold KF, et al. *Anesthesiology*. 2009;111:591–599.
143. Ouyang W, Hemmings HC. *J Pharmacol Exp Ther*. 2005;312:801–808.
144. OuYang W, Hemmings HC. *Anesthesiology*. 2007;107:91–98.
145. Ouyang W, et al. *J Pharmacol Exp Ther*. 2007;322:1076–1083.
146. Ratnakumari L, et al. *Anesthesiology*. 2000;92:529–541.
147. Herold KF, Hemmings HC. *Front Pharmacol*. 2012;3:50.
148. Tang JX, et al. *Alzheimers Dement*. 2011;7:521–531.e521.
149. Barber AF, et al. *Proc Natl Acad Sci U S A*. 2014;111:6726–6731.
150. Kinde MN, et al. *Proc Natl Acad Sci U S A*. 2016;113:13762–13767.
151. Sand RM, et al. *J Gen Physiol*. 2017;149:623–638.
152. Miao N, et al. *Anesthesiology*. 1995;83:593–603.
153. Pocock G, Richards CD. *Br J Anaesth*. 1993;71:134–147.
154. Kameyama K, et al. *Br J Anaesth*. 1999;82:402–411.
155. Study RE. *Anesthesiology*. 1994;81:104–116.
156. Hall AC, et al. *Anesthesiology*. 1994;81:117–123.
157. Takei T, et al. *Neurosci Lett*. 2003;350:41–45.
158. Joksovic PM, et al. *Br J Pharmacol*. 2005;144:59–70.
159. Todorovic SM, et al. *Mol Pharmacol*. 2001;60:603–610.
160. Petrenko AB, et al. *Anesthesiology*. 2007;106:1177–1185.
161. Hanley PJ, et al. *Anesthesiology*. 2004;101:999–1014.
162. Huncke R, et al. *Acta Anaesthesiol Scand*. 2004;48:547–561.
163. Rithalia A, et al. *Anesth Analg*. 2004;99:1615–1622.
164. Huncke R, et al. *Anesthesiology*. 2001;95:999–1006.
165. Stowe DF, et al. *Anesthesiology*. 2000;92:516–522.
166. Davies LA, et al. *Anesthesiology*. 2000;93:1034–1044.
167. Joseph JD, et al. *Anesthesiology*. 2014;121:528–537.
168. Pabelick CM, et al. *Anesthesiology*. 2001;95:207–215.
169. Roberts MC, et al. *Anesthesiology*. 2001;95:716–725.
170. Mickelson JR, Louis CF. *Physiol Rev*. 1996;76:537–592.
171. Yost CS. *Anesthesiology*. 1999;90:1186–1203.
172. Friederich P, et al. *Anesthesiology*. 2001;95:954–958.
173. Franks NP, Lieb WR. *Nature*. 1988;333:662–664.
174. Dickinson R, Franks NP. *Critical care*. 2010;14:229.
175. Tong L, et al. *Br J Anaesth*. 2014;113:157–167.
176. Woll KA, et al. *ACS Chem Biol*. 2017;12:1353–1362.
177. Bertaccini EJ, et al. *ACS Chem Neurosci*. 2014;5:1246–1252.
178. Farwell D, Gollob MH. *Can J Cardiol*. 2007;23(suppl A):16A–22A.
179. Antzelevitch C. *J Electrocardiol*. 2001;34(suppl):177–181.
180. Li J, Correa AM. *Anesthesiology*. 2002;97:921–930.
181. Davies LA, et al. *Br J Pharmacol*. 2000;131:223–230.
182. Stadnicka A, et al. *J Anesth*. 2007;21:212–219.
183. Wojtowich AP, et al. *Anesthesiology*. 2016;124:1065–1076.
184. Sirois JE, et al. *J Physiol*. 2002;541:717–729.
185. Chen X, et al. *J Neurosci*. 2005;25:5803–5814.
186. Robinson RB, Siegelbaum SA. *Annu Rev Physiol*. 2003;65:453–480.
187. Girault JA, et al. In: Hemmings HC, et al, eds. *Foundations of Anesthesia*. Mosby; 2005:31.
188. Rebecchi MJ, Pentyala SN. *Br J Anaesth*. 2002;89:62–78.
189. Peterlin Z, et al. *Mol Cell Neurosci*. 2005;30:506–512.
190. Minami K, et al. *Mol Pharmacol*. 1998;53:148–156.
191. Minami K, et al. *J Pharmacol Exp Ther*. 1997;281:1136–1143.
192. Minami K, et al. *Eur J Pharmacol*. 1997;339:237–244.
193. Hemmings HC. *Toxicol Lett*. 1998;100–101:89–95.
194. Hasegawa J, et al. *Acta Histochem Cytochem*. 2006;39:163–172.
195. Das J, et al. *J Biol Chem*. 2004;279:37964–37972.
196. Shumilla JA, et al. *Anesth Analg*. 2004;99:82–84.
197. Sonner JM, et al. *Anesth Analg*. 1999;89:1030–1034.
198. Inoue S, et al. *Anesthesiology*. 2004;101:75–81.
199. Rasmussen LS, et al. *Acta Anaesthesiol Scand*. 2004;48:1137–1143.
200. Fukuda S, Warner DS. *Br J Anaesth*. 2007;99:10–17.
201. Turner CP, et al. *Neuroscience*. 2012;210:384–392.
202. Pratt PF, et al. *Curr Opin Anaesthesiol*. 2006;19:397–403.
203. Zaugg M, et al. *Br J Anaesth*. 2003;91:551–565.
204. Ludwig LM, et al. *Anesthesiology*. 2004;100:532–539.
205. Song IA, et al. *BMC Anesthesiol*. 2016;16:13.
206. Snyder GL, et al. *Neuropharmacology*. 2007;53:619–630.
207. Hemmings HC, Adamo AI. *Anesthesiology*. 1994;81:147–155.
208. Marota JJ, et al. *Anesthesiology*. 1992;77:365–371.
209. Hamaya Y, et al. *Anesth Analg*. 2000;90:1177–1183.
210. Culley DJ, et al. *Eur J Pharmacol*. 2006;549:71–78.
211. Futterer CD, et al. *Anesthesiology*. 2004;100:302–308.
212. Durieux M, Davis PJ. *Anesth Analg*. 2010;110:1265–1267.
213. Dalla Massara L, et al. *Anesthesiology*. 2016;124:1311–1327.
214. Kullmann DM, et al. *J Physiol*. 1989;412:277–296.
215. Fujiwara N, et al. *J Physiol*. 1988;402:155–175.
216. MacIver MB, Roth SH. *Br J Anaesth*. 1988;60:680–691.
217. Ries CR, Puil E. *J Neurophysiol*. 1999;81:1802–1809.
218. Sirois JE, et al. *J Neurosci*. 2000;20:6347–6354.
219. Semyanov A, et al. *Trends Neurosci*. 2004;27:262–269.
220. Houston CM, et al. *J Neurosci*. 2012;32:3887–3897.
221. Bai D, et al. *Mol Pharmacol*. 2001;59:814–824.
222. Bieda MC, MacIver MB. *J Neurophysiol*. 2004;92:1658–1667.
223. Caraiscos VB, et al. *Proc Natl Acad Sci U S A*. 2004;101:3662–3667.
224. Caraiscos VB, et al. *J Neurosci*. 2004;24:8454–8458.
225. Capogna M, Pearce RA. *Trends Neurosci*. 2011;34:101–112.
226. Rodgers FC, et al. *J Neurosci*. 2015;35:9707–9716.
227. Berg-Johnsen J, Langmoen IA. *Acta Anaesthesiol Scand*. 1992;36:350–355.
228. Kirson ED, et al. *Br J Pharmacol*. 1998;124:1607–1614.
229. Richards CD, Smaje JC. *Br J Pharmacol*. 1976;58:347–357.
230. Wakamori M, et al. *J Neurophysiol*. 1991;66:2014–2021.
231. Yang J, Zorumski CF. *Ann NY Acad Sci*. 1991;625:287–289.
232. Dildy-Mayfield JE, et al. *J Pharmacol Exp Ther*. 1996;276:1058–1065.
233. Minami K, et al. *J Biol Chem*. 1998;273:8248–8255.
234. Morgan PG, et al. *Anesthesiology*. 2002;96:1268–1270.
235. Quintana A, et al. *PLoS One*. 2012;7:e42904.
236. Zimin PI, et al. *Curr Biol*. 2016;26:2194–2201.
237. Ramadasan-Nair R, et al. *PLoS One*. 2017;12:e0188087.
238. Banks MI, Pearce RA. *Anesthesiology*. 1999;90:120–134.
239. Murugaiah KD, Hemmings HC. *Anesthesiology*. 1998;89:919–928.
240. Nishikawa K, MacIver MB. *Anesthesiology*. 2001;94:340–347.
241. Westphalen RI, Hemmings HC. *J Pharmacol Exp Ther*. 2003;304:1188–1196.
242. Westphalen RI, Hemmings HC. *J Pharmacol Exp Ther*. 2006;316:216–223.
243. Baumgart JP, et al. *Proc Natl Acad Sci U S A*. 2015;112:11959–11964.
244. Nagele P, et al. *Anesthesiology*. 2005;103:768–778.
245. van Swinderen B, et al. *Proc Natl Acad Sci U S A*. 1999;96:2479–2484.
246. Hemmings HC, et al. *Mol Pharmacol*. 2005;67:1591–1599.
247. Pearce RA, et al. *Anesthesiology*. 1989;71:591–598.
248. Pearce RA. *J Physiol*. 1996;492(Pt 3):823–840.
249. Ballesteros KA, et al. *Int J Gen Med*. 2012;5:935–942.
250. Simon W, et al. *Anesthesiology*. 2001;94:1058–1065.
251. Jinks SL, et al. *Neuroreport*. 2011;22:655–659.
252. Jinks SL, et al. *Anesthesiology*. 2005;103:567–575.
253. Lewis LD, et al. *Proc Natl Acad Sci U S A*. 2012;109:E3377–E3386.
254. Guidera JA, et al. *Front Neural Circuits*. 2017;11:36.
255. Steriade M, et al. *J Neurosci*. 1993;13:3266–3283.
256. Purdon PL, et al. *Proc Natl Acad Sci U S A*. 2013;110:E1142–E1151.
257. Buzsaki G. *Neuron*. 2002;33:325–340.
258. Bland BH, et al. *Hippocampus*. 2003;13:38–47.
259. Munglani R, et al. *Br J Anaesth*. 1993;71:633–641.
260. Madler C, et al. *Br J Anaesth*. 1991;66:81–87.
261. Buzsaki G, Wang XJ. *Annu Rev Neurosci*. 2012;35:203–225.
262. Dickinson R, et al. *Neuropharmacology*. 2003;44:864–872.
263. Antkowiak B, Hentschke H. *Neurosci Lett*. 1997;231:87–90.
264. Gottschalk A, Haney P. *Anesthesiology*. 2003;98:548–564.
265. Storer KP, Reeke GN. *Anesthesiology*. 2012;117:780–790.
266. Wilson MT, et al. *Anesthesiology*. 2006;104:588–593.
267. Steyn-Ross ML, et al. *Prog Biophys Mol Biol*. 2004;85:369–385.
268. Zhang Y, et al. *Anesth Analg*. 2001;92:1585–1589.
269. Zhang Y, et al. *Anesth Analg*. 2001;92:123–127.
270. Forman SA, Miller KW. *Anesth Analg*. 2016;123:1263–1273.
271. Woll KA, et al. *FASEB J*. 2018;fj201701347R.
272. Nash HA. *Br J Anaesth*. 2002;89:143–155.
273. Kim CK, et al. *Nat Rev Neurosci*. 2017;18:222–235.
274. Roth BL. *Neuron*. 2016;89:683–694.
275. Gelegen C, et al. *Curr Biol*. 2018;28:580–587.e585.
276. Sonner JM, et al. *Mol Pharmacol*. 2005;68:61–68.
277. van Swinderen B, Kottler B. *Bioessays*. 2014;36:372–381.
278. Morgan PG, Sedensky MM. *Anesthesiology*. 1994;81:888–898.
279. Rajaram S, et al. *Proc Natl Acad Sci U S A*. 1998;95:8761–8766.
280. Sedensky MM, et al. *Am J Physiol Cell Physiol*. 2001;280:C1340–C1348.
281. Cascio M, et al. *Anesth Analg*. 2007;105:381–385.
282. Olufs ZPG, et al. *Sci Rep*. 2018;8:2348.
283. Veselis RA, et al. *Anesthesiology*. 2002;97:329–337.
284. Alkire MT, Miller J. *Prog Brain Res*. 2005;150:229–244.

References

1. Perouansky M. The quest for a unified model of anesthetic action. A century in Claude Bernard's shadow. *Anesthesiology*. 2012;117:465–474.
2. Winterstein H. *Die Narkose in ihrer Bedeutung für die allgemeine Physiologie*. Springer; 1919.
3. Eger EI. A brief history of the origin of minimum alveolar concentration (MAC). *Anesthesiology*. 2002;96:238–239.
4. Eger EI, et al. Minimum alveolar anesthetic concentration. A standard of anesthetic potency. *Anesthesiology*. 1965;26:756–763.
5. Franks NP, Lieb WR. Temperature dependence of the potency of volatile general anesthetics. Implications for in vitro experiments. *Anesthesiology*. 1996;84:716–720.
6. Boggs JM, et al. Site and mechanism of anesthetic action. I. Effect of anesthetics and pressure on fluidity of spin-labeled lipid vesicles. *Mol Pharmacol*. 1976;12:127–135.
7. Franks NP, Lieb WR. Where do general anaesthetics act? *Nature*. 1978;274:339–342.
8. Franks NP, Lieb WR. The structure of lipid bilayers and the effects of general anaesthetics. An x-ray and neutron diffraction study. *J Mol Biol*. 1979;133:469–500.
9. Featherstone RM, et al. Interactions of inert anesthetic gases with proteins. *Anesthesiology*. 1961;22:977–981.
10. Ueda I, Kamaya H. Kinetic and thermodynamic aspects of the mechanism of general anesthesia in a model system of firefly luminescence in vitro. *Anesthesiology*. 1973;38:425–436.
11. Franks NP, Lieb WR. Molecular mechanisms of general anaesthesia. *Nature*. 1982;300:487–493.
12. Franks NP, Lieb WR. Do general anaesthetics act by competitive binding to specific receptors? *Nature*. 1984;310:599–601.
13. Franks NP, Lieb WR. Seeing the light. Protein theories of general anesthesia. 1984. *Anesthesiology*. 2004;101:235–237.
14. Franks NP, Lieb WR. Is membrane expansion relevant to anaesthesia? *Nature*. 1981;292:248–251.
15. Franks NP, Lieb WR. Mapping of general anaesthetic target sites provides a molecular basis for cutoff effects. *Nature*. 1985;316:349–351.
16. Franks NP, Lieb WR. Partitioning of long-chain alcohols into lipid bilayers. Implications for mechanisms of general anesthesia. *Proc Natl Acad Sci U S A*. 1986;83:5116–5120.
17. Koblin DD, et al. Polyhalogenated and perfluorinated compounds that disobey the Meyer-Overton hypothesis. *Anesth Analg*. 1994;79:1043–1048.
18. Hall AC, et al. Stereoselective and non-stereoselective actions of isoflurane on the GABA_A receptor. *Br J Pharmacol*. 1994;112:906–910.
19. Dickinson R, et al. Can the stereoselective effects of the anesthetic isoflurane be accounted for by lipid solubility? *Biophys J*. 1994;66:2019–2023.
20. Franks NP, Lieb WR. Stereospecific effects of inhalational general anesthetic optical isomers on nerve ion channels. *Science*. 1991;254:427–430.
21. Herold KF, et al. Clinical concentrations of chemically diverse general anesthetics minimally affect lipid bilayer properties. *Proc Natl Acad Sci U S A*. 2017;114:3109–3114.
22. Franks NP. General anaesthesia. from molecular targets to neuronal pathways of sleep and arousal. *Nat Rev Neurosci*. 2008;9:370–386.
23. Eckenhoff RG. Promiscuous ligands and attractive cavities. How do the inhaled anesthetics work? *Mol Interv*. 2001;1:258–268.
24. Eckenhoff RG, Johansson JS. What are “relevant” concentrations? *Anesthesiology*. 2001;95:1537–1539.
25. Eger EI, et al. Relevant concentrations of inhaled anesthetics for in vitro studies of anesthetic mechanisms. *Anesthesiology*. 2001;94:915–921.
26. Dickinson R, et al. Stereoselective loss of righting reflex in rats by isoflurane. *Anesthesiology*. 2000;93:837–843.
27. Rudolph U, Antkowiak B. Molecular and neuronal substrates for general anaesthetics. *Nat Rev Neurosci*. 2004;5:709–720.
28. Antognini JF, Schwartz K. Exaggerated anesthetic requirements in the preferentially anesthetized brain. *Anesthesiology*. 1993;79:1244–1249.
29. Rampil IJ, et al. Anesthetic potency (MAC) is independent of forebrain structures in the rat. *Anesthesiology*. 1993;78:707–712.
30. Stabernack C, et al. Thiopental produces immobility primarily by supraspinal actions in rats. *Anesth Analg*. 2005;100:128–136.
31. Veselis RA, et al. Drug-induced amnesia is a separate phenomenon from sedation. Electrophysiologic evidence. *Anesthesiology*. 2001;95:896–907.
32. Sanders RD, et al. Unresponsiveness not equal unconsciousness. *Anesthesiology*. 2012;116:946–959.
33. Devor M, Zalkind V. Reversible analgesia, atonia, and loss of consciousness on bilateral intracerebral microinjection of pentobarbital. *Pain*. 2001;94:101–112.
34. Minert A, et al. Location of the mesopontine neurons responsible for maintenance of anesthetic loss of consciousness. *J Neurosci*. 2017;37:9320–9331.
35. Nelson LE, et al. The sedative component of anesthesia is mediated by GABA(A) receptors in an endogenous sleep pathway. *Nat Neurosci*. 2002;5:979–984.
36. Rampil IJ, Laster MJ. No correlation between quantitative electroencephalographic measurements and movement response to noxious stimuli during isoflurane anesthesia in rats. *Anesthesiology*. 1992;77:920–925.
37. Antognini JF, et al. Does the immobilizing effect of thiopental in brain exceed that of halothane? *Anesthesiology*. 2002;96:980–986.
38. Zhang Y, et al. Gamma-aminobutyric acidA receptors do not mediate the immobility produced by isoflurane. *Anesth Analg*. 2004;99:85–90.
39. Liao M, et al. Beta3-containing gamma-aminobutyric acidA receptors are not major targets for the amnesia and immobilizing actions of isoflurane. *Anesth Analg*. 2005;101:412–418.
40. Sonner JM, et al. Effect of isoflurane and other potent inhaled anesthetics on minimum alveolar concentration, learning, and the righting reflex in mice engineered to express alpha1 gamma-aminobutyric acid type A receptors unresponsive to isoflurane. *Anesthesiology*. 2007;106:107–113.
41. Raines DE, et al. Nonhalogenated anesthetic alkanes and perhalogenated nonimmobilizing alkanes inhibit alpha(4)beta(2) neuronal nicotinic acetylcholine receptors. *Anesth Analg*. 2002;95:573–577.
42. Zhang Y, et al. Bidirectional modulation of isoflurane potency by intrathecal tetrodotoxin and veratridine in rats. *Br J Pharmacol*. 2010;159:872–878.
43. Heurteaux C, et al. TREK-1, a K⁺ channel involved in neuroprotection and general anesthesia. *EMBO J*. 2004;23:2684–2695.
44. Linden AM, et al. The in vivo contributions of TASK-1-containing channels to the actions of inhalation anesthetics, the alpha(2) adrenergic sedative dexmedetomidine, and cannabinoid agonists. *J Pharmacol Exp Ther*. 2006;317:615–626.
45. Linden AM, et al. TASK-3 knockout mice exhibit exaggerated nocturnal activity, impairments in cognitive functions, and reduced sensitivity to inhalation anesthetics. *J Pharmacol Exp Ther*. 2007;323:924–934.
46. Pang DS, et al. An unexpected role for TASK-3 potassium channels in network oscillations with implications for sleep mechanisms and anesthetic action. *Proc Natl Acad Sci U S A*. 2009;106:17546–17551.
47. Westphalen RI, et al. Reduced inhibition of cortical glutamate and GABA release by halothane in mice lacking the K⁺ channel, TREK-1. *Br J Pharmacol*. 2007;152:939–945.
48. Jinks SL, et al. Volatile anesthetic effects on midbrain-elicited locomotion suggest that the locomotor network in the ventral spinal cord is the primary site for immobility. *Anesthesiology*. 2008;108:1016–1024.
49. Koch C, et al. Neural correlates of consciousness. progress and problems. *Nat Rev Neurosci*. 2016;17:307–321.
50. Mashour GA, Hudetz AG. Neural correlates of unconsciousness in large-scale brain networks. *Trends Neurosci*. 2018;41:150–160.
51. Sanders RD, et al. Incidence of connected consciousness after tracheal intubation. A prospective, international, multicenter cohort study of the isolated forearm technique. *Anesthesiology*. 2017;126:214–222.
52. Leung LS, et al. Brain areas that influence general anesthesia. *Prog Neurobiol*. 2014;122:24–44.
53. Brown EN, et al. General anesthesia and altered states of arousal, a systems neuroscience analysis. *Annu Rev Neurosci*. 2011;34:601–628.
54. Mashour GA. Top-down mechanisms of anesthetic-induced unconsciousness. *Front Syst Neurosci*. 2014;8:115.

55. Mashour GA, Hudetz AG. Bottom-up and top-down mechanisms of general anesthetics modulate different dimensions of consciousness. *Front Neural Circuits*. 2017;11:44.
56. Tononi G. Consciousness as integrated information. A provisional manifesto. *Biol Bull*. 2008;215:216–242.
57. Tononi G, et al. Integrated information theory. From consciousness to its physical substrate. *Nat Rev Neurosci*. 2016;17:450–461.
58. Lee U, et al. Assessing levels of consciousness with symbolic analysis. *Philos Trans A Math Phys Eng Sci*. 2015;373.
59. Imas OA, et al. Volatile anesthetics disrupt frontal-posterior recurrent information transfer at gamma frequencies in rat. *Neurosci Lett*. 2005;387:145–150.
60. MacIver MB, Bland BH. Chaos analysis of EEG during isoflurane-induced loss of righting in rats. *Front Syst Neurosci*. 2014;8:203.
61. Bullmore E, Sporns O. The economy of brain network organization. *Nat Rev Neurosci*. 2012;13:336–349.
62. van den Heuvel MP, Sporns O. Rich-club organization of the human connectome. *J Neurosci*. 2011;31:15775–15786.
63. Massimini M, et al. Breakdown of cortical effective connectivity during sleep. *Science*. 2005;309:2228–2232.
64. Ferrarelli F, et al. Breakdown in cortical effective connectivity during midazolam-induced loss of consciousness. *Proc Natl Acad Sci U S A*. 2010;107:2681–2686.
65. Alkire MT, et al. Consciousness and anesthesia. *Science*. 2008;322:876–880.
66. Imas OA, et al. Volatile anesthetics enhance flash-induced gamma oscillations in rat visual cortex. *Anesthesiology*. 2005;102:937–947.
67. Imas OA, et al. Isoflurane disrupts antero-posterior phase synchronization of flash-induced field potentials in the rat. *Neurosci Lett*. 2006;402:216–221.
68. John ER, et al. Invariant reversible QEEG effects of anesthetics. *Conscious Cogn*. 2001;10:165–183.
69. Burlingame RH, et al. Subhypnotic doses of isoflurane impair auditory discrimination in rats. *Anesthesiology*. 2007;106:754–762.
70. Ter-Mikaelian M, et al. Transformation of temporal properties between auditory midbrain and cortex in the awake Mongolian gerbil. *J Neurosci*. 2007;27:6091–6102.
71. Lee U, et al. Disruption of frontal-parietal communication by ketamine, propofol, and sevoflurane. *Anesthesiology*. 2013;118:1264–1275.
72. Wacongne C, et al. Evidence for a hierarchy of predictions and prediction errors in human cortex. *Proc Natl Acad Sci U S A*. 2011;108:20754–20759.
73. Raz A, et al. Preferential effect of isoflurane on top-down vs. bottom-up pathways in sensory cortex. *Front Syst Neurosci*. 2014;8:191.
74. Hentschke H, et al. Disruption of cortical network activity by the general anaesthetic isoflurane. *Br J Anaesth*. 2017;119:685–696.
75. Kelz MB, et al. An essential role for orexins in emergence from general anesthesia. *Proc Natl Acad Sci U S A*. 2008;105:1309–1314.
76. Moore JT, et al. Direct activation of sleep-promoting VLPO neurons by volatile anesthetics contributes to anesthetic hypnosis. *Curr Biol*. 2012;22:2008–2016.
77. McCarren HS, et al. Alpha2-Adrenergic stimulation of the ventrolateral preoptic nucleus destabilizes the anesthetic state. *J Neurosci*. 2014;34:16385–16396.
78. Solt K. General anesthesia: activating a sleep switch? *Curr Biol*. 2012;22:R918–R919.
79. Scharf MT, Kelz MB. Sleep and anesthesia interactions. A pharmacological appraisal. *Curr Anesthesiol Rep*. 2013;3:1–9.
80. Taylor NE, et al. Optogenetic activation of dopamine neurons in the ventral tegmental area induces reanimation from general anesthesia. *Proc Natl Acad Sci U S A*. 2016.
81. Alkire MT, et al. Toward a unified theory of narcosis. brain imaging evidence for a thalamocortical switch as the neurophysiologic basis of anesthetic-induced unconsciousness. *Conscious Cogn*. 2000;9:370–386.
82. Baker R, et al. Altered activity in the central medial thalamus precedes changes in the neocortex during transitions into both sleep and propofol anesthesia. *J Neurosci*. 2014;34:13326–13335.
83. Saalmann YB. Intralaminar and medial thalamic influence on cortical synchrony, information transmission and cognition. *Front Syst Neurosci*. 2014;8:83.
84. Dutton RC, et al. The concentration of isoflurane required to suppress learning depends on the type of learning. *Anesthesiology*. 2001;94:514–519.
85. Brown EN, et al. General anesthesia, sleep, and coma. *N Engl J Med*. 2010;363:2638–2650.
86. Alkire MT, Nathan SV. Does the amygdala mediate anesthetic-induced amnesia? Basolateral amygdala lesions block sevoflurane-induced amnesia. *Anesthesiology*. 2005;102:754–760.
87. Dai S, et al. Isoflurane enhances both fast and slow synaptic inhibition in the hippocampus at amnestic concentrations. *Anesthesiology*. 2012;116:816–823.
88. Piao MH, et al. Volatile anesthetic isoflurane inhibits LTP induction of hippocampal CA1 neurons through alpha4beta2 nAChR subtype-mediated mechanisms. *Ann Fr Anesth Reanim*. 2013;32:e135–e141.
89. Zhou C, et al. HCN1 channels contribute to the effects of amnesia and hypnosis but not immobility of volatile anesthetics. *Anesth Analg*. 2015;121:661–666.
90. Kuo MC, Leung LS. Disruption of hippocampal multisynaptic networks by general anesthetics. *Anesthesiology*. 2017;127:838–851.
91. Vertes RP. Hippocampal theta rhythm: a tag for short-term memory. *Hippocampus*. 2005;15:923–935.
92. Pan WX, McNaughton N. The medial supramammillary nucleus, spatial learning and the frequency of hippocampal theta activity. *Brain Res*. 1997;764:101–108.
93. Robbe D, et al. Cannabinoids reveal importance of spike timing coordination in hippocampal function. *Nat Neurosci*. 2006;9:1526–1533.
94. Perouansky M, et al. Amnesic concentrations of the nonimmobilizer 1,2-dichlorohexafluorocyclobutane (F6, 2N) and isoflurane alter hippocampal theta oscillations in vivo. *Anesthesiology*. 2007;106:1168–1176.
95. Seidenbecher T, et al. Amygdalar and hippocampal theta rhythm synchronization during fear memory retrieval. *Science*. 2003;301:846–850.
96. Rudolph U, et al. Benzodiazepine actions mediated by specific gamma-aminobutyric acid(A) receptor subtypes. *Nature*. 1999;401:796–800.
97. Kandel L, et al. Nonanesthetics can suppress learning. *Anesth Analg*. 1996;82:321–326.
98. Mihic SJ, et al. Potentiation of gamma-aminobutyric acid type A receptor-mediated chloride currents by novel halogenated compounds correlates with their abilities to induce general anesthesia. *Mol Pharmacol*. 1994;46:851–857.
99. Zarnowska ED, et al. The gamma-subunit governs the susceptibility of recombinant gamma-aminobutyric acid type A receptors to block by the nonimmobilizer 1,2-dichlorohexafluorocyclobutane (F6, 2N). *Anesth Analg*. 2005;101:401–406.
100. Jevtovic-Todorovic V, et al. Nitrous oxide (laughing gas) is an NMDA antagonist, neuroprotectant and neurotoxin. *Nat Med*. 1998;4:460–463.
101. Gruss M, et al. Two-pore-domain K⁺ channels are a novel target for the anesthetic gases xenon, nitrous oxide, and cyclopropane. *Mol Pharmacol*. 2004;65:443–452.
102. Gries DA, et al. Anxiolytic-like action in mice treated with nitrous oxide and oral triazolam or diazepam. *Life Sci*. 2005;76:1667–1674.
103. Zhang Z, et al. Neuronal ensembles sufficient for recovery sleep and the sedative actions of alpha2 adrenergic agonists. *Nat Neurosci*. 2015;18:553–561.
104. Murphy M, et al. Propofol anesthesia and sleep. A high-density EEG study. *Sleep*. 2011;34: 283–291A.
105. Tung A, et al. Recovery from sleep deprivation occurs during propofol anesthesia. *Anesthesiology*. 2004;100:1419–1426.
106. Nelson AB, et al. Effects of anesthesia on the response to sleep deprivation. *Sleep*. 2010;33:1659–1667.
107. Hentschke H, et al. Neocortex is the major target of sedative concentrations of volatile anaesthetics. Strong depression of firing rates and increase of GABA_A receptor-mediated inhibition. *Eur J Neurosci*. 2005;21:93–102.
108. Franks NP, Lieb WR. Molecular and cellular mechanisms of general anaesthesia. *Nature*. 1994;367:607–614.
109. Zeller A, et al. Inhibitory ligand-gated ion channels as substrates for general anesthetic actions. *Handb Exp Pharmacol*. 2008;31–51.
110. Franks NP, et al. Structural basis for the inhibition of firefly luciferase by a general anesthetic. *Biophys J*. 1998;75: 2205–2211.

111. Bhattacharya AA, et al. Binding of the general anesthetics propofol and halothane to human serum albumin. High resolution crystal structures. *J Biol Chem.* 2000;275:38731–38738.
112. Bertaccini EJ, et al. The common chemical motifs within anesthetic binding sites. *Anesth Analg.* 2007;104:318–324.
113. Howard RJ, et al. Seeking structural specificity. Direct modulation of pentameric ligand-gated ion channels by alcohols and general anesthetics. *Pharmacol Rev.* 2014;66:396–412.
114. Nury H, et al. X-ray structures of general anaesthetics bound to a pentameric ligand-gated ion channel. *Nature.* 2011;469:428–431.
115. Dickinson R, et al. Competitive inhibition at the glycine site of the N-methyl-D-aspartate receptor by the anesthetics xenon and isoflurane. evidence from molecular modeling and electrophysiology. *Anesthesiology.* 2007;107:756–767.
116. Hemmings HC, et al. Emerging molecular mechanisms of general anesthetic action. *Trends Pharmacol Sci.* 2005;26:503–510.
117. Patel AJ, et al. Inhalational anesthetics activate two-pore-domain background K⁺ channels. *Nat Neurosci.* 1999;2:422–426.
118. Franks NP, Honore E. The TREK K2P channels and their role in general anaesthesia and neuroprotection. *Trends Pharmacol Sci.* 2004;25:601–608.
119. Sieghart W. Allosteric modulation of GABA_A receptors via multiple drug-binding sites. *Adv Pharmacol.* 2015;72:53–96.
120. Lynch JW. Molecular structure and function of the glycine receptor chloride channel. *Physiol Rev.* 2004;84:1051–1095.
121. Mihic SJ, et al. Sites of alcohol and volatile anaesthetic action on GABA(A) and glycine receptors. *Nature.* 1997;389:385–389.
122. Solt K, et al. General anesthetic-induced channel gating enhancement of 5-hydroxytryptamine type 3 receptors depends on receptor subunit composition. *J Pharmacol Exp Ther.* 2005;315:771–776.
123. Jenkins A, et al. Actions of general anaesthetics on 5-HT₃ receptors in N1E-115 neuroblastoma cells. *Br J Pharmacol.* 1996;117:1507–1515.
124. Role LW, Berg DK. Nicotinic receptors in the development and modulation of CNS synapses. *Neuron.* 1996;16:1077–1085.
125. Flood P, et al. Alpha 4 beta 2 neuronal nicotinic acetylcholine receptors in the central nervous system are inhibited by isoflurane and propofol, but alpha 7-type nicotinic acetylcholine receptors are unaffected. *Anesthesiology.* 1997;86:859–865.
126. Violet JM, et al. Differential sensitivities of mammalian neuronal and muscle nicotinic acetylcholine receptors to general anesthetics. *Anesthesiology.* 1997;86:866–874.
127. Dingledine R, et al. The glutamate receptor ion channels. *Pharmacol Rev.* 1999;51:7–61.
128. Franks NP, et al. How does xenon produce anaesthesia? *Nature.* 1998;396:324.
129. de Sousa SL, et al. Contrasting synaptic actions of the inhalational general anesthetics isoflurane and xenon. *Anesthesiology.* 2000;92:1055–1066.
130. Solt K, et al. Differential modulation of human N-methyl-D-aspartate receptors by structurally diverse general anesthetics. *Anesth Analg.* 2006;102:1407–1411.
131. Harris RA, et al. Actions of anesthetics on ligand-gated ion channels. Role of receptor subunit composition. *FASEB J.* 1995;9:1454–1462.
132. Sonner JM, et al. The effect of three inhaled anesthetics in mice harboring mutations in the GluR6 (kainate) receptor gene. *Anesth Analg.* 2005;101:143–148.
133. MacIver MB, et al. Volatile anesthetics depress glutamate transmission via presynaptic actions. *Anesthesiology.* 1996;85:823–834.
134. Perouansky M, et al. Anesthetic effects on glutamatergic neurotransmission. Lessons learned from a large synapse. *Anesthesiology.* 2004;100:470–472.
135. Winegar BD, MacIver MB. Isoflurane depresses hippocampal CA1 glutamate nerve terminals without inhibiting fiber volleys. *BMC Neurosci.* 2006;7:5.
136. Haydon DA, Urban BW. The effects of some inhalation anaesthetics on the sodium current of the squid giant axon. *J Physiol.* 1983;341:429–439.
137. Berg-Johnsen J, Langmoen IA. The effect of isoflurane on unmyelinated and myelinated fibres in the rat brain. *Acta Physiol Scand.* 1986;127:87–93.
138. Mikulec AA, et al. Halothane depresses action potential conduction in hippocampal axons. *Brain Res.* 1998;796:231–238.
139. Wu XS, et al. Isoflurane inhibits transmitter release and the presynaptic action potential. *Anesthesiology.* 2004;100:663–670.
140. Yu FH, Catterall WA. The VGL-chanome. A protein superfamily specialized for electrical signaling and ionic homeostasis. *Sci STKE.* 2004; 2004:re15.
141. Catterall WA. Structure and regulation of voltage-gated Ca²⁺ channels. *Annu Rev Cell Dev Biol.* 2000;16:521–555.
142. Herold KF, et al. Isoflurane inhibits the tetrodotoxin-resistant voltage-gated sodium channel Nav1.8. *Anesthesiology.* 2009;111:591–599.
143. Ouyang W, Hemmings HC. Depression by isoflurane of the action potential and underlying voltage-gated ion currents in isolated rat neurohypophyseal nerve terminals. *J Pharmacol Exp Ther.* 2005;312:801–808.
144. Ouyang W, Hemmings HC. Isoform-selective effects of isoflurane on voltage-gated Na⁺ channels. *Anesthesiology.* 2007;107:91–98.
145. Ouyang W, et al. Isoflurane inhibits NaChBac, a prokaryotic voltage-gated sodium channel. *J Pharmacol Exp Ther.* 2007;322:1076–1083.
146. Ratnakumari L, et al. Differential effects of anesthetic and nonanesthetic cyclobutanes on neuronal voltage-gated sodium channels. *Anesthesiology.* 2000;92:529–541.
147. Herold KF, Hemmings HC. Sodium channels as targets for volatile anesthetics. *Front Pharmacol.* 2012;3:50.
148. Tang JX, et al. Anesthesia in presymptomatic Alzheimer's disease. a study using the triple-transgenic mouse model. *Alzheimers Dement.* 2011;7:521–531.e521.
149. Barber AF, et al. Modulation of a voltage-gated Na⁺ channel by sevoflurane involves multiple sites and distinct mechanisms. *Proc Natl Acad Sci U S A.* 2014;111:6726–6731.
150. Kinde MN, et al. Fluorine-19 NMR and computational quantification of isoflurane binding to the voltage-gated sodium channel NaChBac. *Proc Natl Acad Sci U S A.* 2016;113:13762–13767.
151. Sand RM, et al. Isoflurane modulates activation and inactivation gating of the prokaryotic Na(+) channel NaChBac. *J Gen Physiol.* 2017;149:623–638.
152. Miao N, et al. Volatile anesthetics depress Ca²⁺ transients and glutamate release in isolated cerebral synaptosomes. *Anesthesiology.* 1995;83:593–603.
153. Pocock G, Richards CD. Excitatory and inhibitory synaptic mechanisms in anaesthesia. *Br J Anaesth.* 1993;71:134–147.
154. Kameyama K, et al. Isoflurane inhibits neuronal Ca²⁺ channels through enhancement of current inactivation. *Br J Anaesth.* 1999;82:402–411.
155. Study RE. Isoflurane inhibits multiple voltage-gated calcium currents in hippocampal pyramidal neurons. *Anesthesiology.* 1994;81:104–116.
156. Hall AC, et al. Insensitivity of P-type calcium channels to inhalational and intravenous general anesthetics. *Anesthesiology.* 1994;81:117–123.
157. Takei T, et al. Increased sensitivity to halothane but decreased sensitivity to propofol in mice lacking the N-type Ca²⁺ channel. *Neurosci Lett.* 2003;350:41–45.
158. Joksovic PM, et al. Contrasting anesthetic sensitivities of T-type Ca²⁺ channels of reticular thalamic neurons and recombinant Ca(v)3.3 channels. *Br J Pharmacol.* 2005;144:59–70.
159. Todorovic SM, et al. Ca(v)3.2 channel is a molecular substrate for inhibition of T-type calcium currents in rat sensory neurons by nitrous oxide. *Mol Pharmacol.* 2001;60:603–610.
160. Petrenko AB, et al. Mutation of alpha1G T-type calcium channels in mice does not change anesthetic requirements for loss of the righting reflex and minimum alveolar concentration but delays the onset of anesthetic induction. *Anesthesiology.* 2007;106:1177–1185.
161. Hanley PJ, et al. Excitation-contraction coupling in the heart and the negative inotropic action of volatile anesthetics. *Anesthesiology.* 2004;101:999–1014.
162. Huncke R, et al. Effects of volatile anesthetics on cardiac ion channels. *Acta Anaesthesiol Scand.* 2004;48:547–561.
163. Rithalia A, et al. The effects of halothane, isoflurane, and sevoflurane on Ca²⁺ current and transient outward K⁺ current in subendocardial and subepicardial myocytes from the rat left ventricle. *Anesth Analg.* 2004;99:1615–1622.
164. Huncke R, et al. Effects of the anesthetic gases xenon, halothane, and isoflurane on calcium and potassium currents in human atrial cardiomyocytes. *Anesthesiology.* 2001;95:999–1006.

165. Stowe DF, et al. Xenon does not alter cardiac function or major cation currents in isolated guinea pig hearts or myocytes. *Anesthesiology*. 2000;92:516–522.
166. Davies LA, et al. Effects of isoflurane, sevoflurane, and halothane on myofilament Ca²⁺ sensitivity and sarcoplasmic reticulum Ca²⁺ release in rat ventricular myocytes. *Anesthesiology*. 2000;93:1034–1044.
167. Joseph JD, et al. General anesthetic isoflurane modulates inositol 1,4,5-trisphosphate receptor calcium channel opening. *Anesthesiology*. 2014;121:528–537.
168. Pabelick CM, et al. Effects of halothane on sarcoplasmic reticulum calcium release channels in porcine airway smooth muscle cells. *Anesthesiology*. 2001;95:207–215.
169. Roberts MC, et al. Autosomal dominant canine malignant hyperthermia is caused by a mutation in the gene encoding the skeletal muscle calcium release channel (RYR1). *Anesthesiology*. 2001;95:716–725.
170. Mickelson JR, Louis CF. Malignant hyperthermia, excitation-contraction coupling, Ca²⁺ release channel, and cell Ca²⁺ regulation defects. *Physiol Rev*. 1996;76:537–592.
171. Yost CS. Potassium channels. basic aspects, functional roles, and medical significance. *Anesthesiology*. 1999;90:1186–1203.
172. Friederich P, et al. Interaction of volatile anesthetics with human Kv channels in relation to clinical concentrations. *Anesthesiology*. 2001;95:954–958.
173. Franks NP, Lieb WR. Volatile general anaesthetics activate a novel neuronal K⁺ current. *Nature*. 1988;333:662–664.
174. Dickinson R, Franks NP. Bench-to-bedside review. Molecular pharmacology and clinical use of inert gases in anesthesia and neuroprotection. *Critical care*. 2010;14:229.
175. Tong L, et al. Activation of K(2)P channel-TREK1 mediates the neuroprotection induced by sevoflurane preconditioning. *Br J Anaesth*. 2014;113:157–167.
176. Woll KA, et al. Photoaffinity ligand for the inhalational anesthetic sevoflurane allows mechanistic insight into potassium channel modulation. *ACS Chem Biol*. 2017;12:1353–1362.
177. Bertaccini EJ, et al. Molecular modeling of a tandem two pore domain potassium channel reveals a putative binding site for general anesthetics. *ACS chemical neuroscience*. 2014;5:1246–1252.
178. Farwell D, Gollob MH. Electrical heart disease. Genetic and molecular basis of cardiac arrhythmias in normal structural hearts. *Can J Cardiol*. 2007;23(suppl A):16A–22A.
179. Antzelevitch C. Molecular biology and cellular mechanisms of Brugada and long QT syndromes in infants and young children. *J Electrocadiol*. 2001;34(suppl):177–181.
180. Li J, Correa AM. Kinetic modulation of HERG potassium channels by the volatile anesthetic halothane. *Anesthesiology*. 2002;97:921–930.
181. Davies LA, et al. Effects of halothane on the transient outward K(+) current in rat ventricular myocytes. *Br J Pharmacol*. 2000;131:223–230.
182. Stadnicka A, et al. Volatile anesthetic-induced cardiac preconditioning. *J Anesth*. 2007;21:212–219.
183. Wojtovich AP, et al. Cardiac Slo2.1 is required for volatile anesthetic stimulation of K⁺ transport and anesthetic preconditioning. *Anesthesiology*. 2016;124:1065–1076.
184. Sirois JE, et al. Convergent and reciprocal modulation of a leak K⁺ current and I(h) by an inhalational anaesthetic and neurotransmitters in rat brainstem motoneurones. *J Physiol*. 2002;541:717–729.
185. Chen X, et al. HCN subunit-specific and cAMP-modulated effects of anesthetics on neuronal pacemaker currents. *J Neurosci*. 2005;25:5803–5814.
186. Robinson RB, Siegelbaum SA. Hyperpolarization-activated cation currents. from molecules to physiological function. *Annu Rev Physiol*. 2003;65:453–480.
187. Girault JA, Hemmings HCJ. In: Hemmings HC, Hopkins PM, eds. *Foundations of Anesthesia*. Mosby; 2005:31.
188. Rebecchi MJ, Pentyala SN. Anesthetic actions on other targets. protein kinase C and guanine nucleotide-binding proteins. *Br J Anaesth*. 2002;89:62–78.
189. Peterlin Z, et al. Selective activation of G-protein coupled receptors by volatile anesthetics. *Mol Cell Neurosci*. 2005;30:506–512.
190. Minami K, et al. Effects of ethanol and anesthetics on type 1 and 5 metabotropic glutamate receptors expressed in *Xenopus laevis* oocytes. *Mol Pharmacol*. 1998;53:148–156.
191. Minami K, et al. Inhibition of 5-hydroxytryptamine type 2A receptor-induced currents by n-alcohols and anesthetics. *J Pharmacol Exp Ther*. 1997;281:1136–1143.
192. Minami K, et al. Inhibitory effects of anesthetics and ethanol on muscarinic receptors expressed in *Xenopus* oocytes. *Eur J Pharmacol*. 1997;339:237–244.
193. Hemmings HC. General anesthetic effects on protein kinase C. *Toxicol Lett*. 1998;89–95, 100–101.
194. Hasegawa J, et al. Sevoflurane stimulates MAP kinase signal transduction through the activation of PKC alpha and betaII in fetal rat cerebral cortex cultured neuron. *Acta Histochem Cytochem*. 2006;39:163–172.
195. Das J, et al. Identification of a general anesthetic binding site in the diacylglycerol-binding domain of protein kinase Cdelta. *J Biol Chem*. 2004;279:37964–37972.
196. Shumilla JA, et al. Inhibition of spinal protein kinase C-epsilon or -gamma isozymes does not affect halothane minimum alveolar anesthetic concentration in rats. *Anesth Analg*. 2004;99:82–84.
197. Sonner JM, et al. Mouse strain modestly influences minimum alveolar anesthetic concentration and convulsivity of inhaled compounds. *Anesth Analg*. 1999;89:1030–1034.
198. Inoue S, et al. Combination of isoflurane and caspase inhibition reduces cerebral injury in rats subjected to focal cerebral ischemia. *Anesthesiology*. 2004;101:75–81.
199. Rasmussen LS, et al. Postoperative cognitive dysfunction. true deterioration versus random variation. *Acta Anaesthesiol Scand*. 2004;48:1137–1143.
200. Fukuda S, Warner DS. Cerebral protection. *Br J Anaesth*. 2007;99:10–17.
201. Turner CP, et al. Strategies to defeat ketamine-induced neonatal brain injury. *Neuroscience*. 2012;210:384–392.
202. Pratt PF, et al. Cardioprotection by volatile anesthetics. New applications for old drugs? *Curr Opin Anaesthesiol*. 2006;19:397–403.
203. Zaugg M, et al. Anaesthetics and cardiac preconditioning. Part I. Signalling and cytoprotective mechanisms. *Br J Anaesth*. 2003;91: 551–565.
204. Ludwig LM, et al. Protein kinase C translocation and Src protein tyrosine kinase activation mediate isoflurane-induced preconditioning in vivo. potential downstream targets of mitochondrial adenosine triphosphate-sensitive potassium channels and reactive oxygen species. *Anesthesiology*. 2004;100:532–539.
205. Song IA, et al. The involvement of protein kinase C-epsilon in isoflurane induced preconditioning of human embryonic stem cell-derived Nkx2.5(+) cardiac progenitor cells. *BMC Anesthesiol*. 2016;16:13.
206. Snyder GL, et al. General anesthetics selectively modulate glutamatergic and dopaminergic signaling via site-specific phosphorylation in vivo. *Neuropharmacology*. 2007;53:619–630.
207. Hemmings HC, Adamo AI. Effects of halothane and propofol on purified brain protein kinase C activation. *Anesthesiology*. 1994;81: 147–155.
208. Marota JJ, et al. Selective effects of pentobarbital and halothane on c-fos and jun-B gene expression in rat brain. *Anesthesiology*. 1992;77:365–371.
209. Hamaya Y, et al. The effects of pentobarbital, isoflurane, and propofol on immediate-early gene expression in the vital organs of the rat. *Anesth Analg*. 2000;90:1177–1183.
210. Culley DJ, et al. Altered hippocampal gene expression 2 days after general anesthesia in rats. *Eur J Pharmacol*. 2006;549: 71–78.
211. Futterer CD, et al. Alterations in rat brain proteins after desflurane anesthesia. *Anesthesiology*. 2004;100:302–308.
212. Durieux M, Davis PJ. The Safety of Key Inhaled and Intravenous Drugs in Pediatrics (SAFEKIDS). An update. *Anesth Analg*. 2010;110:1265–1267.
213. Dalla Massara L, et al. General anesthesia causes epigenetic histone modulation of c-Fos and brain-derived neurotrophic factor, target genes important for neuronal development in the immature rat hippocampus. *Anesthesiology*. 2016;124:1311–1327.
214. Kullmann DM, et al. Reduction by general anaesthetics of group Ia excitatory postsynaptic potentials and currents in the cat spinal cord. *J Physiol*. 1989;412:277–296.
215. Fujiwara N, et al. Changes in spontaneous firing patterns of rat hippocampal neurones induced by volatile anaesthetics. *J Physiol*. 1988;402:155–175.

216. MacIver MB, Roth SH. Inhalation anaesthetics exhibit pathway-specific and differential actions on hippocampal synaptic responses in vitro. *Br J Anaesth.* 1988;60:680–691.
217. Ries CR, Puil E. Ionic mechanism of isoflurane's actions on thalamocortical neurons. *J Neurophysiol.* 1999;81:1802–1809.
218. Sirois JE, et al. The TASK-1 two-pore domain K⁺ channel is a molecular substrate for neuronal effects of inhalation anesthetics. *J Neurosci.* 2000;20:6347–6354.
219. Semyanov A, et al. Tonically active GABA A receptors modulating gain and maintaining the tone. *Trends Neurosci.* 2004;27:262–269.
220. Houston CM, et al. Are extrasynaptic GABA A receptors important targets for sedative/hypnotic drugs? *J Neurosci.* 2012;32:3887–3897.
221. Bai D, et al. Distinct functional and pharmacological properties of tonic and quantal inhibitory postsynaptic currents mediated by gamma-aminobutyric acid(A) receptors in hippocampal neurons. *Mol Pharmacol.* 2001;59:814–824.
222. Bieda MC, MacIver MB. Major role for tonic GABA A conductances in anesthetic suppression of intrinsic neuronal excitability. *J Neurophysiol.* 2004;92:1658–1667.
223. Caraiscos VB, et al. Tonic inhibition in mouse hippocampal CA1 pyramidal neurons is mediated by alpha5 subunit-containing gamma-aminobutyric acid type A receptors. *Proc Natl Acad Sci U S A.* 2004;101:3662–3667.
224. Caraiscos VB, et al. Selective enhancement of tonic GABAergic inhibition in murine hippocampal neurons by low concentrations of the volatile anesthetic isoflurane. *J Neurosci.* 2004;24:8454–8458.
225. Capogna M, Pearce RA. GABA A,slow. Causes and consequences. *Trends Neurosci.* 2011;34:101–112.
226. Rodgers FC, et al. Etomidate impairs long-term potentiation in vitro by targeting alpha5-subunit containing gabaa receptors on nonpyramidal cells. *J Neurosci.* 2015;35:9707–9716.
227. Berg-Johansen J, Langmoen IA. The effect of isoflurane on excitatory synaptic transmission in the rat hippocampus. *Acta Anaesthesiol Scand.* 1992;36:350–355.
228. Kirson ED, et al. Presynaptic and postsynaptic actions of halothane at glutamatergic synapses in the mouse hippocampus. *Br J Pharmacol.* 1998;124:1607–1614.
229. Richards CD, Smaje JC. Anaesthetics depress the sensitivity of cortical neurones to L-glutamate. *Br J Pharmacol.* 1976;58:347–357.
230. Wakamori M, et al. Effects of two volatile anesthetics and a volatile convulsant on the excitatory and inhibitory amino acid responses in dissociated CNS neurons of the rat. *J Neurophysiol.* 1991;66:2014–2021.
231. Yang J, Zorumski CF. Effects of isoflurane on N-methyl-D-aspartate gated ion channels in cultured rat hippocampal neurons. *Ann N Y Acad Sci.* 1991;625:287–289.
232. Dildy-Mayfield JE, et al. Anesthetics produce subunit-selective actions on glutamate receptors. *J Pharmacol Exp Ther.* 1996;276:1058–1065.
233. Minami K, et al. Sites of volatile anesthetic action on kainate (Glutamate receptor 6) receptors. *J Biol Chem.* 1998;273:8248–8255.
234. Morgan PG, et al. Mitochondrial defects and anesthetic sensitivity. *Anesthesiology.* 2002;96:1268–1270.
235. Quintana A, et al. Altered anesthetic sensitivity of mice lacking Ndufs4, a subunit of mitochondrial complex I. *PLoS One.* 2012;7:e42904.
236. Zimin PI, et al. Glutamatergic neurotransmission links sensitivity to volatile anesthetics with mitochondrial function. *Curr Biol.* 2016;26:2194–2201.
237. Ramadasan-Nair R, et al. Regional knockdown of NDUF54 implicates a thalamocortical circuit mediating anesthetic sensitivity. *PLoS One.* 2017;12:e0188087.
238. Banks MI, Pearce RA. Dual actions of volatile anesthetics on GABA(A) IPSCs. Dissociation of blocking and prolonging effects. *Anesthesiology.* 1999;90:120–134.
239. Murugaiah KD, Hemmings HC Jr. Effects of intravenous general anesthetics on [3H]GABA release from rat cortical synaptosomes. *Anesthesiology.* 1998;89:919–928.
240. Nishikawa K, MacIver MB. Agent-selective effects of volatile anesthetics on GABA A receptor-mediated synaptic inhibition in hippocampal interneurons. *Anesthesiology.* 2001;94:340–347.
241. Westphalen RI, Hemmings HC. Selective depression by general anesthetics of glutamate versus GABA release from isolated cortical nerve terminals. *J Pharmacol Exp Ther.* 2003;304:1188–1196.
242. Westphalen RI, Hemmings HC. Volatile anesthetic effects on glutamate versus GABA release from isolated rat cortical nerve terminals. 4-aminopyridine-evoked release. *J Pharmacol Exp Ther.* 2006;316:216–223.
243. Baumgart JP, et al. Isoflurane inhibits synaptic vesicle exocytosis through reduced Ca²⁺ influx, not Ca²⁺-exocytosis coupling. *Proc Natl Acad Sci U S A.* 2015;112:11959–11964.
244. Nagele P, et al. Volatile anesthetics bind rat synaptic snare proteins. *Anesthesiology.* 2005;103:768–778.
245. van Swinderen B, et al. A neomorphic syntaxin mutation blocks volatile-anesthetic action in *Caenorhabditis elegans*. *Proc Natl Acad Sci U S A.* 1999;96:2479–2484.
246. Hemmings HC, et al. The general anesthetic isoflurane depresses synaptic vesicle exocytosis. *Mol Pharmacol.* 2005;67:1591–1599.
247. Pearce RA, et al. Effect of volatile anesthetics on synaptic transmission in the rat hippocampus. *Anesthesiology.* 1989;71:591–598.
248. Pearce RA. Volatile anaesthetic enhancement of paired-pulse depression investigated in the rat hippocampus in vitro. *J Physiol.* 1996;492(Pt 3):823–840.
249. Ballesteros KA, et al. Effects of inhaled anesthetic isoflurane on long-term potentiation of CA3 pyramidal cell afferents in vivo. *Int J Gen Med.* 2012;5:935–942.
250. Simon W, et al. Isoflurane blocks synaptic plasticity in the mouse hippocampus. *Anesthesiology.* 2001;94:1058–1065.
251. Jinks SL, et al. Anesthetic effects on fictive locomotion in the rat isolated spinal cord. *Neuroreport.* 2011;22:655–659.
252. Jinks SL, et al. Isoflurane disrupts central pattern generator activity and coordination in the lamprey isolated spinal cord. *Anesthesiology.* 2005;103:567–575.
253. Lewis LD, et al. Rapid fragmentation of neuronal networks at the onset of propofol-induced unconsciousness. *Proc Natl Acad Sci U S A.* 2012;109:E3377–E3386.
254. Guidera JA, et al. Sevoflurane induces coherent slow-delta oscillations in rats. *Front Neural Circuits.* 2017;11:36.
255. Steriade M, et al. Intracellular analysis of relations between the slow (< 1 Hz) neocortical oscillation and other sleep rhythms of the electroencephalogram. *J Neurosci.* 1993;13:3266–3283.
256. Purdon PL, et al. Electroencephalogram signatures of loss and recovery of consciousness from propofol. *Proc Natl Acad Sci U S A.* 2013;110:E1142–E1151.
257. Buzsaki G. Theta oscillations in the hippocampus. *Neuron.* 2002;33:325–340.
258. Bland BH, et al. Effect of halothane on type 2 immobility-related hippocampal theta field activity and theta-on/theta-off cell discharges. *Hippocampus.* 2003;13:38–47.
259. Munglani R, et al. A measure of consciousness and memory during isoflurane administration. the coherent frequency. *Br J Anaesth.* 1993;71:633–641.
260. Madler C, et al. Sensory information processing during general anaesthesia. effect of isoflurane on auditory evoked neuronal oscillations. *Br J Anaesth.* 1991;66:81–87.
261. Buzsaki G, Wang XJ. Mechanisms of gamma oscillations. *Annu Rev Neurosci.* 2012;35:203–225.
262. Dickinson R, et al. The effects of general anaesthetics on carbachol-evoked gamma oscillations in the rat hippocampus in vitro. *Neuropharmacology.* 2003;44:864–872.
263. Antkowiak B, Hentschke H. Cellular mechanisms of gamma rhythms in rat neocortical brain slices probed by the volatile anaesthetic isoflurane. *Neurosci Lett.* 1997;231:87–90.
264. Gottschalk A, Haney P. Computational aspects of anesthetic action in simple neural models. *Anesthesiology.* 2003;98:548–564.
265. Storer KP, Reeke GN. Gamma-Aminobutyric acid receptor type A receptor potentiation reduces firing of neuronal assemblies in a computational cortical model. *Anesthesiology.* 2012;117:780–790.
266. Wilson MT, et al. General anesthetic-induced seizures can be explained by a mean-field model of cortical dynamics. *Anesthesiology.* 2006;104:588–593.
267. Steyn-Ross ML, et al. Modelling general anaesthesia as a first-order phase transition in the cortex. *Prog Biophys Mol Biol.* 2004;85:369–385.
268. Zhang Y, et al. Both cerebral GABA(A) receptors and spinal GABA(A) receptors modulate the capacity of isoflurane to produce immobility. *Anesth Analg.* 2001;92:1585–1589.
269. Zhang Y, et al. Neither GABA(A) nor strychnine-sensitive glycine receptors are the sole mediators of MAC for isoflurane. *Anesth Analg.* 2001;92:123–127.

270. Forman SA, Miller KW. Mapping general anesthetic sites in heteromeric gamma-aminobutyric acid type A receptors reveals a potential for targeting receptor subtypes. *Anesth Analg*. 2016;123:1263–1273.
271. Woll KA, et al. Identification of binding sites contributing to volatile anesthetic effects on GABA type A receptors. *FASEB J*. 2018;fj201701347R.
272. Nash HA. In vivo genetics of anaesthetic action. *Br J Anaesth*. 2002;89:143–155.
273. Kim CK, et al. Integration of optogenetics with complementary methodologies in systems neuroscience. *Nat Rev Neurosci*. 2017;18:222–235.
274. Roth BL. DREADDs for neuroscientists. *Neuron*. 2016;89:683–694.
275. Gelegen C, et al. Excitatory pathways from the lateral habenula enable propofol-induced sedation. *Curr Biol*. 2018;28:580–587.e585.
276. Sonner JM, et al. Alpha 1 subunit-containing GABA type A receptors in forebrain contribute to the effect of inhaled anesthetics on conditioned fear. *Mol Pharmacol*. 2005;68:61–68.
277. van Swinderen B, Kottler B. Explaining general anesthesia. A two-step hypothesis linking sleep circuits and the synaptic release machinery. *Bioessays*. 2014;36:372–381.
278. Morgan PG, Sedensky MM. Mutations conferring new patterns of sensitivity to volatile anesthetics in *Caenorhabditis elegans*. *Anesthesiology*. 1994;81:888–898.
279. Rajaram S, et al. Unc-1, a stomatin homologue controls sensitivity to volatile anesthetics in *Caenorhabditis elegans*. *Proc Natl Acad Sci U S A*. 1998;95:8761–8766.
280. Sedensky MM, et al. Model organisms, new insights into ion channel and transporter function. Stomatin homologues interact in *Caenorhabditis elegans*. *Am J Physiol Cell Physiol*. 2001;280:C1340–C1348.
281. Cascio M, et al. Mouse chromosome 7 harbors a quantitative trait locus for isoflurane minimum alveolar concentration. *Anesth Analg*. 2007;105:381–385.
282. Olufs ZPG, et al. Genetic variability affects absolute and relative potencies and kinetics of the anesthetics isoflurane and sevoflurane in *Drosophila melanogaster*. *Sci Rep*. 2018;8:2348.
283. Veselis RA, et al. A neuroanatomical construct for the amnesic effects of propofol. *Anesthesiology*. 2002;97:329–337.
284. Alkire MT, Miller J. General anesthesia and the neural correlates of consciousness. *Prog Brain Res*. 2005;150:229–244.

STUART A. FORMAN and YUMIKO ISHIZAWA

KEY POINTS

- The alveolar anesthetic concentration (F_A) or partial pressure (P_{alv}) is important because it is the driving force determining anesthetic uptake into blood and target tissues in the central nervous system, and it can be monitored as a readout of anesthetic dosage. P_{alv} is influenced by both delivery and uptake of anesthetic gas.
- Inhaled anesthetic delivery to patients can be increased with larger fresh carrier gas flows, vaporizer output settings, and minute ventilation.
- Initial anesthetic uptake into blood increases with greater pulmonary blood flow (cardiac output) and high blood solubility of anesthetic gas. Increased uptake (as with a highly blood-soluble drug or high cardiac output) slows anesthetic induction because it slows the rate of rise of P_{alv} . Conversely, low anesthetic solubility in blood is associated with rapid onset and offset of anesthesia.
- Uptake of anesthetic into blood slows as blood and tissue partial pressures increase, resulting in higher anesthetic partial pressure in mixed venous blood.
- The higher the inspired anesthetic concentration, the less it diminishes because of uptake (the concentration effect). At 100% inspired concentration of a gas, uptake reduces the volume of gas in alveoli, but does reduce P_{alv} . During inhalation of anesthetic mixtures containing high nitrous oxide (N_2O) concentrations, the reduction of alveolar volume produced by rapid N_2O uptake sustains or increases the concentrations of other alveolar gases (the second gas effect).
- Factors that affect anesthetic uptake similarly affect pulmonary clearance of anesthetics. The rate of clearance is also context sensitive—that is, equivalent drops in alveolar and brain anesthetic concentrations are slower after a long exposure to inhaled anesthetic compared to a short exposure of equal depth.
- Toxicities of inhaled anesthetics that last beyond the exposure period are primarily associated with their biotransformation (metabolism). These toxic effects are usually produced in the tissues, such as liver and kidney, in which metabolism occurs. Modern inhaled anesthetics undergo less metabolism than older drugs, resulting in less hepatic and renal toxicity.
- Halothane hepatitis is a potentially fatal syndrome of fulminant liver damage after exposure to reactive metabolites produced by oxidation of volatile anesthetics. These metabolites covalently modify liver proteins, creating neohaptens that elicit an immune response against hepatocytes. The incidence of the syndrome varies with different anesthetics, paralleling the extent of drug metabolism: halothane >> enflurane > isoflurane > desflurane.
- Defluorination of inhaled anesthetics occurs in both the liver and kidney, producing high fluoride concentrations in blood. Renal toxicity characterized by high-output renal failure is almost exclusively associated with prolonged exposure to methoxyflurane. Sevoflurane metabolism also results in high fluoride levels in blood but does not damage kidneys. Factors that enhance the toxicity of methoxyflurane relative to sevoflurane include its higher tissue solubility, slower clearance, and higher degree of renal metabolism, resulting in high intrarenal fluoride levels for an extended time.
- In laboratory mammals, including nonhuman primates, all general anesthetics alter synapse and neural circuit formation during critical periods of brain development, resulting in abnormal memory and behavior. Clinical studies in children suggest that lengthy (>4 hours) anesthetic exposures at under 2 years of age are associated with detectable but quite small neurocognitive deficits, relative to unexposed controls (also see [Chapter 77](#)). Postoperative delirium and cognitive decline/dysfunction (POCD) in elderly patients is also a growing concern (see [Chapter 83](#)). Based on animal and clinical studies, both postsurgical neuroinflammation and exposure to general anesthesia may contribute to POCD.
- Anesthetics react with strong bases, particularly potassium hydroxide (KOH), in carbon dioxide (CO_2) absorbents, resulting in production of several potentially toxic substances. Sevoflurane

degrades to form compound A, which is associated with renal damage in rodents, but not in humans. This differential toxicity is associated with differential renal metabolism in rodents versus humans. Dry CO₂ absorbents in the breathing circuit react with inhaled anesthetics, releasing carbon monoxide and heat. New CO₂ absorbent materials that lack strong base chemicals prevent these reactions and subsequent potential harm to patients.

- N₂O is unique among anesthetics in its ability to inhibit methionine synthase by oxidizing a cofactor, vitamin B₁₂. In certain susceptible patients or with multiple frequent exposures to N₂O, methionine synthase inhibition can lead to hematologic and neurologic dysfunction. After prolonged N₂O exposure, methionine synthase inhibition also increases blood homocysteine, which is hypothesized to increase vascular inflammation and the risk of thrombosis. Large clinical trials show that N₂O exposure does not increase the risk of cardiovascular morbidity in most patients, but N₂O should be avoided in patients with deficiencies in dietary B₁₂ intake or absorption or B₁₂-dependent metabolism.
- Inhaled anesthetics, when scavenged and ejected into the atmosphere, contribute to both global warming and ozone depletion. Minimizing the environmental impact of inhaled anesthetics requires reducing waste, through the routine use of low fresh gas flows and/or by use of new technologies that trap scavenged anesthetic gases. Reprocessing and reusing trapped anesthetic gases further reduce the environmental impact of drug production.

Introduction

Modern inhaled anesthetics are important pharmacologic tools for reversibly altering central nervous system (CNS) functions in patients. Because inhaled anesthetics are both taken up and eliminated through alveolar blood-gas exchange, drug dosage can be monitored in expired alveolar gases and tissue-dependent metabolism is unnecessary for drug clearance. Optimal delivery of systemic drugs via inhalation requires a full understanding of the factors influencing how gas-phase compounds move into and out of various body tissues and how they are metabolized (pharmacokinetics) together with knowledge of where and how these drugs and their metabolism affect tissue functions. Reversible anesthetic effects on the nervous, respiratory, and cardiovascular systems (pharmacodynamics) are covered elsewhere in this book (see Chapters 11, 14, 19, and 21).

Uptake and Distribution of Inhaled Anesthetics

In the first part of this chapter, we review and apply some of the basic principles of chemical equilibria to illuminate major factors influencing inhaled anesthetic uptake and distribution in patients. For this, we use a physiologic model that closely simulates clinical observations. The model, an elaboration of that introduced in 1973 by Mapleson,¹ is described both qualitatively and quantitatively (using mathematical expressions) to convey important concepts to readers with different learning styles.

BIOPHYSICAL PROPERTIES OF INHALED ANESTHETICS: PARTIAL PRESSURE, HYDROPHOBICITY, AND PARTITION COEFFICIENTS

Inhaled anesthetics are administered as a component of a gas mixture. Biophysical properties of inhaled anesthetics are summarized in Table 20.1.²⁻¹¹ **Partial pressure** is the portion of total pressure contributed by one component of

a gas mixture, where each component contributes pressure in direct proportion to its molar fraction. For example, 1.5% isoflurane in air (21% O₂ and 79% N₂) at 1 standard atmosphere (atm) (760 mm Hg) is a mixture of O₂ at 157.2 mm Hg, N₂ at 591.4 mm Hg, and isoflurane at 11.4 mm Hg. The partial pressure of an anesthetic gas is a measure of its thermodynamic activity and determines its pharmacologic effect. The partial pressure of an anesthetic is usually reported as the percentage (or fraction) of the delivered gas mixture, where atmospheric pressure is near 1 atm (760 mm Hg). Correcting these values to absolute partial pressure is important under conditions when local atmospheric pressure differs significantly from standard, such as at high altitude, underwater, or in a hyperbaric chamber. The same inhaled concentration of an anesthetic gas results in a reduced pharmacologic effect at higher altitudes because the partial pressure of the anesthetic is lower. Because partial pressure is the thermodynamic force for gas transfer between compartments in a system, anesthetics move from regions of high partial pressure to low partial pressure, unaffected by the other components of the gas mixture, and equilibrium is achieved when the partial pressure of an anesthetic is equal in the different compartments.

The maximum partial pressure of a volatile compound is its **vapor pressure**; this is the partial pressure of volatile anesthetic (VA) within the drug reservoir of a vaporizer. Vapor pressure is unique to each anesthetic and increases with increasing temperature. VAs are defined by a vapor pressure less than 1 atm at 20°C and a boiling point above 20°C (see Table 20.1). Gaseous anesthetics are defined by a vapor pressure above 1 atm at 20°C and a boiling point below 20°C (see Table 20.1). VAs typically compose a small fraction of the gas mixture delivered to patients. In contrast, gaseous anesthetics such as nitrous oxide (N₂O) and xenon, because of their relatively low anesthetic potencies, typically compose a large fraction of an inhaled gas mixture, and thus produce additional effects (e.g., concentration effect, second gas effect, and airspace expansion) that are negligible with VAs.

Hydrophobicity is a molecular property of certain chemicals, including most general anesthetics that do not

TABLE 20.1 Chemical Structures and Properties of Inhaled Anesthetics

Anesthetic	Nitrous Oxide	Halothane	Methoxyflurane	Enflurane	Isoflurane	Desflurane	Sevoflurane
Year Introduced into Clinic	1840s	1956	1960	1966	1969	1990	1981
Chemical structure	$ \begin{array}{c} \text{N} \equiv \text{N} - \ddot{\text{O}} \\ \uparrow \quad \downarrow \\ \text{N} = \text{N} = \text{O} \end{array} $	$ \begin{array}{c} \text{F} \quad \text{Br} \\ \quad \\ \text{F} - \text{C} - \text{C} - \text{H} \\ \quad \\ \text{F} \quad \text{Cl} \end{array} $	$ \begin{array}{c} \text{Cl} \quad \text{F} \quad \text{H} \\ \quad \quad \\ \text{H} - \text{C} - \text{C} - \text{O} - \text{C} - \text{H} \\ \quad \quad \\ \text{Cl} \quad \text{F} \quad \text{H} \end{array} $	$ \begin{array}{c} \text{F} \quad \text{F} \quad \text{F} \\ \quad \quad \\ \text{H} - \text{C} - \text{C} - \text{O} - \text{C} - \text{H} \\ \quad \quad \\ \text{Cl} \quad \text{F} \quad \text{F} \end{array} $	$ \begin{array}{c} \text{F} \quad \text{H} \quad \text{F} \\ \quad \quad \\ \text{F} - \text{C} - \text{C} - \text{O} - \text{C} - \text{H} \\ \quad \quad \\ \text{F} \quad \text{Cl} \quad \text{F} \end{array} $	$ \begin{array}{c} \text{F} \quad \text{F} \quad \text{F} \\ \quad \quad \\ \text{F} - \text{C} - \text{C} - \text{O} - \text{C} - \text{H} \\ \quad \quad \\ \text{F} \quad \text{H} \quad \text{F} \end{array} $	$ \begin{array}{c} \text{CF}_3 \quad \text{H} \\ \quad \\ \text{H} - \text{C} - \text{O} - \text{C} - \text{F} \\ \quad \\ \text{CF}_3 \quad \text{H} \end{array} $
Molecular weight	44	197.4	165.0	184.5	184.5	168	200.1
Boiling point (°C)	-88.5	50.2	104.8	56.5	48.5	22.8	58.6
Density (g/ml)	1.84×10^{-3}	1.86	1.42	1.52	1.5	1.45	1.50
Vapor pressure (mm Hg)	43,880	243	22.5	175	238	664	157
Oil/gas partition coefficient at 37°C	1.3	197	950	98.5	90.8	19	47-54
Blood/gas partition coefficient at 37°C	0.47	2.5	12	1.9	1.4	0.45	0.65
MAC-immobility (% atm/mm Hg)*	104/800	0.75/5.7	0.2/1.52	1.58/12.0	1.28/9.7	6.0/45.6	2.05/15.6
MAC-aware*	71/540	0.41/3.21	0.081/0.62	0.51/3.88	0.43/3.27	2.4/19	0.63/4.79

*MAC is minimal alveolar concentration for subjects approximately age 40 years.

Partition coefficients are from the following references²⁻⁶:

MAC-immobility and MAC-aware values are from the following references^{2,7-11}:

Properties are measured at standard temperature (20°C) and pressure (1 atm) unless otherwise specified.

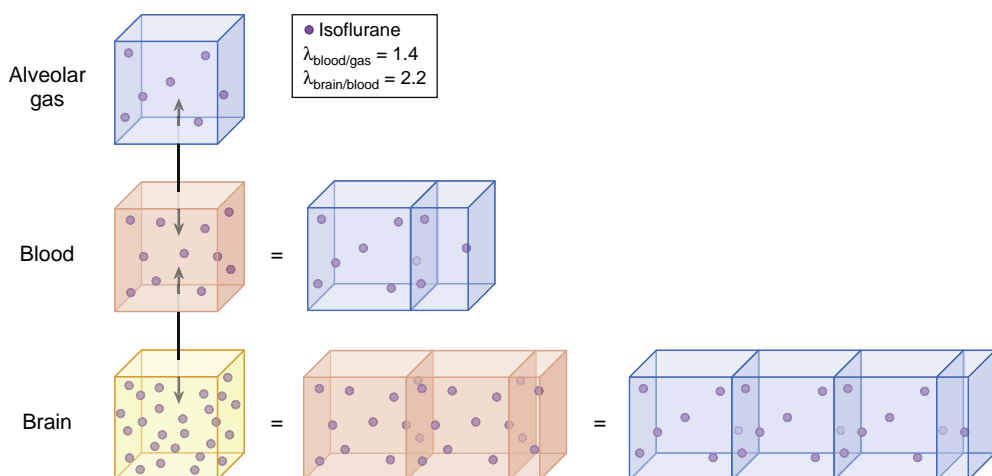


Fig. 20.1 Partitioning of anesthetic gases between different biophases. Left, Depicts the partitioning of isoflurane between gas phase (blue), blood (red) and brain (yellow). The blood:gas partition coefficient ($\lambda_{\text{b/g}}$) for isoflurane is 1.4 and the brain:blood partition coefficient ($\lambda_{\text{CNS/blood}}$) is 2.2 (see Table 20.2). At equilibrium, defined as equal isoflurane partial pressure in all compartments, a volume of blood contains 1.4-fold the quantity of isoflurane as the same volume of alveolar gas, whereas a volume of brain tissue contains 2.2-fold the quantity of isoflurane as the same volume of blood. Right, We also depict partition coefficients as effective (equivalent) volumes of another biophase. For example, 1 volume of blood contains the same amount of isoflurane as 1.4 volumes of alveolar gas, whereas 1 volume of brain contains the same amount of isoflurane as 2.2 volumes of blood or 3.1 volumes of gas.

readily form hydrogen bonds and therefore display low water solubility. Hydrophobic compounds are also usually *lipophilic*, demonstrating high solubility in low polarity solvents such as oils. Common measures of hydrophobicity are **partition coefficients** between water and olive oil (which is mostly oleic acid, an 18-carbon fatty acid) or between water and n-octanol. Usually represented by the Greek letter lambda (λ), a partition coefficient is the ratio of two solute concentrations *at equilibrium* (i.e., at equal partial pressure) in two separate but adjacent solvents or compartments such that the solute moves freely between the compartments (Fig. 20.1). Another useful way to conceptualize a partition coefficient is that it represents the *relative volume of two phases or compartments that contain an equal amount of the solute at equilibrium* (see Fig. 20.1).

Anesthetic partition coefficients between blood and gas ($\lambda_{\text{b/g}}$) and between tissue and blood ($\lambda_{\text{t/b}}$) are important factors in uptake and distribution of inhaled drugs as they move from pulmonary airspace to pulmonary blood and then from blood to various tissues (Tables 20.1 and 20.2).^{6,12-15} The blood solubility of anesthetic gases (and other gases such as O₂, N₂, and CO₂) increases as temperature decreases.^{16,17} Because most anesthetics are hydrophobic, they tend to display high solubility in tissues with high lipid content (e.g., fat), and also bind to many proteins that form hydrophobic or amphiphilic pockets.¹³ Anesthetic partitioning into blood (blood solubility) increases after ingestion of fatty foods¹⁸ and may decrease in anemic or malnourished patients. Methoxyflurane (no longer in clinical use) and halothane are notable for high blood solubility. N₂O, sevoflurane, and desflurane are characterized by low blood solubility.

ANESTHETIC DELIVERY, UPTAKE, AND DISTRIBUTION: A MULTICOMPARTMENTAL MODEL

Delivering an inhaled anesthetic agent to patients is analogous to an intravenous drug infusion with two major differences: (1) entry of drug into the body is via transalveolar

exchange from gas to blood, and (2) clearance is mostly via the same route. Thus inhaled anesthetic delivery is dependent on pulmonary ventilation, whereas uptake and clearance of inhaled anesthetics are also dependent on pulmonary perfusion.

Upstream and Downstream Compartments and Anesthetic Transfer: Bulk Flow and Pressure Gradients

Uptake and distribution of inhaled anesthetic can be readily understood as a series of transfer steps from upstream compartments with high partial pressure to downstream compartments with low partial pressure as depicted in Fig. 20.2. First, drug is transferred from an anesthesia delivery device, typically an anesthesia machine with a vaporizer designed to deliver specified concentrations (in percent atm) of VA agent, into a fresh gas mixture flowing in a breathing circuit. Second, ventilation transfers gases from the circuit to the alveolar airspace in lung. Third, anesthetic moves by transcapillary diffusion into pulmonary venous blood. Fourth, arterial blood distributes anesthetic to various tissues including the primary target tissue, the CNS. Fifth, venous outflow from tissues converges in the pulmonary artery, and sixth, the mixed venous blood passes through alveolar capillaries where it again equilibrates with alveolar gases.

Gas flow from the anesthesia machine into the breathing circuit is unidirectional. Blood circulation is also largely unidirectional. In transfers from the anesthesia machine (the fresh gas outlet) to breathing circuit and then to alveolar airspace, anesthetic flow can simply be understood as exchange from upstream compartments into downstream compartments. In later steps, such as exchange between alveolar gases and pulmonary capillary blood, flow of anesthetic molecules occurs via diffusion between adjacent compartments separated by a permeable membrane. For simplicity, we have not treated blood as a separate compartment in our model. Distribution of anesthetic to and from various tissues involves both bulk transfer via blood flow

TABLE 20.2 Uptake and Distribution Model Parameters for Inhaled Anesthetics

Tissue	Blood		Heart		Kidney		Liver		CNS		Muscle		Fat		VPT	
	Blood Flow (L/min)	Volume (L)	Blood Flow (L/min)	Volume (L)	Blood Flow (L/min)	Volume (L)	Blood Flow (L/min)	Volume (L)	Blood Flow (L/min)	Volume (L)	Blood Flow (L/min)	Volume (L)	Blood Flow (L/min)	Volume (L)	Blood Flow (L/min)	Volume (L)
	5	5	0.2	0.28	1.07	0.32	1.2	3.9	0.62	1.43	0.75	30	0.5	13	0.35	7
Anesthetic Agent	V_{eff} (L)*	$\lambda_{tissue/blood}$	V_{eff} (L)	τ (min)	$\lambda_{tissue/blood}$	V_{eff} (L)	τ (min)	$\lambda_{tissue/blood}$	V_{eff} (L)	τ (min)	$\lambda_{tissue/blood}$	V_{eff} (L)	τ (min)	$\lambda_{tissue/blood}$	V_{eff} (L)	τ (min)
Nitrous oxide	2.35	0.87	0.24	1.2	0.93	0.3	0.3	1.1	4.1	3.4	1.1	1.6	2.6	1.2	36	48
Halothane	12.5	2.9	0.8	4.0	1.5	0.5	0.4	2.5	9.8	8.0	2.7	3.9	3.3	2.5	75	100
Methoxyflurane	60	1.2	0.34	1.7	2.3	0.74	.69	2.5	9.8	8	2	2.9	4.7	1.6	48	64
Enflurane	9	1.3	0.36	1.8	2.0	0.64	0.6	2.1	8.2	6.7	1.4	2.0	3.3	1.7	51	68
Isoflurane	7	1.3	0.36	1.8	2.3	0.74	0.69	2.4	9.4	7.6	1.5	2.1	3.5	2.9	87	116
Desflurane	2.25	1.3	0.36	1.8	1.0	0.32	0.3	1.4	5.5	4.5	1.3	1.9	3.0	2.0	60	80
Sevoflurane	3.25	1.3	0.36	1.8	2.3	0.74	0.69	2.4	9.4	7.7	1.7	2.4	4.0	3.1	93	120

Based on a 70 kg pt at rest. Blood and tissue partition coefficients are from references 6 and 12-14. Tissue volumes and blood flow values are approximate (Kennedy et al.¹⁵ and Levitt¹³). Effective volumes are calculated as tissue volume $\times \lambda_{tissue/blood}$ and exchange time constant (τ) for each compartment is $V_{eff}/$ blood flow.

*Blood/gas partition coefficients for anesthetic agents are given in Table 20.1.

CNS, Central nervous system; VPT, vessel-poor tissues (e.g., skin, bone, and connective tissues).